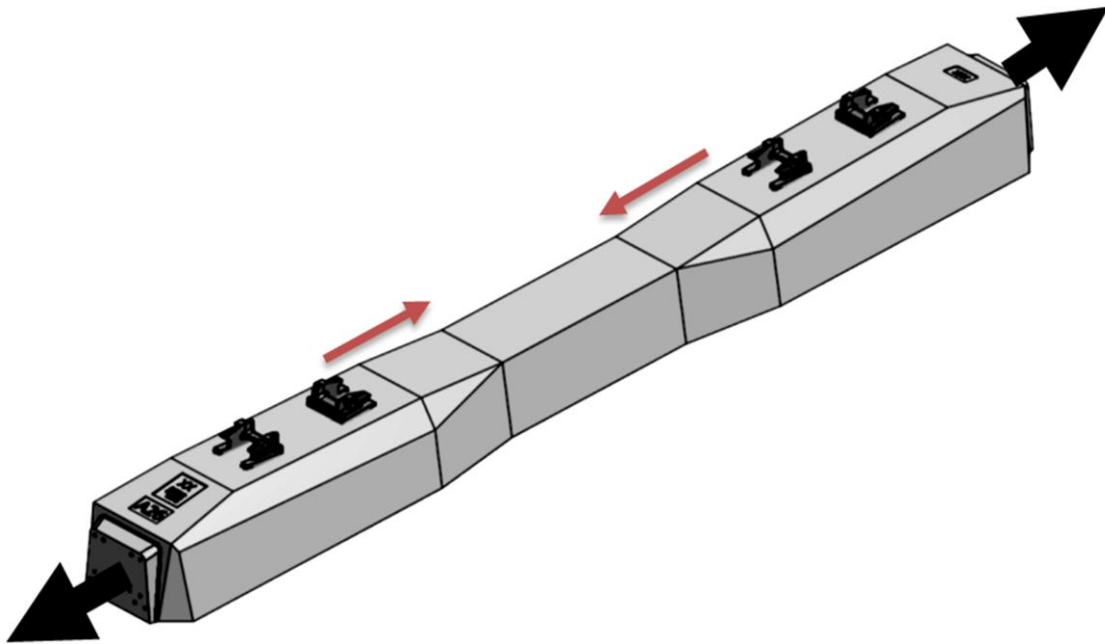


CHALMERS



Process induced prestress losses in long bed systems for railway sleepers

Master of Science Thesis in the Master's Programme Structural Engineering and Building Performance Design

SIMON CARLSSON
ERIK HOLMBOM

Department of Civil and Environmental Engineering
Division of Structural Engineering
Concrete Structures
CHALMERS UNIVERSITY OF TECHNOLOGY
Göteborg, Sweden 2012
Master's Thesis 2012:86

MASTER'S THESIS 2012:86

Process induced prestress losses in long bed systems for railway sleepers

*Master of Science Thesis in the Master's Programme Structural Engineering and
Building Performance Design*

SIMON CARLSSON

ERIK HOLMBOM

Department of Civil and Environmental Engineering
*Division of Structural Engineering
Concrete Structures*

CHALMERS UNIVERSITY OF TECHNOLOGY

Göteborg, Sweden 2012

Process induced prestress losses in long bed systems for railway sleepers

Master of Science Thesis in the Master's Programme Structural Engineering and Building Performance Design

CARLSSON SIMON

HOLMBOM ERIK

© SIMON CARLSSON, ERIK HOLMBOM, 2012

Examensarbete / Institutionen för bygg- och miljöteknik,
Chalmers tekniska högskola 2012:86

Department of Civil and Environmental Engineering

Division of Structural Engineering

Concrete Structures

Chalmers University of Technology

SE-412 96 Göteborg

Sweden

Telephone: + 46 (0)31-772 1000

Cover:

Illustration of a typical design of a prestressed concrete sleeper produced by Abetong:s "The Long Line Method".

Chalmers Reproservice / Department of Civil and Environmental Engineering
Göteborg, Sweden 2012

Process induced prestress losses in long bed systems for railway sleepers

Master of Science Thesis in the Master's Programme Structural Engineering and Building Performance Design

SIMON CARLSSON

ERIK HOLMBOM

Department of Civil and Environmental Engineering

Division of Structural Engineering

Concrete Structures

Chalmers University of Technology

ABSTRACT

The tendency in recent years has been to optimise the railway sleepers for higher axle loads with existing geometry of the sleepers due to the high investment cost for new moulds. The optimization requires deeper knowledge than the general relations specified in existing standards. The qualities of prestressed concrete sleepers during the manufacturing process called “The Long Line Method” vary widely depending on initial conditions. Mainly, the initial prestress on the steel reduces significantly during the first approximately eighteen hours after tensioning. The purpose of this thesis was to identify the causes of these prestress losses, to explain how the main parameters influence, and to propose solutions that reduce the prestress losses during the production process. This was done through literature studies, modelling with non-linear finite element analysis in DIANA and parameter studies. The analyses included a thermal part and a structural part which are coupled. The thermal part includes temperature- and maturity development during the curing process when heat is generated by the concrete hydration, where ambient- and initial temperature are important factors. The structural part includes bond-slip behaviour and stiffness development, dependent of maturity from the thermal analysis. It also includes thermal effects such as expansion and contraction, which are coupled to the temperature achieved in the thermal analysis. The production at three factories with different conditions, located in the cities Vislanda, Marijampolė and Sollenau were studied. Furthermore, the results from FE-models were compared with measurements made at the different plants and a parameter study was made on the most important initial conditions. The result shows that temperature and maturity development controls the most important phenomena's; contraction, expansion, bond-slip behaviour and evolution of stiffness. The parameter study shows that there are many parameters influencing the development of temperature and maturity; initial concrete temperature, ambient temperature, sheeting properties, casting times and bed arrangement. Control of these parameters gives a uniform steel stress variation, which results in lower induced prestress losses in the last casted end which has been showed having the lowest prestress.

Key words: Prestressed concrete sleeper, Prestress loss, The Long Line Method, young concrete, thermal properties of young concrete, mechanical properties of young concrete, hydration process, heat development, bond behaviour, maturity, non-linear finite element analysis.

Förspänningsförluster under produktion med långa bäddsystem för järnvägssliprar
Examensarbete inom Structural Engineering and Building Performance Design
SIMON CARLSSON

ERIK HOLMBOM

Institutionen för bygg- och miljöteknik

Avdelningen för konstruktionsteknik

Betongbyggnad

Chalmers tekniska högskola

SAMMANFATTNING

Tendensen under de senaste åren har varit att optimera järnvägssliprar för högre axel-laster med befintlig geometri av sliprarna på grund av den höga inversteringskostnaden för nya former. Optimeringen kräver djupare kunskap än vad som finns i nuvarande standarder. Kvalitén på förspända betongsliprar under tillverkningsprocessen kallad ”The Long Line Method” har visat sig variera väsentligt beroende på initiala förhållanden. Huvudsakligen minskar den initiella förspänningen på stålet avsevärt redan under de första cirka arton timmarna från uppspanning. Syftet med detta examensarbete är att identifiera orsakerna till dessa spänningsförluster, för att kunna förklara hur de viktigaste parametrarna påverkar, och att föreslå lösningar som reducerar förspänningsförlusterna under produktion. Detta utfördes genom litteraturstudier, analyser med finit element modellering i DIANA och en parameterstudie. Analyserna inkluderar en termisk och en strukturell del, vilka är kopplade med varandra. Den termiska delen innehåller temperatur- och mognadsutveckling under härdningsprocessen då betongens hydration, omgivande temperatur och initiell betongtemperatur är viktiga parametrar. Den strukturella delen innehåller vidhäftning-glidning beteende och betongens styvhetstillväxt, vilka är beroende på betongens mognadsgrad från den termiska analysen. Den innehåller också termiska effekter såsom expansion och kontraktion, vilka är kopplade till temperaturutvecklingen från den termiska analysen. Produktionen på tre fabriker med olika förutsättningar, belägna i städerna Vislanda, Marijampolé och Sollenau har studerats. Resultaten visar att temperature- och mognadsgradsutveckling kontrollerar de flesta viktiga fenomen; expansion, kontraktion, vidhäftning-glidning beteende och utvecklingen av betongens styvhet. Parameterstudien visar att det finns många faktorer som inverkar på utvecklingen av temperatur och mognadsgrad; initiell betongtemperatur, omgivande temperatur, täckande materialets egenskaper, gjuttider och bäddutförande. Kontroll av dessa parametrar resulterar i en produktion med jämn förspänningskraft, där en jämn produktion i sin tur leder till lägre förspänningsförluster i den sist gjutna bädden som visat sig vara den som har sämst förspänning.

Nyckelord: Förspänd betong slipper, förspännings förluster, The Long Line Method, ung betong, termiska egenskaper av ung betong, mekaniska egenskaper av ung betong, hydratiseringsprocessen, värme utveckling, vidhäftning-bindning beteende, mognadsgrad, olinjär analys med finit element metod.

Contents

1	INTRODUCTION	2
1.1	Background	2
1.2	Purpose and objectives	3
1.3	Scope and method	3
1.4	Limitations	4
1.5	Outline of contents	4
2	MATERIAL BEHAVIOURS	5
2.1	Young concrete	5
2.1.1	Introduction	5
2.1.2	Thermal properties of young concrete	7
2.1.3	Mechanical properties of young concrete	22
2.2	Prestressing steel	29
2.2.1	Introduction	29
2.2.2	Thermal properties of prestressing steel	29
2.2.3	Mechanical properties of prestressing steel	31
2.3	Interaction between young concrete and prestressing steel	37
2.3.1	Bond behaviour	37
2.3.2	Transfer of prestressing force	40
3	THE LONG LINE METHOD	44
3.1	General about concrete sleepers	47
4	MEASURED PRESTRESS LOSSES DURING SLEEPER PRODUCTION WITH “THE LONG LINE METHOD”	49
4.1	Different production conditions	49
4.1.1	Vislanda – warm surroundings and sections of moulds	49
4.1.2	Marijampolé – cold surroundings and continuous set of moulds	50
4.1.3	Sollenau – warm surroundings and continuous set of moulds	51
4.1.4	Results from test measurements	52
4.1.5	Summary of the factories	58
5	DEVELOPMENT OF FINITE ELEMENT MODEL	60
5.1	Introduction	60
5.2	Element selection	60
5.2.1	Young concrete	61
5.2.2	Heat transfer	61
5.2.3	Prestressed steel	61
5.2.4	Interaction between young concrete and prestressed steel strands	62
5.3	Verification of the thermal properties in the FE-model	63
5.3.1	Input parameters for the thermal analyses	63

5.3.2	Hydration process of young concrete and heat transfer	64
5.3.3	Casting of young concrete in sequences	70
5.4	Verification of the mechanical properties in the FE-model	72
5.4.1	Input parameters to the mechanical analyses Fel! Bokmärket är inte definierat.	
5.4.2	Thermal expansion due to constant temperature	73
5.4.3	Shrinkage of young concrete	81
5.4.4	Development of Young's modulus of elasticity	81
5.4.5	Bond-slip behaviour between concrete and steel strand	84
5.4.6	Verification of the relationship between all parameters	87
5.5	Description of the FE-models	90
5.5.1	Geometry conditions	90
5.5.2	Casting Sequences	92
5.5.3	Boundary conditions	92
5.5.4	Adiabatic temperature	94
5.6	Results of FE-analyses in phase 2 with reference values compared to measurements	97
5.6.1	Vislanda	98
5.6.2	Marijampolé	104
5.6.3	Sollenau	108
5.6.4	Comments to results	113
6	PARAMETER STUDY	114
6.1	The ambient air temperature	114
6.2	Initial temperature of the steel strands	116
6.3	Different curing methods	116
6.4	Bed arrangements of "The Long Line Method"	118
6.5	Different casting times	120
6.6	Expansion behaviour	122
6.7	Summary of results obtained in the parameter study	124
7	ACHIEVED KNOWLEDGE OF PRINCIPAL PHENOMENA INFLUENCING PRESTRESS LOSSES DURING DIFFERENT PHASES OF THE SLEEPER PRODUCTION	125
7.1	Before casting	126
7.2	From casting to release of prestress	126
7.3	Release of prestress	130
7.4	Comparison of prestress variation during the production between results from FE-analysis with reference values, hand calculation and measurement	130
8	FINAL REMARKS	134
8.1	Discussion	134

8.2	Conclusions	135
8.3	Further studies	136
9	REFERENCES	137
APPENDIX A	HAND CALCULATIONS	140
APPENDIX B	INPUT DATA FILES FOR DIANA	194

Preface

In this master thesis, the prestress losses of prestressed steel strands in sleepers during the manufacturing process called The Long Line Method were studied. The project was initiated by the company Abetong, and was carried out between January 2012 and June 2012 at the Department of Civil and Environmental Engineering, Division of Structural Engineering, Concrete Structures, Chalmers University of Technology.

First of all, we would like to thank our two supervisors Ph. D. Rikard Bolmsvik, Abetong, and Professor Karin Lundgren, who also was the examiner, for their helpful support, guidance and understanding during entire master thesis.

Furthermore, we would like to thank our opponents Fabian Narin and Olle Wiklund for their feedbacks and comments during this project. Finally, special thanks to Nicklas Karlsson who reviewed parts of the report.

Göteborg, June, 2012



Simon Carlsson



Erik Holmbom

Notations

Roman upper case letters

A	Frequency factor [J/mol]
A_p	Area of the prestressing steel [m ²]
C	Cement content [kg cement/m ³]
\bar{C}	Dimensionless matrix dependent on Poisson's ratio [-]
C_{const}	Coefficient with recommend value 2 [-]
C_m	Moister correction factor [-]
C_p	Specific heat capacity [J/kg°C]
$C_{p\infty}$	Specific heat capacity of mature concrete [J/kg°C]
CTC	Coefficient of thermal contraction [μ /°C]
CTE	Coefficient of thermal expansion [μ /°C]
\bar{D}	Dimensionless matrix dependent on Poisson's ratio [-]
E_a	Apparent activation energy [J/mol]
E_{cm}	Modulus of elasticity of concrete [GPa]
$E_c(t_e)$	Modulus of elasticity depending on equivalent age [GPa]
$E_c(28)$	Modulus of elasticity after 28 days [GPa]
E_p	Modulus of elasticity of prestressed steel [GPa]
$E(t, \tau)$	Relaxation function [GPa]
$E_a(\tau)$	Time dependent stiffness of the model [GPa]
$J(t, \tau)$	Creep function, according to Kelvin Chain model [-]
K	Constant depending casting temperature and cement type [°C]
P_{max}	Maximum prestressing force [MPa]
$P_{m,t}$	Mean prestressing force [MPa]
P_{m0}	Initial prestressing force [MPa]
ΔP_{c+s+r}	Time dependent losses due to short term relaxation [MPa]
ΔP_i	Immediate losses [MPa]
ΔP_e	Specific thermal prestress loss [MPa]
ΔP_{el}	Immediate losses due to elastic deformations of concrete [MPa]
ΔP_r	Immediate losses due to short term relaxation [MPa]
ΔP_{sl}	Immediate losses due to anchorage slip [MPa]
Q	Amount of hydrated heat generated within the body [W/m ³]
Q_c	Total developed heat energy [J/m ³]
R	Restraint degree [-]
R	Universal gas constant [J/mol·K]
T	Actual temperature at a specific time [°C]
T_a	Temperature of the surrounding air [°C]
T_{adiab}	Adiabatic Temperature [°C]
T_c	Curing temperature [°C]
T_{max}	Maximum temperature [°C]
T_{ref}	Reference temperature [°C]
T_0	Temperature of surrounding [°C]
ΔT_0	Temperature difference between concrete and surroundings when casting starts [°C]
ΔT_{max}	Maximum temperature increase [°C]
T_u	Temperature after cooling period [°C]
$T_{(\Delta t_1)}$	Temperature during the time interval Δt_i [°C]
dT	Temperature difference between air and surface [°C]

$\frac{\partial T}{\partial x}$	Temperature gradient [°C]
$V_{agg,i}$	Volume of aggregate in the concrete mixture [m ³]
V_{conc}	Total volume of concrete in the concrete mixture [m ³]
V_{paste}	Volume of cement paste in the concrete mixture [m ³]

Roman lower case letters

c	Constant value, recommended to f_t [MPa]
c	Specific heat capacity [J/kgK]
f_{ck}	Characteristic compressive strength of concrete [MPa]
f_{cm}	Mean compressive strength [MPa]
$f_{cm}(t)$	Mean compressive strength a time t [MPa]
$f_c(t_e)$	Compressive strength depending on equivalent age [MPa]
$f_c(28)$	Compressive strength after 28 days [MPa]
f_t	Reinforcement tensile stress [MPa]
$f_t(t_e)$	Tensile strength depending on equivalent age [MPa]
$f_t(28)$	Tensile strength after 28 days [MPa]
f_p	Prestressing tensile stress [MPa]
$f_{p0,1k}$	0,1 % prestressed characteristic proof stress [MPa]
f_{yk}	Characteristic yield stress of the reinforced steel [MPa]
h_c	Convection heat transfer coefficient [W/m ² °C]
h_r	Irradiation heat transfer coefficient [W/m ² °C]
k	Thermal conductivity coefficient [W/m°C]
k_h	Coefficient that depends on size of the cross-section [-]
k_7	Constant value [-]
k_8	Constant value [-]
k_∞	Thermal conductivity coefficient of mature concrete [W/m°C]
l_t	Transmission length [m]
n_E	Model parameter describing the age dependence [-]
n_t	Model parameter describing the age dependence [-]
q	Heat flux [W/m]
q_c	Heat transfer by convection [W/m ²]
q_u	Hydration heat degree after completed hydration [J/kg cement]
s	Model parameter describing the age dependence [-]
s	Maximum slip [mm]
s_1	Constant slip value [mm]
s_2	Constant slip value [mm]
s_3	Clear rib spacing [mm]
t_e	Equivalent age
t_1	Hydration parameter [-]
t_0	Age at where significant mechanical properties starts to develop [-]
Δu_t	Shear slip [mm]
Δu_t^0	Where the curve reaches the plateau [mm]
w	Wind speed [m/s]

Greek letters

$\alpha_{agg,i}$	CTE of i th aggregate [μ /°C]
α_{adia}	Constant depending casting temperature and cement type [°C]

α_{conc}	Weighted average of the aggregate- and cement volume for the CTE value of young concrete [$\mu / ^\circ\text{C}$]
α_{cTc}	Coefficient of thermal contraction of concrete, CTC [$\mu / ^\circ\text{C}$]
α_{cTe}	Coefficient of thermal expansion of concrete, CTE [$\mu / ^\circ\text{C}$]
α_{paste}	CTE of i^{th} cement paste [$\mu / ^\circ\text{C}$]
α_{psTe}	Coefficient of thermal expansion of prestressing steel, CTE [$\mu / ^\circ\text{C}$]
α_u	The final hydration degree
$\frac{d\alpha}{dt}$	Acceleration of the hydration process [-]
β_{add}	Factor that considers the effect of additives [-]
$\beta_{as}(t)$	Time function of autogenous shrinkage [-]
$\beta_{as}(t, t_s)$	Time function of drying shrinkage [-]
$\beta_c(t, t_0)$	Time function of the creep coefficient considers actual age of concrete, non-adjusted duration of loading, national size of the cross section and the ambient relative humidity [-]
β_{RH}	Factor that considers relative humidity in concrete [-]
β_T	Factor that considers temperature [-]
γ	Age conversion factor [-]
ε	Coefficient of emissivity of surface [-]
ε	Strains [-]
$\varepsilon_{ca}(t)$	Concrete autogenous shrinkage strain [-]
$\varepsilon_{ca}(\infty)$	Final value of concrete autogenous shrinkage [-]
$\varepsilon_{cd}(t)$	Concrete drying shrinkage strain [-]
$\varepsilon_{cd,0}$	Basic value of concrete drying shrinkage depending on relative humidity, concrete class and type of cement [-]
ε_{ct}	Concrete stress-dependent strain [-]
ε_{cT}	Total concrete stress-independent strain due to temperature [-]
ε_{cTc}	Concrete stress-independent strain due to temperature contraction [-]
ε_{cTe}	Concrete stress-independent strain due to temperature expansion [-]
ε_{psTe}	Stress-independent strain of prestressed steel due to temperature expansion [-]
$\Delta\varepsilon$	Total change in strain [-]
κ_1	Hydration parameter [-]
λ_α	Relaxation time [s]
λ_1	Hydration parameter [-]
μ	Quota between σ_{pi} and f_p [-]
ν	Poisson's ratio [-]
ρ	Density [kg/m^3]
ρ_{1000}	Value of relaxation loss at 1000 hours after tensioning [%]
σ	Stefan-Boltzmann constant [$\text{W}/\text{m}^2\text{K}^4$]
σ_c	Concrete stresses [MPa]
$\sigma_{m0}(x)$	Stress in the tendon immediately after transfer [MPa]
σ_s	Steel stresses [MPa]
$\Delta\sigma_{pr}$	Absolut value of the relaxation losses of the prestress [MPa]
σ_{pi}	Maximum tensile stress applied to the tendon minus the immediate losses occurred during the stressing process [MPa]
τ	Age parameter [-]
τ_b	Bond stress [MPa]

τ_{max}	Final value of bond stress [MPa]
t_t	Bond shear traction [MPa]
φ_0	National creep coefficient considers relative humidity, concrete strength and age when the concrete was loaded [-]
ψ	The degree of hydration [-]

1 Introduction

The railway has been an important branch of transport in the society since the last one and a half centuries. It started with steam powered trains with simple timber sleepers tracks. Development of both trains and the railway structure has then been made over the years. Today electric powered trains are used at tracks with prestressed concrete sleepers. The sleepers are important components in the railway structure which interact with both the rail and the embankment, see Figure 1.1.

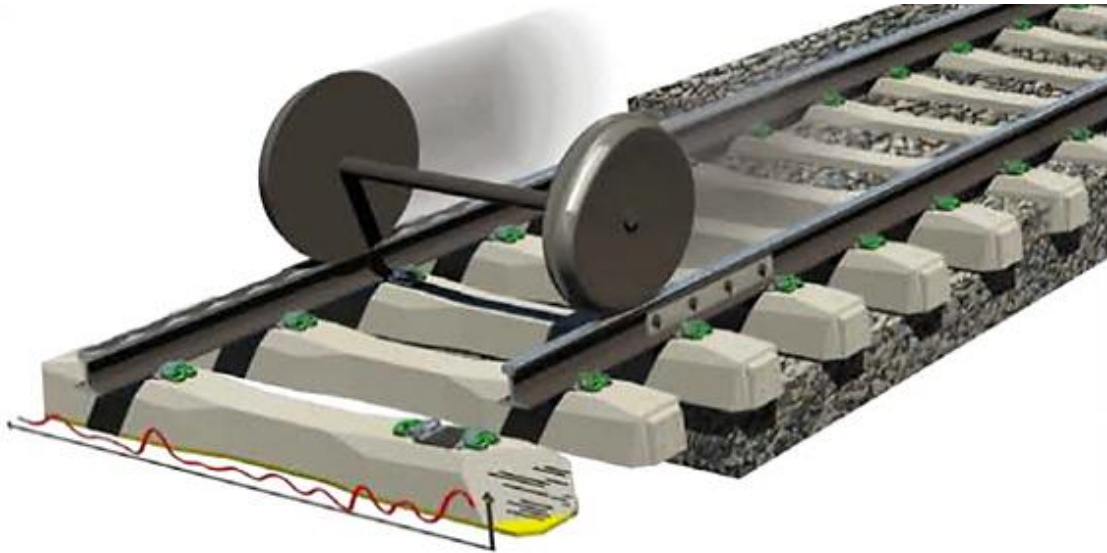


Figure 1.1 Components in the railway influencing the prestressed concrete sleeper design, modified from Abetong (2012).

The capacity requirements regarding the railway are constantly increasing in terms of axle load and speed of the trains. High speeds are given by the new passenger trains that run at 250 km/h and above. The constantly increasing need of freight transport increasing the axle load up to 30 tonnes and more.

Another aspect in the railway industry is to achieve better economy, which means using less material and more efficient production method.

1.1 Background

The idea of this master thesis was presented by the company Abetong AB. The company produces prefabricated concrete members and is a part of the Heidelberg Cement Group which is one of the largest manufactures of building materials. Abetong has produced prestressed concrete sleepers since the middle of 1960's. They use a prestressed production method called "The Long Line Method" which is developed by themselves. The main function of the method is based on rational production with long casting beds including quadruple sleeper moulds. See Chapter 3 for a detailed description of "The Long Line Method".

To increase the knowledge about prestress losses during production, the company Abetong has made measurements at three different factories with different conditions: Vislanda (Sweden), Marijampolė (Lithuania) and Sollenau (Austria). The measurements include the variation of temperature and strain, which is directly related to the prestressing force, during the production. What can be observed in the different re-

sults is that the prestressing force decreases when the temperature increases due to hydration. It can also be seen that the prestressing force decreases significantly when the prestressing force is released (which is expected due to elastic shortening), but other reductions of the prestressing force during production are more difficult to understand and relate to a physical phenomenon.

Bending tests of the sleepers indicates that the model in Eurocode does not coincide with the actual behaviour of the prestressed concrete sleepers, in terms of the given prestress loss during production. Eurocode only presents recommendations and it is up to the designer to decide how the recommendations should be used or if a detailed investigation is needed. Thus, no appropriate model exists, capable of describing the prestress losses indicated by the comparison of results from design calculations and bending tests.

Current sleeper production results in sleepers with sufficient capacity. However, improved knowledge is needed in order to handle the variations in surrounding conditions present at various parts of the world, and to enable further optimization of the sleeper design without unnecessary safety margins.

1.2 Purpose and objectives

The aim with the master thesis is to obtain better understanding about losses in prestressing force during production and to explain which main parameters that influence the given prestress loss.

To get more understanding of the problem, a milestone was to establish a FE-model of the entire bed in “The Long Line Method” at an appropriate detail level that produced similar results that has been found in the different measurements during the production.

The objective was therefore to create a model that takes into account temperature increases over time due to heat of hydration, stepwise casting, development of Young’s modulus and bond-slip with maturity dependence. When principal understanding has been obtained and the model is sufficiently extended, the purpose was to have control of the prestress losses induced during the production of sleepers and to propose appropriate measures.

1.3 Scope and method

The method used was to first do a theoretical literature study of the subject, meantime FE-models was set up, analysed and verified. The FE-models were gradually expanded to include more verified parameters and realistic boundary conditions to obtain a more accurate model. Linear analysis was used in the first models but when the hydration process was introduced a non-linear analysis had to be done. A parameter study was then performed to achieve knowledge of how different parameters influenced the prestress variation.

1.4 Limitations

The thesis includes phenomena that occur during the production process, which means approximately the first day after casting. Thus, only young concrete is considered. As the sleepers are to remain uncracked, cracking was not included in the finite element analyses. FE-analyses were made with two-dimensional plane-stress assumption and consider only the period from concrete casting until pre-tensioning. Furthermore, assumptions regarding free movements of concrete against the underneath steel moulds were made, hence no frictional forces were taken into account. The steel strands were assumed to have linear elastic behaviour. Deeper investigation of the concrete hydration process, i.e. the reaction between water and cement, was not included in the thesis.

1.5 Outline of contents

Chapter 1 presents an introduction to the subject. It includes background, purpose and objectives, scope and methods and limitations. In Chapter 2, a general behaviour of concrete, prestressed steel and an interaction between the materials are presented. The production process, “The Long Line Method”, is described in Chapter 3. In Chapter 4, an explanation of the measured prestress losses during sleeper production is presented. Chapter 5 illustrates the development of different FE-models. In Chapter 6, the knowledge gained from the measurements and simulations concerning the prestress losses obtained during sleeper production are presented. Finally, Chapter 7 contains final remarks. It includes discussion, conclusions and further studies.

2 Material behaviours

In the following subchapters, a literature study has been made on young concrete, prestressed steel and heat transfer in, between and from the two materials.

2.1 Young concrete

2.1.1 Introduction

Traditionally, interest is focused on properties of concrete at an age of 28 days or higher. But it is very important to also know the behaviour of concrete at early ages. This is relevant to the production methods with fast production and early demoulding, adhesion between the concrete and the steel in pretension concrete structures, risk of cracking due to hydration heat, development of thermal and mechanical properties of concrete etc., see Ljungkrantz (1994).

According to Eurocode 2, concrete is considered to be mature after 28 days of curing. Therefore, many properties of concrete are tested at this age and used as standard values, for example the modulus of elasticity, compression strength and tensile strength. The expression young concrete is mainly used before the degree of maturity is fulfilled, but can be related to anything from few hours to days after casting. An upper limit for young concrete could be defined as when the external climate conditions no longer has a significant influence on the development of structure, see Lundgren (2005). The hardening process of concrete can be separated in different phases, fresh concrete, young concrete, hardening concrete and hardened concrete, see Figure 2.1. This report treats only fresh and young concrete, during the production, with an age up to one day.

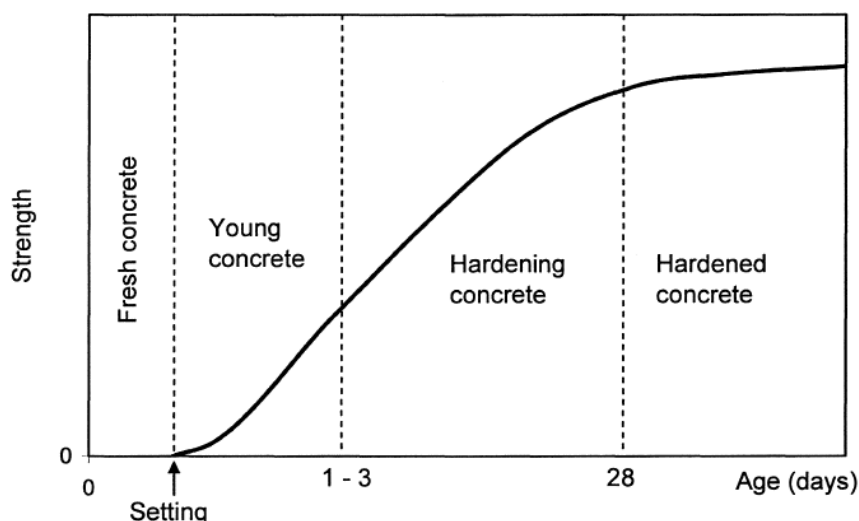


Figure 2.1 Different phases of the hardening process of concrete, Lundgren (2005).

During the first phase of the hardening process of concrete, fresh concrete, the concrete is designated as fresh. Slightly stiffness occurs but the concrete can be readily formed. In phase two, young concrete, the establishment stiffness starts and the change of the concrete properties is rapid. The concrete is in this phase sensitive to humidity, temperature variations and early loading. During the third phase, hardening concrete, the effects of the concrete properties is significantly lower or not at all influenced of the external conditions. The concrete has similar function as the hardened concrete, phase four, but the mechanical properties are not fully developed, see Ljungkrantz (1994).

Studies made on the development of different properties of young concrete show that changes are much more rapid during the first hours up to several days then the rate of change after one week, as Figure 2.1 illustrates above, see Lundgren (2005).

2.1.1.1 The development and use of concrete as a building material

Structural concrete is one of the most commonly used building materials in the society today. Simple concrete technology was already used by the ancient Egyptians in sorts of calcined impure gypsum. Later the Greeks and Romans developed the first concrete in history, by mixing calcined limestone with sand and crushed stone or brick and broken tiles. This was a huge discovery, larger and more durable structures could be built. But the knowledge and use of the building material disappeared with the defeat of the Empire. It was not until the eighteenth century before an advance in the knowledge of concrete occurred, see Neville (2002).

Modern concrete contains almost the same ingredients as the Greeks and Romans with coarse and fine aggregate, cement and water. The main different is that different admixture is added to the concrete today to achieve a specific behaviour. Examples of admixtures are accelerators, retarders, air entrainments, plasticizers, corrosion inhibitors, fly ash, silica fume etc. The strength and durability of concrete depends on many factors and varies a lot. The major factors that affect the strength of the concrete are water- cement ratio, method of mixing and curing, age of concrete, properties and proportions of concrete constituents and shape and dimensions of the tested specimen, see Hassoun (2002).

The name structural concrete summarizes all types of concrete used in structural applications. It can be plain, reinforced, prestressed or partially prestressed. The most frequently used form of concrete is reinforced concrete, where concrete cooperate with the steel reinforcement. If the materials are used properly, they can together form a structural member which can withstand many types of loadings. Concrete should be used to resist compression and steel reinforcement to resist tension forces. What can be mentioned is that concrete has relatively high compressive strength, but not as compared to steel (the ratio is approximately 1:10 depending on materials), see Hassoun (2002). The reason to use steel reinforcement in concrete is because concrete has a low tensile strength, around one-tenth of its compressive strength. See Figure 2.2 for uniaxial stress-strain curve for concrete.

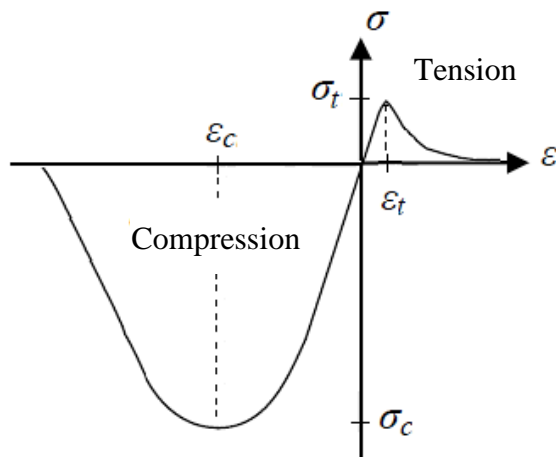


Figure 2.2 Typical uniaxial stress-strain relation for concrete, modified from Plos (2000).

2.1.2 Thermal properties of young concrete

Concrete is a heterogeneous material consisting of several components with different thermal properties. Some of the most common thermal properties for young concrete are the development of heat, specific heat capacity and heat conductivity, see Byfors (1980). These thermal properties are affected by various factors, such as types of material used in the concrete mixture, volume ratios of aggregate, water content, concrete temperature, porosity, additional admixtures, etc., see Kim (2000).

2.1.2.1 Hydration process of concrete

The hardening development of concrete is called hydration process, which initiates when water comes in contact with the cement. The silicates and aluminates in the cement react with the water and form products of hydration. This mixture is called cement paste, which is the bonding agent in the concrete. In the beginning of the hydration process the cement paste is pouring like a liquid, but after time becomes a firm and hard mass. The term hydration degree is used to indicate how much cement that has reacted at a certain time, see Neville (2002). Figure 2.3 shows the development of the cement hydration during the hydration process.

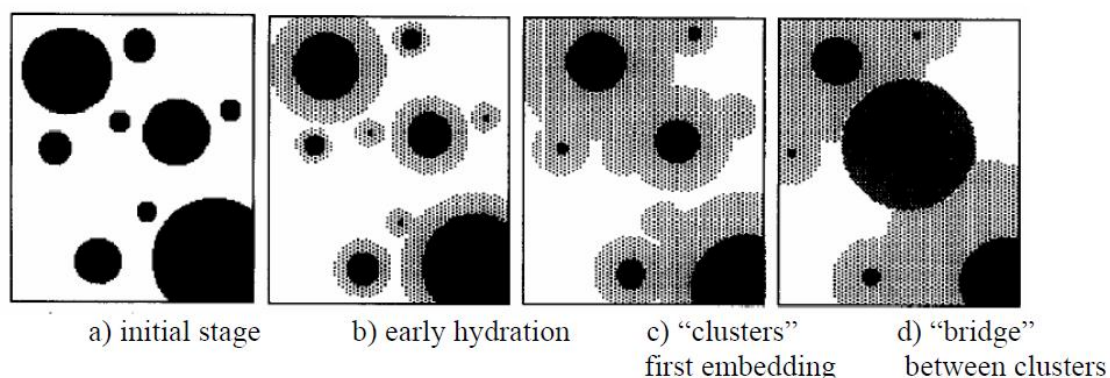


Figure 2.3 Illustration of formation of microstructure between during the hydration process of concrete, from Ji (2008).

Firstly, hydration product is formed and expanded around larger cement particle. Smaller particles are thereafter included and the larger cement particle creates hydration clusters and consolidates them. The level of consolidation inside the cement paste is represented by the cross-linked particles, which is closely associated with the development of strength and elastic modulus, see Ji (2008).

The final hydration degree, α_u , specifies the amount of finally hydrated cement comparing to the total amount of cement. If the value is equal to one, it means that all cement in the concrete has been hydrated. The final hydration degree varies a lot depending on the size and type of cement particles, grinding time and the amount of watering, see Neville (2002). Equation 2.1 shows the definition of the final hydration degree.

$$\alpha_u = \frac{\text{Amount of finally hydrated cement}}{\text{Total amount of cement}} \quad (2.1)$$

What is well known is that the degree of hydration increases continuously, which means that there's a possibility that a varying amount of unhydrated cement may remain after the hydration process is completed, If the conditions are assumed to be constant during the entire hydration process, the hydration degree can be expressed by the ratio of the evolved heat at a certain time and the total heat develop at complete hydration. Similarly, the hydration degree can also be expressed by means of cement relative strength, which is much easier to control, see Neville (2002).

The chemical reaction between water and cement that occurs during the hydration process release heat and consume water, an exothermic process. The main cement compounds that reacts in the hydration process is C_3A (tricalcium aluminate), C_3S (tricalcium silicate) and C_2S (dicalcium silicate). The reaction process of C_3A can be divided into three different stages. Firstly occurs a hydration on the surface, which happens during the first one to two hours and the rate of evaluation of heat is very high. The secondly hydration happens around the tenth hour after casting, the diffusion through the pores is an important factor. A third reaction can occur after approximately 30 hours due to a regeneration of the C_3A :s. The rate of hydration decreases along the three different stages of C_3A hydration, see Neville (2002). The chemical reactions 2.2a-c illustrates the chemical reaction formula between C_3S , C_2S and C_3A with water.



The cement silicate C_3S is most important for the strength development of young concrete and C_2S is most important for hardened concrete. The chemical reaction results in carbonation shrinkage due to reduction of the original volumes, which leads to self-desiccation of the concrete, see Chapter 2.1.2 for more information about carbonation shrinkage, see Neville (2002). The hydration process is relative complex and depends of many different parameters, therefore a deeper explanation of the reaction process between water and cement will be out of the scope of this thesis.

2.1.2.2 Development of hydration heat

The total developed heat energy, Q_C , produced when hydration heat releases due to chemical reaction between water and cement, is assumed to be proportional to the cement content and to the final hydration degree of the cement, see Equation 2.3. Thus the more cement hydrates, the more heat is produced, see Engström (2011).

$$Q_C = \alpha_u \cdot q_u \cdot C \quad (2.3)$$

Where Q_C = Total developed heat energy [J/m³]

α_u = Final hydration degree [-]

q_u = Hydration heat degree after complete hydration
[J/kg cement]

C = Cement content [kg cement/m³]

In the production of high performance concrete mineral additives such as silica fume, blast furnace slag and fly ash is used to increase the properties of the concrete. By replacing cement with pozzolanic material (fly ash, blast furnace slag etc.) the hydration heat can be significantly reduced. High strength concrete contains high cement content and low water cement ratio. Consequently, the hydration degree is less than in ordinary concrete, see Ji (2008).

As already mentioned, the hydration process produces hydration heat, which increase the temperature of the concrete mass. According to Engström (2011) leads this temperature increase to an acceleration of the hydration process, i.e. the speed in which the cement is hydrated, $\frac{d\alpha}{dt}$, see Equation 2.4.

$$\frac{d\alpha}{dt} = a_0 \cdot \beta_T \cdot \beta_{RH} \cdot \beta_{add} \quad (2.4)$$

Where a_0 = Hydration rate for specific type of cement under reference condition [-]

β_T = Factor that considers temperature [-]

β_{RH} = Factor that considers relative humidity in concrete [-]

β_{add} = Factor that considers the effect of additives [-]. If $\beta_{add} > 1$ results in acceleration otherwise retardation.

The hydration process ceases if the relative humidity decreases below 75% - 80%, see Engström (2011).

Hydration heat can be determined in two different ways, by an adiabatic- or semi-adiabatic calorimeter test. The two different test methods works in similar manner. A concrete sample is cast into a box immediately after mixing. Thereafter the box is closed and the development of the temperature in the concrete sample is recorded by induced temperature sensors linked to a computer. The difference between an adiabatic- and a semi-adiabatic calorimeter test is the amount of isolation around the box. In an adiabatic calorimeter test, no heat is allowed to be transported from the box. All the heat produced by the hydration is assumed to be kept inside the box, due to sufficient isolation. However, if heat transport between the concrete and the surrounding

is allowed, a semi-adiabatic calorimeter test is performed, see Figure 2.4 for illustration of results from the different calorimeter test. The total heat evolution is defined as the sum of the heat corresponding to the temperature increase and the heat loss to the surrounding due to the insufficient insulation. The heat flux from the box is assumed to be proportional to the temperature difference between the concrete sample and the ambient air, see Ji (2008).

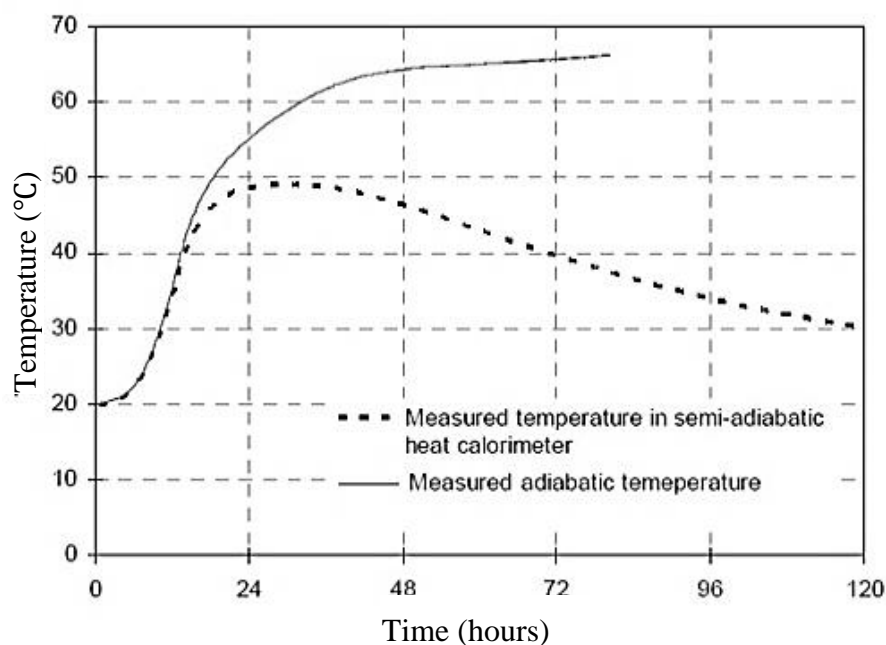


Figure 2.4 Illustration of typical curves from adiabatic- and semi-adiabatic heat calorimeter test, modified from Ji (2008).

According to Tanabe (1986), the adiabatic temperature, T_{adiab} , from the heat of hydration can be calculated as

$$T_{adiab} = T_c + K \cdot (1 - e^{-\alpha_{adia} \cdot t}) \quad (2.5)$$

- Where
- T_c = Initial temperature of the concrete/curing temperature [°C]
 - K = Constant depending on casting temperature and cement content, see Figure 2.5 [°C]
 - α_{adia} = Constant depending on casting temperature and cement content, see Figure 2.5 [-]
 - t = Time [hours]

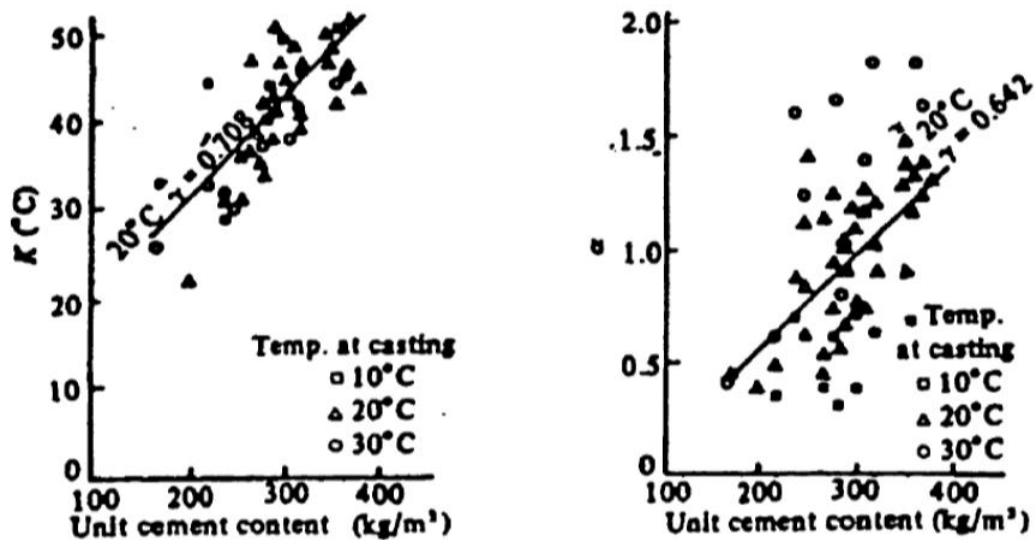


Figure 2.5 K and α_{adia} values of adiabatic temperature rise, from Tanabe (1986).

Regarding the semi-adiabatic case, the temperature development can be divided into different periods, heating and cooling, see Figure 2.6. For adiabatic conditions, there is only a heating period.

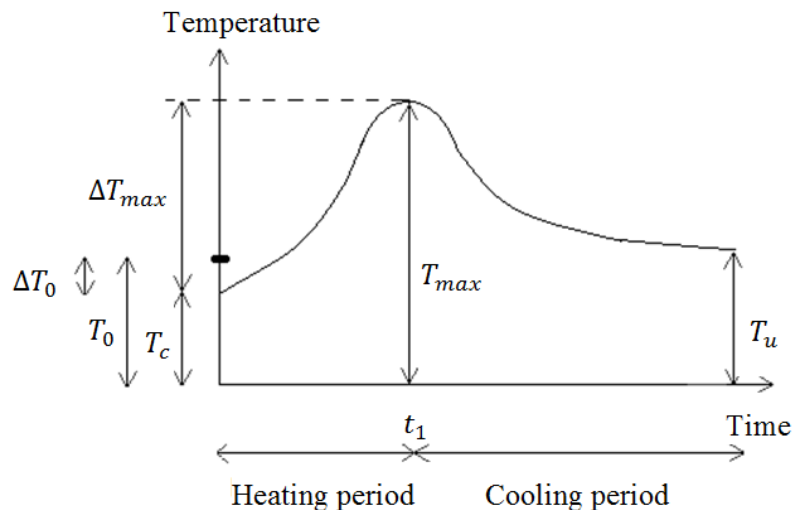


Figure 2.6 Temperatures versus time during the hydration process, where T_0 is the temperature of the surrounding and ΔT_0 is the temperature difference between the young concrete and surroundings when casting starts. See Equation 2.5 for explanations of the other variables, modified from Engström (2011).

According to Eurocode 2, the maximum temperature increase, ΔT_{max} , depends on the curing temperature, T_c , and the maximum temperature, T_{max} , that appears during the hydration, see Equation 2.6. Figure 2.6 explains the different temperature variables included in Equation 2.6 over time.

$$\Delta T_{max} = T_{max} - T_c \quad (2.6)$$

Where T_{max} = Maximum temperature [°C]

T_c = $T_0 - \Delta T_0$, Curing temperature [°C]

Heating period

During the heating period, the temperature increases due to hydration heat which results in expansion of especially the cement paste. The coefficient of thermal expansion, CTE, of hardened cement paste can vary between 10 and 20 $\mu / ^\circ\text{C}$, see Domone & Illston (2010). The variation depends mainly on the moisture content.

The CTE of common concrete aggregates, for example granite, varies between 6 and 10 $\mu / ^\circ\text{C}$, see Domone & Illston (2010), which is less than the value for cement paste. In contrast to the CTE of the cement paste, the CTE for the aggregates is independent of the concrete age. Consequently, CTE of the cement paste governs the overall expansion of the young concrete mixture during curing process, see McCullough (1998). In Eurocode 2, the CTE of concrete is recommended to 10 $\mu / ^\circ\text{C}$ independent of aggregate type.

The CTE of the cement depends on several factors such as fineness, age, moisture content and the chemical composition of the cement. Figure 2.7 shows the CTE of Portland cement depended of curing age. The CTE of the Portland cement is very high after only a few hours after casting, maximum 170 $\mu / ^\circ\text{C}$, then decreases the value rapidly and stabilizes around 20 $\mu / ^\circ\text{C}$ after approximately 30 hours.

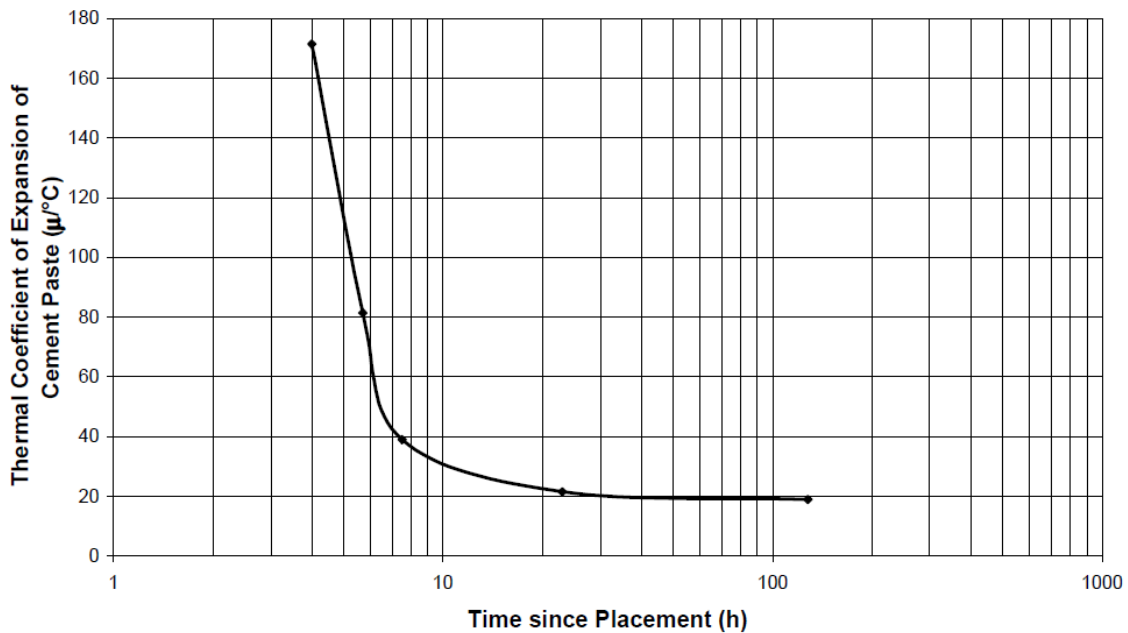


Figure 2.7 The coefficient of thermal expansion, CTE, of Portland cement depended of age after curing, from McCullough (1998).

According to McCullough (1998) the CTE of hardened cement paste can be estimated from a weighted average of the aggregate- and cement volumes and an approximation of the CTE as a function of age is made, see Equation 2.7.

$$\alpha_{conc} = C_m \cdot \left[\sum_{i=1}^{\# \text{ of aggs}} (\alpha_{agg,i} \cdot \frac{V_{agg,i}}{V_{conc}}) + \alpha_{paste} \cdot \frac{V_{agg,i}}{V_{conc}} \right] \quad (2.7)$$

Where α_{conc} = Weighted average of the aggregate- and cement volume for the CTE value of young concrete [$\mu / ^\circ\text{C}$]

C_m = Moisture correction factor, derived from Figure 2.8

$$\begin{aligned}\alpha_{agg,i} &= \text{CTE of } i^{\text{th}} \text{ aggregate } [\mu/\text{°C}] \\ \alpha_{paste} &= \text{CTE of } i^{\text{th}} \text{ cement paste } [\mu/\text{°C}] \\ V_{agg,i} &= \text{Volume of aggregate in the mixture } [\text{m}^3] \\ V_{paste} &= \text{Volume of cement paste in the mixture } [\text{m}^3] \\ V_{conc} &= \text{Total volume of concrete in the mixture } [\text{m}^3]\end{aligned}$$

As Figure 2.8 illustrates the CTE for saturated concrete is largest in intermediate relative humidities (around 60-80 %), see McCullough (1998).

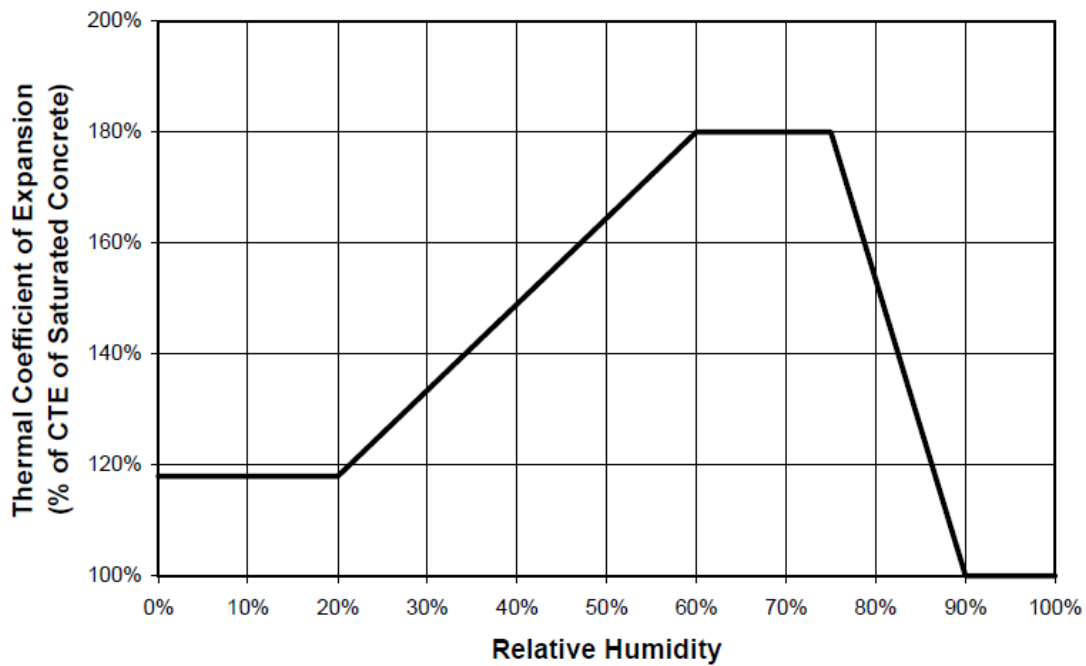


Figure 2.8 Relative humidity dependence of the coefficient of thermal expansion of saturated concrete, see McCullough (1994).

Cooling period

After the maximum temperature, T_{max} , is reached, the cooling period starts, see Figure 2.6. The coefficient of thermal contraction, CTC, varies depending on cement type and water/cement ratio, but is normally around $8 \mu/\text{°C}$, see Engström (2012).

2.1.2.3 Maturity concept

The speed in which chemical reactions occurs can also be expressed with the Arrhenius function, where the derivation of the degree of hydration depending on time is expressed as an exponential function, called age conversion factor, γ , see Equation 2.8.

$$\gamma = A \cdot e^{\frac{E_a}{R} \left(\frac{1}{T_{ref}} - \frac{1}{T} \right)} \quad (2.8)$$

Where A = Frequency factor [J/mol]
 E_a = Apparent activation energy [J/mol]
 R = Universal gas constant, 8.314 J/mol·K
 T_{ref} = Reference temperature, usually set to 20°C / 293 K
 T = Actual temperature at a specific time [°C/K]

The frequency factor, a proportionality constant, describes the frequency of collision and the probability that the molecules are favourable oriented for reaction. The activation energy was invented by Svante Arrhenius to explain why chemical reactions do not occur instantaneously when reactants was put together. The activation energy can be defined as the energy needed to overcome an energy barrier so the reactants in the cement hydration start to react, see Carino (2001).

The term maturity is used to be able to translate a curing with another temperature than the reference temperature at 20°C. Maturity is defined as the equivalent time the concrete has been hardening, see Øverli (2002). The equivalent curing age is the time the cement has to cure to achieve the same degree of hydration as the actual temperature and time. The equivalent curing age can be calculated by knowledge about a temperature sensitivity association, see Carino (2001).

Freiesleben, Hansen and Pedersen invented a new equivalent function, to calculate a maturity index from the temperature history of the concrete. This function was based on the Arrhenius equation, which describes the effect of temperature on the rate of a chemical reaction. The new function allowed the calculation of the equivalent age, t_e , of concrete as

$$t_e = \sum_0^t \gamma \Delta t = \sum_0^t A \cdot e^{\frac{E_a}{R} \left(\frac{1}{T_{ref}} - \frac{1}{T} \right)} \Delta t \quad (2.9)$$

Where γ is the age conversion factor, explained in Equation 2.8 and T is the actual temperature at a specific time [°C/K], see Carino (2001).

According to McCullough (1998), the degree of hydration, ψ , can also be defined as

$$\psi = e^{-\lambda_1 \cdot (\ln \tau)^{\kappa_1}} \quad (2.10)$$

Where τ = Age parameter, defined as: $1 + \left(\frac{t_e}{t_1} \right)$, t_e can be obtained in Equation 2.8.

λ_1, κ_1, t_1 = Hydration shape and time factors, see Table 2.1

The degree of hydration varies between 0-1.0.

Table 2.1 Thermal material parameters for different cement types, adopted from McCullough (1998).

Cement type	Total heat of hydration, Q [J/g]	Activation energy, E _a , [J/mol]	Hydration parameter, λ ₁	Hydration parameter, t ₁	Hydration parameter, ter, κ ₁
CEM I	460	41750	2.42	2.12	0.85
CEM IP	410	41715	2.42	2.12	0.85
CEM II	406	39050	3.16	2.06	1.07
CEM III	468	44150	3.52	1.1	0.97
CEM V	373	36350	3.90	2.0	1.29

2.1.2.4 Temperature effects

Temperature effects are important phenomena and influences the behaviour of young concrete structures. Changes in temperature can produce stresses in concrete structures, but only if thermal expansion or contraction is restrained. As been mentioned, hydration of cement generates heat during the hardening process due to chemical reaction. If the removal of re-radiation and convection is smaller than the heat created by the hydration, a significant rise of temperature takes place in especially thick concrete members. The temperature gradient between the interior part and the surface is larger for thicker concrete members, see Gahli (2002).

Heat can either be transferred by radiation, irradiation, conduction or convection, see Figure 2.9 for an illustration of the different heat transfer phenomena. The three-dimensional heat transfer equation based on Fourier's law is expressed as

$$k \frac{\partial^2 T}{\partial x^2} + k \frac{\partial^2 T}{\partial y^2} + k \frac{\partial^2 T}{\partial z^2} + Q = \rho \cdot C_p \frac{\partial T}{\partial t} \quad (2.11)$$

- Where
- k = Thermal conductivity coefficient [W/m°C]
 - T = Temperature at any point (x,y) at any time [°C]
 - Q = Amount of hydrated heat generated within the body [W/m³]
 - ρ = Density [kg/m³]
 - C_p = Specific heat capacity [J/kg°C]

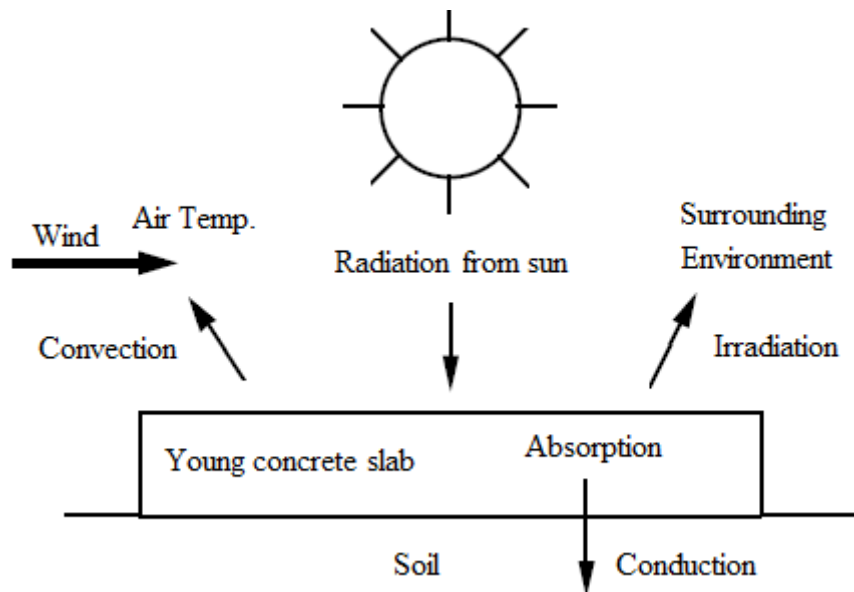


Figure 2.9 Illustrations of different phenomena of heat transfer in a young concrete slab, modified from McCullough (1998).

Specific heat capacity, C_p , is the quantity of heat required to increase the temperature of the unit mass of the material by one degree, see Gahli (2002). It is considered to be important relative to the temperature change of the young concrete material. The aggregate, both in content and type, affect the specific heat capacity and it is also dependent on the temperature of the cement paste. Equation 2.12 shows furthermore that C_p is a function of the degree of hydration, see McCullough (1998).

$$C_p = C_{p\infty} \cdot (1,25 - 0,25\psi) \quad (2.12)$$

Where $C_{p\infty}$ = Specific heat capacity of mature concrete [J/kg°C]

ψ = Degree of hydration, see Equation 2.8.

Specific heat capacity of mature concrete, $C_{p\infty}$, can generally be set to between 0,8-1,0 kJ/kg°C, it is lower than the value for the fresh concrete which normally can be set between 1,0-1,1 kJ/kg°C. The variations on the parameters depends on the concrete type, see Ljungkrantz (1994). Figure 2.10 illustrates the linearly variation of the specific heat capacity depending on the degree of hydration. Equation 2.10 is used for the calculation on the specific heat capacity. The specific heat capacity of mature concrete is assumed to be 1,0 kJ/kg°C in Figure 2.10.

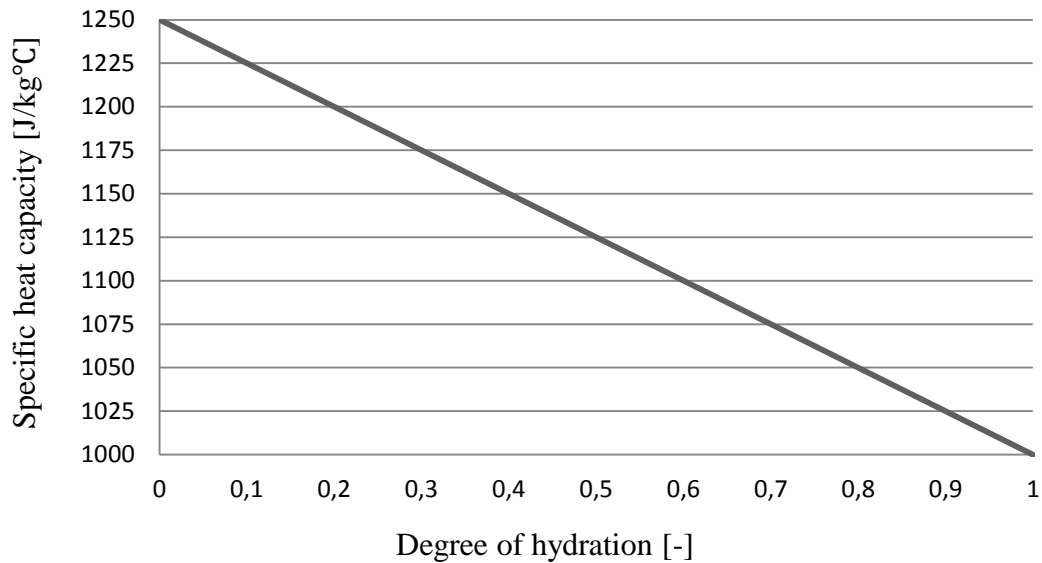


Figure 2.10 Variation of the specific heat capacity, C_p , with the degree of hydration, ψ , the specific heat capacity of mature concrete is set to $1 \text{ kJ}/\text{kg}^\circ\text{C}$.

Thermal heat capacity is the quantity of heat required to increase the temperature of one cubic meter of a specific material by one degree. It consist of a product of the density, ρ , and the specific heat capacity, C_p , and has the unit $[\text{J}/\text{m}^3^\circ\text{C}]$, see Nevander (2006). The thermal heat capacity varies normally between $2,3\text{-}2,6 \text{ MJ}/\text{m}^3^\circ\text{C}$ for young concrete, depending on the density of the young concrete.

If the thermal conductivity coefficient, defined below, is divided with the thermal capacity the thermal diffusivity is obtained. Thermal diffusivity is defined as the time dependent penetration depth in a specific material and has the unit $[\text{m}^2/\text{s}]$, see Nevander (2006).

Irradiation

Radiation is the transfer of energy to or from a body by means of the emission or absorption of electromagnetic radiation. The amount of irradiation from a concrete surface to the ambient air can be calculated by Stefan-Boltzmann law, see Equation 2.13.

$$q_r = h_r(T - T_a) \quad (2.13)$$

Where h_r = Irradiation heat transfer coefficient $[\text{W}/\text{m}^2^\circ\text{C}]$

T = Temperature of the surface $[\text{°C}]$

T_a = Temperature of the surrounding air $[\text{°C}]$

The irradiation heat transfer coefficient depends on Stefan-Boltzmann constant and emissivity of the surface, see Gahli (2002). The surface emissivity is highly affected of the surface colour, an ideal black-body has a value of 1. Concrete has a emissivity coefficient between $0,8\text{-}0,9$, see McCullough (1998). According to Ghali (2002) the irradiation heat transfer coefficient, h_r , can be given by

$$h_r = \sigma \cdot \varepsilon \cdot ((T + 273)^2 + (T_a + 273)^2) \cdot (T + T_a + 546) \quad (2.14)$$

- Where h_r = Irradiation heat transfer coefficient [W/m²°C]
 T = Temperature of the surface [°C]
 T_a = Temperature of the surrounding air [°C]
 σ = Stefan-Boltzmann constant, 5.67×10^{-8} [W/m²K⁴]
 ε = Coefficient of emissivity of the surface [-]

Figure 2.11 shows different values of the irradiation heat coefficient of concrete dependent of ambient air temperatures, Temperature of the surface and coefficient of emissivity from concrete surface. The emissivity coefficient of the concrete surface is assumed to be constant 0,85.

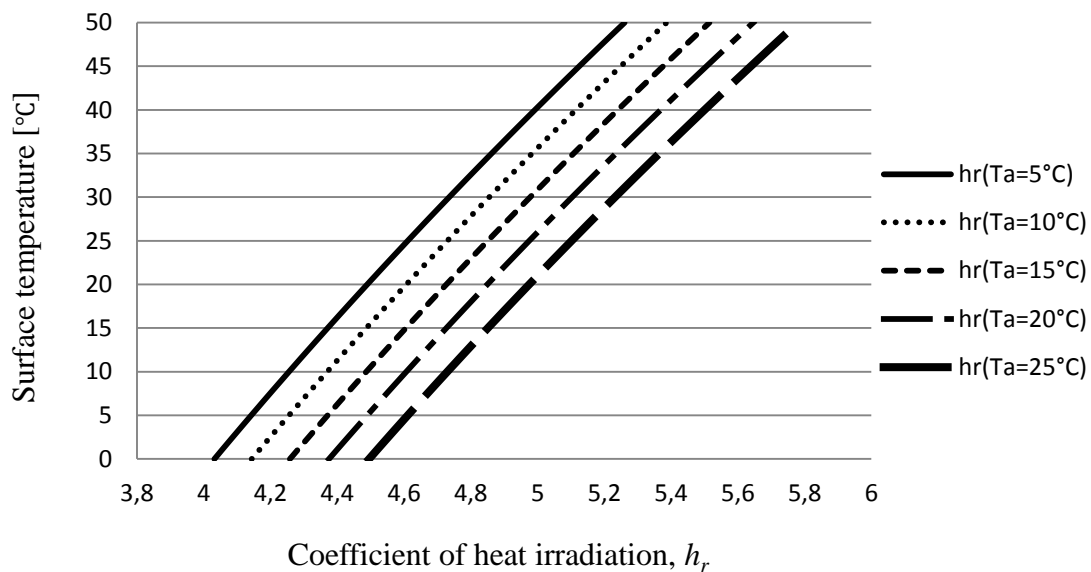


Figure 2.11 Variation of irradiation heat transfer coefficient, h_r , dependent of concrete surface temperature and ambient air temperature, T_a . The emissivity coefficient of the concrete surface is set to constant 0,85.

Conduction

Heat conduction can be defined as the transfer of energy in an object or between objects that are in physical contacts. Transfer of energy from a specific area is a common term of conduction, named heat flux, q , see Equation 2.15 for the one-dimension form of Fourier's law. Heat flux flows from media with high temperature to media with lower temperature, see Lienhard (2011).

$$q = -k \frac{\partial T}{\partial x} \quad (2.15)$$

- Where k = Thermal conductivity coefficient [W/m°C]
 $\frac{\partial T}{\partial x}$ = Temperature gradient [°C]
 q = Heat flux [W/m]

The thermal conductivity coefficient, k , is an important thermal material property in young concrete, it is defined as the rate of heat flow through a known thickness of a

specific material between two phases of uniform areas which are exposed to a large temperature difference. The thermal conductivity coefficient of the cement paste is generally not affected by the temperature increase under normal ranges of curing. However, it is significantly affected by moisture content, an increase in moisture content within the cement results in an increase in thermal conductivity, see McCullough (1998). It has been proved to be a function of the degree of hydration at early ages, see Equation 2.16 below.

$$k = k_{\infty} \cdot (2 - \psi) \quad (2.16)$$

Where k = Thermal conductivity coefficient [W/m°C]
 k_{∞} = Thermal conductivity coefficient of mature concrete [W/m°C]
 ψ = Degree of hydration, see Equation 2.10.

The thermal conductivity coefficient of mature concrete, k_{∞} , can generally be set to 1,2 W/m°C, see Nevander (1994). But it varies a bit depending on the concrete type. The variation of the thermal conductivity coefficient depending on the degree of hydration varies linearly from two times the k_{∞} (around 2,4 W/m°C) to k_{∞} , according to Equation 2.16.

Convection

Convection is the transfer of energy between an objects surface and its environment, due to fluid motion. Newton's second law of cooling gives the amount of heat transfer by convection, q_c , see Equation 2.17.

$$q_c = h_c(T - T_a) \quad (2.17)$$

Where h_c = Convection heat transfer coefficient [W/m²°C]
 T = Temperature of the surface [°C]
 T_a = Temperature of the surrounding air [°C]

The convection heat transfer coefficient can be separated in forced and natural convection. Forced convection is when wind occurs at the surface and can be calculated in two different ways depending of the amount of wind speed, see Equation 2.18a-b and Figure 2.12.

$$h_c = 6 + 4 \cdot u \quad u \leq 5 \text{ m/s} \quad (2.17a)$$

$$h_c = 7,4 \cdot u^{0,78} \quad u > 5 \text{ m/s} \quad (2.17b)$$

Where u = Wind speed [m/s]

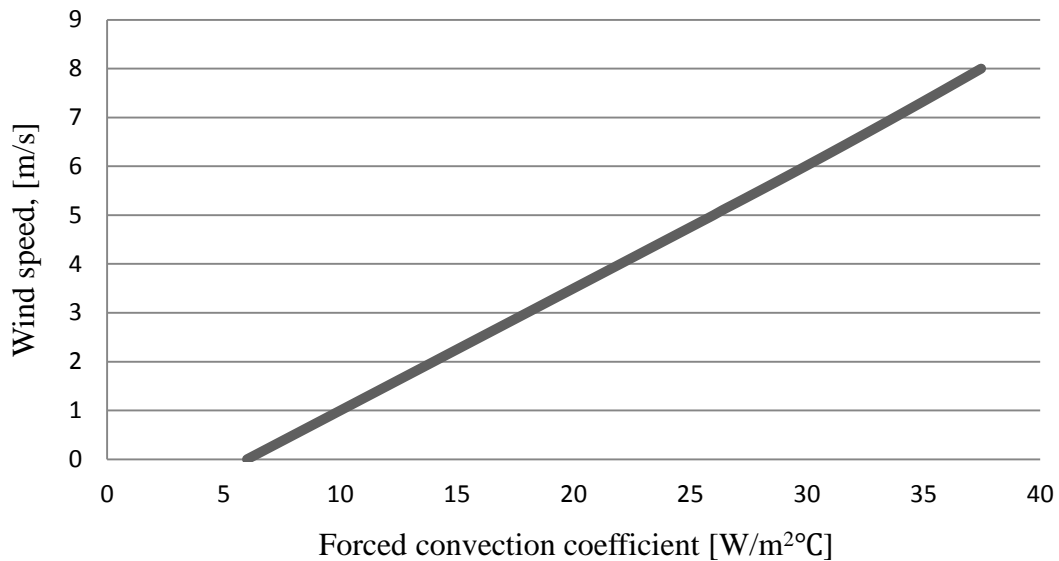


Figure 2.12 Variation of the forced convection coefficient dependent of wind speed.

Natural convection depends on air current that arise due to temperature differences between air and surface, dT , see Figure 2.13. The momentum is the density difference between colder and warmer air, warm air tends always to transition to colder areas, Nevander (2006). The natural convection can be calculated as

$$h_c = C_{const} \cdot dT^{0,25} \quad (2.19)$$

Where C_{const} = Coefficient with recommend value around 2
 dT = Temperature difference between air and surface [°C/K]

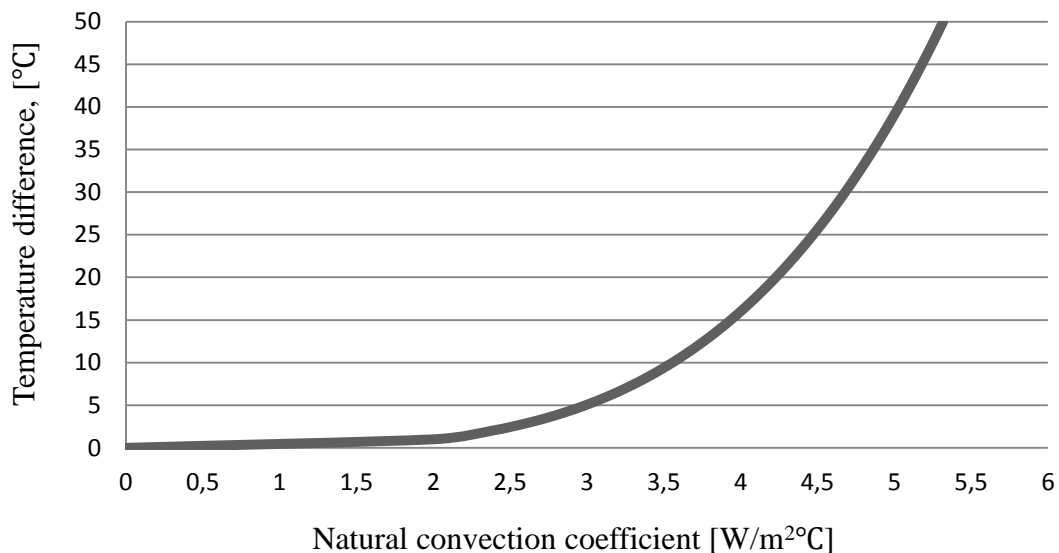


Figure 2.13 Variation of natural convection coefficient dependent of temperature difference between concrete surface and the ambient air.

Heat flow by convection and irradiation can be expressed by one combined expression, $q = q_c + q_r$, see q in Equation 2.14. The same applies for the convection heat

transfer coefficient and the irradiation heat transfer coefficient which can be expressed as $h = h_c + h_r$.

The convection heat transfer coefficient, h_c , depends mainly on wind speed and some degree of surface conditions and type of material, see Ghali (2002). Regarding concrete structures, it is also a function of different curing methods used during the concrete hardening process, which is used to minimize excess moisture-loss through evaporation. Common curing methods are liquid membrane, polyethylene sheeting and cotton mats. Liquid membrane is often wax-based, which is applied at the concrete surface. Curing with polyethylene sheeting is very beneficial in retaining moisture if it is used properly. The sheeting prevents the moisture to evaporate, instead it remains near the concrete surface. The behaviour and advantages with cotton mats is similar to polyethylene sheeting, the difference is that the cotton mats is wetted and thus provide free moisture instead of almost completely block it, see McCullough (1998). Table 2.2 shows the heat transfer coefficient as a function of the different curing methods.

Table 2.2 Expression of convective heat transfer coefficient for different curing methods as a function of the wind speed, w , in miles/hour.

Curing method	Convective heat transfer coefficient, h_c
None or liquid membrane	$-0,0022 \cdot w^2 + 0,6522 \cdot w + 1,9521$
Polyethylene sheeting (tarpaulin)	$-0,0072 \cdot w^2 + 0,4152 \cdot w + 1,8526$
Cotton mat	$0,223 \cdot \ln(w) + 1,1132$

Figure 2.14 shows the convection heat transfer coefficient for polyethylene sheeting, which was applied during the concrete curing in all the plants.

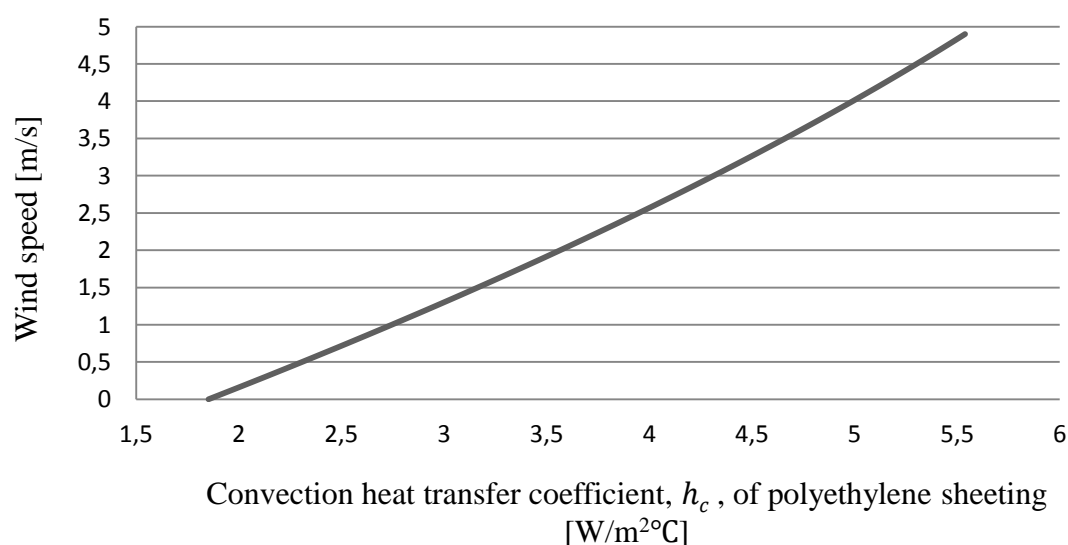


Figure 2.14 Convection heat transfer coefficient for Polyethylene sheeting, calculated according to the equation in Table 2.2.

2.1.3 Mechanical properties of young concrete

Some of the most important mechanical properties of young concrete are strength development (modulus of elasticity, tensile strength and compressive strength) and viscoelastic behaviour (creep and shrinkage of young concrete due to temperature effects, see Lundgren (2005)).

2.1.3.1 Strength development of young concrete

During the first hours up to some days after the casting the development of the mechanical properties is most obvious and fastest. At early age, the modulus of elasticity develops at highest rate and the compressive strength develops at lowest rate. Temperature of the surrounding is shown to have significant effect on the strength development. The rate of the strength development decreases if the surrounding temperature is cold and increases if it is warmer see Lundgren (2005). In what magnitude the elevated temperatures affect the mechanical properties of concrete depends on the concrete composition, moisture conditions and the drying conditions of the concrete, see Ji (2008).

The strength development of young concrete depends mainly on the hydration process, which in turn depends on time, temperature and type of concrete. Different codes calculate the variation of the mechanical properties during the hydration of concrete in different ways. According to Eurocode 2, the variation of the mean modulus of elasticity with time ($E_{cm}(t)$) is calculated as

$$E_{cm}(t) = \left(\frac{f_{cm}(t)}{f_{cm}}\right)^{0,3} \cdot E_{cm} \quad (2.20)$$

Where f_{cm} = Mean compressive strength [MPa]
 E_{cm} = $22 \cdot (f_{cm}/10)^{0,3}$, modulus of elasticity [GPa]
 $f_{cm}(t)$ = Mean compressive strength at time t [MPa]

According to the modified version of CEB-FIB Model Code 1990 the modulus of elasticity, E_c , tensile strength, f_t , and compressive strength, f_c , is calculated with an equivalent time, t_e , see equation 2.21a-c.

$$E_c(t_e) = E_c(28) \cdot \exp \left[s \cdot \left(1 - \sqrt{\frac{28}{t_e - t_0}} \right) \right]^{n_E} \quad (2.21a)$$

$$f_t(t_e) = f_t(28) \cdot \exp \left[s \cdot \left(1 - \sqrt{\frac{28}{t_e - t_0}} \right) \right]^{n_t} \quad (2.21b)$$

$$f_c(t_e) = f_c(28) \cdot \exp \left[s \cdot \left(1 - \sqrt{\frac{28}{t_e - t_0}} \right) \right] \quad (2.21c)$$

Where the $E_c(28)$, $f_t(28)$, $f_c(28)$ are the strength after 28 days, s , n_E , n_t are the model parameters and describes the age dependence. The equivalent age, t_e , takes account for the temperature history and t_0 is the age at where significant mechanical properties starts to develop, see Øverli (2002).

The variation of the E-modulus can also be calculated according to Reinhardt Model from DIANA (2008) as

$$E(t) = E_{cm} \cdot \int_0^t \gamma(\tau) \cdot \dot{\tau}(\tau) \cdot \left(1 - e^{-\beta_0 \frac{t-\tau}{\alpha(\tau)}}\right) d\tau \quad (2.22a)$$

$$\text{with } \gamma(\tau) = \left(\frac{T_0 - T(t)}{273}\right)^7 \quad \text{and} \quad \alpha(t) = \left(\frac{T_0 - T(t)}{273}\right)^6 \quad (2.22b)$$

Where T_0 = Temperature factor considering in which unit the temperature is given, if $T(t)$ is inserted in degree then is $T_0 = 0$ and other way around is $T_0 = 273$ if kelvin is used [°C/K]

E_{cm} = Stiffness modulus [GPa]

β_0 = First model parameter, recommended 0,075 [-]

τ, t = Time factors [s]

Another important mechanical property for young concrete is the Poisson's ratio, ν , it can be defined as the ratio between lateral and longitudinal strength when a uniaxial load is applied on a specific concrete specimen. It is included in Hooke's law equation for plain stress assumption and can be defined in Equation 2.23, see Mase (2000).

$$\begin{bmatrix} \sigma_{xx} \\ \sigma_{yy} \\ \sigma_{xy} \end{bmatrix} = \frac{E}{1-\nu^2} \cdot \begin{bmatrix} 1 & \nu & 0 \\ \nu & 1 & 0 \\ 0 & 0 & 1-\nu \end{bmatrix} \cdot \begin{bmatrix} \varepsilon_{xx} \\ \varepsilon_{yy} \\ \varepsilon_{xy} \end{bmatrix} \quad (2.23)$$

Where E = Young's modulus of elasticity [GPa]

ν = Poisson's ratio [-]

ε = Strains [-]

σ = Stresses [MPa]

Generally the value of Poisson's ratio for concrete is in the range between 0,17 and 0,2, see Neville (2002). According to Oluokun (1991) the Poisson's ratio for early age concrete is relatively constant during all stages of curing and may be set to approximately 0,18, while the Young's modulus should vary with time.

2.1.3.2 Shrinkage of young concrete

According to Eurocode 2 the shrinkage strain is composed of two main components, the autogenous shrinkage strain and the drying shrinkage strain. The autogenous shrinkage strain is basically a linear function of the concrete strength and develops during hardening of the concrete (major parts develops in the first days after casting). The drying shrinkage strain progresses slowly as it depends on the transport of water from the concrete even after hydration has been achieved. Read more about the different shrinkage types in the following subchapters. The value of total shrinkage strain at a certain concrete age t , can be determined as

$$\varepsilon_{cs}(t) = \varepsilon_{ca}(t) \cdot \varepsilon_{cd}(t) \quad (2.24)$$

Where $\varepsilon_{ca}(t) =$ Autogenous shrinkage strain [-]
 $\varepsilon_{cd}(t) =$ Drying shrinkage strain [-]

Plastic shrinkage

Plastic shrinkage occurs at an early stage of the concrete hardening process before any strength of the concrete has developed. The fresh cast concrete surface loses its moisture by evaporation and starts to dry out, which can result in cracking on the concrete surface (plastic-shrinkage cracking). Surface drying initiates when the evaporation rate exceeds the bleeding rate, see ACI Committee (1999). Bleeding is a phenomenon where some of the water tends to rise upwards (almost freely water transport) within the recently casted concrete to the exposed surface, see Neville (2003). The rate of bleeding depends on the concrete type, depth of concrete, consolidation and after-treatments. The evaporation of the surface water on the other hand depends on environmental factors. It increases with high concrete temperature, high wind speed and low humidity, see ACI Committee (1999).

Autogenous shrinkage

When no moisture movement is permitted in a concrete specimen, shrinkage due to self-desiccation takes place. This shrinkage is called autogenous shrinkage and occurs in the interior of a concrete mass. Autogenous shrinkage is three-dimensional and increases at higher temperatures, higher cement content and with cement contains of high tricalcium silicate (C_3A) and high tetracalcium aluminoferrite (C_4AF). But constant bleeding and higher content of fly ash decreases the autogenous shrinkage, see Neville (2003). High strength concrete with low water/cement ratio is prone to significant autogenous shrinkage Ji (2008). The autogenous shrinkage strain can be expressed as in Equation 2.25, see CEN (2004).

$$\varepsilon_{ca}(t) = \beta_{as}(t) \cdot \varepsilon_{ca}(\infty) \quad (2.25)$$

Where $\beta_{as}(t) =$ Time function of autogenous shrinkage [-]
 $\varepsilon_{ca}(\infty) =$ Final value of autogenous shrinkage [-]

Drying shrinkage

Drying shrinkage occurs after the concrete has gathered its final set and a large part of the cement gel has been hydrated. The definition of drying shrinkage is when a concrete element decreases in volume due to moisture losses by evaporation. The reason for drying shrinkage is because greater amount of water is used than the hydration process requires, due to the need of good workability during casting for example. Swelling means increasing of volume by water absorption and is the opposite of drying shrinkage. Factors that increase the degree of drying shrinkage are for example: Low aggregate content, higher water/cement ratio, less size of the concrete element, low relative humidity, high content of admixtures etc., see Nawy (2000). The development of drying shrinkage strain with time can be seen in Equation 2.26 see CEN (2004).

$$\varepsilon_{cd}(t) = \beta_{ds}(t, t_s) \cdot k_h \cdot \varepsilon_{cd,0} \quad (2.26)$$

Where $\beta_{as}(t, t_s)$ = Time function of drying shrinkage [-]
 k_h = Coefficient that depends on size of the cross-section [-]
 $\varepsilon_{cd,0}$ = Basic value of drying shrinkage depending on relative humidity, concrete strength class and type of cement [-]

According to Eurocode 2 develops the shrinkage strain slowly, since it is a function of the migration of the water through the hardening concrete. Therefore it should not be included considering during the hydration process of young concrete.

Carbonation shrinkage

Carbonation shrinkage occurs on exposed concrete surfaces due to carbonation. Some of the experimental data made on drying shrinkage includes the effect of carbonation shrinkage. Carbonation of concrete takes place when the air containing carbon dioxide (CO₂), in presence of moisture, reacts with the hydrated cement. Due to the carbon dioxide being fixed by the hydrated cement paste, the concrete mass increases as a result of increasing of the hydrated cement paste. But the volume of the reactants decreases compared to the volume of the product, due to water consuming. At intermediate humidities (between 25 and 100 per cent) carbonation has its greatest effect and increases the shrinkage. The sequence of drying and carbonation is an important factor which affects the total shrinkage. Simultaneous drying and carbonation gives lower total shrinkage than shrinkage due to drying and subsequent carbonation, see Figure 2.15. The effect of the carbonation is that the pH of the pore water reduces, which can cause corrosion of the embedded reinforced steel, see Neville (2002).

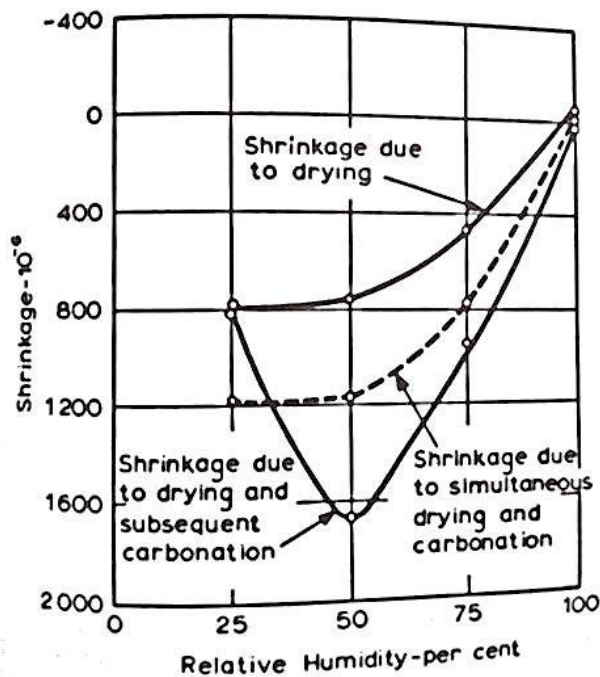


Figure 2.15 Influence of the sequence of drying and carbonation gives different shrinkage at different humidities, from Neville (2002).

2.1.3.3 Thermal deformation

A need for thermal deformation occurs in young concrete subjected to temperature changes. As explained in Chapter 2.1.2.2 two different types of deformations are either thermal expansion, during heating period, or thermal contraction, during cooling period.

Thermal expansion

Thermal expansion is used to calculate strains due to increasing of thermal gradients under the heating period, e.g. from heat of hydration, explained in Chapter 2.1.2.2. Equation 2.27 illustrates the stress-independent strain, ε_{cTe} , due to temperature increase. Stress-independent strain occurs in concrete structures without any restraint and results in free deformation without stresses, see Engström (2011). Restraint is defined in a subchapter below.

$$\varepsilon_{cTe} = \alpha_{cTe} \cdot \Delta T_{max} \quad (2.27)$$

Where ε_{cTe} = Stress-independent strain (no restraint) [-]
 α_{cTe} = Coefficient of thermal expansion, CTE, of young concrete during the heating period
 ΔT_{max} = Maximum temperature increase [°C], see Equation 2.27

Thermal contraction

During the cooling period, after the maximum temperature, T_{max} , is reached, the concrete structure gets a need of thermal contraction. The stress-independent strain, ε_{cTc} , due to temperature decrease is expressed as

$$\varepsilon_{cTc} = \alpha_{cTc} \cdot (T_{max} - T_u) \quad (2.28)$$

Where T_u = Final temperature after cooling [°C]
 T_{max} = Maximal temperature [°C]
 α_{cTc} = Coefficient of thermal contraction of hardening concrete during the cooling period

Restraints

Restraint is a phenomenon that somehow prevents a structure to move freely. The restraint degree expresses the ratio between imposed strain, which is equal to the stress-dependent strain, and the strain in case of full restraint, which is equivalent to the stress-independent strain. If the restraint degree is equal to 1, the structure is completely prevented to move freely, i.e. full restraint. In the opposite way, if the restraint degree is 0, the structure is allowed to free movements. If the restraint degree is something between 0-1, it is called partial restraint, see Engström (2011).

If there is no deformation after the heating and cooling period, fully restraint, a remaining concrete stress-independent strain, ε_{cT} , can be calculated as a difference of

the thermal contraction (Equation 2.28) and thermal expansion (Equation 2.27) during the periods, see Equation 2.29.

$$\varepsilon_{cT} = \varepsilon_{cTc} - (1 - k_0) \cdot \varepsilon_{cTe} \quad (2.28)$$

Where $(1 - k_0) \cdot \varepsilon_{cTe}$ = Elastic part of the thermal expansion

Considering partial restraint, the thermal concrete strain, ε_{cT} , dependent on the restraint degree, R , must be in equilibrium with the elastic tensile concrete strain, ε_{ct} , according to Equation 2.30. For a fully restraint structure, the restraint degree is equal to 1 as mentioned above.

$$\varepsilon_{ct} + R \cdot \varepsilon_{cT} = 0 \quad (2.30)$$

Where ε_{cT} = Total concrete stress-independent strain due to temperature (no restraint)

ε_{ct} = Concrete stress-dependent strain (full restraint)

R = Restraint degree [-], see Engström (2011)

Concrete structures can both have external and/or internal restraint, either full or partial restraints, see the definitions below for internal- and external restraint.

When a structure is prevented from moving freely by being attached to its supports or boundaries, external restraint occurs. A structure can be exposed to different types of external restraints by variation of fixation in different supports, resulting in variation of restraint degree in different directions within the structure. The length in relation to the height in a structure is an important factor considering longitudinal movements, the longer the structure is in relation to the height, and the greater the restraint is. This can be reduced by shorter sections with movement joints in between, see Engström (2011).

Internal restraint can be defined as the relation between stress-independent strains in different parts of a structure, because these parts can prevent free deformation of each other's, see Engström (2011).

2.1.3.4 Creep and relaxation of young concrete

Creep of young concrete depends on internal and external factors which vary after casting. The internal factors are related to the material properties of the concrete mixture, while the external factors are type, duration and level of load. The different type of external load can be thermal loads, such as moisture and temperature differences, and mechanical loads consisting of point loads, distributed loads, etc, see Ji (2008).

Time-dependent increasing of strain under a sustained stress is a general definition of creep. The deformation can be divided into an immediate elastic strain and a creep strain, see Figure 2.16. The elastic strain appears first when a load is applied on a concrete specimen and an instantaneous deflection takes place. The creep strain on the other hand increases with time, but converge to a final creep value after long time. If the load is removed for some reason an instantaneous elastic recovery occurs, followed by a creep relaxation over time. The result will be an irreversible creep depending on the loading time, see Engström (2011).

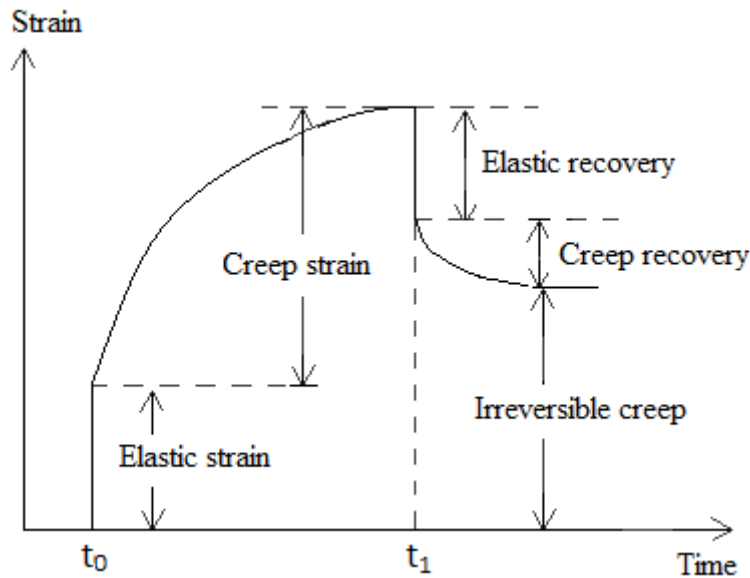


Figure 2.16 Strain-time curve for concrete loaded at time t_0 and unloaded at time t_1 , modified from Ljungkrantz (1994).

Creep strain can be separated into basic creep and a drying creep. Basic creep occurs if the concrete is sealed or if it is no moisture movement to or from the ambient medium. The additional creep caused by drying (drying creep) is when the concrete is allowed to dry out under sustained load. The total creep is the sum of the basic and drying creep.

During the hardening of young concrete, the modulus of elasticity increases with time which results in a gradually decreases of the elastic deformation. To simplify calculations, the modulus of elasticity is often set to a constant value and creep is taken as an increase in strain above the initial elastic strain, see Neville (2002). In Eurocode 2 can the creep coefficient be calculated as

$$\varphi(t, t_0) = \beta_c(t, t_0) \cdot \varphi_0 \quad (2.31)$$

Where $\beta_c(t, t_0)$ = Time function of the creep coefficient considers actual age of concrete, non-adjusted duration of loading, national size of the cross section and the ambient relative humidity [-]

φ_0 = National creep coefficient considers relative humidity, concrete strength and age when the concrete was loaded

Creep occurs in the hardened cement structure around the aggregates. It may be due to slippage along the plane within the crystal lattice, internal stresses caused by changes in the structure or loss of water in the concrete. The main parameter that influence the creep of concrete are the level of stress, duration of load, strength and age of concrete, type of curing, ambient conditions, cement amount, water/cement ratio etc., see Hassoun (2002).

2.2 Prestressing steel

2.2.1 Introduction

Prestressing steel is used in concrete structures in order to obtain higher capacities, which enables longer spans and slimmer structures. The idea to prestress concrete structures is not new, patent was registered containing tensioning of the reinforcing steel in reinforced concrete by the end of the 1800 century. However, due to insufficient knowledge about long term deformations of concrete due to creep and shrinkage, the prestressing effect was lost with time. Another factor that influenced the prestressing effect negatively was the limited strength of the steel.

The French engineer Eugène Freyssinet, also called the “father” of prestressed concrete, studied the behaviour of concrete for many years. He received a patent in 1928 where he pointed out the importance of having high strength prestress steel in order to limit time dependent effect due to concrete creep. At this time high strength steel was available and the prestressing technology started, see Engström (2011).

Prestressed steel can be achieved in two different production ways, pretensioning or post-tensioning. It works as the names point out, pretensioning means that the reinforcement steel is tensioned before the concrete is casted and post-tensioning is when the steel is tensioned after the concrete has hardened. This report only focuses on pretensioned reinforcement steel, because “The Long Line Method” (production method of sleepers at Abetong) uses pretensioning.

2.2.2 Thermal properties of prestressing steel

The most important thermal properties of prestressing steel are the thermal expansion coefficient, specific heat capacity, heat conduction in the steel and heat convection from the steel surface. These properties will vary depending on the type of steel and the steel quality, see Narang (2005).

2.2.2.1 Thermal expansion of prestressed steel

The thermal strain due to expansion of prestressing steel, ε_{psTe} , can be expressed as

$$\varepsilon_{psTe} = \Delta T \cdot \alpha_{psTe} \quad (2.32)$$

- Where
- ε_{psTe} = Prestressed steel stress-independent strain due to temperature expansion [-]
 - ΔT = Total changes in temperature of the prestressed steel [°C]
 - α_{psTe} = Thermal expansion coefficient, CTE, of prestressing steel [μ /°C]

According to Nevander (2006) the CTE for steel is equal to 12μ /°C. But a experimentally test made by Chen (2011) of the thermal expansion coefficient for different prestressed steel structures, showed that the CTE was $18,38 \mu$ /°C, for a strand com-

posed of three steel wires with a diameter of 4,2 mm each. CEB-FIB model (1990) suggest that the coefficient of thermal expansion for prestressed steel should be set to $10 \mu / ^\circ\text{C}$.

Table 2.3 presents different values of the coefficient of thermal expansion for various steel types, in a temperature range from room temperature up to 100°C , see ASM (2002).

Table 2.3 Coefficient of thermal expansion, CTE, for different steel types, temperature range from room temperature up to 100°C . From lowest to highest CTE value, from ASM (2002).

Type of steel	CTE [$\mu / ^\circ\text{C}$]
Structural steel	12
High strength structural steel	9,9-13
Hot work tool steel	8,9-12
Cold work tool steel	11-14
High-carbon high-chromium cold work tool steel	10-12
High strength low-alloy steel (HSLA)	12-13
Austenitic stainless steel	9,8-25
Proprietary alloy steel	9,7-19

Table 2.3 shows that the CTE value can vary between $8,9 - 25 \mu / ^\circ\text{C}$ depending on the steel type. Differences in the CTE value obtained from the different experiments can therefore be explained by the different types of steel which has been used in the tests.

The coefficient of thermal contraction is assumed to be equal as the CTE. It will result in equal deformation but in opposite direction if an arbitrary steel wire firstly expand due to a temperature increase and then decreases due to a temperature decrease of the same size as the temperature increase.

2.2.2.2 Thermal conductivity of steel

Thermal conductivity is the material property that indicates the rate at which heat can flow through an arbitrary material under a temperature gradient. If one side is warmer than the other side of the material, the rate of heat flow from the warmer side to the cooler is proportional to the thermal conductivity, see ASM (2002). See Chapter 2.1.2.4, temperature effects, for a deeper explanation of the subject. Table 2.4 shows different values of the thermal conductivity coefficient for different steel types, in a temperature range from room temperature up to 100°C , see ASM (2002).

Table 2.4 Thermal conductivity coefficient, k , for different steel types, temperature range from room temperature up to 100°C. From lowest to highest k -value, from ASM (2002).

Type of steel	k [W/m°C]
Ultrahigh strength steel	25-58
Hot work tool steel	17-42
Cold work tool steel	20-32
High-manganese carbon steel	46-50
High strength low-alloy steel (HSLA)	50-51
Mould steel	29-72
Austenitic stainless steel	11-21

2.2.2.3 Specific heat capacity of steel

For normal steel the specific heat capacity, c , is around 460 J/kgK at heating below 100°C, see Nevander (2006). See Chapter 2.1.2.4, temperature effects, for a deeper explanation of specific heat capacity. The thermal heat capacity is therefore 3611 kJ/m³°C for the prestressed steel (specific heat capacity times the density of 7850 kg/m³).

2.2.2.4 Heat convection from steel surface

The heat convection from a steel surface is the same as for concrete, see Chapter 2.1.2.4, temperature effects, for a deeper explanation of heat convection.

2.2.3 Mechanical properties of prestressing steel

Prestressed reinforcement steel can have different forms, e.g. single wires, strands composed of many wires twisted together, a group of strands forming a tendon (which is used in post-tensioned member), high strength bars etc. A prestressing wire is a single component made of steel, the most common diameters of the wires are 2,5 3,0, 4,0, 5,0, 7,0 and 8,0 mm. It can have two different configurations, plain wire with no indentations on the surface or indented wire with either circular or elliptical indentations. The different prestressing strands are composed of two, three or seven wires spun together in a spiral shape, see Nawy (2000). The plant in Vislanda use indented low-relaxation strands composed of three twisted steel wires with a diameter of 3,0 mm each, this results in a total diameter of approximately 6,5 mm for one steel strand, see Figure 2.17.

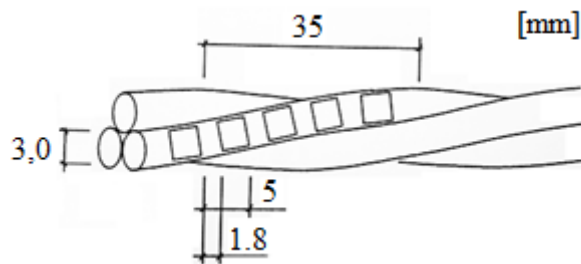


Figure 2.17 Illustration of the strand consisting of three twisted steel wires used in the plant at Vislanda with indentation according to prEn 10380, modified from Gustavsson (2002).

The prestressed steel is treated in the following process to meet the desired properties:

- Cold working: Altering the shape by plastic deformation, rolling, pressing, spinning etc. Hardness and tensile strength increases while ductility is lowered.
- Stress relieving: Heating the strands to around 350 °C and cooling slowly, plastic deformation of the steel is reduced after the onset of yielding.
- Strain tempering for low relaxation: Heating the strands to around 350 °C while they are under tension, this further reduce the plastic deformation and the relaxation, see Vincenzo (1999).

The mechanical properties of prestressing steel are high strength, adequate ductility, high bond, low relaxation, bendability and minimum corrosion, provided that the steel has good quality. The stiffness is given by the initial modulus of elasticity which depends on the form of the prestressing steel and the manufactory process, see Table 2.5. The mean density of prestressing tendons is normally taken as 7850 kg/m³ in design, see CEN (2004). Poisson's ratio for steel can vary between 0,27-0,30, see Gere (1997).

Table 2.5 Design values of modulus of elasticity, E_p , depending on type of steel and manufactory process, from CEN (2004).

Type of steel	E_p [kN/mm ²], average (range)
Cold-drawn wires	205 (195-210)
High tensile steel bars	205 (195-210)
Strands	195 (185-210)

The values given in Table 2.5 above may be assumed to be valid within a temperature range between - 40°C and + 100°C.

In comparison to ordinary reinforcing steel, prestressed steel has much higher capacity. Figure 2.18 shows a comparison of a typical prestressed steel and hot rolled reinforcing steel, where f_p is the prestressed tensile stress, $f_{p0,1k}$ is the 0,1 % prestressed characteristic proof stress, f_t is the reinforcement tensile stress and f_{yk} is the characteristic yield stress of the reinforced steel, see CEN (2004). Prestressing wires and strands have characteristic 0,1 % proof stress of around 1400-1600 MPa and a characteristic tensile strength of about 1600-1900 MPa. At tensioning the allowable stress is

approximately 85 % of the characteristic 0,1 % proof stress, but not more than 75 % of the characteristic tensile strength, see Engström (2011).

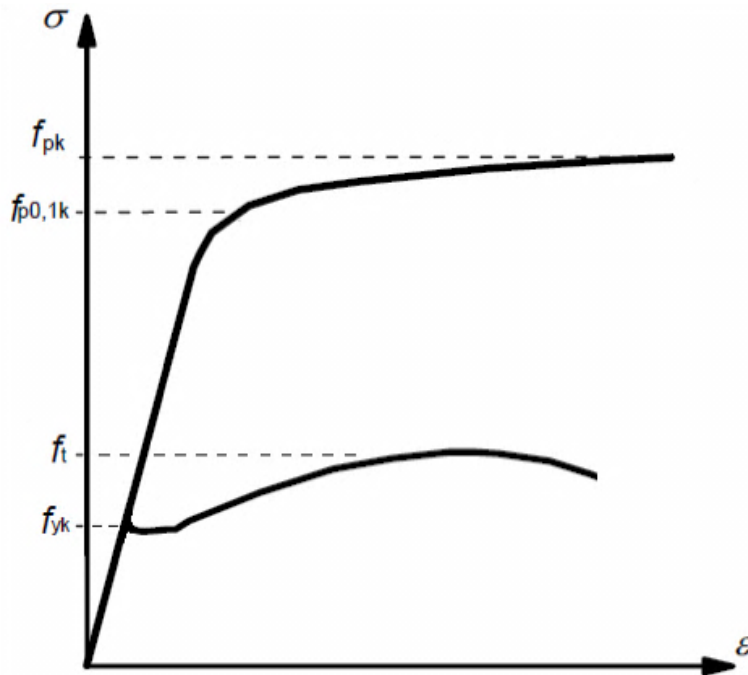


Figure 2.18 Stress-strain curve for typical prestressed steel (uppermost curve) and typical hot rolled reinforcing steel (bottom curve), modified from CEN (2004).

2.2.3.1 Losses of prestressing force

Losses of prestressing force in the prestressed steel strands can be separated in different phases; immediate loss of prestressing, losses of prestressing due to thermal properties, relaxation of prestressing steel and time dependent losses of prestress for pre-tensioning, see following subchapters.

Immediate loss of prestressing

According to Eurocode 2 the value of the initial prestressing force, $P_{m0}(x)$, is applied to the young concrete after transfer of prestressing, obtained by subtracting from the force at tensioning, P_{max} , the immediate losses, $\Delta P_l(x)$. The initial prestressing force should not exceed the following value:

$$P_{m0}(x) = A_p \cdot \sigma_{m0}(x) \quad (2.33)$$

Where $\sigma_{m0}(x)$ is the stress in the tendon immediately after transfer, which should be taken as minimum value of $(k_7 \cdot f_p, k_8 \cdot f_{p0,1k})$. Recommended values for k_7 and k_8 are 0,75 and 0,85 respectively.

When determining the immediate losses, $\Delta P_l(x)$, the following immediate influences should be considered; losses due to elastic deformation of concrete ΔP_{el} , losses due to short term relaxation ΔP_r , losses due to anchorage slip ΔP_{sl} .

Following losses should be considered in order to describe what occurs during pre-tensioning.

- During the stressing process: loss due to friction at the bends (in the case of curved wires or strands) and losses due to wedge draw-in of the anchorage devices.
- Before the transfer of prestress to concrete: loss due to relaxation of the pre-tensioning tendons during the period which elapses between the tensioning of the tendons and prestressing of the concrete. In case of heat curing, losses due to shrinkage and relaxation are modified and should be assessed accordingly; direct thermal effect should also be considered.
- At the transfer of prestress to concrete: loss due to elastic deformation of concrete as the result of the action of pre-tensioned tendons when they are released from the anchorages, see CEN (2004).

Losses of prestressing due to thermal properties

Prestress losses in the prestress steel, P_{loss} [kN], due to changes in strain can be expressed as:

$$P_{loss} = \Delta\varepsilon \cdot E_p \cdot A_p \quad (2.34)$$

Where

$$\begin{aligned} \Delta\varepsilon &= \text{Total changes in strain of the prestressed steel [m]} \\ E_p &= \text{Modulus of elasticity of prestressed steel [kN/mm}^2\text{]} \\ A_p &= \text{Area of the prestressed steel [m}^2\text{]} \end{aligned}$$

Eurocode 2 has a special treatment for thermal loss in the case of heat curing of pre-cast concrete elements, ΔP_e .

$$\Delta P_e = 0,5 \cdot A_p \cdot E_p \cdot \alpha_{cTe} \cdot (T_{max} - T_0) \quad (2.35)$$

Where

$$\begin{aligned} \alpha_{cTe} &= \text{Linear coefficient of thermal expansion for concrete.} \\ T_{max} &= \text{Maximum temperature near the tendons [}^\circ\text{C]} \\ T_0 &= \text{Initial temperature near the tendons [}^\circ\text{C]} \end{aligned}$$

Relaxation of prestressing steel

Relaxation of prestressing steel is the loss of prestress when the steel strands are subjected to substantially constant strain. It can be compared with creep in concrete, the difference is that creep is a change in strain while steel relaxation is loss in steel stress, see Nawy (2000). According to Eurocode 2, the effect on the relaxation losses for pre-tensioned members should be considered when the temperature increases during concrete curing. Relaxation increases rapidly with increasing temperature, see Ghali (2002). The relaxation increases also with increased ratio between the initial steel stress and the tensile strength and varies depending on steel type of prestressing steel, see Engström (2011).

In Eurocode 2 the following three classes of relaxation are defined

- Class 1: Wire or strand – Ordinary relaxation, $\rho_{1000} = 8 \%$

- Class 2: Wire or strand – Low relaxation, $\rho_{1000} = 2,5 \%$
- Class 3: Hot rolled and processed bars, $\rho_{1000} = 4 \%$

These classes have different equations when considering relaxation losses, see Equation 2.36a for class 1 and 2.36b for class 2.

Class 1:

$$\frac{\Delta\sigma_{pr}}{\sigma_{pi}} = 5,39 \cdot \rho_{1000} \cdot e^{6,7 \cdot \mu} \cdot \left(\frac{t}{1000}\right)^{0,75 \cdot (1-\mu)} \cdot 10^{-5} \quad (2.36a)$$

Class 2:

$$\frac{\Delta\sigma_{pr}}{\sigma_{pi}} = 0,66 \cdot \rho_{1000} \cdot e^{9,1 \cdot \mu} \cdot \left(\frac{t}{1000}\right)^{0,75 \cdot (1-\mu)} \cdot 10^{-5} \quad (2.36b)$$

- Where
- $\Delta\sigma_{pr}$ = Absolut value of the relaxation losses of the prestress [MPa]
 - σ_{pi} = Maximum tensile stress applied to the tendon minus the immediate losses occurred during the stressing process [MPa]
 - t = Time after tensioning [h]
 - μ = $\frac{\sigma_{pi}}{f_p}$ where f_p is the characteristic value of the tensile strength of the prestressing steel
 - ρ_{1000} = Value of relaxation loss [%] at 1000 hours after tensioning and at a mean temperature of 20°C

Time dependent losses may be calculated by considering the following to reduction of stress:

- Due to reduction of strain, caused by the deformation of concrete due to creep and shrinkage, under the permanent loads.
- The reduction of stress in the steel due to the relaxation under tension. The relaxation of steel depends on the concrete deformation due to creep and shrinkage. This interaction can generally and approximately be taken into account by a reduction factor 0,8, see CEN (2004).

An equivalent time, t_e , should be used in the relaxation time function, to take into account for the effects of the heat treatment on the prestress loss due to relaxation of the prestressing steel. The equivalent time can be estimated from

$$t_e = \frac{1,14 T_{max}^{-20}}{T_{max} - 20} \cdot \sum_{i=1}^n (T_{(\Delta t_i)} - 20) \Delta t_i \quad (2.37)$$

- Where
- t_e = Equivalent time [h]
 - $T_{(\Delta t_i)}$ = Temperature during the time interval Δt_i [°C]
 - T_{max} = Maximum temperature during the heat treatment [°C]

According to Eurocode 2 t_e is put into the relaxation loss equation for class 2 wires, which take into account for the equivalent time, see Equation 2.38.

$$\sum_1^{J-1} \Delta\sigma_{pr,J} = 0,66 \cdot \rho_{1000} \cdot e^{9,09 \cdot \mu} \cdot \left(\frac{t_e}{1000}\right)^{0,75 \cdot (1-\mu)} \left\{ \sigma_{pr,J}^* + \sum_1^{J-1} \Delta\sigma_{pr,J} \right\} \cdot 10^{-5} \quad (2.38)$$

- Where
- $\Delta\sigma_{pr}$ = Absolut value of the relaxation losses of the prestress
 - σ_{pi} = Maximum tensile stress applied to the tendon minus the immediate losses occurred during the stressing process
 - t_e = Equivalent time [h]
 - μ = $\frac{\sigma_{pi}}{f_{pk}}$ where f_{pk} is the characteristic value of the tensile strength of the prestressing steel
 - ρ_{1000} = Value of relaxation loss [%] at 1000 hours after tensioning and at a mean temperature of 20°C

According to DIANA (2008) the stress relaxation on the steel strand can be calculated with Maxwell Chain Model with viscoelasticity assumption as

$$\sigma(t) = \int_{-\infty}^t E(t, \tau) \cdot \bar{D} \cdot \dot{\varepsilon} \cdot d\tau \quad (2.39a)$$

with $E(t, \tau) = E_\alpha(\tau) \cdot e^{-\frac{t-\tau}{\lambda_\alpha}}$ (2.39b)

and $\varepsilon(t) = \int_{-\infty}^t J(t, \tau) \cdot \bar{C} \cdot \dot{\sigma}(\tau) \cdot d\tau$ (2.39c)

and $J(t, \tau) = \frac{1}{E_\alpha(\tau)} \cdot \left(1 - e^{-\frac{t-\tau}{\lambda_\alpha}}\right)$ (2.39d)

- Where
- $\sigma(t)$ = Time dependent stresses [MPa]
 - $E(t, \tau)$ = Relaxation function [GPa]
 - \bar{D}/\bar{C} = Dimensionless matrix dependent on Poisson's ratio [-]
 - $J(t, \tau)$ = Creep function, according to Kelvin Chain model [-]
 - $E_\alpha(\tau)$ = Time dependent stiffness of the model [GPa]
 - λ_α = Relaxation time [s]
 - t = Time [s]
 - τ = Time factor [s]

2.3 Interaction between young concrete and prestressing steel

2.3.1 Bond behaviour

The bond behaviour of steel strands to young concrete is caused by adhesion, Hoyer's effect and mechanical interlocking. Hoyer's effect and mechanical interlocking contributes both to friction, therefore is it not listed as a separate mechanism. Without friction, the amount of bond from Hoyer's effect would be zero and mechanical interlocking's effect would be reduced, see Russell (1993). These mechanisms are active in different stages of the bond stress, τ_b , - slip, s , curve, see Figure 2.19. The initial bond behaviour is primarily due to adhesion between steel and concrete. Different parameters of the strands and the concrete results in different bond behaviour. Increased roughness of the strand surface will improve the bond capacity. This can be done by use of indents or surface treatments, see Gustavsson (2002).

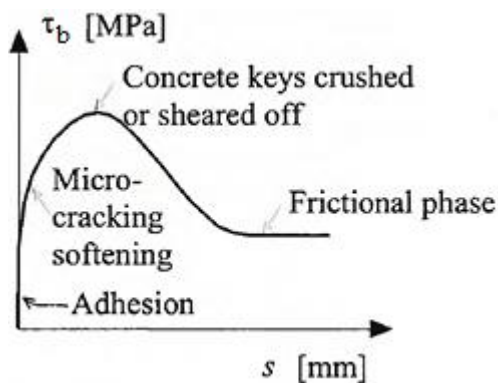


Figure 2.19 Typical bond stress-slip relation between steel and concrete, modified from Engström (2011).

In CEB-FIB Model Code 1990 is the typical bond stress-slip relation simplified, see Figure 2.20. The different phases in the bond stress-slip curve are characterized with different equations, see Equations 2.40a-d.

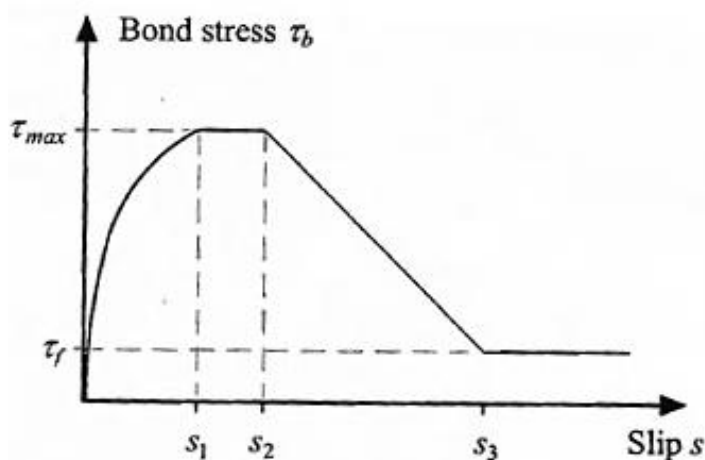


Figure 2.20 Simplified bond stress-slip relation between steel and concrete with different phases; s_1 , s_2 and s_3 , according to CEB-FIB (1993).

$$\tau_b = \tau_{max} \cdot \left(\frac{s}{s_1}\right)^{0,4} \quad \text{if } s \leq s_1 \quad (2.40a)$$

$$\tau_b = \tau_{max} = 2,5 \cdot \sqrt{f_{ck}} \quad \text{if } s_1 < s \leq s_2 \quad (2.40b)$$

$$\tau_b = \tau_{max} - (s - s_2) \cdot \frac{\tau_{max} - \tau_{lim}}{s_3 - s_2} \quad \text{if } s_2 < s \leq s_3 \quad (2.40c)$$

$$\tau_b = \tau_{lim} = 0,4 \cdot \tau_{max} \quad \text{if } s \leq s_3 \quad (2.40d)$$

- Where
- τ_b = Bond stress [MPa]
 - τ_{max} = Maximum bond stress [MPa]
 - τ_{lim} = Final value of bond stress [MPa]
 - f_{ck} = Characteristic compressive strength of concrete [MPa]
 - s = Maximum slip [mm]
 - s_1 = 1.0 [mm]
 - s_2 = 3.0 [mm]
 - s_3 = Clear rib spacing [mm], see CEB-FIB (1993)

In the Finite element program DIANA bond-slip models for interfaces elements are set as nonlinear relation between shear traction, t_t , and shear slip, Δu_t . Shear traction are the same as bond stress, τ_b , and shear slip is the same as slip, s . But it is a linear relationship between normal traction and normal relative displacements. There are three different bond-slip models available; cubic-, power law- and multi-linear function. The cubic bond-slip model can be used in combination of maturity dependence of the cubic function, see Figure 2.21. Equation 2.41.a-b shows the mathematic expression of the cubic function, see DIANA (2008).

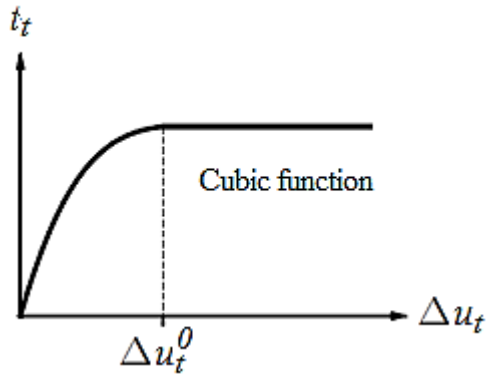


Figure 2.21 Bond stress versus slip curve of the cubic function, used in DIANA, from DIANA (2008).

$$t_t = c \cdot \left(5 \cdot \left(\frac{\Delta u_t}{\Delta u_t^0}\right) - 4,5 \cdot \left(\frac{\Delta u_t}{\Delta u_t^0}\right)^2 + 1,4 \cdot \left(\frac{\Delta u_t}{\Delta u_t^0}\right)^3 \right) \quad \text{if } 0 \leq \Delta u_t < \Delta u_t^0 \quad (2.41a)$$

$$t_t = 1,9 \cdot c \quad \text{if } \Delta u_t \geq \Delta u_t^0 \quad (2.41b)$$

- Where
- t_t = Bond stress [MPa]

- c = Constant value, recommended value is tensile strength of concrete, f_t [MPa]
- Δu_t = The slip [mm]
- Δu_t^0 = Where the curve reaches the plateau, recommended value is 0,06 [mm]

With the bond-slip model multi-linear function, a prescribed bond-slip relation can be deployed, see Figure 2.21 for an illustration.

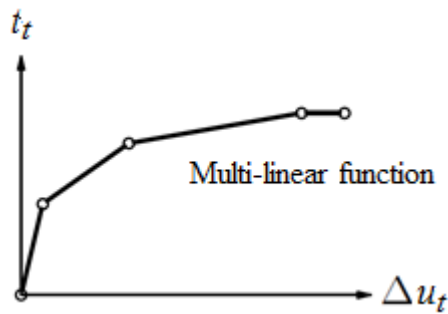


Figure 2.22 Multi-linear bond-slip curve with the shear traction, t_t , and slip, Δu_t , from DIANA (2008).

Bond stresses between the prestressed steel strands and the young concrete are not easy to define in advance. The concrete can be able to crack in the transfer zone. Strands slip relative to the concrete during expansion of the materials and upon de-tensioning. During tensioning of the strands, they tend to untwist to relieve their tension, but they cannot regain their original shape. Due to temperature increase, the strands expand against the concrete causing normal force, which in turn creates friction restraint, see Russell (1993).

2.3.1.1 Adhesion

The adhesion between concrete and steel is a major factor considering the interaction between construction elements, not least for the interaction between the young concrete and the prestressed steel wires during the sleeper production process. The adhesion zone is exposed to different stresses, shear stresses due to different length expansions between the two materials, which occur due to moisture or temperature variations and normal stresses. In the interaction zone between steel and concrete it also occur tensile- and compressive stresses. Shrinkage after concrete casting results in shear stresses in the interaction zone, different temperature expansion and modulus of elasticity between the materials, see Ljungkrantz (1994).

The adhesion can be measured with a bond-slip test, where a machine pulls out the steel wire and measures the force and displacements between the concrete specimen and the steel wire, see Ljungkrantz (1994). The age of the concrete is an important factor that should be taken into account. If many similarly tests are done with different age of the concrete, a bond-slip maturity dependent relationship can be set up. The adhesion between the steel wire and the surrounding concrete increases with increasing maturity.

As has been mentioned, adhesion is the glue between the young concrete and the prestressed steel. The glue line is very thin and the resulting bond stress versus slip has

rigid-brittle behaviour, it means that failure of the glue is always brittle, see Russell (1993).

2.3.1.2 Hoyer's effect

The researcher E.Hoyer investigated the mechanism that anchored the pretensioned force to the concrete. The mechanism is therefore named after him. The Hoyer's effect is explained by considering the production of a prestressed concrete element consisting of steel strands. After the steel strands are pretensioned, the diameter of the strands reduces by Poisson's ratio as it is elongated. At detensioning the steel strands lose their initial prestress at the end face of the concrete element. The strands trying to regain their original form, which results in a radial expansion of the strands at the element ends, see Figure 2.23. A normal force is imposed at the boundary between concrete and steel, which activates a frictional force at the interface. This friction force restraining the prestressing strands in tension. A certain end anchorage is achieved by the Hoyer's effect, when the radial expanding strands tend to slip into the concrete, see Russell (1993).

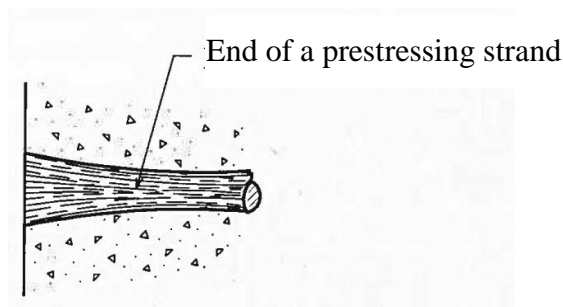


Figure 2.23 Expansion of the end of a prestressing strand, from Engström (2011).

2.3.1.3 Mechanical interlocking

Consider twisted prestressed three-wire strands; when concrete is cast around these not-uniform strands, a certain pattern occurs in the concrete which perfectly match the strands surface. When the strands slip against the concrete surface without twisting, friction forces are created because movement is resisted. This resistance is called mechanical interlocking, see Russell (1993).

2.3.2 Transfer of prestressing force

Transfer of prestressing force can be explained by considering what happens with an arbitrary prestressed concrete specimen before and after the prestress force is applied, see Figure 2.24.

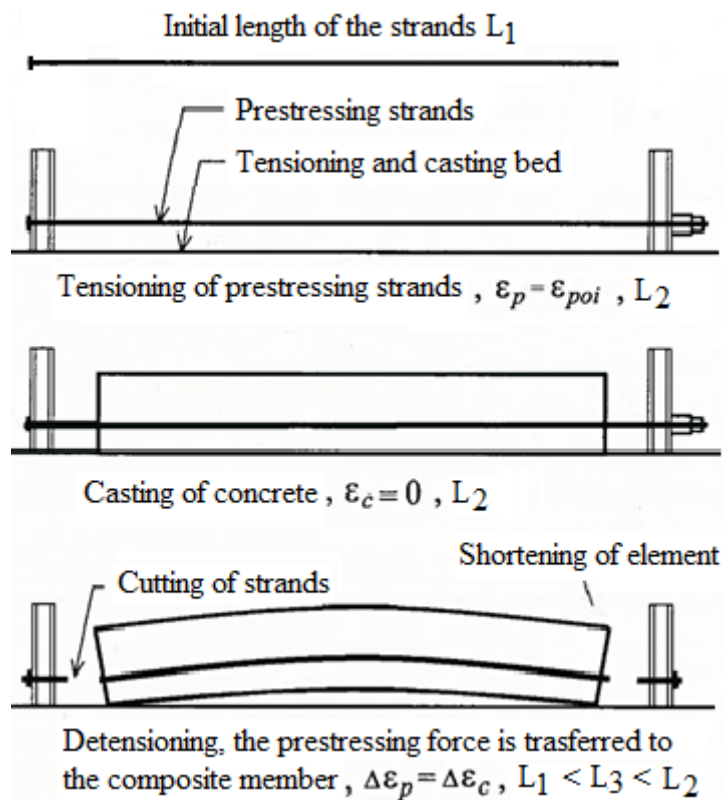


Figure 2.24 Illustration of different phases during prestressing of an arbitrary concrete specimen, modified from Engström (2011).

Before tensioning, the steel strand has an original length L_1 . Then the tensioning force elongates the steel strand to a length L_2 . After casting of concrete, the in-casted steel strand still has the same length (L_2). But when the initial prestressing force (P_i) releases, elastic shortening appears and the final length (L_3) becomes something between the original length of the steel strand and the original length of the concrete specimen. Important notation is that the steel strand and the concrete specimen receive the same length (L_3). Figure 2.25 shows the concrete stresses, σ_c , steel stresses, σ_s , bond stress, τ_b , the transmission length, l_t , and changes in strain along the arbitrary prestressed concrete member in the prestressing bed.

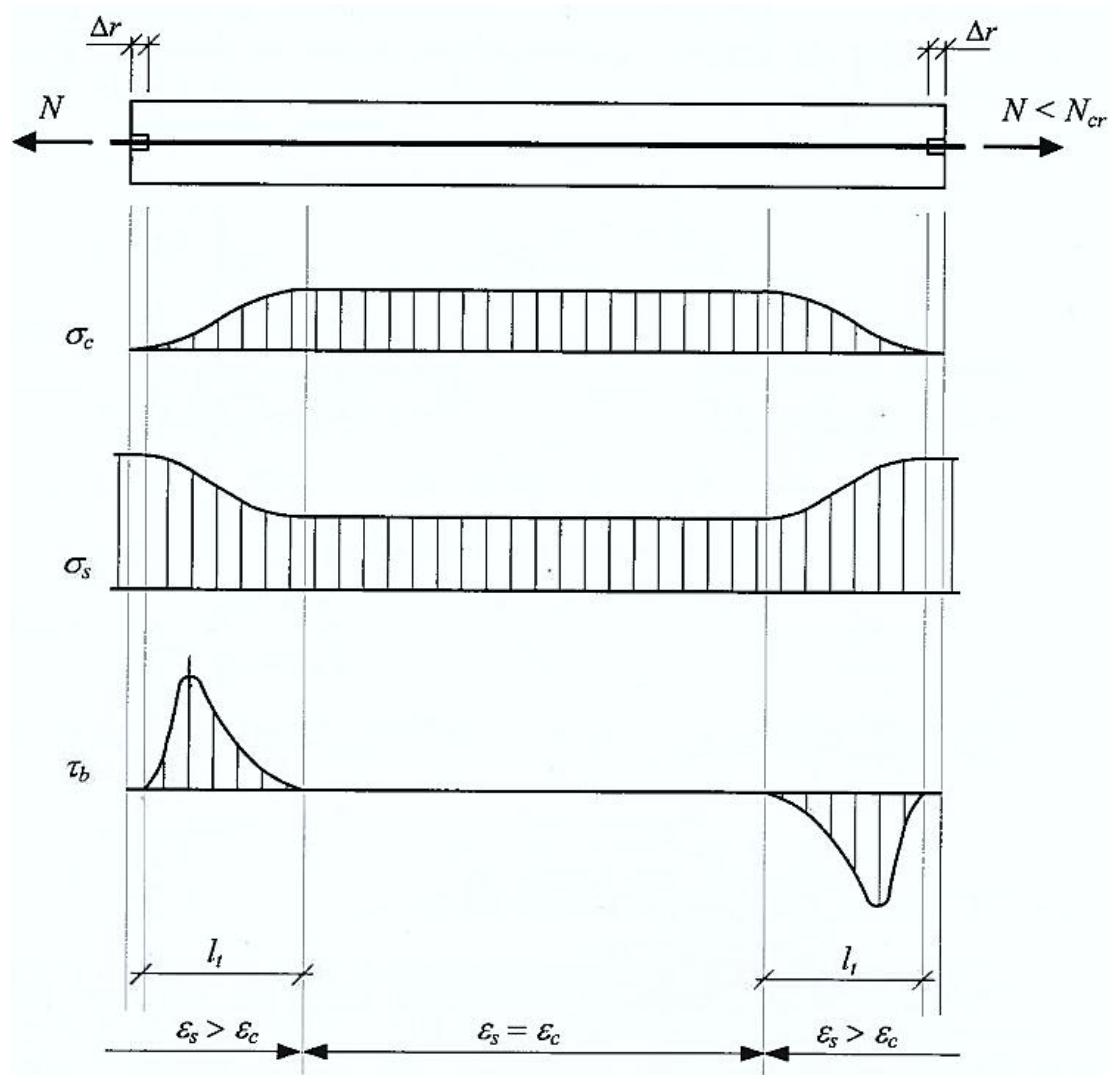


Figure 2.25 Illustration of concrete stresses, σ_c , steel stresses, σ_s , bond stress, τ_b , the transmission length, l_t , and changes in strain along an arbitrary prestressed concrete member in the prestressing bed, from Engström (2011).

2.3.2.1 Elastic shortening of concrete

The transfer of prestressing force is the phenomenon that occurs in pre-tensioned concrete structures, known as elastic shortening. When the initial prestress force is released, instantaneous elastic shortening of the casted concrete takes place. This happens because the in-casted steel strands want to shrink back to its original length and therefore creates a pressure force that the concrete tries to resist. Hence, force is transferred from the prestressed strands to the concrete. The result of this shortening will be an immediate partial prestress loss of the initial prestress force, see Bennitz (2008).

The transmission length, l_t , is the needed distance to transfer the fully effective prestressing force, see Figure 2.26. At the end of the strands, the prestressed force is zero, in the transmission length the prestress increases approximately linearly up to the fully effective prestress. The concrete behaves in a similar way. Slip between the

strands and the concrete occurs in the transmission length. When fully effective prestress is achieved, no slip occurs and the prestressed force is constant. At this point are the incremental strains equal in the both materials, which results in that the concrete and strand forces must be in equilibrium at every point along this length. Therefore, the tension in the strands is always balanced by equivalent and opposite compression in the concrete along this length, see Russell (1993).

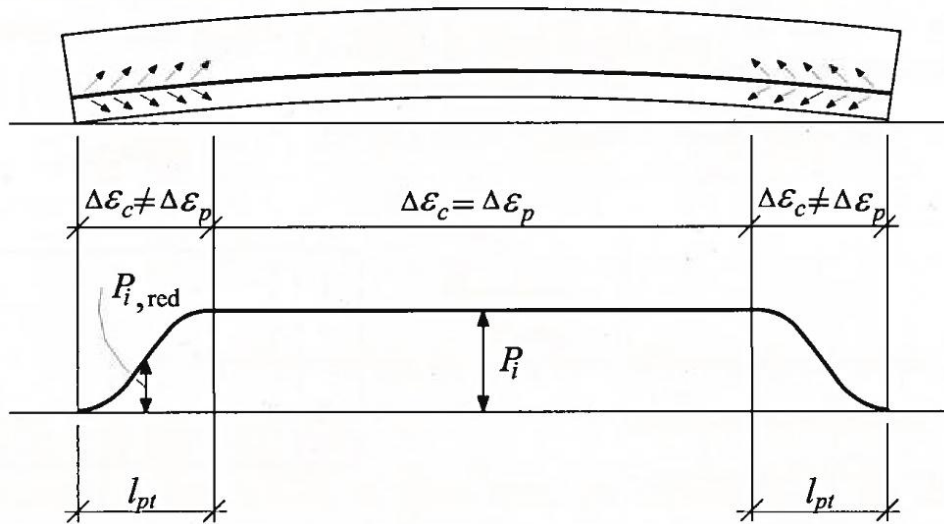


Figure 2.26 Elastic shortening of an arbitrary concrete specimen during the prestress process with a transmission length, l_t , from Engström (2011).

3 The Long Line Method

As mentioned, Abetong uses a production method called “The Long Line Method” to produce prestressed concrete sleepers. The following facts about “The Long Line Method” were gathered during a site visit at Abetong sleeper plant in Vislanda, Sweden¹. The method was invented already in 1960 and was licensed six years later. Today the method is used in 35 sleeper plants all around the world, see Figure 3.1.



Figure 3.1 Plants utilizing the Abetong Long Line Method around the world, modified from Abetong (2012).

The basic idea of “The Long Line Method” is to have a rational production, i.e. produce sleepers as quick, easy and cheap as possible. Of course, the concrete sleepers also have to meet various requirements to obtain a certain quality.

To obtain a rational production, long beds around 110 meters with quadruple moulds are placed after each other's, see Figure 3.3. The long bed has two different ends, the passive and the active end. The passive end resist the force (steel wires are fixed) and in the active end the steel wires are first tensioned, then fixed and finally released of prestressing force after a certain time. Figure 3.2 shows an illustration of the boundary conditions of the bed in different stages.

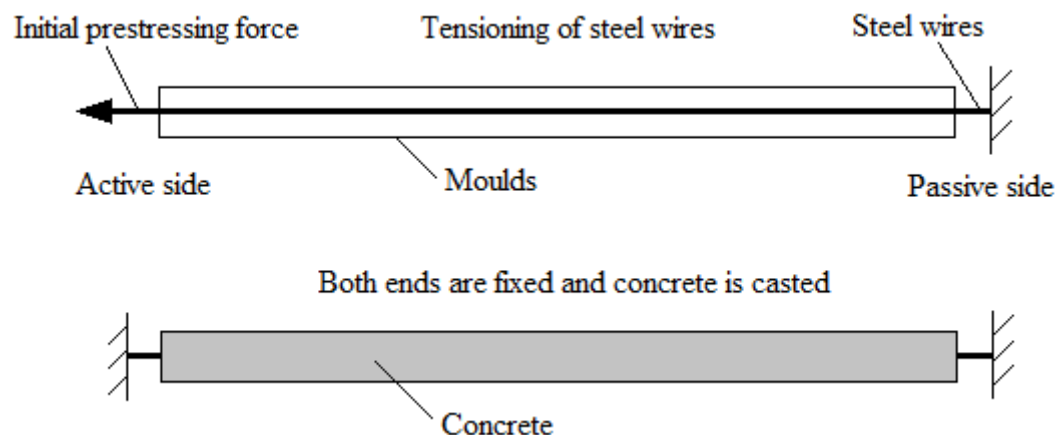


Figure 3.2 Illustration of boundary condition during tensioning and curing.

¹Study trip to the factory in Vislanda with Rikard Bolmsvik, 12 december 2011.

“The Long Line Method” is not executed exactly the same way in all plants. Parameters that differ are for example; the length of the bed, indoor climate, casting process, etc. Another major difference is if the sleepers are casted all together as a long beam or if there is some space (naked steel wire) between for example every fourth sleepers, as in the factory in Vislanda.

The first step in the production is to clean and oil the moulds after the previous casting process. This is made by a special cleaning machine which is placed on top of the bed, see Figure 3.3 for different machines used in the production. Next step is to put a specific number of steel wires at different predetermined positions in the moulds, this is made by another machine that pulls out the wires from cable rolls over the bed and attaches them to the passive side. Thereafter the steel wires are pre-tensioned on the active side by a hydraulic jack up to a certain initial prestress force. The quality of the steel is very high compared to normal reinforcement; the factory in Vislanda use steel with a yield capacity of 1860 MPa.



Figure 3.3 “The Long Line Method” with its production equipment, from Abetong (2012).

When the initial steel stress is reached a special machine is used to lift up the moulds which were lowered during the previous process. Afterwards the casting process starts. An automatic casting machine is placed on the bed and moves sequentially along the bed, usually from passive side to active side, and casting fresh concrete meanwhile. The casting process takes from 1-3 hours, but the most common time is two hours. Directly after casting, the bed is covered with tarpaulins to keep some of the generated hydration heat.

After approximately sixteen hours when a certain bond capacity is reached between concrete and steel, the sleepers are demoulded and the prestressing is released. Sufficient bond capacity is controlled by checking the compressive strength of the concrete. The minimum compressive strength that needs to be obtained before release of prestress is 35 MPa. Bed trolleys are installed so the whole bed can be transferred to the cutting machine. Depending on if the sleepers are casted as one long specimen or not, the cutting process is different. The most common production processes with Long Line Method is to cast the sleepers as one long beam and after releasing of the prestressing force cut it into final sleepers length. One more step is needed in the Vislanda plant; firstly the bed is cutted into a group of four sleepers to empty the bed faster so a new casting can take place. These groups of sleepers are then placed in a storage place in anticipation of being cut into final length by another diamond saw. The sleepers are then controlled and rail fastenings are installed before they are ready to be transported to the customer, see Figure 3.4 for a description the production process.



Figure 3.4 Schematic production description of “The Long Line Method”, starts at the top.

3.1 General about concrete sleepers

Concrete sleepers forming together with the embankment and the steel rail the track structure of the railway. A main advantage of the sleepers is that climate influences have little effects, because of the material properties of the concrete. Some of the most important functions and requirements of the sleepers is to provide support and restraining facilities for rail foot and fasteners, maintaining rail forces and transfer them as uniform as possible to the embankment and to preserve track gauge and rail inclination. More benefits with concrete sleepers are that they have long service life provided that the fasteners obtain good quality or can easily be replaced, relatively easy to produce and create a lot of freedom in design and construction. The most important disadvantage is that it is susceptible to corrosion and can break due to impacts from fatigue loading and derailment, see Esveld (2001).

The most common sort of sleepers today is the prestressed mainline monoblock sleeper, see Figure 3.5. The dimensional requirements for the monoblock sleepers are that the area of the bottom must be sufficiently large so the average ballast pressure under full load does not exceed a certain value (normally 0,5-0,4 MPa), the end face

should be of such character to withstand the maximum resistance to lateral movements and the shape of the sleepers should be tapered from both ends to the centre in height and width with smooth changes to prevent stress concentrations, see Gustavsson (2002).

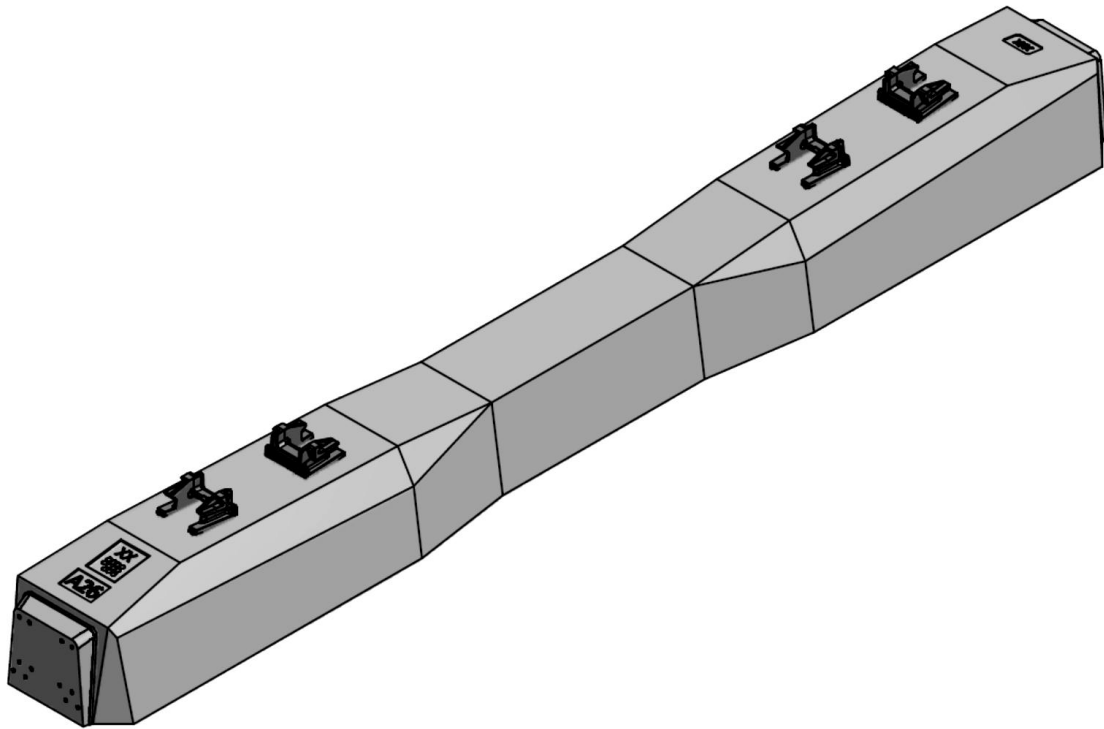


Figure 3.5 Typical geometry of a prestressed concrete sleeper produced with “The Long Line Method”, from Abetong (2012).

4 Measured prestress losses during sleeper production with “The Long Line Method”

4.1 Different production conditions

To increase the knowledge about prestress losses during sleeper production with “The Long Line Method”, measurements have been made by the company Abetong at three different factories with different boundary conditions. The factory included in the test experiment was Vislanda (Sweden), Marijampolė (Lithuania) and Sollenau (Austria), see the following subchapters for description of the measurements with specific conditions.

4.1.1 Vislanda – warm surroundings and sections of moulds

Following data was taken from Andersen (2011), which is an internal report of the measurements made in Vislanda year 2010 and 2011. Table 4.1 shows different properties of the concrete and steel strands used in Vislanda.

Table 4.1 *Properties of the concrete and steel strands used Vislanda factory².*

Concrete	
Cement type	CEM I 52,5 R (Skövde)
Concrete	SH
W/C-value	0,42
Density of mature concrete	2400 kg/m ³
Admixtures	Non, 100 % cement
Compressive strength after 17.0 h	35 MPa at least
Ballast type	Granit
Cub compressive strength 28 days	73 MPa
Tensile strength 28 days	5,2 MPa
E-Modulus 28 days	38 MPa
Prestressed steel strand	
Steel strand type	Low relaxation D=4,9 mm
Number of steel strand	14
Total area of steel strands*	2,9696E-4 m ²
Perimeter of all steel strands	0,238 m
Initial steel stress	1343 MPa

*The perimeter of all steel strands was assumed to be 60 % of the actual perimeter, because they are twined together. This applies for all plants.

² Properties of the concrete and the prestressed steel have been obtained from Rikard Bolmsvik, supervisor to the thesis and employed at Abetong.

4.1.1.1 Initial conditions

- Indoor temperature was regulated so that at least 20°C always was kept in the production hall. The steel strands will have the same temperature as the indoor temperature, because they are stored in the same hall.
- Starting curing temperature of concrete was regulated if necessary (preheating of the ballast). The temperature of the fresh concrete mix varies between 10 and 20°C, depending of the season.
- No additional heating was supplied to the sleeper beds during curing of concrete.
- The sleeper beds were covered with tarpaulins directly after casting, which results in that a certain amount of the produced hydration heat was kept inside the sleepers.
- Sections of moulds, four sleepers in each mould. Totally 11 moulds, which results in 44 sleepers along the bed.
- The distance between the moulds, “naked” steel strands, is five centimetre.
- The length of the naked steel strands in the ends is 0.5 meters each.
- The total length of the bed is 111.5 meters.
- The minimum compressive strength that needs to be obtained before release of prestress is 35 MPa.
- Five different tests at different times were made in the plant.

4.1.2 Marijampolé – cold surroundings and continuous set of moulds

The plant in Marijampolé consists of one set of moulds and has generally cold surroundings in the production hall. Initial conditions during the measurements can be seen in subchapter below and properties of concrete and steel strands used at the plant can be seen in Table 4.2

Table 4.2 Properties of the concrete and steel strands used in Marijampolė factory.

Concrete	
Cement type	CEM I 52,5 R
Concrete	C50/60
W/C-value	0,37
Density of mature concrete	2400 kg/m ³
Admixtures	BASF/ACE 30 1,9 l/m ³
Compressive strength after 17.0 h	37 Mpa
Ballast type	Granit
Cub compressive strength 28 days	65 MPa
Tensile strength 28 days	4,8 MPa
E-Modulus 28 days	38 MPa
Prestressed steel strand	
Steel strand type	3x3,15 mm indented 1860 S3
Number of steel strand	12
Total area of steel strands	2,806E-4 m ²
Perimeter of all steel strands	0,214 m
Initial steel stress	1395 MPa

4.1.2.1 Initial conditions

- A heating system is installed under the casting bed and was switched on all the time during the measurements of the steel strain.
- Indoor temperature was 6°C in the surrounding and at the steel strands before tensioning.
- Both heated aggregates and hot water were used to start the hydration of the concrete faster. Initial temperature of the concrete mix was 17°C.
- The concrete bed consists of continuous sets of moulds.
- The sleeper bed was covered with tarpaulins directly after casting, as in Vislanda.
- Before release of the prestressed force, two concrete cubes were tested in compression strength, showing a capacity of 43 and 44 MPa.
- The length of the bed is totally 109 meters, due to 40 sleepers along the entire bed and each sleeper is approximately 7 meters. The ends consist also of 0,5 meters “naked” steel strands.

4.1.3 Sollenau – warm surroundings and continuous set of moulds

The plant in Sollenau consists of one set of moulds and has generally warm surroundings in the production hall. Initial conditions during the measurements can be seen in subchapter below and properties of concrete and steel strands used at the plant can be seen in Table 4.3.

Table 4.3 Properties of the concrete and the steel strands used in Sollenau factory, from Scmöllerl (2011).

Concrete	
Cement type	CEM I 52,5 R
Concrete	C50/60
W/C-value	0,39
Density of mature concrete	2400 kg/m ³
Admixtures	Sika FF86 8,5 l/m ³
Compressive strength after 17.0 h	54 Mpa
Ballast type	Dolomite
Cub compressive strength 28 days	95 MPa
Tensile strength 28 days	6,3 MPa
E-Modulus 28 days	40 MPa
Prestressed steel strand	
Steel strand type	Φ6mm ST 1570/1770
Number of steel strand	14
Total area of strands	3,958E-4 m ²
Perimeter of all steel strands	0,264 m
Initial steel stress	1275 MPa

4.1.3.1 Initial conditions

- The concrete bed consists of continuous sets of moulds.
- Initial temperature of concrete mix was 25°C.
- Temperature of the surrounding was 25°C.
- The length of the bed is totally 105 meters, due to 40 sleepers along the entire bed and each sleeper is approximately 2,6 meters. The ends consist also of 0,5 meters “naked” steel strands.
- The sleeper bed was covered with tarpaulins directly after casting, as in the other factories.
- No additional heating during the hardening process.

4.1.4 Results from test measurements

The test measurements made at the different factories includes the variation of temperature and strain, which is directly related to the prestressing force, during the production. The similarity between the different results is that the prestressing force decreases when the temperature increases due to hydration, see Figure 4.1. The change of rate of the prestress loss is directly linked to a change of rate of the temperature. After the maximum temperature was reached the prestress was almost constant. A decrease of the prestress force was observed directly after that the strands were prestressed. This loss can be explained by inner friction loss in the anchorage, see stage one in Figure 4.1. It can also be seen that the prestressing force decreases significantly when the prestressing force was released, due to elastic shortening, see stage three in Figure 4.1.

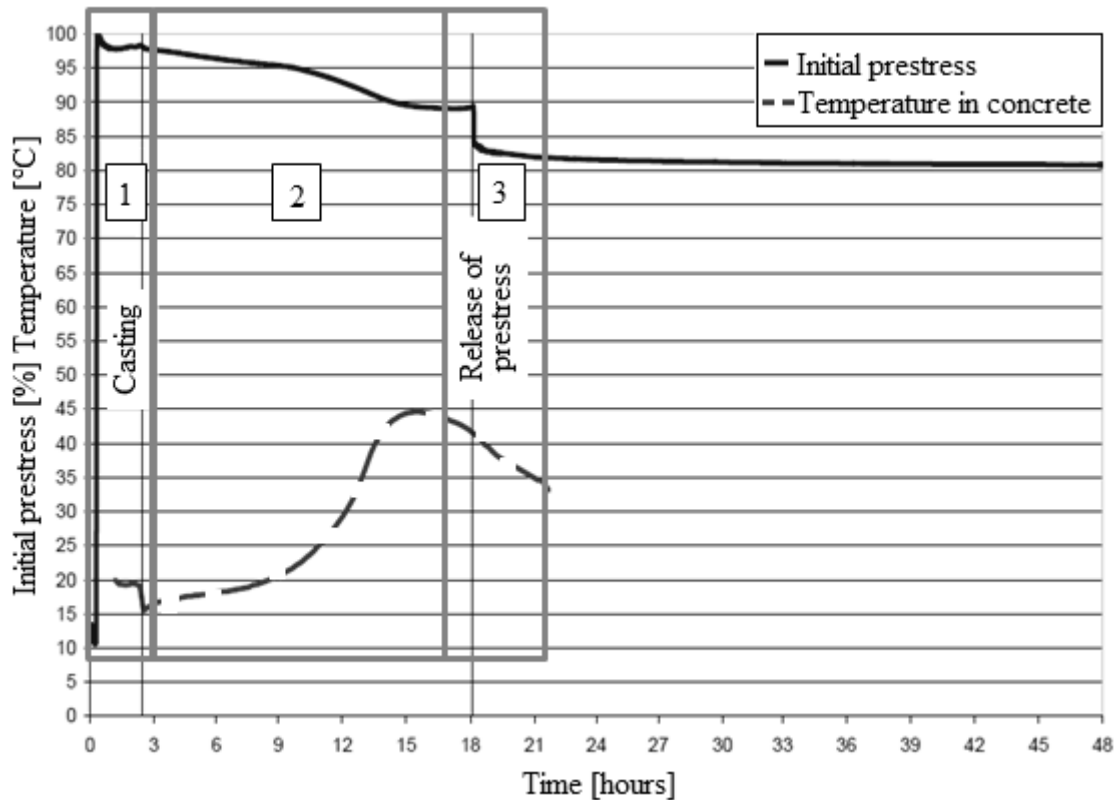


Figure 4.1 Result from the first test measuring made at Vislanda factory. The figure illustrates also the three most important stages when considering the loss of the prestress during the production method of sleepers. Stage 1 is the time from that the steel strands are prestressed until the casting of concrete, stage 2 starts after casting and extends until just before the release of prestress, and stage 3 is when the force is released, modified from Andersen (2011).

4.1.4.1 Vislanda

Table 4.4 below shows data and results over three different tests made at different times in Vislanda factory (test 1 was made at 2010-02-03, test 2; 2010-02-16 and test three; 2010-03-02). The results are more or less equal. Table 4.4 shows that the initial temperature of the concrete mix depends on the time to the maximum temperature which has influence on the prestress loss during the second stage. Lower initial temperature results in longer time to reach the maximum temperature.

Two more measurements including movement of anchor plate has further been made in Vislanda. The results show that a very limited movement was obtained for the anchor plate during the production. The result shows also that the hydraulic lock was keeping the anchor plate more or less still during the entire production process. Hence, the prestress loss could not be determined by the movements of the anchor plate, see Andersen (2011).

Table 4.4 Data and results over three different test measurements made in the Vislanda factory. The time is expressed in hours after casting of the concrete, from Andersen (2011).

Test	Concrete mix temperature [°C]	Max. temp. point in concrete [°C/hours]	Release of the force [hours]	Prestress loss in stage 1 [%]	Prestress loss in stage 2 [%]	Prestress loss in stage 3 [%]
1	16	45/12,5	15,7	2,5	8	6
2	18,6	43,6/12	18,2	2	6	7
3	12,3	45/13,5	64,5	0	7,5	8

The third test measurements in Vislanda included also measurements of the naked steel strands between every fourth sleeper mould. The results shows that the prestress loss of the naked steel strands differed from the prestress loss of the steel strands embedded in the concrete. The prestress loss was constant up to approximately seven hours, thereafter the prestress decreased in the naked steel strands until the maximum temperature was obtained in the concrete. Afterwards, when the temperature decreased, the prestress in the naked steel strands increases to 115 % (more stresses than the initial ones), while the prestress loss in the embedded steel strands did not change. A suggested explanation is that the bond starts to develop between the embedded steel strands and the concrete at around seven hours, see Figure 4.2 below. Full bond was assumed when the maximum temperature in the concrete has occurred, because the prestress loss of the embedded steel strands had stopped, see Andersen (2011).

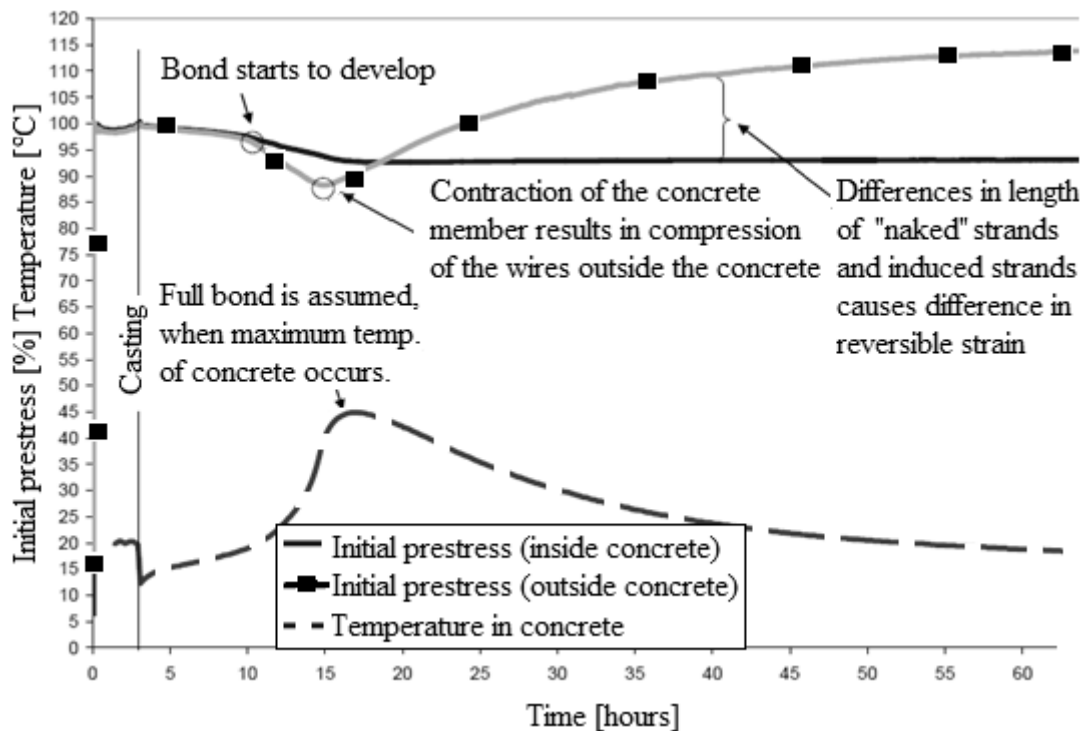


Figure 4.2 Explanations of different phenomenon that occurs during curing of concrete, modified from Andersen (2011).

4.1.4.2 Marijampolė

Measurements made at the factory in Marijampolė, date 2011-03-22, include temperature and prestress losses at four different places in the first sleeper in the long casting bed, see Figure 4.3.

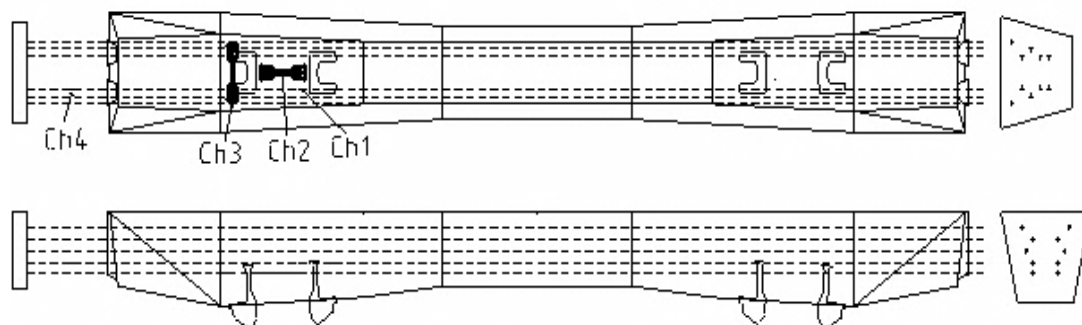


Figure 4.3 Placement of four different strain gauges were placed, Ch1; at a steel strand embedded in the centre section of the end of the first concrete sleeper, Ch2; at the rail seat section placed outside the concrete surface, Ch3; near the Pandrol shoulder and Ch4; at a naked steel strand between the anchor plate and the first sleeper, from Andersen (2011).

The measurements were made by a ConReg instrument at the active side of the bed, where the hydraulic jack tensions the steel strands. Two strain gauges were mounted in Ch1, at the steel strands embedded in the concrete. Two other strain gauges were

placed at Ch4, between the anchor plate and the end of the first concrete sleeper. Table 4.5 shows the results from the different measurements.

Table 4.5 Results from the measurements at the factory in Marijampolé, from Andersen (2011). The time is specified after casting.

Test	Concrete mix temperature [°C]	Max. temp. point in concrete [°C/hours]	Release of the force [hours]	Prestress loss in stage 1 [%]	Prestress loss in stage 2 [%]	Prestress loss in stage 3 [%]
ConReg	17	33/14	21	5	36	4

As Table 4.5 shows, the prestress loss in stage two was 36 %, which is very large compared to the losses in Vislanda that were between 6-8 %. But the behaviour in stage one and three was similar for the two factories.

4.1.4.3 Sollenau

Measurements of strains in steel strands have been made in Sollenau date 2010-07-27, see Table 4.6 and Figure 4.4 for the results obtained.

Table 4.6 Results from the measurement at the factory in Sollenau, from Schmöllerl (2011). The time is specified after casting.

Test	Concrete mix temperature [°C]	Max. temp. point in concrete [°C/hours]	Release of the force [hours]	Prestress loss in stage 1 [%]	Prestress loss in stage 2 [%]	Prestress loss in stage 3 [%]
1	25	55.0/10	18	0	8	5.5

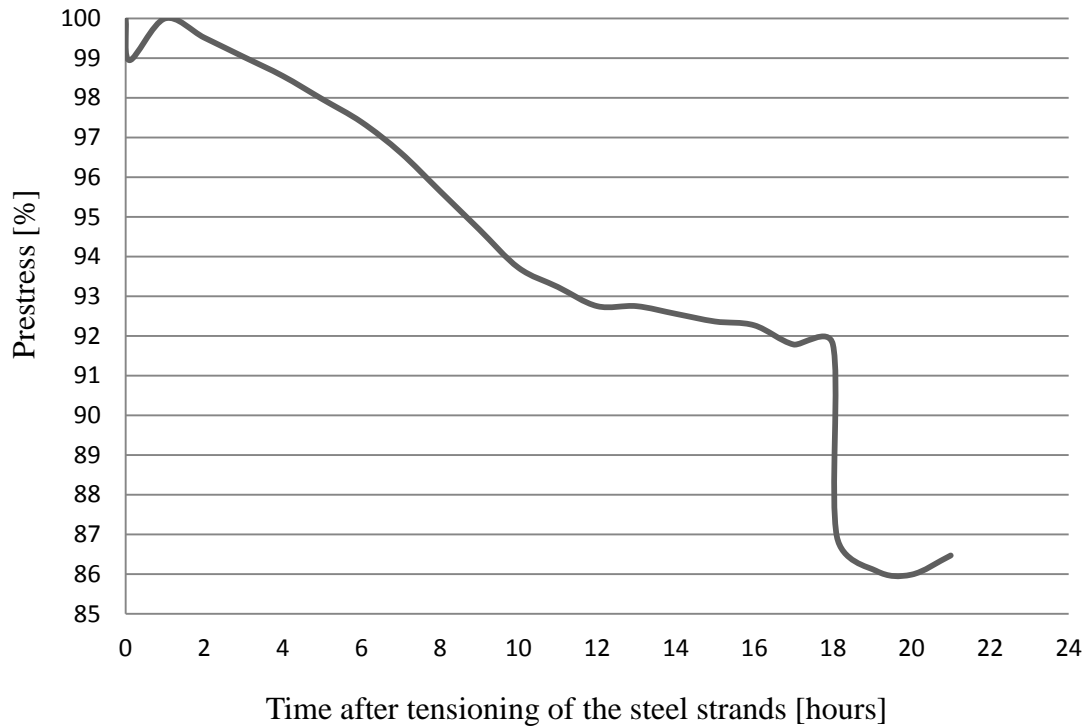


Figure 4.4 Prestress of steel strands in measuring made at Sollenau, date 2010-07-29, modified from Scmöllerl (2011).

As Figure 4.4 shows, the prestress force decreased first with 1 % and then increased with the same in stage 1. This is probably due to re-tensioning of the steel strands. The total prestress loss after 21 hours was approximately 13,5 %.

4.1.5 Summary of the factories

A comparison of the prestressing force and temperature development between the factories can be seen in Figure 4.5 and in Table 4.7.

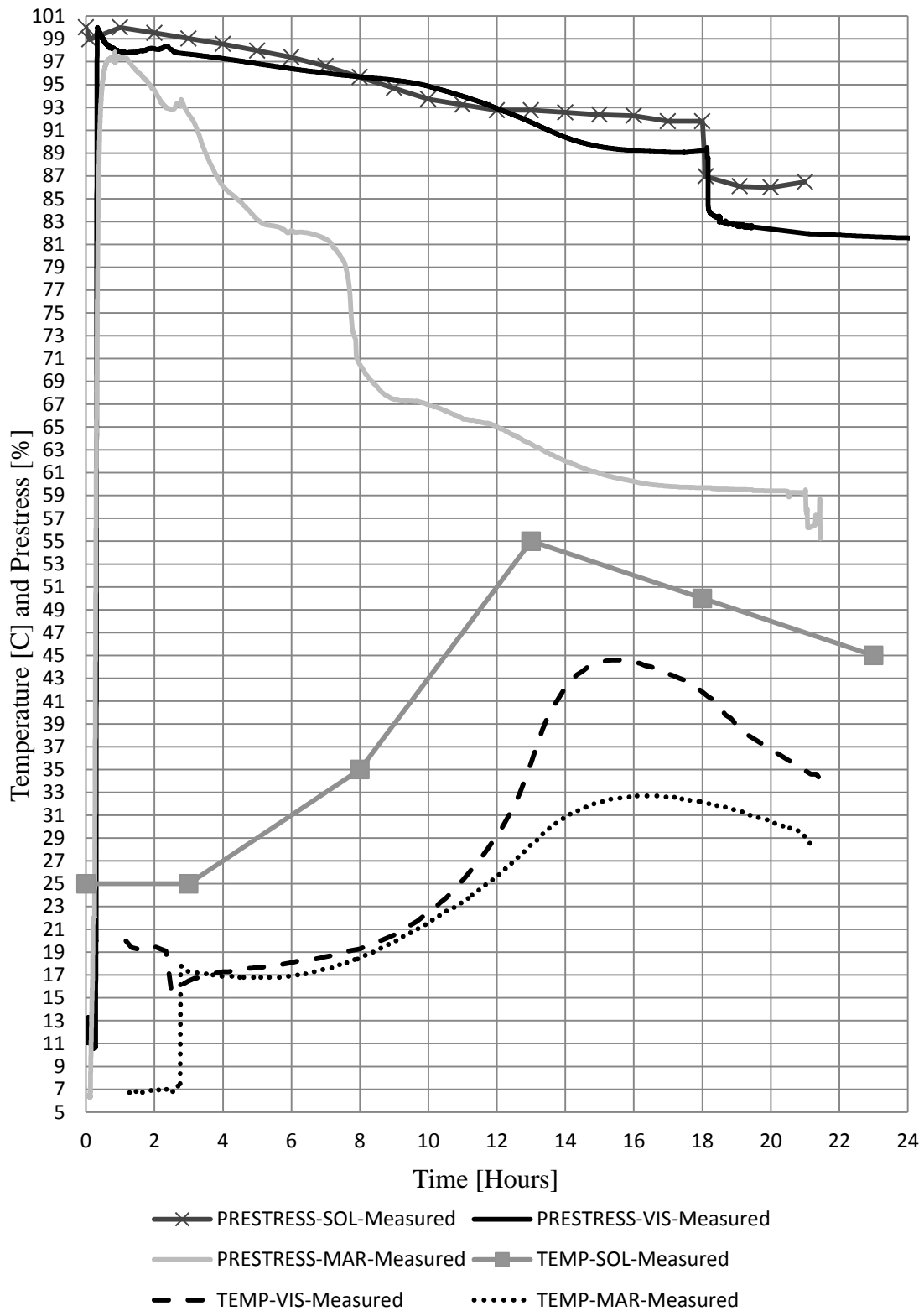


Figure 4.5 Comparison of prestressing force and developed temperature between the factories, during the first 24 hours after casting. Test2 was chosen from Vislanda factory.

Table 4.7

Summary of prestress losses in the factories at different stages.

Factory	Prestress loss in stage 1 [%]	Prestress loss in stage 2 [%]	Prestress loss in stage 3 [%]	Total loss [%]
Vislanda	2	6	7	15
Marijampolé	5	36	4	45
Sollenau	0	8	5,5	13,5

Losses of prestressing force are quite similar for the Vislanda and Sollenau plants, but for the factory in Marijampolé the loss was much more. This can maybe be explained by the low temperature of the surroundings in the Marijampolé factory compared to the others.

The temperature development for the Sollenau factory was only included with very few measurement points in Figure 4.5, due to lack of information. It would have been more accurate to include more readings, in order to get improved understanding of exactly how the temperature develop.

It can be observed in Figure 4.5 that the plant in Sollenau reached its maximum temperature fastest, resulting in a rapid decay of the prestress loss at that point. The same behaviour occurs for the two other plants but the time for the maximum temperature was delayed.

The reduction of the prestressing force after casting until the force was released, stage 2 in Figure 4.1, could not be explained enough; this was an important reason why this master thesis was initiated. In Chapter 5, Development of Finite Element Method, this part was modelled by the Finite Element program DIANA to explain the losses of the prestressing force.

5 Development of Finite Element model

5.1 Introduction

The Finite element program DIANA was used to analyse and model the behaviour of the young concrete sleepers manufactured by using “The Long Line Method”. In order to understand and verify the behaviour of the concrete sleepers during the production, first simplified FE-models were established with different boundary conditions. These models were thereafter gradually updated and verified. Initially the whole casting bed was only modelled as ten meters, to simplify the mesh and the calculations. Later, the real length was introduced, approximately 105-112 meters depending on the factory, with more accurate element and node composition. The design of the sleeper was also simplified; the cross-sectional area was assumed to be constant $0,2 \times 0,2 \text{ m}^2$.

The model was specified during the period from casting of the young concrete to the prestressing force was released. The goal with the FE-model was to establish a sufficient detailed model that captures the behaviour of the young concrete and the steel strands in this stage. The development of the finite element method is explained by verification of thermal- and mechanical properties, which contains the following parameters:

Thermal properties

- Hydration process of the young concrete and heat transfer
 - Adiabatic conditions
 - Semi-adiabatic conditions
- Casting of young concrete in several sequences

Mechanical properties

- Thermal expansion due to constant temperature
- Shrinkage of young concrete
- Development of the E-modulus
- Bond-slip behaviour between young concrete and induced steel strands
 - Bond-slip with prescribed curve
 - Bond-slip depending on maturity

See Chapter 5.3 and 5.4 for the verification of the thermal- respective mechanical properties. Descriptions of the FE-models can be found in Chapter 5.5.

5.2 Element selection

The following subchapter contains descriptions of the specific elements selected to capture the behaviour of and between the various materials used in the models.

5.2.1 Young concrete

The young concrete was modelled with Q8MEM element which is a four-node quadrilateral isoparametric plane stress element, see Figure 5.1.

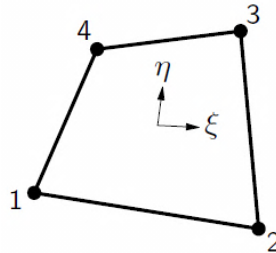


Figure 5.1 Q8MEM element based on linear interpolation and Gauss integration, from DIANA (2008).

The four-node plane stress element creates strains in both x - and y -direction. The strain ϵ_{xx} , is constant in x direction and varies linearly in y direction. The strain ϵ_{yy} works in the same manor: constant in y direction and varies linearly in x direction. The shear strain ϵ_{xy} , is constant over the element area, see DIANA (2008).

In the 1D model the young concrete was modelled with straight two nodes, truss L2TRU element, see chapter 5.2.3 below for an explanation.

5.2.2 Heat transfer

To be able to describe the heat transfer between the young concrete and the surrounding, B2HT, heat flux elements, were added around the Q8MEM elements. B2HT element is a two-node isoparametric boundary element for flow analysis. The two-node straight boundary elements creates a flux q_y perpendicular to the boundary and varying linearly along this boundary, see Figure 5.2.

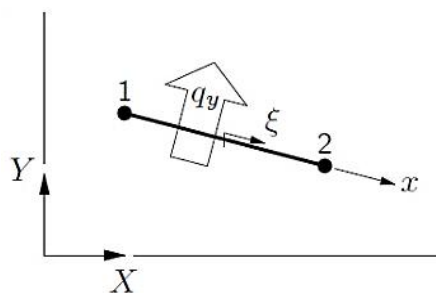


Figure 5.2 B2HT element based on linear interpolation and Gauss integration, from DIANA (2008).

5.2.3 Prestressed steel

The steel strands in the FE-models were modelled with straight, two nodes, L2TRU elements, see Figure 5.3. The L2TRU element is a two-node truss element which is possible to use in one-, two-, and three-dimensional models.

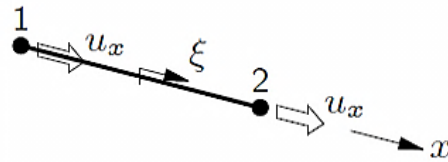


Figure 5.3 The L2TRU two-node element gives a strain, ϵ_{xx} , which is constant along the bar axis, from DIANA (2008).

With the same explanation as for the concrete, B2HT heat flux elements were added between the same nodes as for the truss elements.

5.2.4 Interaction between young concrete and prestressed steel strands

In order to model the heat transfer and the bond-slip between the concrete and the steel strands, the interface elements L8IF and IL4HT were placed between the materials. The L8IF element is a structural interface element in a two-dimensional configuration between two lines, consisting of four nodes. The elements take into account the bond-slip between the materials. IL4HT is a interface heat element which transfer heat.

As Figure 5.4 shows that the local coordinate system, xy , for the displacements, is evaluated in the first node. The element is based on linear integration and by default applies DIANA a three point Newton-Cotes integration scheme, see DIANA (2008).

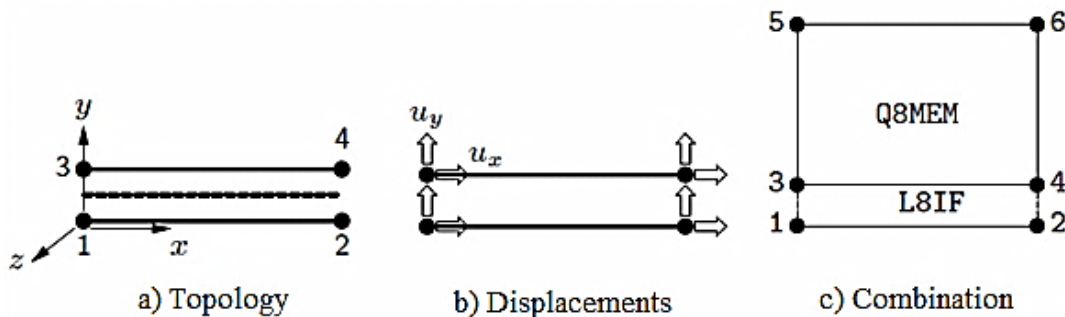


Figure 5.4 Description of topology, displacements and the use of the L8IF interface element, from DIANA (2008).

IL4HT is a potential flow interface element between two lines, see Figure 5.5. As the name illustrates, the element takes into account the heat flow between materials. The element is based on linear interface and describes a relation between the potential difference and the flux. The flux is perpendicular to the interface and varying linearly along this interface, see DIANA (2008).

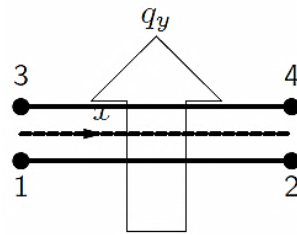


Figure 5.5 Explanation of the IL4HT element, from DIANA (2008).

5.3 Verification of the thermal properties in the FE-model

The following subchapters explain the different verifications made of the thermal properties during development of the FE-model. These thermal properties are described in Chapter 2.1.2.

5.3.1 Input parameters for the thermal analyses

To capture the behaviour of the hardening process of the young concrete and the heat transfer within and between the concrete, prestress steel and the surroundings, different thermal properties are assumed, see Table 5.1. These parameters are chosen according to the literature study in Chapter 2, especially Chapter 2.1.2, and they are used in all the analyses in the verification part.

Table 5.1 Reference parameters of the thermal properties of young concrete and prestressed steel used in the analyses.

Reference thermal parameters	Young concrete	Prestressed steel
Convection coefficient, adiabatic conditions [kJ/m ² s°C]	~1E-200	
Convection coeff., semi-adiabatic conditions [kJ/m ² s°C]	0,002	3,6E-6
Thermal conductivity coefficient [kJ/ms°C]	0,0024	0,05
Coefficient of thermal expansion [x10 ⁻⁶]	80	12
Density, ρ [kg/m ³]	2400	7850
Specific heat capacity, C_p [kJ/kg°C]	1,1	0,460
Thermal heat capacity, $\rho \cdot C_p$ [kJ/m ³ °C]	2640	3611
Cement type	RS	
Ambient relative humidity [%]	50	
Analysis time [hour]	48/24*	

*Depending on the type of analysis, the running time is different.

Table 5.2 shows the boundary conditions on different temperatures used in all the analyses.

Table 5.2 *Temperature boundary conditions used in the analyses, except the models with constant temperature load.*

Temperature boundary conditions	
Initial concrete mix temperature [°C]	25
Initial temperature on the steel strands [°C]	25
Ambient temperature [°C]	25

5.3.2 Hydration process of young concrete and heat transfer

In order to verify the hydration process of young concrete and the heat transfer between the concrete surface and the surrounding, two different models were created; a model with adiabatic conditions and another model with semi-adiabatic conditions. The first case of internal heat of hydration was modelled with adiabatic conditions, which means that there is no heat flux between the concrete surface and the surrounding, all produced heat stays inside the material. The second case was modelled with semi-adiabatic conditions, which means that some of the heat from the hydration was allowed to leave the concrete specimen, see chapter 2.1.2.2 for a more detailed explanation of the mechanisms.

5.3.2.1 Hydration of young concrete with adiabatic conditions

A homogeneous concrete 2D model with fixed ends and constant temperature, casted in one sequence was set up and analysed, see Figure 5.6.

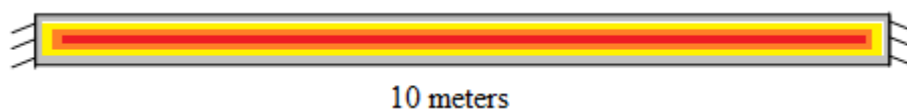


Figure 5.6 *Illustration of internal heat of hydration within the concrete beam with adiabatic conditions.*

The concrete 2D-model was build up with Q8MEM elements, see Chapter 5.2.1. The concrete specimen was given an internal heat of hydration with adiabatic temperature conditions for a slow hardening concrete, received from DIANA (2008), see Figure 5.7. Thermal material data were added to the Q8MEM elements in form of conductivity, convection, capacitance and adiabatic temperature time dependent for the young concrete, etc., see Table 5.1 for the thermal parameters assumed for the young concrete. Non-linear FE-analysis was used because the heat of hydration varied with time.

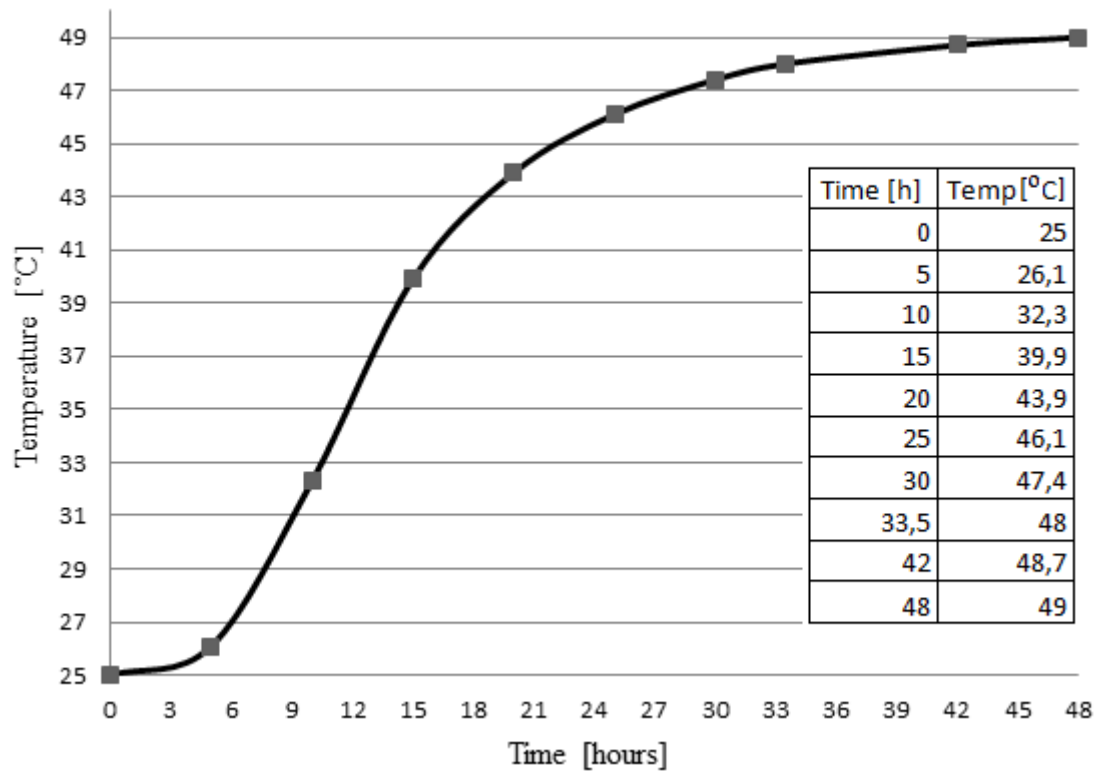


Figure 5.7 Adiabatic temperature conditions for a slow hardening concrete used as input value in DIANA, from DIANA (2008).

5.3.2.2 Hydration of young concrete with semi-adiabatic conditions

To obtain a more realistic behaviour of the model, heat flux was added between the concrete surfaces and the surrounding, which correspond to semi-adiabatic conditions. B2HT element was chosen around the models to capture the external load, in case of ambient temperature, because it works as a transfer zoon of heat flux, see Chapter 5.2.2.

FE-models in DIANA with semi-adiabatic behaviour can be made in three different ways. Either by direct input of the produced heat as a function of degree of reaction to simulate the heat production, with additional information about the parameters of thermal properties for the young concrete such as conductivity, capacitance and convection. Or instead, by deterring the temperature time dependent development from an adiabatic calorimeter test, pre-processing from the adiabatic curve, with additional parameters of thermal properties. Or else, by user-supplied subroutine see DIANA (2012). Two different cases with various semi-adiabatic conditions were performed and analysed, the first consisted of heat flux out from all the concrete surfaces, see Figure 5.8.

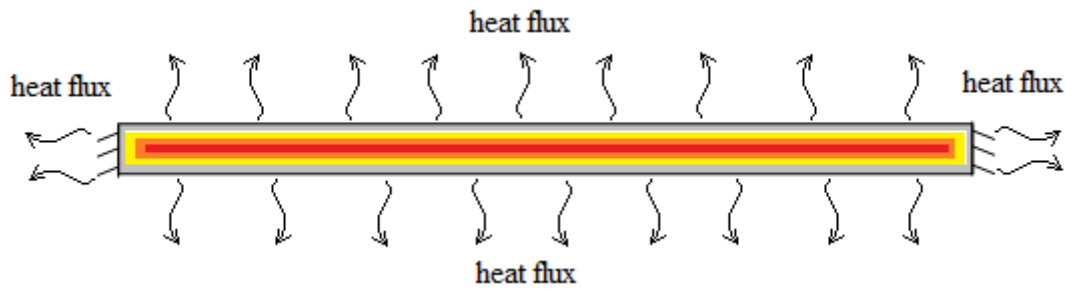


Figure 5.8 Internal heat of hydration within the beam with heat flux out from all four surfaces, semi-adiabatic conditions.

In the second case, heat flux was only allowed to be transferred from the top surface, see Figure 5.9, which is similar to the actual conditions in the sleeper production due to surrounding moulds.

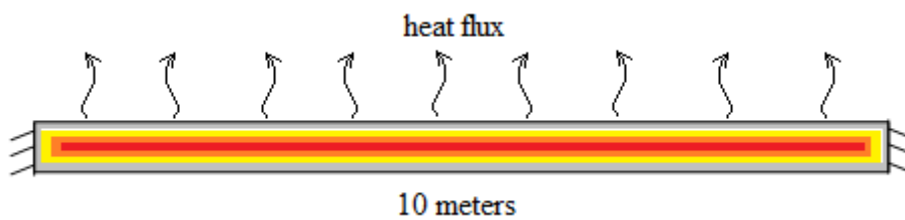


Figure 5.9 Internal heat of hydration with heat flux out from the top surface which is attached to the surrounding, semi-adiabatic conditions.

5.3.2.3 Results and comparisons between the thermal models

Thermal analyses have been made on the different models explained above. For all cases, except semi-adiabatic condition with heat flux out from the top surface, the results shown are from the center node in the middle of the length and height of the concrete beam. As Table 5.1 specifies, the initial temperature of both the concrete mix and the surrounding temperature was 25°C.

Figure 5.10 shows the results between hand calculations and input- and output values in DIANA of the temperature development during 48 hours with adiabatic conditions. The output temperature was given with different initial degree of reaction, DGR, 1% and 0,01%. The output temperatures with 1 % initial degree of reaction corresponds better to the inserted adiabatic temperature in DIANA compared to the hand calculated temperatures and the output temperatures with 0,01%. But all curves reach the same maximum temperature, around 49°C, which verifies that the model with adiabatic conditions, no heat fluxes out from the specimen, conforms to its desired behaviour. Unfortunately, very low initial DGR results in misaligned output temperatures from DIANA in form of delayed temperature evolution, compared to the given temperatures.

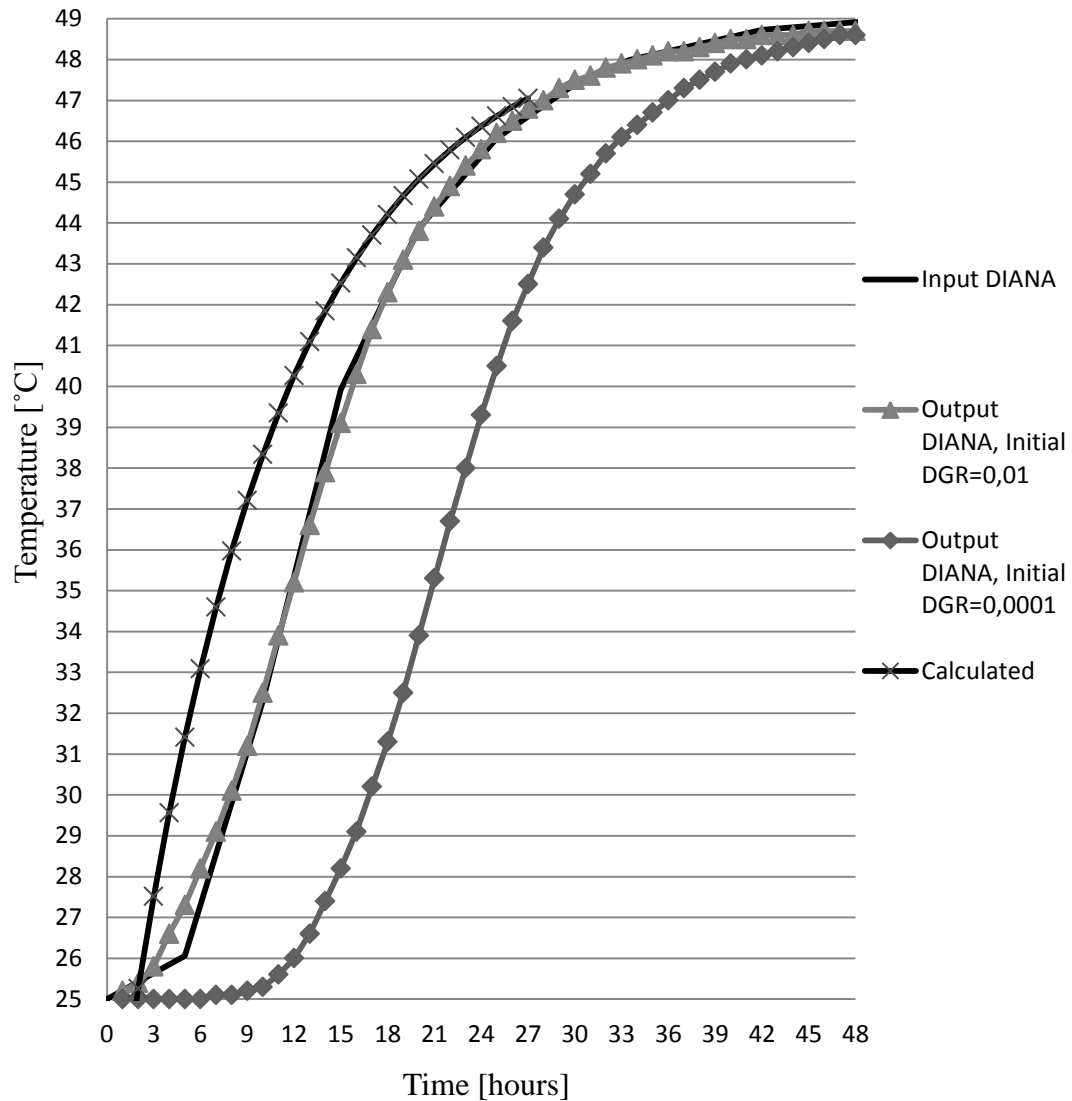


Figure 5.10 Comparison of hydration process with adiabatic conditions between input-, output- and calculated temperatures. The output temperature has been analysed with two different initial degree of reaction, DGR.

In the semi-adiabatic case, the convection coefficient was further changed from a negligible value to 0,002 kJ/m²s°C. This resulted in temperature losses within the concrete specimen. The two different cases of semi-adiabatic conditions, heat flux from all surfaces and heat flux from only the top surface, compared with the adiabatic conditions with 1 % DGR from Figure 5.10 can be seen in Figure 5.11.

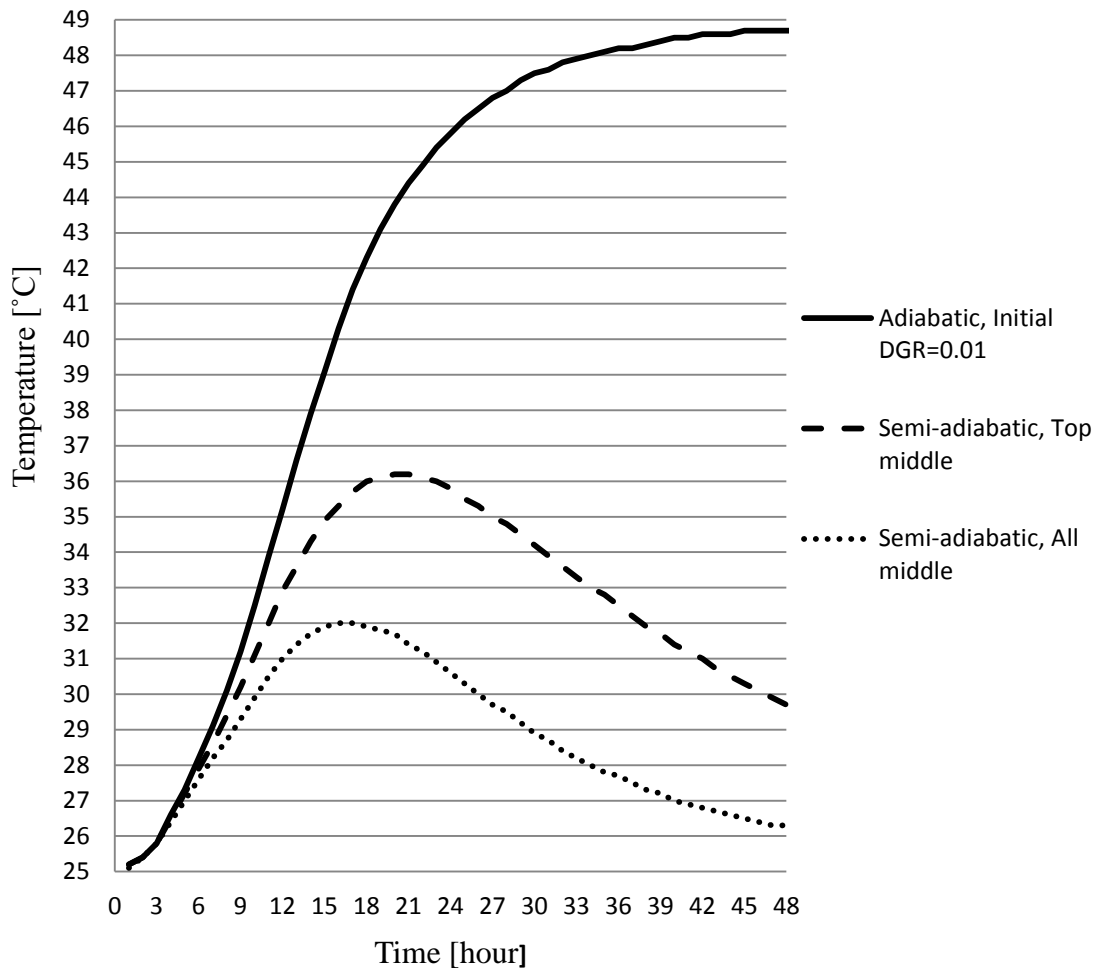


Figure 5.11 Comparison of temperature development between the adiabatic condition with initial degree of reaction, *DGR*, of 1% and semi-adiabatic conditions with heat flow out from all surfaces and heat flow from only the top surface.

The results from the comparison between all the three cases in Figure 5.11 was as expected, the temperature decreases when heat is allowed to be transferred from the concrete beam. If heat flux is prevented out from some surfaces, as in the case with only heat flux out from the top surface, the temperature increased compared to fully permitted heat flux. Consequently, the adiabatic and semi-adiabatic conditions are verified.

Figure 5.12 and Figure 5.13 illustrates 2D contour plots of the temperature development within the concrete specimen during several time steps of the two different cases of semi-adiabatic conditions, heat flux from all surfaces and heat flux from only the top, respectively.

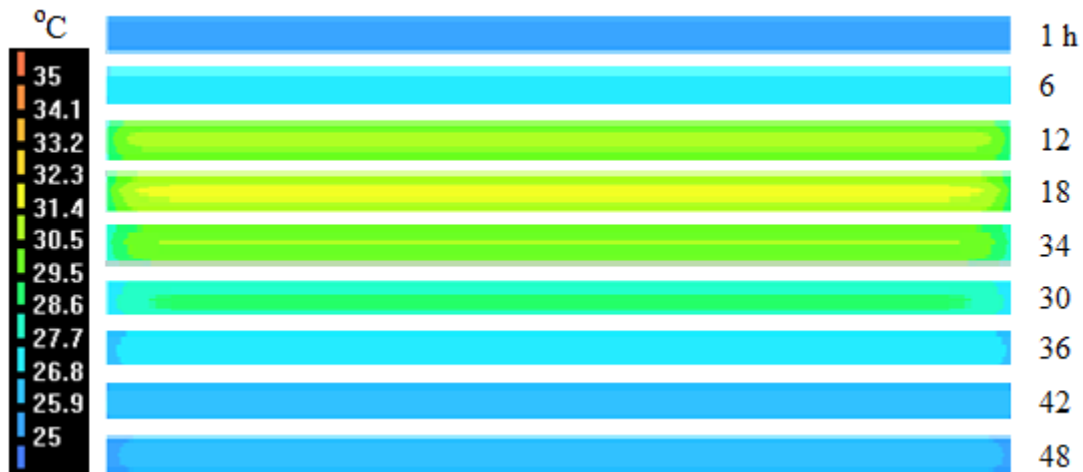


Figure 5.12 2D Contour plot of the temperature development within the young concrete specimen in Figure 5.8, with semi-adiabatic conditions and heat flow out from all surfaces.

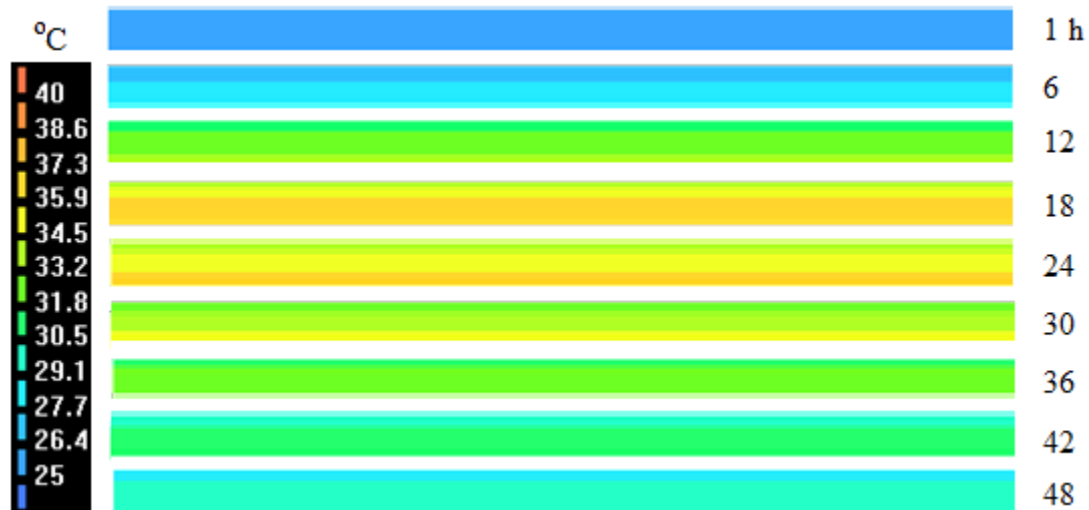


Figure 5.13 2D Contour plot of the temperature development within the young concrete specimen in Figure 5.9, with semi-adiabatic conditions and heat flow out from only the top surfaces.

The differences between the two semi-adiabatic conditions, heat flux out from all surfaces and only from the top surface, can be obtained if Figure 5.12 are compared with Figure 5.13. The differences are obvious, the temperature decreases near the top surface and increases over the height for the case with heat flux out from only the top surface. In the other case, heat flux out from all surfaces, decreases the temperature along all the surfaces and the heat loss is greatest in the longitudinal direction. These seem to be reasonable and heat flux in the different models works as it should.

Results of temperature development over time with semi-adiabatic condition and heat flux out from only the top surface can be seen in Figure 5.14 below. It contains of results from three different nodes placed in the middle of the length of the concrete beam at top surface, middle part and at the bottom surface of the height. Due to heat flux from the top surface, the temperature decreased with the height of the concrete beam.

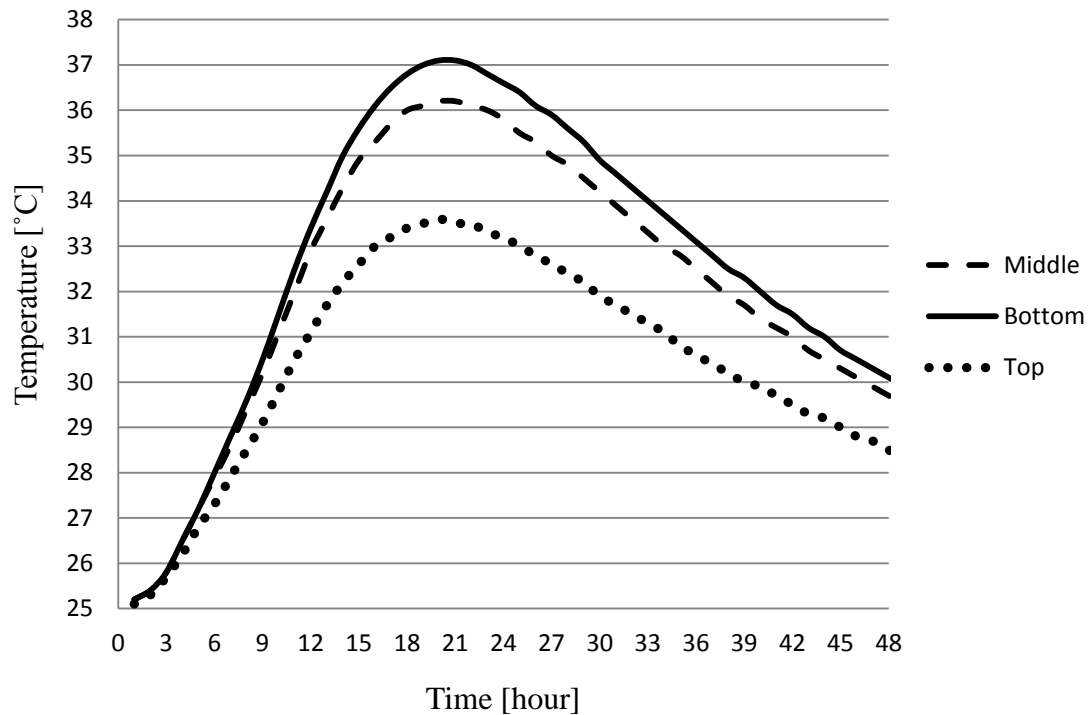


Figure 5.14 Comparison between the temperature development in the top-, middle- and bottom part of the young concrete specimen in Figure 5.9, especially in Figure 5.13, with semi-adiabatic conditions and heat flow out from only the top surfaces.

5.3.3 Casting of young concrete in sequences

The FE-model was further updated to increase the suitability in relation to the actual production process and to verify the behaviour when casting in several sequences. The FE-model with semi-adiabatic conditions with heat flux out from only the top surface, in chapter 5.3.2.2, was used and separated into two equally casting sequences, see Figure 5.15.

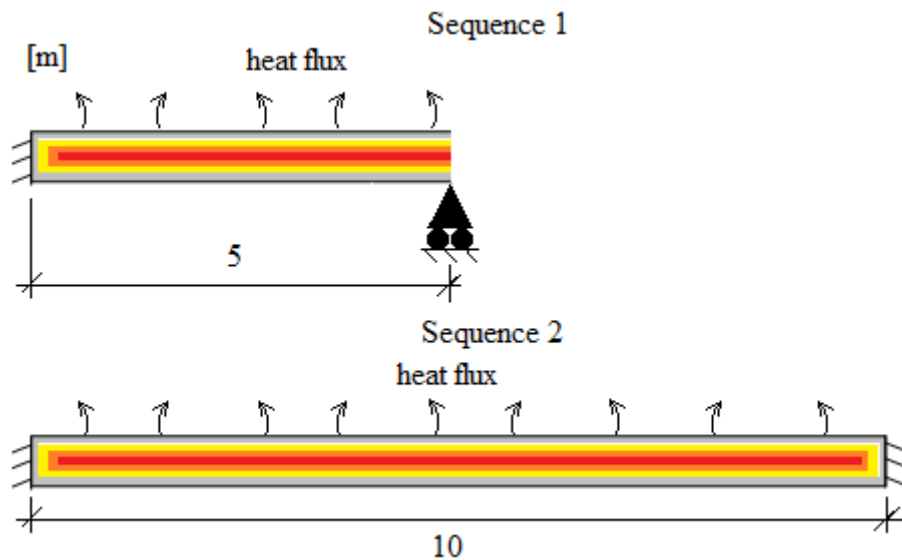


Figure 5.15 Illustration of casting of the concrete in two equal sequences with semi-adiabatic condition with heat flux from only the top surface.

The first casting sequence, half of the bed, was assumed to take one hour and the second sequence started after the first one was finished and continued until the end of the running time.

5.3.3.1 Results

Figure 5.16 illustrates the difference in the temperature development along the concrete specimen when casting in two separate steps.

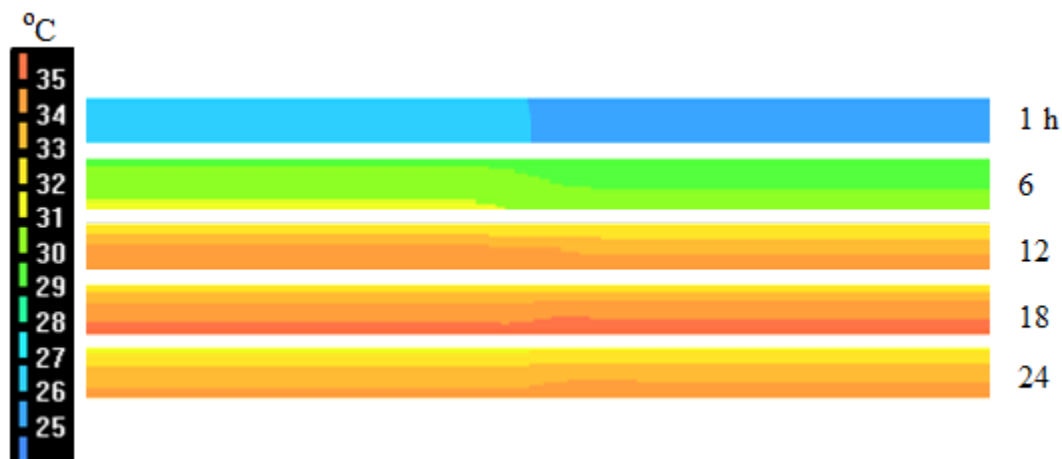


Figure 5.16 Result of casting of concrete in two sequences depending on time according to Figure 5.15 above. The second sequence was casted 1 hour after the first, then was the model analysed in 24 hours.

The temperature development was delayed in the second case, which caused a temperature exchange in between the sequences. Comparing to the case when casting the concrete at the same time, see Figure 5.13, the temperature was not constant along the concrete length in the sequence case. In the first hours after casting the temperature in the first sequence was larger at the bottom part of the height and less at the top sur-

face, see the sixth and twelfth hour after casting in Figure 5.16. But after 24 hours the situation was reversed; this can be explained by the delaying of the temperature development combined with the heat loss from top surface. Around the twentieth curing hours the first sequences reached its maximum temperature, thereafter the temperature decreased according to Figure 5.11. Consequently, the maximum temperature in the second sequence was delayed one hour, the variation of the temperature development along the length of the concrete specimen was therefore affected.

This behaviour seems to be correct and casting in several sequences in the FE-program DIANA was thus verified, see Appendix B.1.2 for the input data file in DIANA.

5.4 Verification of the mechanical properties in the FE-model

This section describes the different verification of the mechanical properties, included in the FE-model, that have been made.

5.4.1 Input parameters to the mechanical analyse

Table 5.3 shows the mechanical properties of the young concrete and prestressed steel that were used in the FE-analyses in DIANA.

Table 5.3 Reference parameters of the mechanical properties of young concrete and the prestressed steel used in the analyses.

Reference mechanical parameters	Young concrete	Prestressed steel
E-modulus, 28 days [GPa]	38	205
Poisson's ratio [-]	0,2	0,3
Compressive strength, 28 days [MPa]	73	
Tensile strength, 28 days [MPa]	5,5	
Bond-slip value with full interaction [MPa/m]	785E5	
Bond-slip with maturity, D-stiff [MPa/m]	7.85E-3	
Initial steel stress [GPa]		1400
Number of steel strands		14
Number of steel wires in one steel strand		3
Total number of steel wires		42
Diameter of one steel strand [m]		0,00163
Thickness [m]	0,05/0,2*	0,00008764**
Thickness of interface element between concrete and steel [m]	0,129***	
Notional size [m]	0,1	

*The thickness for the concrete was inserted in DIANA as the thickness of the concrete, 0,05 for the maturity and E-modulus verifications else 0,2.

**The thickness for the prestressed steel was inserted in DIANA as the total area of the prestressed steel strands.

***The thickness of the interface element was calculated as the total perimeter of all the steel strands in the sleeper currently produced in Vislanda, see Appendix A.1 for the calculation.

5.4.2 Thermal expansion due to constant temperature

Thermal expansion due to constant temperature should follow the relation in Equation 2.27, presented in Chapter 2.1.3.3.

To check the need for thermal expansion of concrete and steel strands during constant heating, four different models were created and studied. The first two models consist-

ed of a homogenous concrete specimen, the third consisted only of steel strands and the fourth was a model with full interaction between concrete and steel strand, see Chapter 5.4.2.1, 5.4.2.2 and Chapter 5.4.2.3 respectively. In the first three cases the conditions for the steel strands and the concrete were the same; restrained ends, length of 10 meters, constant external temperature load of 45 °C, initial temperature of 0°C, except the coefficient of thermal expansion, CTE, which was set to different values for concrete and steel. For the fourth case, the model was analysed with hydration process, semi-adiabatic conditions, with heat flux out from only the top surface.

5.4.2.1 Fixed homogeneous concrete specimen

A homogeneous concrete member casted in one sequence was firstly modelled. Two different FE-models were set up and analysed, one-dimensional model with truss bar element, L2TRU, and a two-dimensional model with quadrilateral isoparametric plane stress element, Q8MEM. To capture the real behaviour of external temperature both models were modelled with surrounding two-node isoparametric boundary flow element, B2HT, see Figure 5.17. The CTE for young concrete was assumed to be $80 \mu / ^\circ\text{C}$.

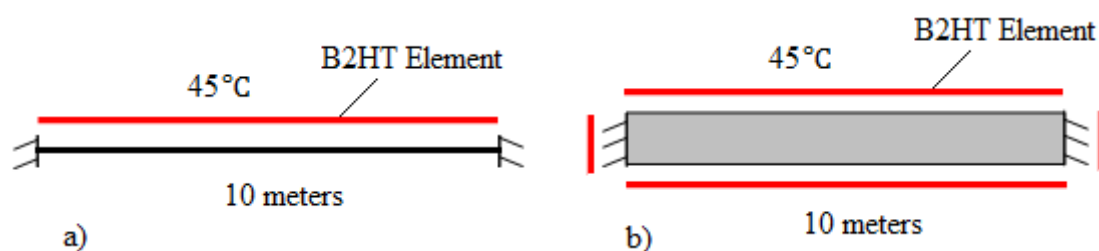


Figure 5.17 Illustration of the homogenous concrete beam casted in one sequence with constant temperature load on B2HT elements and fixed ends, a) 1D model b) 2D model.

Results and comparison between the 1D and 2D models

To capture the behaviour of the models and to verify the results; strains and displacements were given along the beam as an output from the 1D and 2D models.

The strains and displacements were constant along the concrete beam for the 1D model case. This is correct since the model had linear material behaviour, E-modulus was constant, with constant load, ΔT and CTE were constant. The strains and displacements were zero in the 1D model. This can be explained by the boundary conditions; the model was restrained in the end nodes in x- and y-direction and thus did not allow any displacements. The compressive stress-independent strains that occur in the concrete beam due to temperature load and restraint was constant 136,8 MPa. This value can be perceived as very large, but in fact it is due to large temperature increase of 45°C, large value of the CTE of the young concrete and restrained ends.

Regarding the 2D model the stresses and strains were constant along the beam as in the 1D model case. The displacements were almost constant zero along the length in x- and z-direction, but vary along the length in y-direction. This was because the 2D model was fixed in all the outermost nodes of the beam in x-direction but only fixed in one position in y-direction. Therefore the beam could deform in y-direction be-

tween the two outermost nodes, but the displacement was very small. The magnitudes of the compressive stresses in x-direction are same as in the 1D model case i.e 136,8 MPa. The strains in the x-direction were zero (same as in the 1D model) but were 3,6e-3 in y-direction, because it was free to move in y-direction. See Appendix B.2.1.1 and Appendix B.2.1.2 for the input data files in DIANA regarding the 1D- and 2D model respectively.

Verification of the model were also made hand calculations, which agree with the results from FE-analysis, see Appendix A.4.

5.4.2.2 Fixed steel strand

A similar verification as for the homogeneous concrete specimen was also made for a fixed steel strand. Two 1D models with truss elements, L2TRU, with constant temperature load of 45°C were analysed. One model with no initial stress and another with initial stresses, σ_{si} , of 1400 MPa, see Figure 5.18. The CTE for the steel strand was assumed to be 12 μ /°C, which correspond to high strength low-alloy steel.

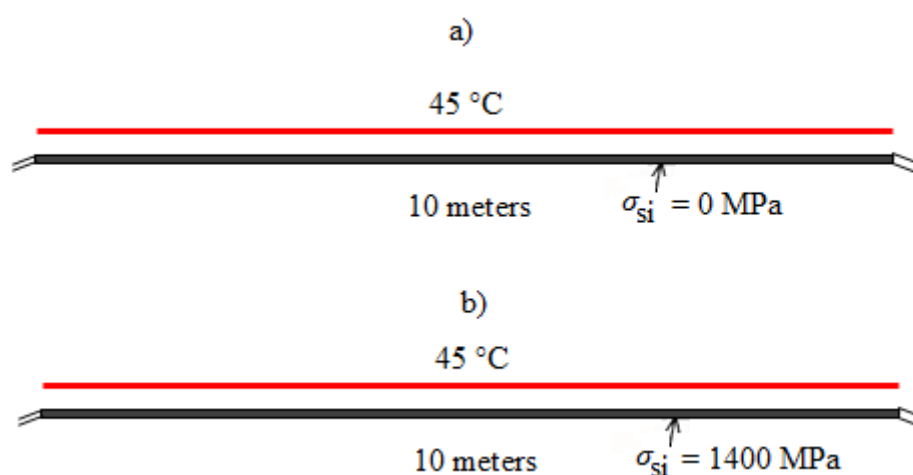


Figure 5.18 Illustration of fixed steel strand with temperature load of 45 degrees and a) no initial stress b) Initial stress, σ_{si} , of 1400 MPa.

Simplification regarding the arrangement of the steel strands in a concrete sleeper was made. The carefully selected positions of the fourteen steel strands³ used in Vislanda, were assumed to be at the same place and represented as only one strand consisting of the same cross-section area as the fourteen steel strands, see Table 5.3 and Appendix A.4 for the hand calculation made on the steel strands. The steel strands were also assumed to have linear elastic behaviour, see Figure 5.19.

³ One steel strand consists of three steel wires with a diameter of 3,0 mm each.

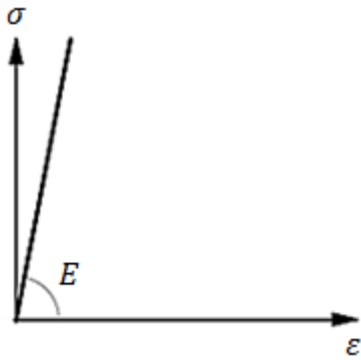


Figure 5.19 Illustration of linear elastic stress-strain relation for the steel strand in FE-analyses, from DIANA (2008).

Results

Due to temperature increase and restrained ends, the steel stress became 110,7 MPa compression for the model without initial stress and 1289,3 MPa for the model with initial stress.

This seems to be correct since the loss of steel stress of the model with initial stress corresponds to the stress increase of the model without initial stress. The same result was obtained in the hand calculations, which verifies the accuracy of the models.

5.4.2.3 Full interaction between concrete and induced steel strand

To verify the interaction between the concrete and the steel strand during heating two different models was set up. The first model consisting of a temperature load of 45°C and the other consisting of heat development assuming semi-adiabatic conditions with heat transfer from the top surface. Steel strands with fixed ends were added in the middle of the young concrete cross-section and additional steel parts of half a meter were also added in both ends of the model. In both models the concrete was cast in one sequence and the bottom surface of the concrete specimen was restrained to prevent expansion of the young concrete in that part, due to the mould. Furthermore full interaction between the concrete and the steel was assumed and fixations of the concrete ends were deleted to allow expansion, see Figure 5.20 for the geometry and boundary condition of the models.

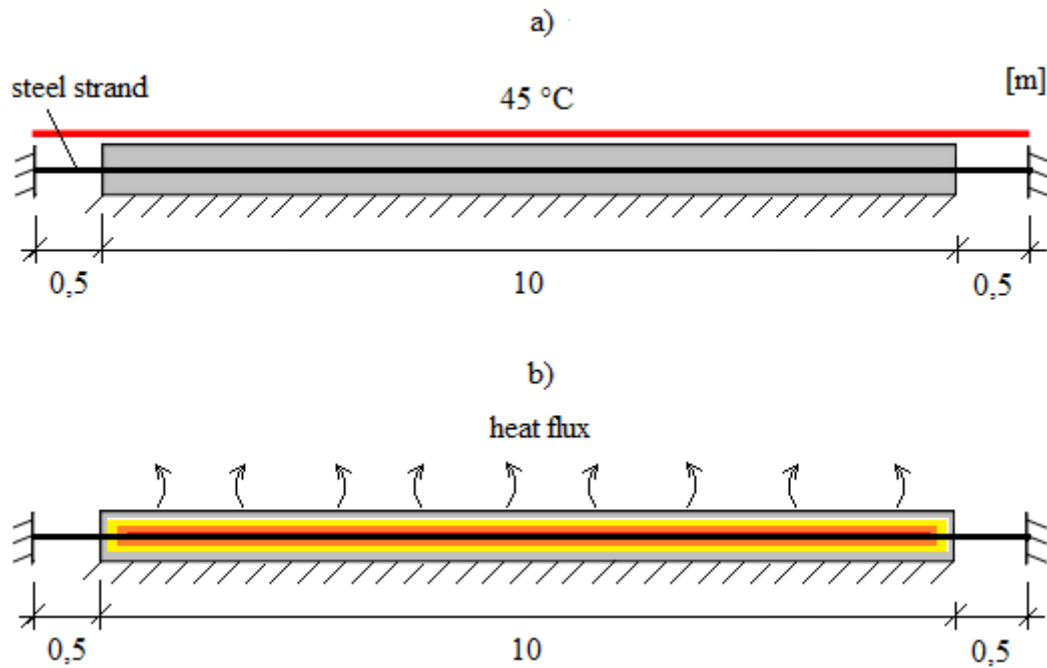


Figure 5.20 Illustration of full interaction between the concrete and the induced steel strand with fixed ends, consisting of a) temperature load of 45 degrees b) heat development assuming semi-adiabatic condition with heat flux from only top surface. The bottom surface of the concrete was also supported for deformations in vertical direction for the two cases.

Results and comparison

The steel stresses and the concrete stresses along the length of the model with constant temperature load can be seen in Figure 5.21 and Figure 5.22 respectively.

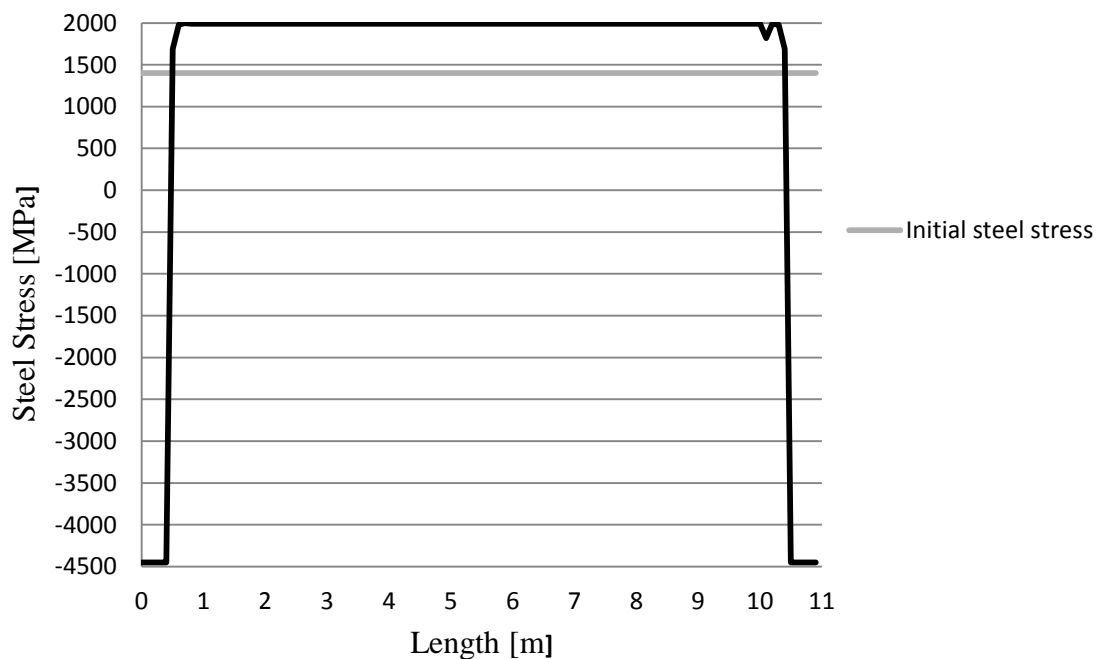


Figure 5.21 Stresses in the prestressed steel along the length for the case with constant temperature load of 45 degrees, according to Figure 5.20a.

As Figure 5.21 shows, the stresses in the steel strand increased inside the concrete, while the stress in the naked steel strands at the ends decreased significantly. The phenomena can be explained by the differences in the CTE values between the materials. The CTE value of the young concrete is greater than the CTE value of the prestressed steel, which causes a larger expansion of the young concrete when the constant temperature load applies and pulls the prestressed strand due to full interaction between the materials. Consequently, the initial tensile stresses increases in the cast in steel strand, while the naked steel strands are subjected to huge compression due to full interaction between the materials. In other words, the naked steel strands can be seen as compressed. The size of the stresses in the steel strand within the concrete can be explained by full interaction between the materials to early and the sizes of the CTE values.

A small error occurred in the analysis which can be seen in the concrete element at approximately 9,5 meters in Figure 5.21 and Figure 5.22. Causes are unknown but probably due to equilibrium condition in the model.

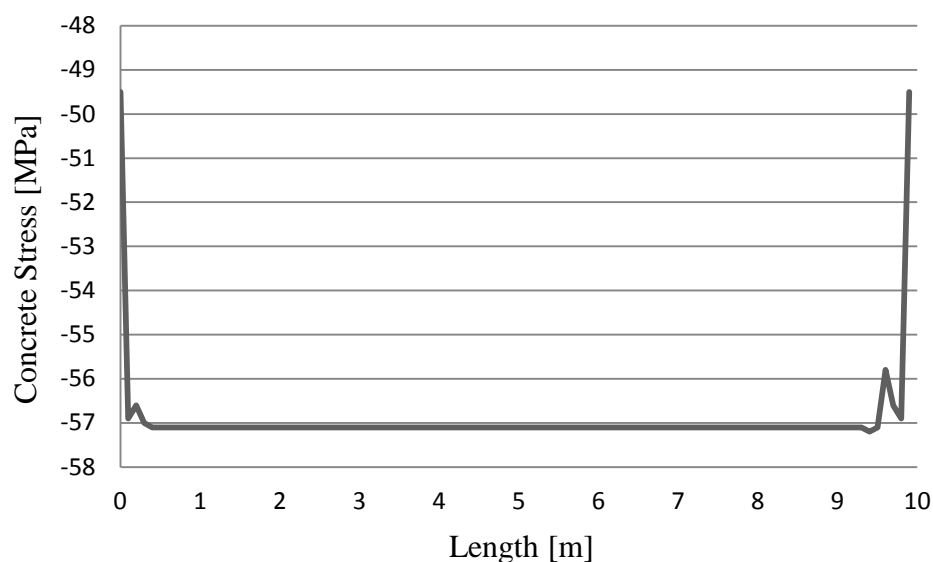


Figure 5.22 Illustration of concrete stress along the length of the concrete specimen for the case with constant temperature load, according to Figure 5.20a.

As Figure 5.22 illustrates, the concrete is subjected to a compressive stress of 57 MPa almost constant along the length, except the ends of the concrete specimen which decreased. The size of concrete stress seems to be reasonable since the case with only concrete and fixed ends, see Chapter 5.4.2.1, had a compressive stress of 136,8 MPa.

Regarding the model with heat development with semi-adiabatic conditions and heat flux out from the top surface, the result of the steel stress along the length of the model during 24 hours after casting can be seen in Figure 5.23. The stresses of the cast in steel increases during the first time steps, and then after slightly decreases a bit after 18 hours. The stresses in the naked steel strands decreases up to 18 hours, then increases.

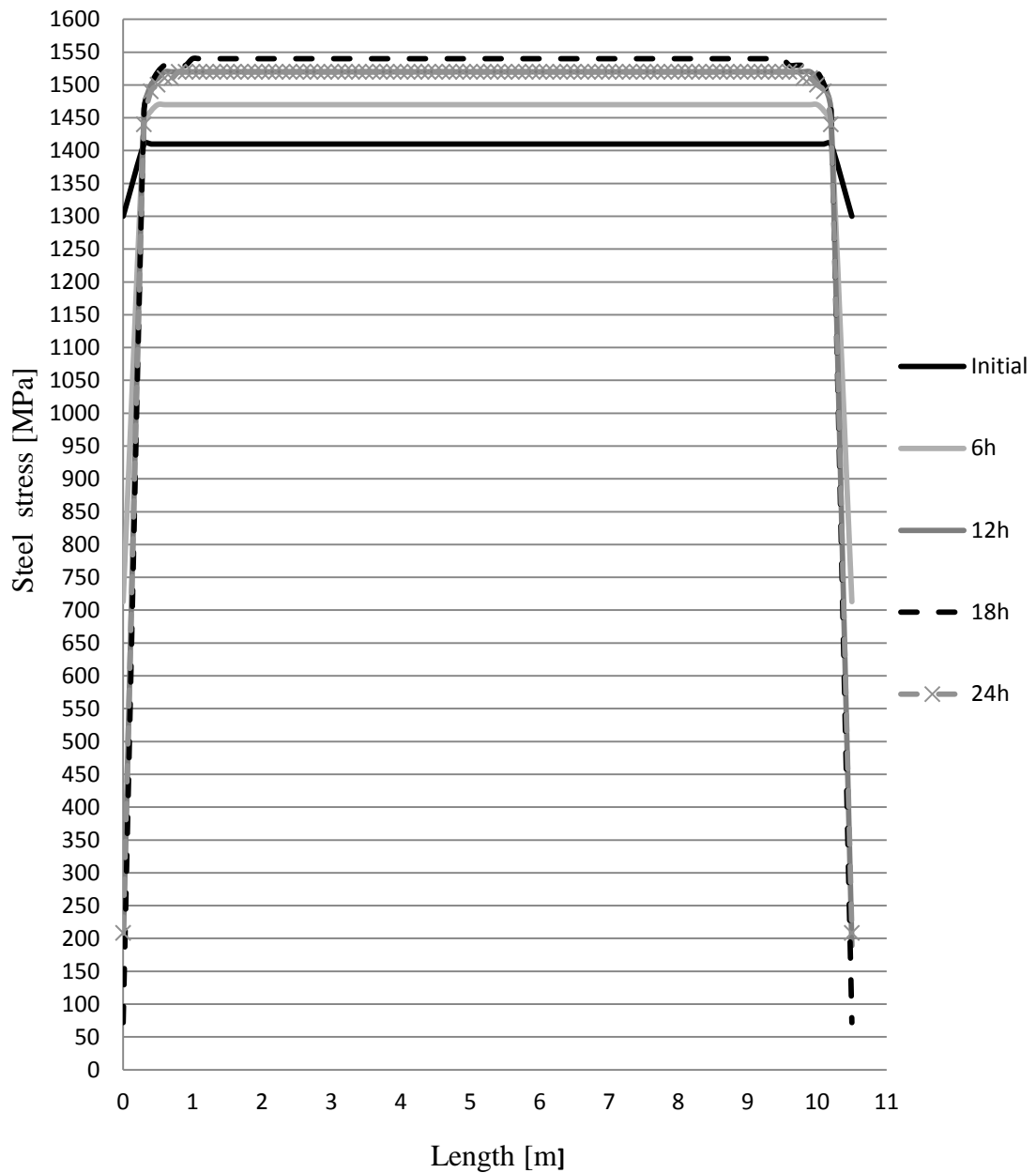


Figure 5.23 Stresses in the steel strand along the length during 24 hours.

Figure 5.24 and Figure 5.25 below illustrates the stresses in the upper and lower part of the concrete, along the length after 6, 12, 18 and 24 hours. Concrete stresses are higher in the lower elements due to fixation of the bottom surface in vertical direction.

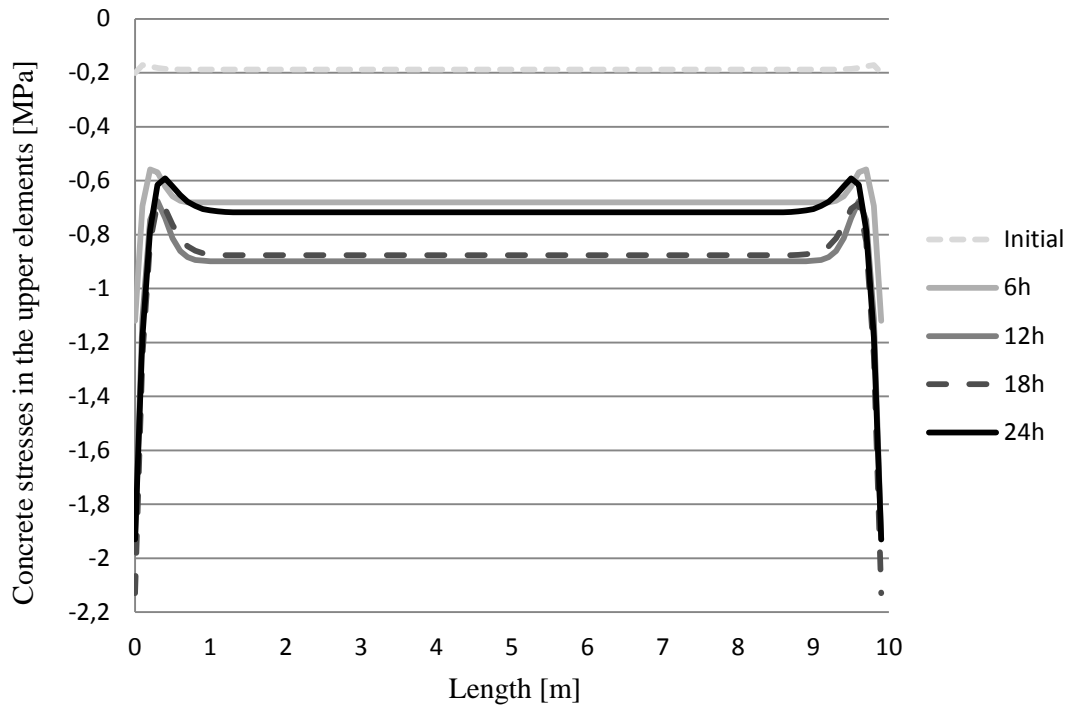


Figure 5.24 Concrete stresses in the upper element along the length of the concrete specimen during 24 hours.

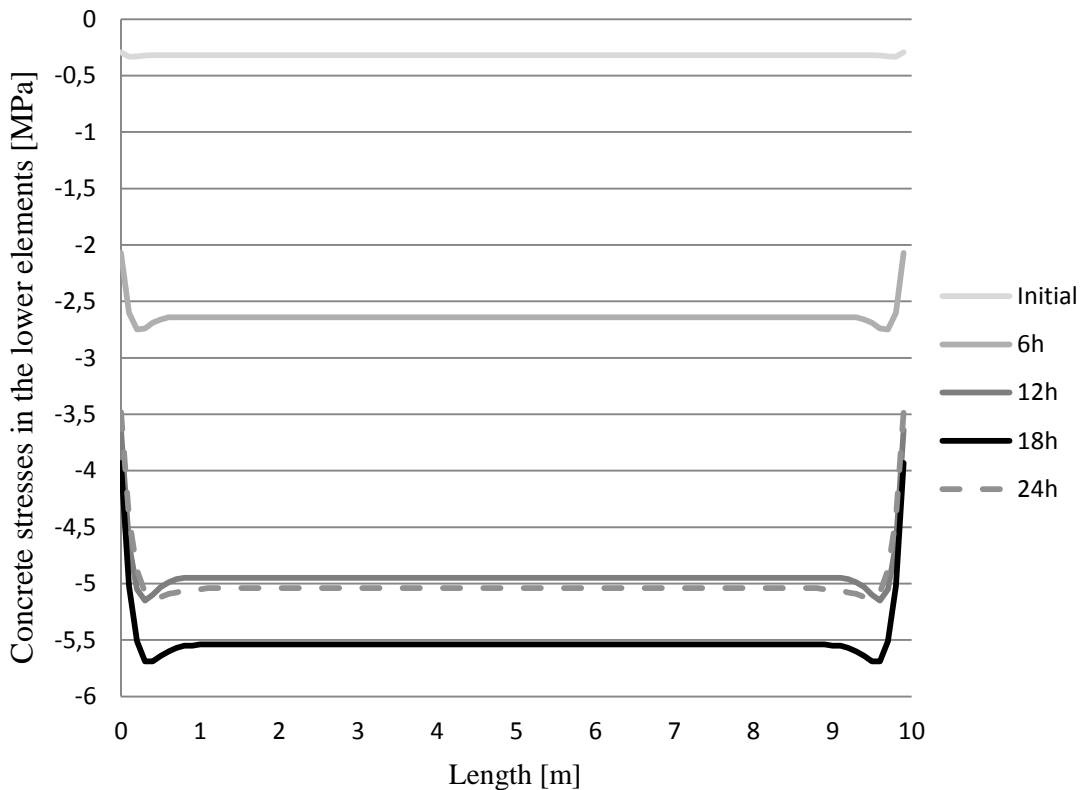


Figure 5.25 Concrete stresses in the lower element along the length of the concrete specimen during 24 hours.

Comparison of the steel and concrete stresses between the models shows that the stresses are higher for the case with constant temperature. This can be explained by

the greater temperature difference of 45°C in the constant temperature case due to no temperature of the surroundings. When heat development occurs, the temperature difference is only around 20°C, due to 25°C of the surroundings and maximum temperature of approximately 45°C.

5.4.3 Shrinkage of young concrete

The same model used in Chapter 5.4.2.1, especially Figure 5.17b, was further used to verify the influences of shrinkage effects during the first 24 hours after casting, see Figure 5.26 for the initial conditions of the model used in the FE-analyse. For the shrinkage analysis, the compressive strength, notional size, cement type, relative ambient humidity, and curing time are needed, see Table 5.3 and Table 5.1 for these values.

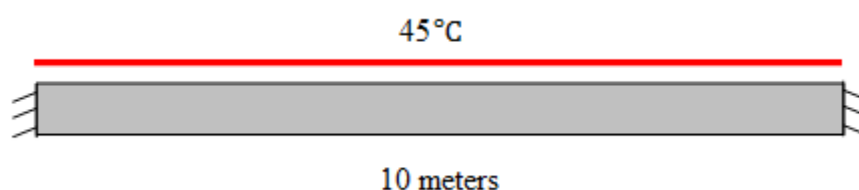


Figure 5.26 Concrete specimen with temperature load of 45 degrees and shrinkage effects according to DIANA.

5.4.3.1 Results

The result from the FE-analyse in DIANA showed that the stress in the concrete was the same, 136,8 MPa, as the case when shrinkage was not included, see Chapter 5.4.2.1. Additional hand calculations on the shrinkage effects according to both Eurocode 2 and CEB FIB Model Code 1990 have also been made. The results showed almost the same result as the FE-analysis, very small strains occurred due to shrinkage during the first 19 hours after casting. According to CEB-FIB Model Code 1990 (used in DIANA) the prestress loss was around 0,02 % in the factories, which can be seen as negligible in comparison to the strains from the temperature increase. Consequently, shrinkage effects do not affect the stresses to any larger extent during the first 19 hours after casting and can be seen as negligible. Same assumption was made in Eurocode 2 for shrinkage of concrete during heat curing. However, the results from hand calculation of shrinkage effects according to Eurocode 2 showed a prestress loss between 0,34 – 0,39 % in the different factories, during the first 19 hours after casting, which also can be seen as negligible, see Appendix A.3 for the hand calculation and Appendix B.2.3 for the input data file in DIANA made on the shrinkage effect.

5.4.4 Development of Young's modulus of elasticity

To verify the development of the modulus of elasticity during the hardening process, a quadratic model was constructed, consisting of Q8MEM elements with dimensions 0,05x0,05 meters. The model was exposed to prescribed compression forces, F , at the top nodes, which was increased stepwise up to 100 N, afterwards the displacement was measured. To capture the increase of the young concrete hardening, three differ-

ent cases were analysed: 1 hour, 10 hours, and 48 hours after casting. The right hand side surface of the model was restrained for deformations in longitudinal direction and the bottom surface was fixed in vertical direction, see Figure 5.27.

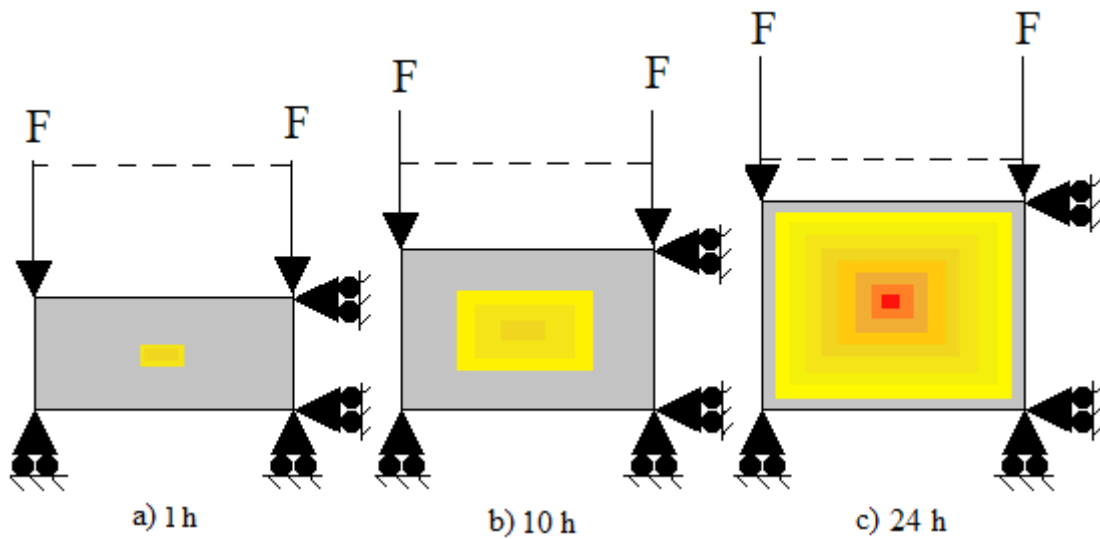


Figure 5.27 Illustration of three different loading tests made on the young concrete specimen with certain boundary conditions. Forces, F , of 100 N were placed at the two top nodes. The models were tested after a) 1 hour b) 10 hours and c) 24 hours after casting.

As mentioned in Chapter 2.1.3.1, the evolution of Young's modulus of elasticity can be calculated according to CEB-FIB Model Code 1990 or Reinhardt Model, see Equation 2.21a and 2.22a respectively. To include this in the FE-model in DIANA, visco elasticity must be assumed and Double Power Law has to be activated, see DIANA (2008).

5.4.4.1 Results

The results were as expected. The modulus of elasticity of the young concrete increased with time, due to the hardening process of the concrete. Figure 5.9 shows the results from the load-displacement tests made in DIANA at three different times after casting, which illustrates the development of the E-modules with time due to increasing of the slope of the curves with time.

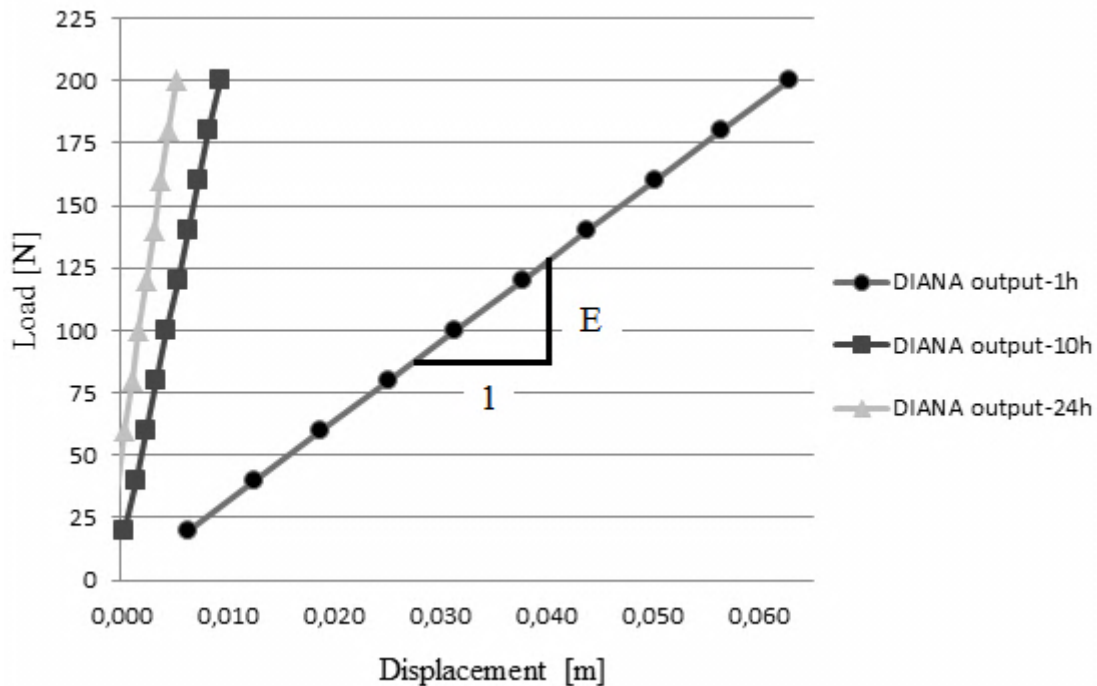


Figure 5.28 Load-displacement curves of outputs from DIANA at three different times after casting. The different slopes illustrates that the E-modules increased with time.

To verify that the results of the young modulus of elasticity from DIANA corresponds to the actual developing of E-modulus of young concrete, a comparison was made between calculations of the E-modulus with equivalent time according to CEB-FIB Model Code 1990 and the results from DIANA, see Figure 5.29.

As Figure 5.29 shows, results from DIANA and hand calculations are consistent. Thus, the development of the E-modulus of the young concrete is verified to work correctly in the FE-program DIANA. See Appendix A.1 for the hand calculation and Appendix B.2.4 for the input data file in DIANA.

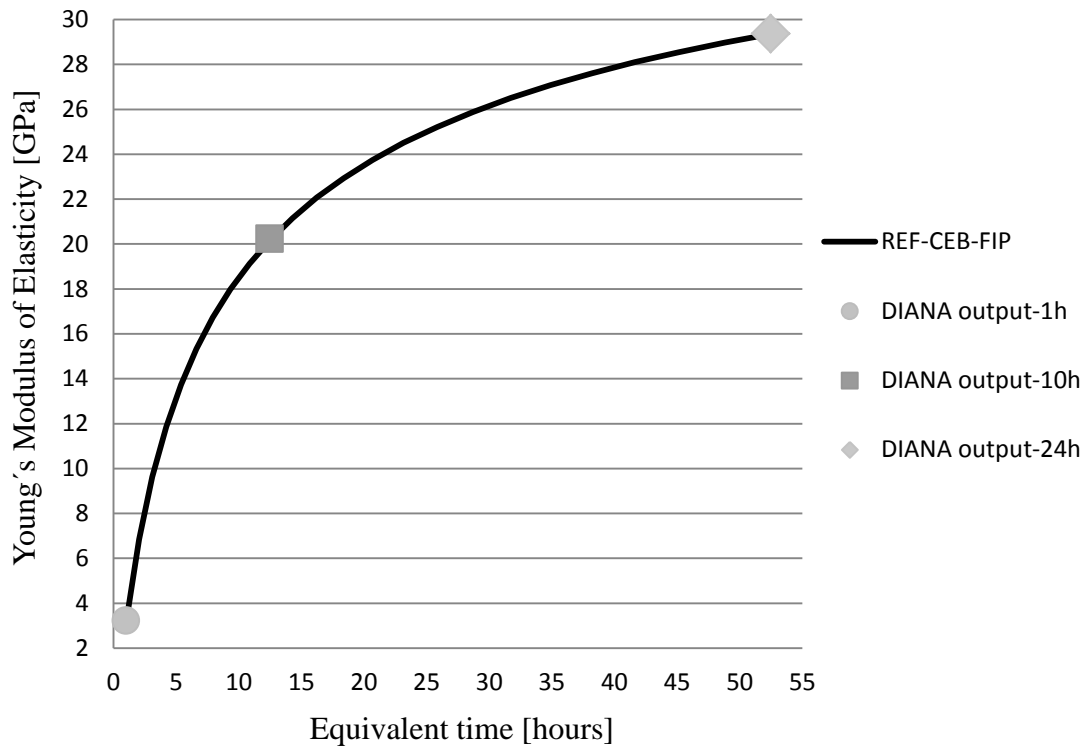


Figure 5.29 Comparison of the E-modulus with equivalent time between calculation according to CEB-FIP Model Code 1990 and Output values from DIANA at three different times: 1 hour, 10 hours and 24 hours.

5.4.5 Bond-slip behaviour between concrete and steel strand

To capture that the bond behaviour between the steel strand and the young concrete is maturity dependent, a model was performed to verify the behaviour, see Figure 5.30. Heat of hydration with adiabatic conditions was assumed. Q8MEM element were used for the concrete, L2TRU elements for the steel strand and L8IF interface element in between the materials to describe the bond-slip behaviour, see Chapter 5.2.4. Figure 5.30 illustrates the element setup and the boundary conditions of the models, the dimension of the quadratic concrete specimen was set to 0,05x0,05 meters. The bond-slip test consisted of a prescribed displacement, δ , of the steel strand, that was iterated in ten steps up to its maximum prescribed displacement.

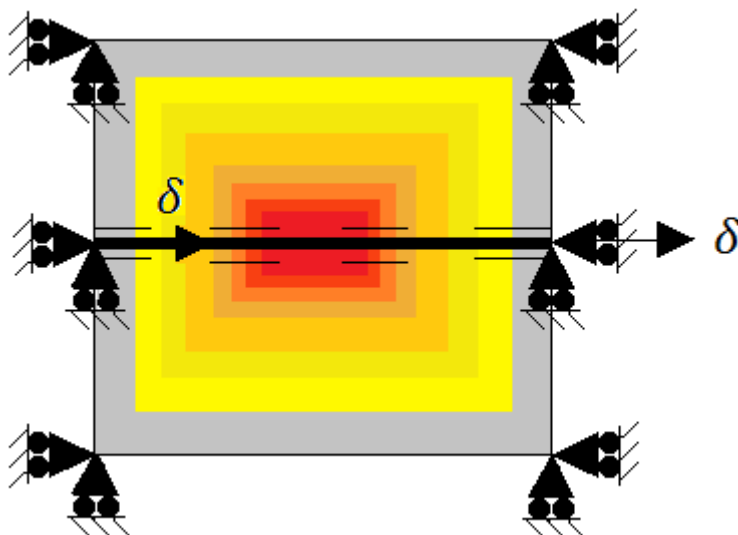


Figure 5.30 Illustration of the boundary conditions and element setup for the bond-slip test with maturity dependence. Same boundary conditions were assumed as for the bond-slip test with prescribed curve.

The cubic function was used to capture the bond-slip behaviour with maturity dependence, see Chapter 2.3.1. DIANA provided an in-build function to capture the maturity dependence bond-slip behaviour, but due to unknown reason the function did not worked as expected. In order to capture the maturity dependence, a subroutine was instead created based on cubic-function variation and equivalent age of concrete according to Equation 2.9 in Chapter 2.1.2.3. In the subroutine the bond-stress was assumed to be zero the first seven hours after casting, according to results from the measurements. Thereafter, the bond strength was assumed to increase linearly until reaching its maximum value at 24 hours and then remaining constant, see Appendix B.2.5.3 for the input data files and explanation of the sub-routine used in the analyses. It is worth to note that the bond stress was assumed to depend on the total slip; i.e. also slip that took place when the concrete had a low maturity will generate bond stresses when larger maturity is reached. This can be questioned, but was considered to be out of the scope of this thesis.

5.4.5.1 Results

The results from bond-slip with maturity dependence analyses after 1, 7, 12, 18 and 24 hours can be seen in Figure 5.31. The figure shows also the evaluation between input and output data from the FE-analyses, which are almost entire consistent. The bond-stress development was as expected, zero the first seven hours (see FE output after 1 and 7 hours in Figure 5.31), then increasing up to 24 hours.

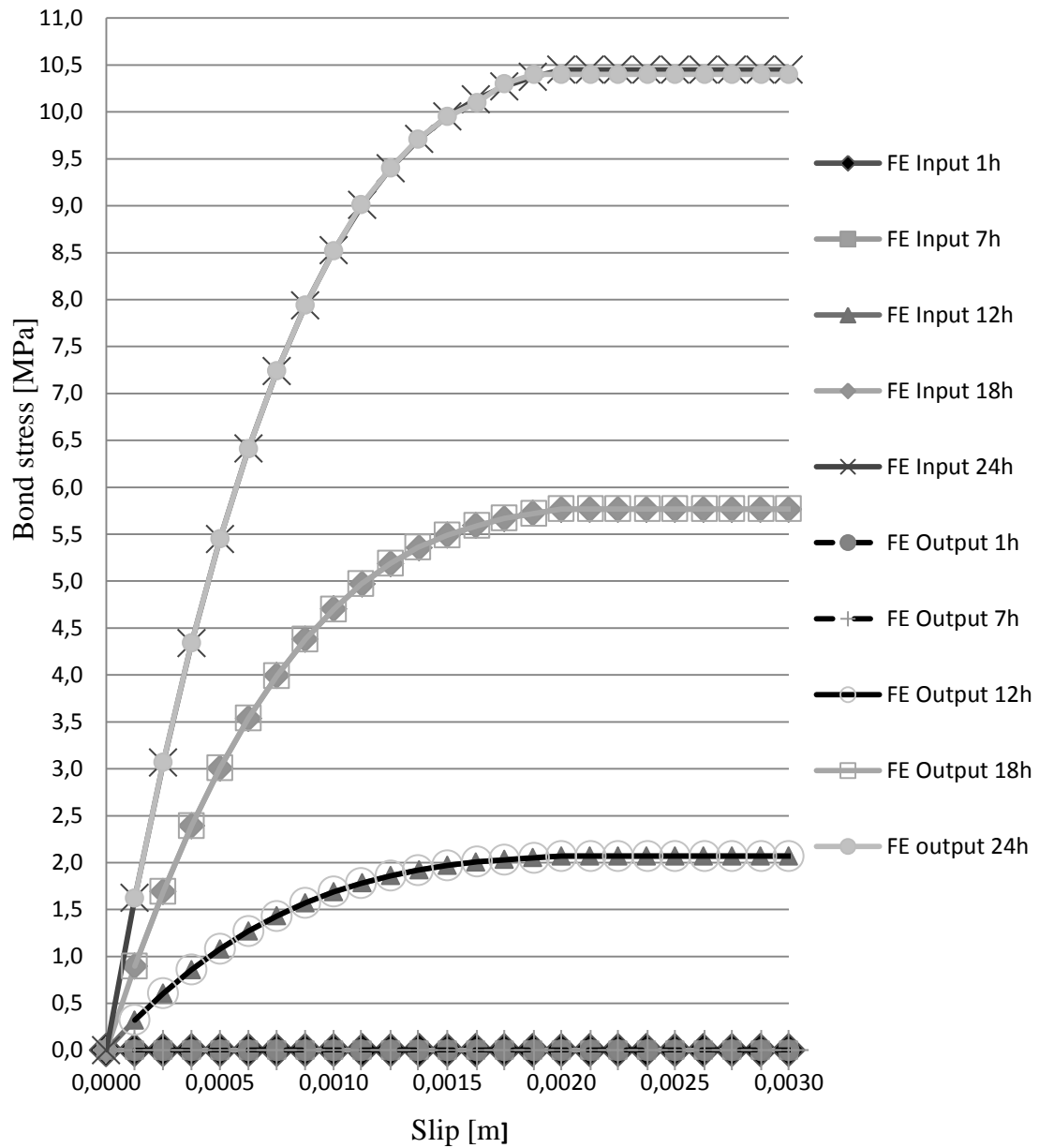


Figure 5.31 Bond-slip curves illustrating comparison between input and output data from FE-analyses of the maturity dependence shear traction in between young concrete and steel after 1, 7, 12, 18 and 24 hours.

Comparison between the cubic bond-slip with maturity dependence after 24 hours and the results used as input are shown in Figure 5.32. There are some differences between the curves, which are due to the cubic-function assumption. However, the general behaviour is captured with same maximum bond-stress.

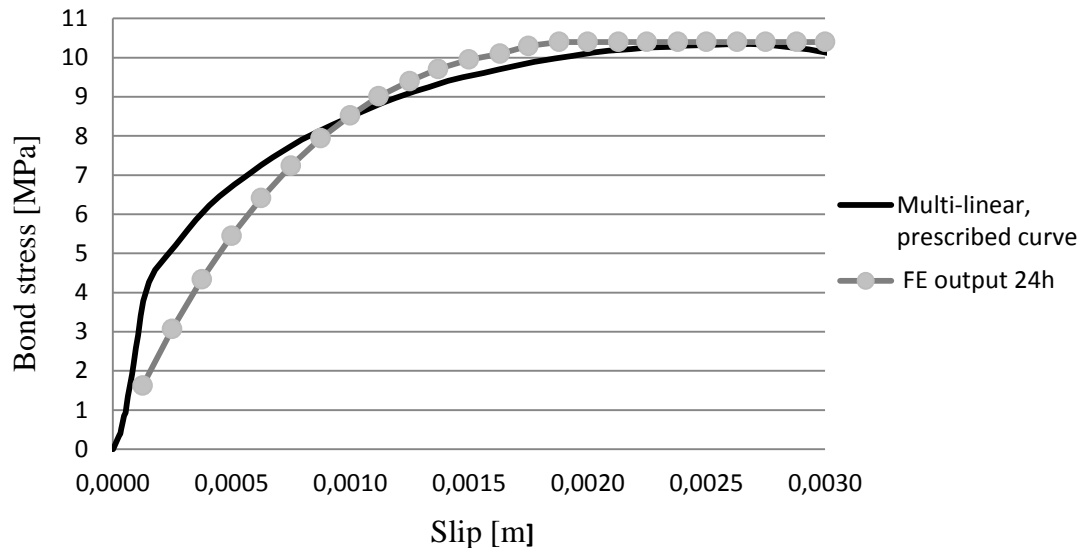


Figure 5.32 Bond-slip comparison between measured prescribed curve and output from FE-analysis after 24 hours.

5.4.6 Verification of the relationship between all parameters

The simplified ten meters concrete-steel model from Chapter 5.4.2.3, especially Figure 5.20b, with adiabatic conditions and heat flux out from the top surface was further updated. Development of the modulus of elasticity, bond-slip with maturity dependence using cubic-function and casting in two steps was added to the model. The first part of the concrete specimen was assumed to take one hour to cast, then the second part was added and the whole bed was analysed during 24 hours, see Figure 5.33.

Thermal and mechanical reference values according to Table 5.1, Table 5.2 and Table 5.3 were used in the model, except for the CTE values, which were changed to $20E-6$ for both the young concrete and the steel strand. The CTE values were changed according to Figure 2.7, due to increased knowledge of the thermal expansion behaviour during curing.

The initial stress of 1400 MPa was still applied in the steel strands.

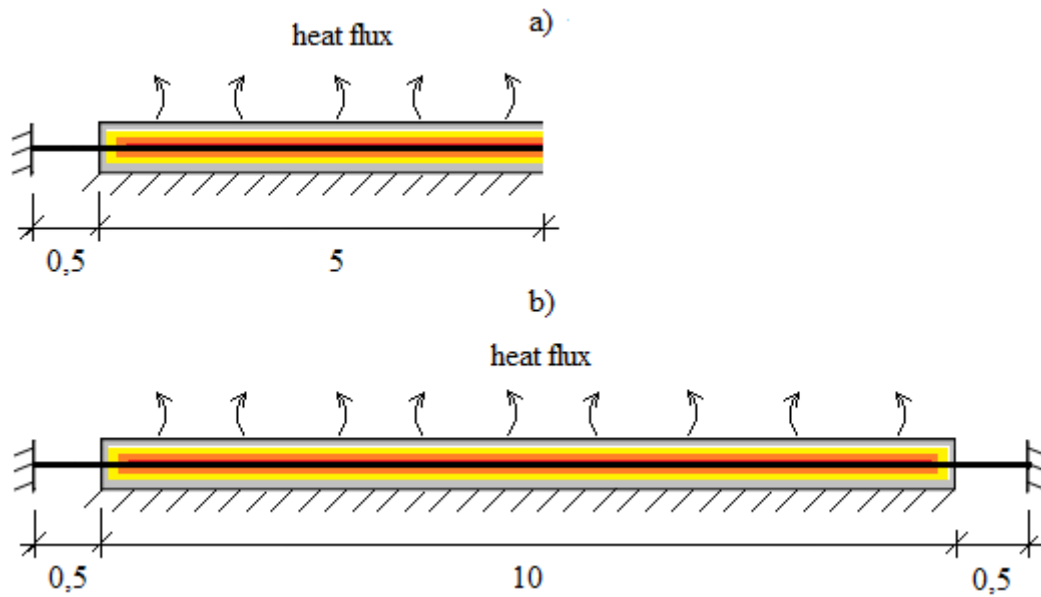


Figure 5.33 Illustration of the 10 meters concrete model with all verified parameters included; heat development with heat flux out from the top surface, induced steel strand and steel strand at the ends, casting in steps, development of E-modulus and bond-slip with maturity dependence.

The results concerning the steel stress, concrete stress and bond-stress along the length of the model during the first 24 hours after casting can be seen in Figure 5.34, Figure 5.35 and Figure 5.36 respectively. Appendix B.2.6 contains the input file for FE-analysis in DIANA.

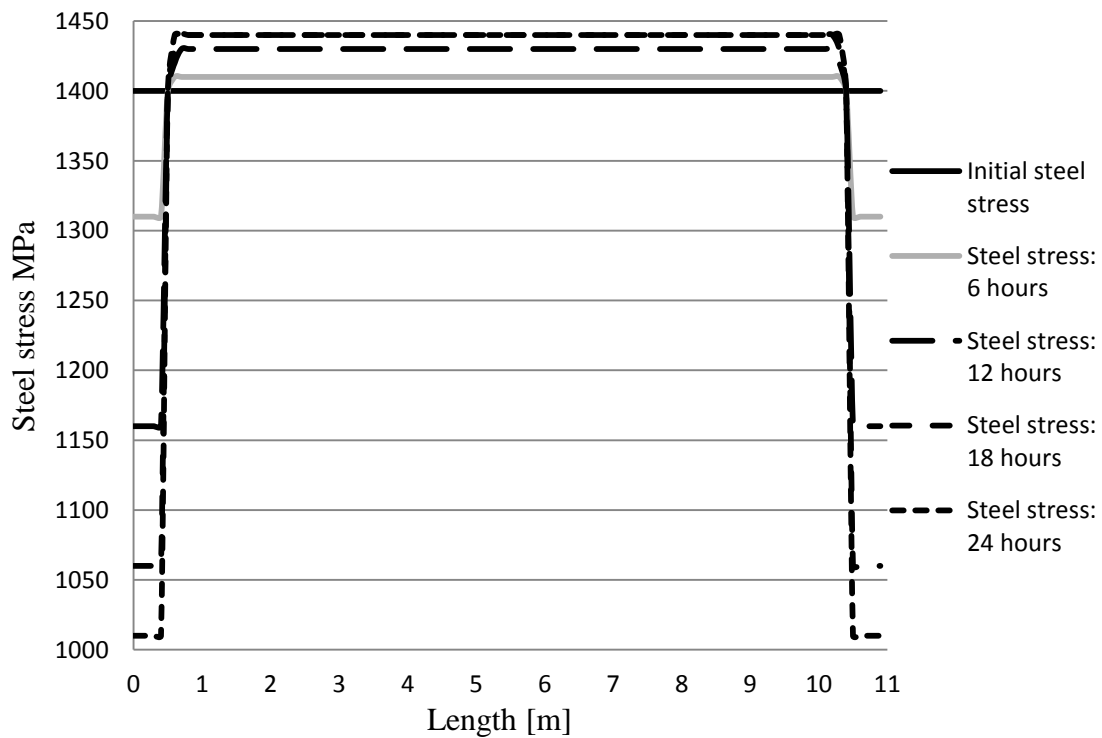


Figure 5.34 Illustration of stresses in the steel strand during different times; 6, 12, 18 and 24 hours after casting.

The stress in the steel strand cast in the concrete increased with time and the stress in the naked steel parts at both ends decreased with time.

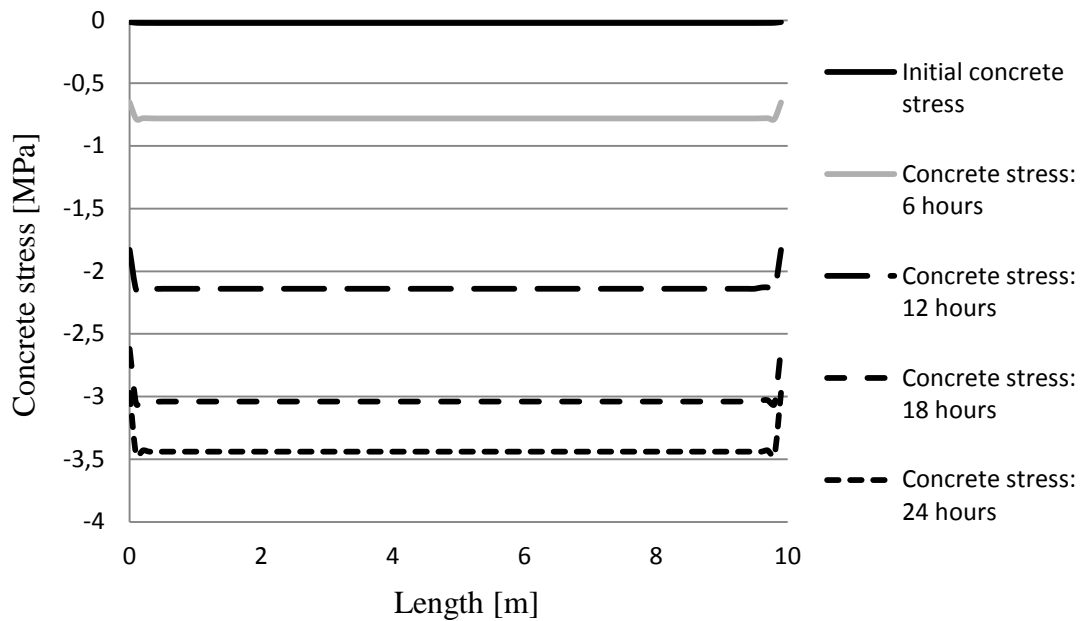


Figure 5.35 Concrete stresses over the length of the concrete specimen during the first 24 hours after casting.

The stresses in the concrete tended to increase with time, but were small. The concrete wanted to expand but were not allowed to do this freely because bond to the steel.

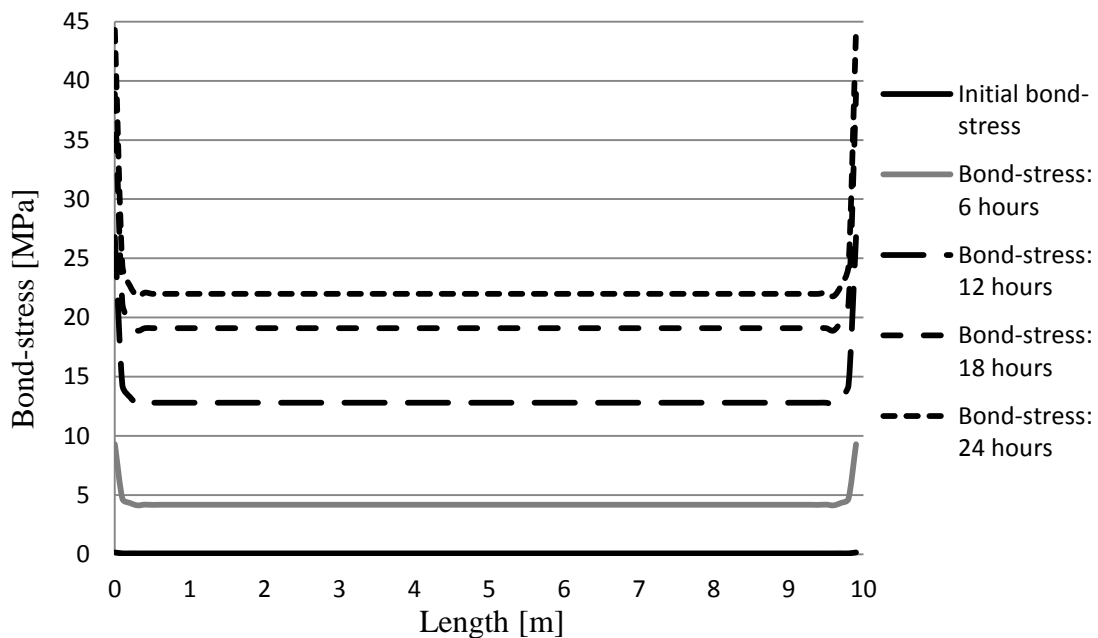


Figure 5.36 Illustration of bond-stresses between the young concrete and steel strand during different times; 6, 12, 18 and 24 hours after casting.

Bond-stress in the interface element increased with time and seems to grow too early and too fast.

5.5 Description of the FE-models

Three different finite element models were created with different boundary and geometry conditions, trying to the plants in Vislanda, Marijampolé and Sollenau. All plants have different boundary conditions according to the measured conditions, see Chapter 4.1. Following subchapter describes the production conditions in the three models, which were constructed with help of the thermal and mechanical verifications presented in Chapter 5.3 and 5.4 respectively. The models take into account the following parameters:

- Heat transfer between the materials and the surroundings
- Temperature development of the hardening process of young concrete
- Time dependent relaxation of steel strands
- Development of Young's modulus of elasticity
- Bond-slip behaviour in between the materials
- Casting in several steps

Shrinkage effects of the young concrete were not included in the FE-models. This choice was based on the results of the analysis made in Chapter 5.4.3, which showed negligible effects.

The finite element models were used in staggered flow-stress analysis, which is a combination of a potential heat flow analysis and a subsequent transient non-linear structural analysis. DIANA will automatically transform the results from the potential flow analyse to input data, loads or temperature and maturity, for the structural analyse, see DIANA (2008).

The concrete were constructed using 2D elements with plane-stress assumption and the prestress steel with 1D line elements, exactly as the simplified models in the verification analyses, see Chapter 5.2 for the different types of elements that was selected for and in between the materials.

5.5.1 Geometry conditions

5.5.1.1 Vislanda

The simplified model with semi-adiabatic conditions and heat transfer from the top surface with induced steel strand, see Chapter 5.4.2.3, in combination with casting in several sequences was used and further developed. Five centimetres "naked" steel strands were added in between every fourth sleepers and tarpaulin consisting of polyethylene sheeting was also added at the top surface of the concrete, see Figure 5.37 for an illustration of the two first sets of moulds from the left side of the bed. Totally, the model consists of 11 moulds with four sleepers in each mould.

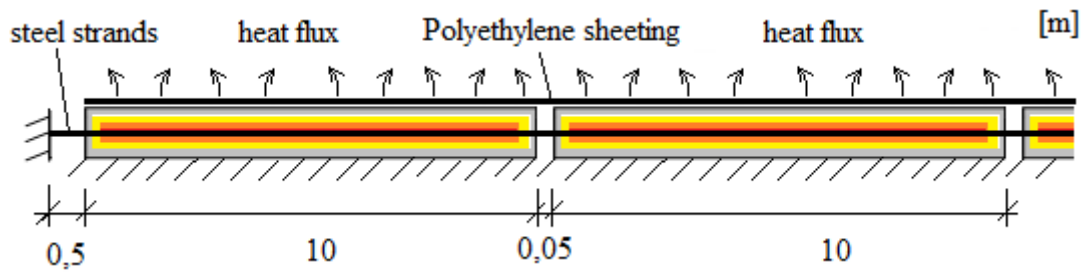


Figure 5.37 Illustration of the boundary conditions of the two first sets of moulds from left side in the model of Vislanda plant.

5.5.1.2 Marijampolé

Contrasting to the model for the Vislanda factory, the factory in Marijampolé consists of one set of moulds of 108 meters. The bottom surface of the concrete specimen was modelled with an additional heating of 15 °C, due to heating system during curing in the factory. The other conditions are the same as the plant in Vislanda, see Figure 5.38 for the boundary conditions.

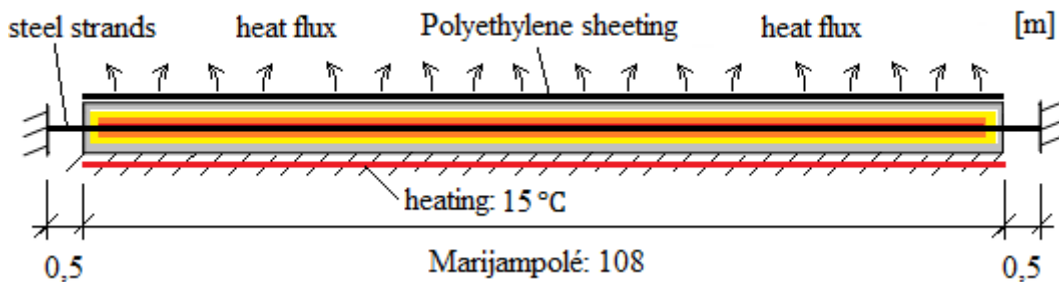


Figure 5.38 Boundary conditions of the model of the factory in Marijampolé, note the additional heating of 15 degrees on the bottom surface of the concrete under the bed.

5.5.1.3 Sollenau

Due to one set of moulds in both the Marijampolé and Sollenau plants was the FE-model almost the same for the two factories. The only difference is the lengths of the moulds, which is 104 meters in the plant in Sollenau, and that no additional heating occurred in the factory, see Figure 5.39 for the boundary conditions.

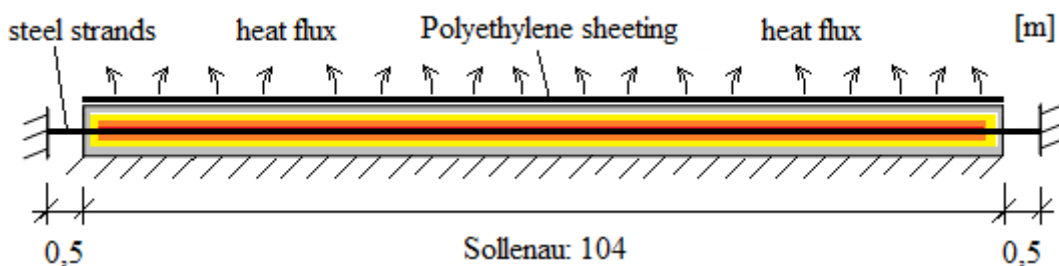


Figure 5.39 Boundary conditions of the model of the factory in Sollenau.

5.5.2 Casting Sequences

As mentioned, the models take into account casting in several steps. An average casting was assumed to take 120 minutes in all the factories and every casting step contained of 1 m^3 concrete, which results in approximately 5 meters of moulding each casting step. Therefore, every casting step was assumed to include two sleepers which resulted in a casting time of five and a half minutes for each casting step. Figure 5.40 illustrates the first three casting sequences in the Vislanda factory: the same principle was also assumed for the plants in Marijampolė and Sollenau.

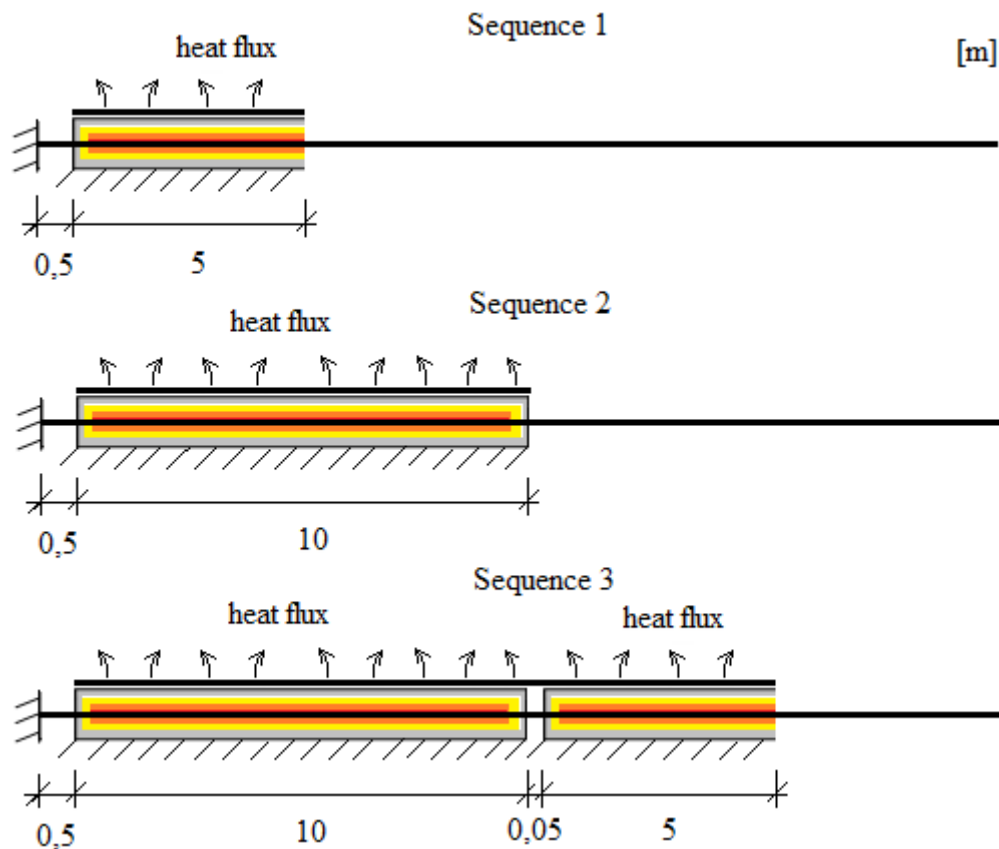


Figure 5.40 Illustration of casting in several sequences, the first three casting steps, in the model of the Vislanda factory.

5.5.3 Boundary conditions

The boundary conditions used in the different FE-models are the same as the boundary conditions from measurements in Chapter 4. Table 5.4 shows the different temperature boundary conditions and Table 5.5 shows the mechanical boundary condition used in the FE-models.

Table 5.4 Different temperature boundary conditions used in the three FE-models.

Temperature boundary conditions	Vislanda	Marijampolé	Sollenau
Initial temperature of the concrete mix [°C]	18,6	17	25
Initial temperature on the steel strands [°C]	20	6	25
Temperature of the surrounding [°C]	20	6	25

Table 5.5 Mechanical properties used in the three FE-models.

Mechanical properties	Vislanda	Marijampolé	Sollenau
Concrete properties (28 days)			
E-modulus [GPa]	38	38	40
Compressive strength [MPa]	73	65	95
Tensile strength [MPa]	5,2	4,8	6,3
Steel strand properties			
Initial steel stress [MPa]	1343	1395	1275
Total area of steel strands [m ²]	2,97E-4	2,806E-4	3,958E-4
Perimeter of all steel strands [m]	0,238	0,214	0,264

Young's modulus of elasticity and tensile strength of the different concrete used in the FE-analysis can be seen in Figure 5.41 and Figure 5.42 respectively.

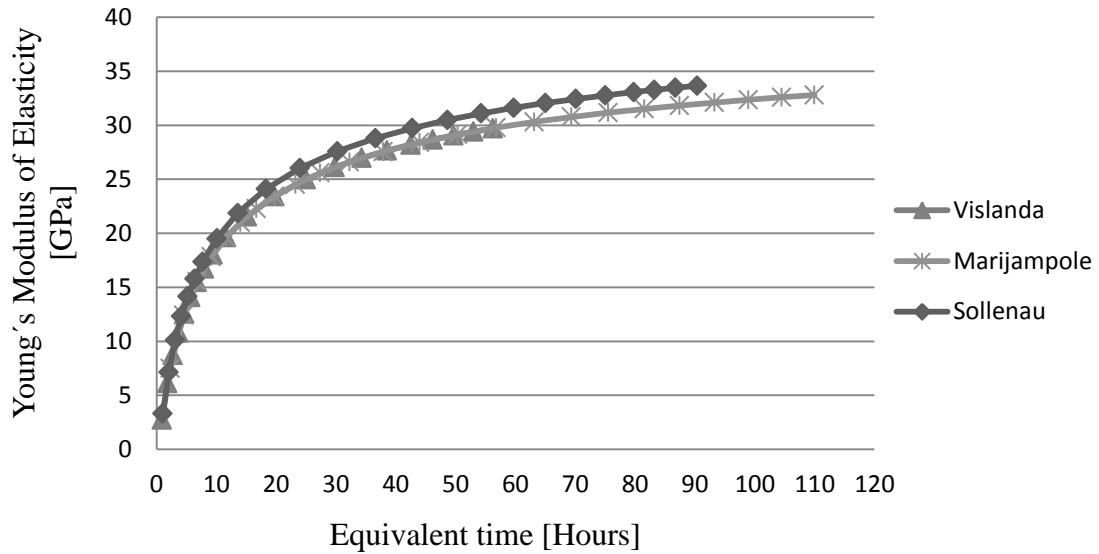


Figure 5.41 Young's modulus of elasticity versus equivalent time; the curves end at 24 hours.

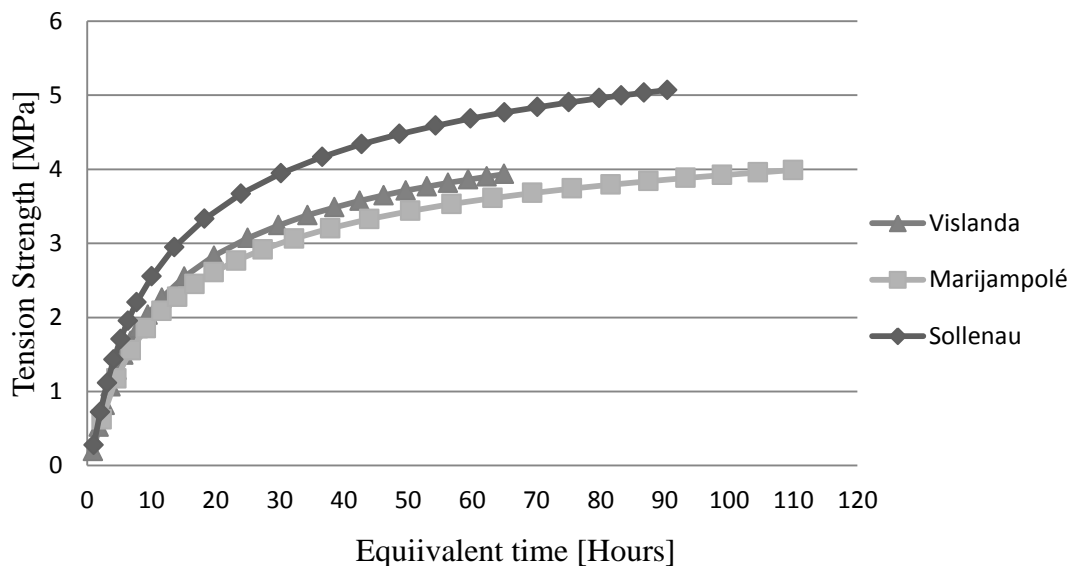


Figure 5.42 Tensile strength versus equivalent time; the curves end at 24 hours.

5.5.4 Adiabatic temperature

Due to lack of knowledge of the temperature that develops in the concrete in the different sleeper factories, hand calculation was made on the adiabatic rise of the temperature according to Equation 2.5. Assumptions regarding the constant values K and α_{adiab} were made for the different plants. Values were chosen so the curves corresponded most accurately to the measured temperature curves, Figure 5.43 illustrates the adiabatic temperature development and in Table 5.6 the constant values used in the equation can be seen.

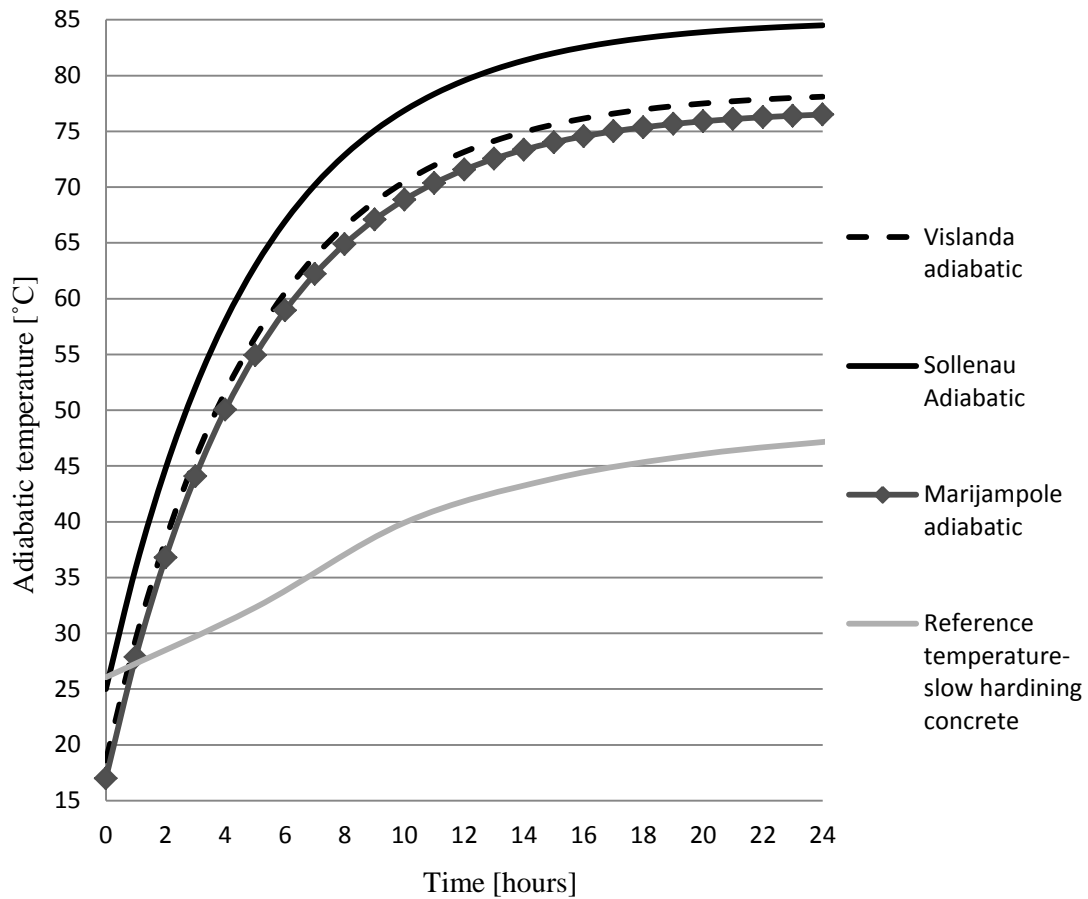


Figure 5.43 Adiabatic temperature curves chosen as indata for the different factories, K and α_{adiab} coefficients are assumed to be 60 and 0,2 respectively in the calculations.

Table 5.6 Properties used in the three FE-models.

Properties	Vislanda	Marijampolé	Sollenau
Concrete properties			
Constant value α_{adiab}	0,2		
Constant value K	50	40	60
Bond-behaviour			
Time, bond starts [hours*]	4	4	3
Equivalent time, bond starts [hours*]	3.7	9.3	3,1
Time, max. bond occurs [hours*]	12	13	10
Equivalent time, max. bond [hours*]	24	48	22,9

*Hours after casting.

The adiabatic curves were then used as input and thermal analyses were made in DIANA. The resulting semi-adiabatic curves compared to measured values can be seen in Figure 5.44.

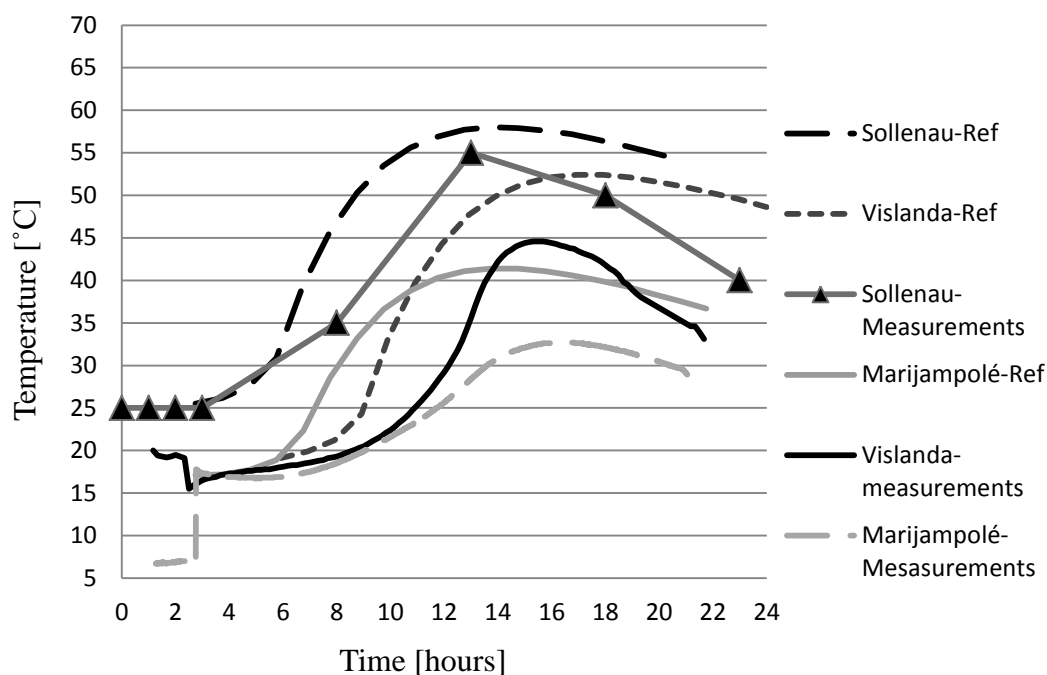


Figure 5.44 Comparison of semi-adiabatic curves of the steel inside the concrete between measurements and output from DIANA, where reference values was used to characteristic the temperature development.

Due to large differences between the output results from Diana and the results from measurements, the input of the adiabatic curves was modified. The curves and equations were improved so the maximum temperature and the time when the maximum temperature occurred almost was equivalent with the measurements in the factories. It was an iterative process with many re-analyses. Results can be seen in Figure 5.45. The new semi-adiabatic results correspond well to the measured temperature variation during curing for the plants in Vislanda and Marijampolé, but not with high accuracy in the factory in Sollenu: this can be explained by the lack of information about the temperature during curing in this plant.

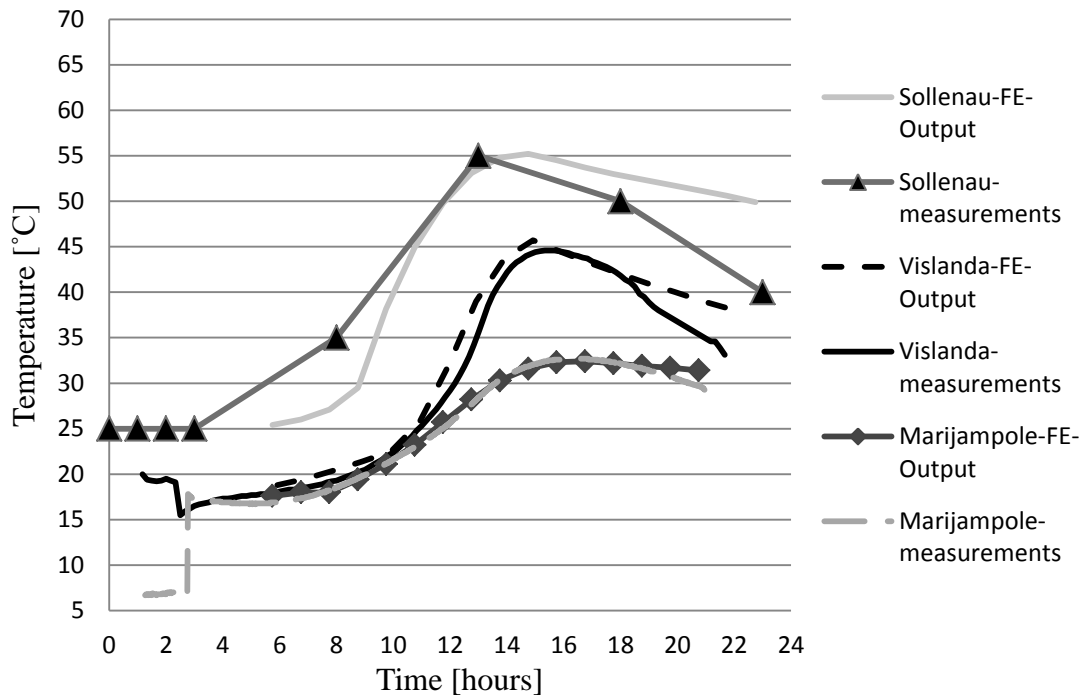


Figure 5.45 Differences of the temperature development in the steel inside the concrete, after some iteration, between measurements and results from DIANA.

5.6 Results of FE-analyses in phase 2 with reference values compared to measurements

The reference parameters of the young concrete and steel strand used in the verification of the thermal- and mechanical properties were furthermore used as input data in the different factories, see Table 5.1 and Table 5.3 in Chapter 5.3 and Chapter 5.4 respectively for the reference parameters. The different boundary conditions for the factories can be seen in Table 5.4 and Table 5.5.

A convection coefficient of the polyethylene sheeting of $1,853 \text{ J/m}^2\text{s}^\circ\text{C}$ was further added in place of the semi-adiabatic convection coefficient on the top surface. This value was calculated according to Table 2.2, assuming no wind speed. The CTE of the young concrete and the steel was also changed to $20\text{E-}6 \text{ 1/}^\circ\text{C}$ for both materials.

Prestress of the steel strand, within the first bed, last bed, “naked” steel strand and along the bed were analysed from casting to release of the force (phase 2). Results were taken as a mean value of the first and last element which is 1,25 meters. Temperature was taken in the node point placed 1,25 meters within the bed. Concrete stress and bond stress were also analysed and the results of the factories; Vislanda, Marijampolé and Sollenau can be seen in subchapters 5.6.1, 5.6.2 and 5.6.3 respectively.

Results from FE-analyses in the subchapters below are rounded using three digits in DIANA output files which unfortunately create uneven curves, but the principal behaviours are captured.

Generally, the results from the finite element analyses show principal behaviour; i.e. how various phenomenon affect the prestress in the steel strands. The Parameters were chosen as reference values obtained from the literature study, therefore the results from FE-analysis do not properly describe the quantitative effects of all different phenomenon. Consequently, FE-results do not describe the entire behaviour of the prestress losses in steel strands compared to results from measurements. To investigate the influence of some parameters, a parameter study was made, see Chapter 6.

5.6.1 Vislanda

FE-results of the prestress losses in the Vislanda factory using the reference values, along the bed, from casting to release of the prestress force can be seen in Figure 5.46. The “naked” steel strands between the concrete packages of four sleepers and at the ends becomes compressed due to expansion of concrete, because of temperature increase, meanwhile bond develops between steel strands and concrete which causes tension of the steel strands within the concrete. Generally, the prestress decreased from active to passive side up to maximum temperature when concrete expanded, thereafter the prestress stabilized along the length during contraction phase of the temperature. “Naked” steel strands between the packages of concrete make the prestress of the package ends decrease. For boundary conditions of the bed in Vislanda factory, see Figure 5.37.

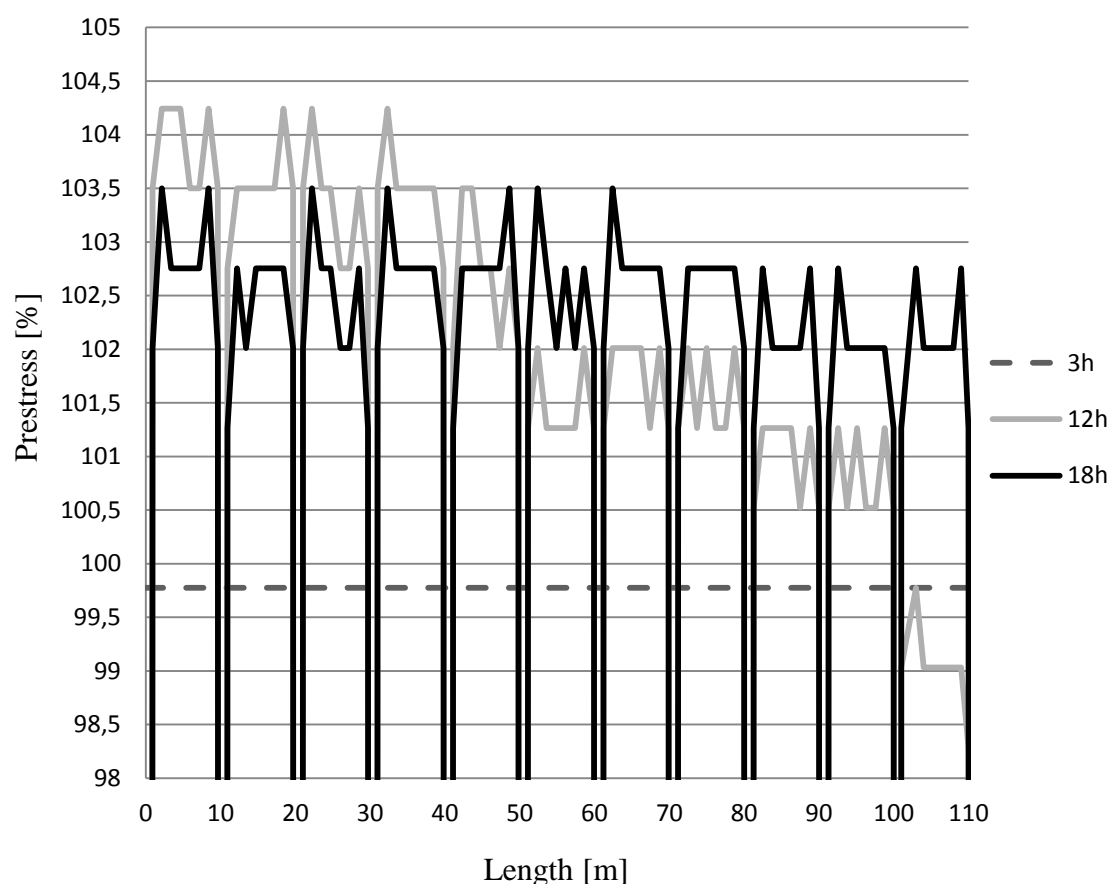


Figure 5.46 Results from FE-analysis of prestress variation in the steel strand along the bed during different times, 3, 12 and 18 hours after casting for Vislanda factory according to reference values.

Results of prestress and temperature development of the last bed compared to measured temperature and prestress loss can be seen in Figure 5.47. As can be seen, the prestress in the analysis was much larger in the measurements. Furthermore, at twelve hours from tensioning, the strain in the analysis increased, which does not agree with the measurements. A possible explanation is that the bond increased too much and too early in the analysis.

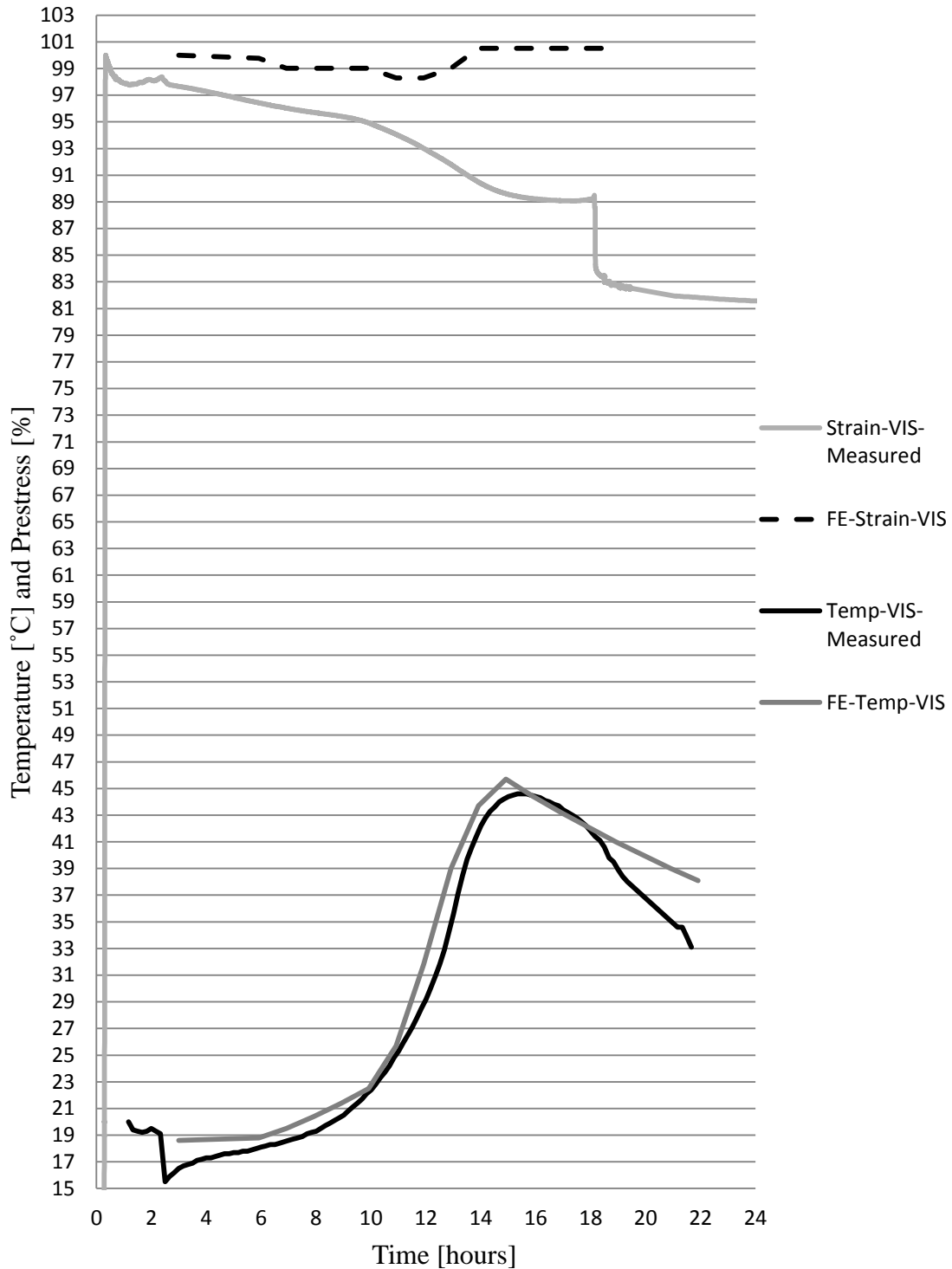


Figure 5.47 Results of prestress loss and temperature development from the FE-analysis compared to measures values in the steel strand within the concrete in the last bed (passive side) for Vislanda factory.

The results of prestress variation in the first sleeper during phase 2, show an increase of the stress up to around ten hours (maximum temperature); thereafter the stress decreased until unloading, see Figure 5.48.

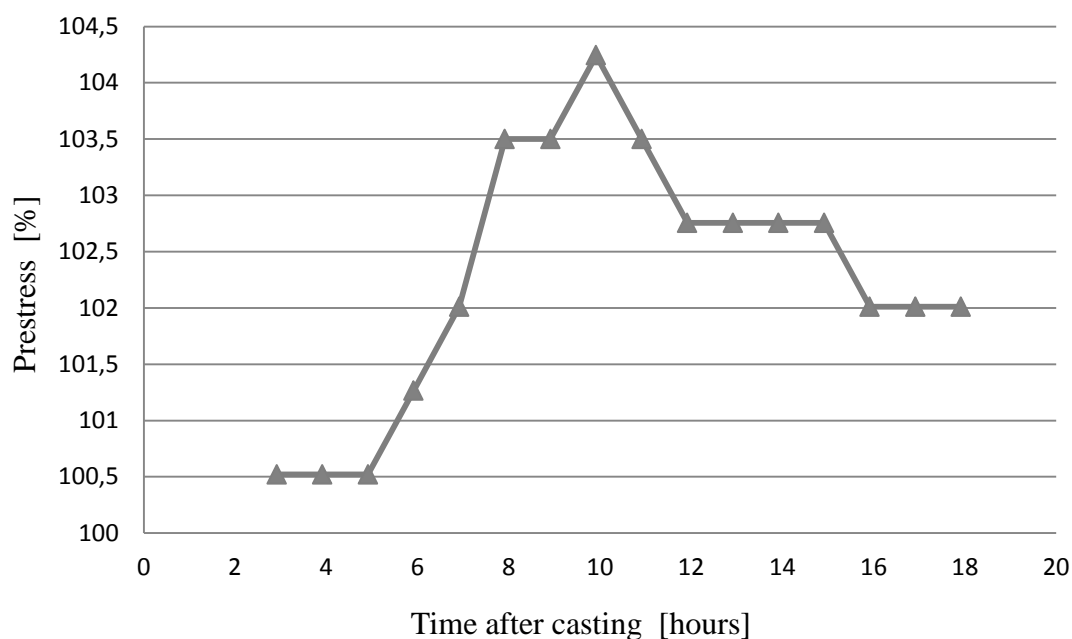


Figure 5.48 Illustrating of the variation of prestress in the steel strand within the concrete in the first sleeper on the active side of the bed during curing with reference values in Vislanda factory.

The FE-results of prestress variation in the ends of the “naked” steel strands can be seen in Figure 5.57. Both first and last “naked” steel parts show the same behavior which is largely temperature dependent. Maximum temperature occurs in the last sleeper after eleven hours from casting which correspond to the turning point of the prestress. Because too much and too early bond stresses, the behavior of the stress variation was excessive but the shape of the curve corresponded to the measurements. The bed can freely move between the steel ends and is therefore at all times in equilibrium, due to the assumption of no friction in the model.

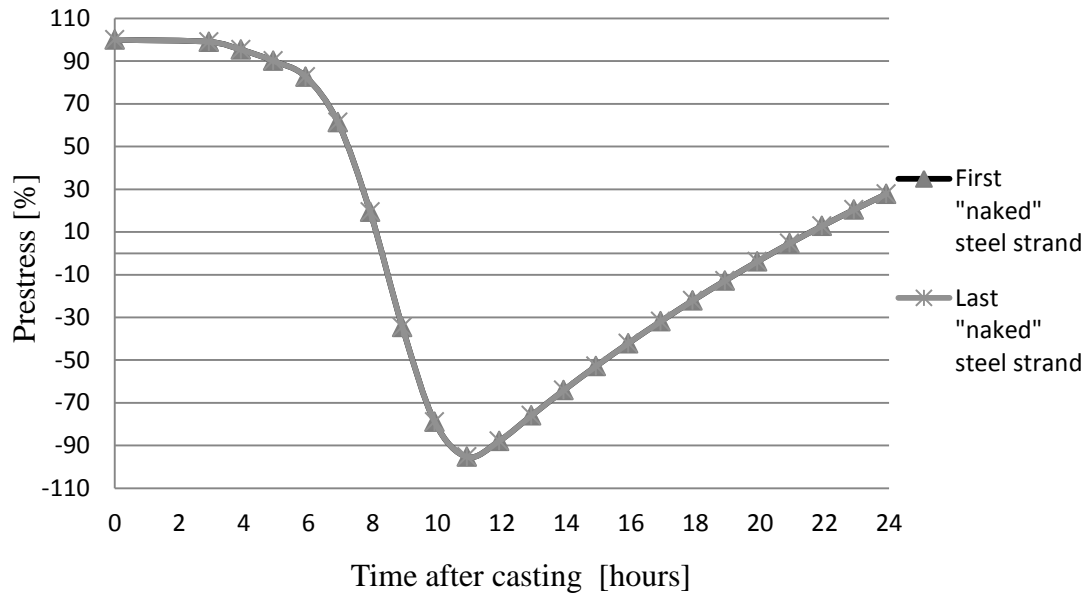


Figure 5.49 Variation of prestress of the “naked” steel strands in the ends according to reference values in Vislanda factory.

Concrete stresses in the first and last bed, in both upper and lower elements, are illustrated in Figure 5.50. The concrete became compressed when it wanted to expand because of the temperature development. The behaviour of the curve was in opposite way as the temperature curve. The upper elements became less compressed than the lower ones and highest stresses occurred in the first sleeper in lower element.

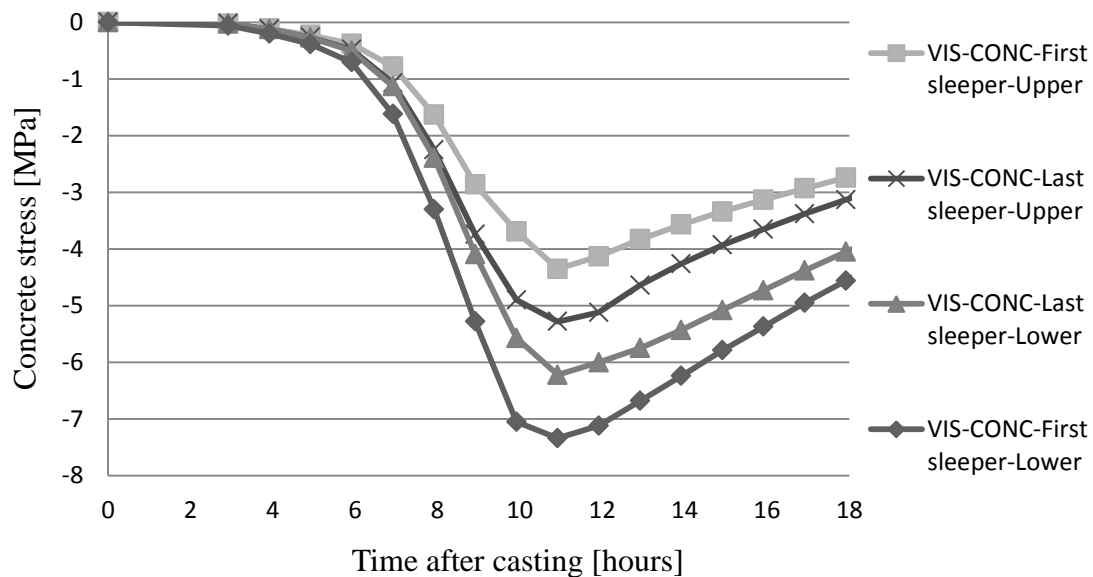


Figure 5.50 Concrete stresses in last and first sleepers of the bed in both upper and lower elements of the height according to reference values in Vislanda factory.

FE-results of bond stresses during the curing period in first and last sleeper can be seen in Figure 5.51. Corresponding bond stresses along the entire bed is illustrated in Figure 5.52. The results show increased bond stress in the last sleeper until maximum temperature occurred, thereafter the bond decreased. The behaviour is opposite in the

first sleeper. Another important observation is that the bond stress in Figure 5.52 was not constant along the length. Due to package of four concrete sleepers with “naked” steel part in between, the prestress force needed to be transferred from the “naked” steel to the ends of the concrete packages every 10 meters, which results in higher bond stress in the ends of the concrete packages, see Figure 5.53. The behaviour corresponds to the literature where the prestress requires a certain length, transmission length, to transfer the prestress force, see Figure 2.25.

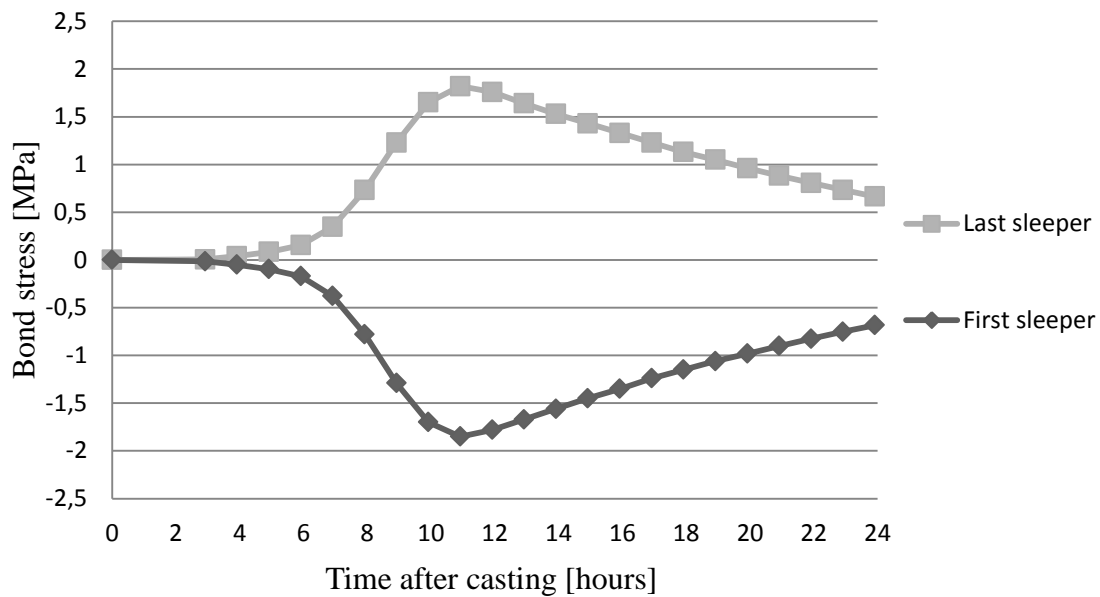


Figure 5.51 Bond stress depending on time after curing for the first and last sleepers with reference values in Vislanda factory.

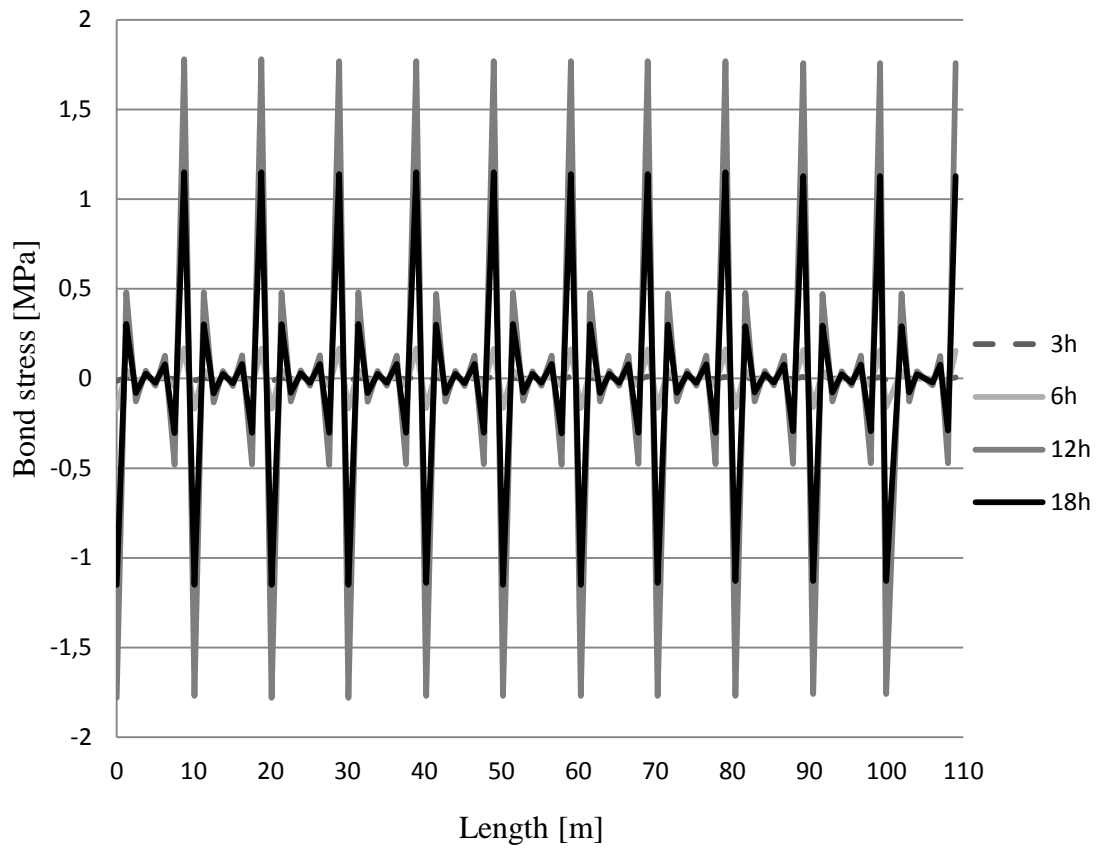


Figure 5.52 Variation of bond stress over the entire casting bed depending on different times according to reference values in Vislanda factory.

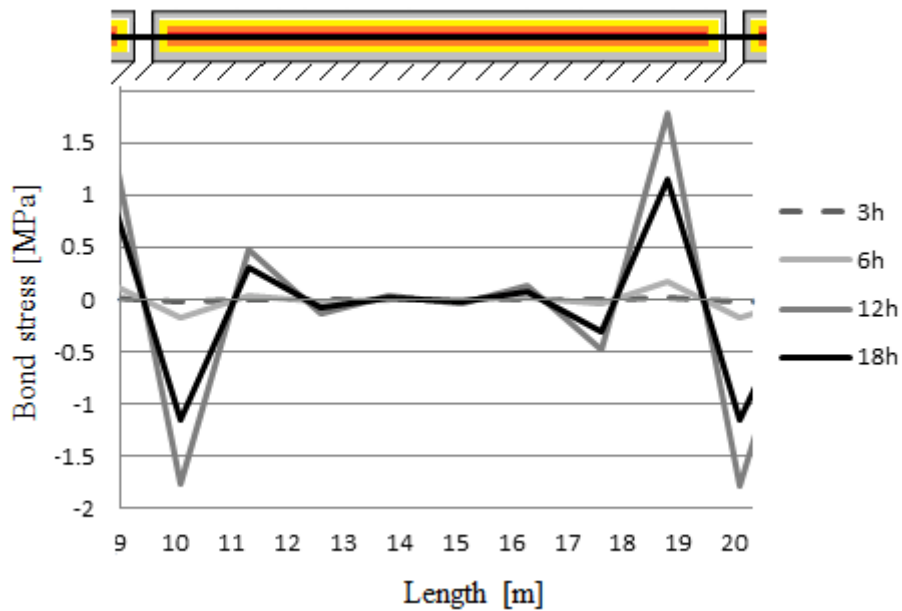


Figure 5.53 Close-up of Figure 5.52 illustrating the variation of bond stresses in second concrete package from the active side of the bed in Vislanda factory.

5.6.2 Marijampolé

The FE-results of the prestress losses in the Marijampolé factory according to reference values, along the bed, from casting to release of the prestress force can be seen in Figure 5.54. The overall behaviour of the prestress along the length during curing can be explained as irregular and is difficult to understand, but stress variation is small. The “naked” steel strands decrease significantly to approximately 45 % of the initial stress at eighteen hours after casting.

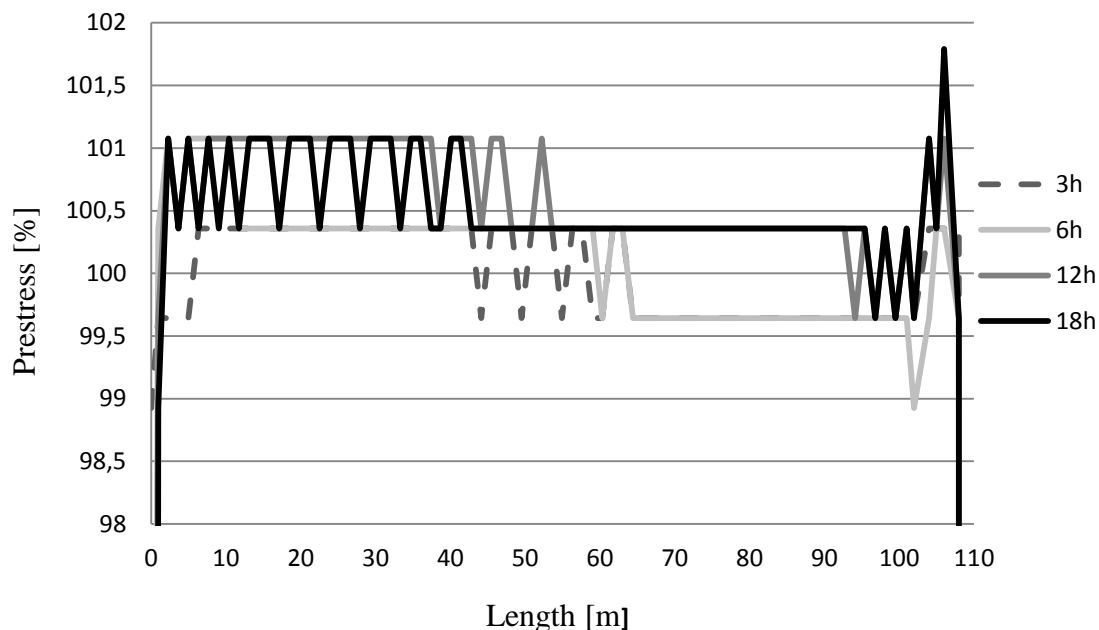


Figure 5.54 Results from FE-model of prestress in steel strand within the concrete along the bed during different times, 3, 6, 12 and 18 hours after casting for Marijampolé factory according to reference values.

Result of prestress and temperature development of the last bed compared to measured temperature and prestress loss can be seen in Figure 5.55. FE-results shows almost no variation of stresses during curing. Differences between FE- and measured results are large although almost same temperature development.

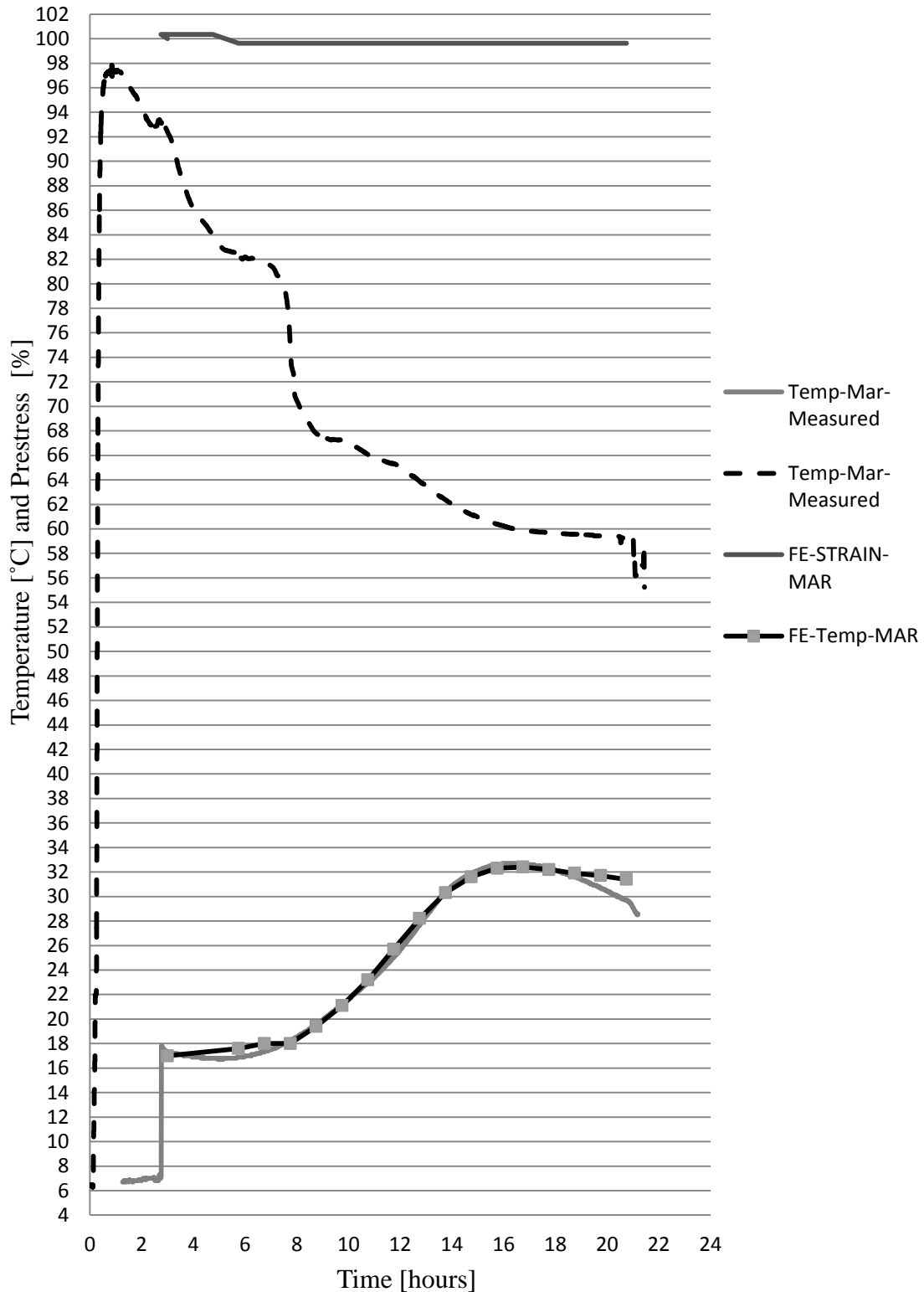


Figure 5.55 Results from the FE-analysis of prestress loss and temperature development compared to measures values in the steel strand within the concrete in the last bed (passive side) for Marijampolé factory.

FE-results of prestress and temperature development in the first bed during phase 2 can be seen in Figure 5.56. Variations of prestress are small, but increases up to around six hours after casting and thereafter decreases.

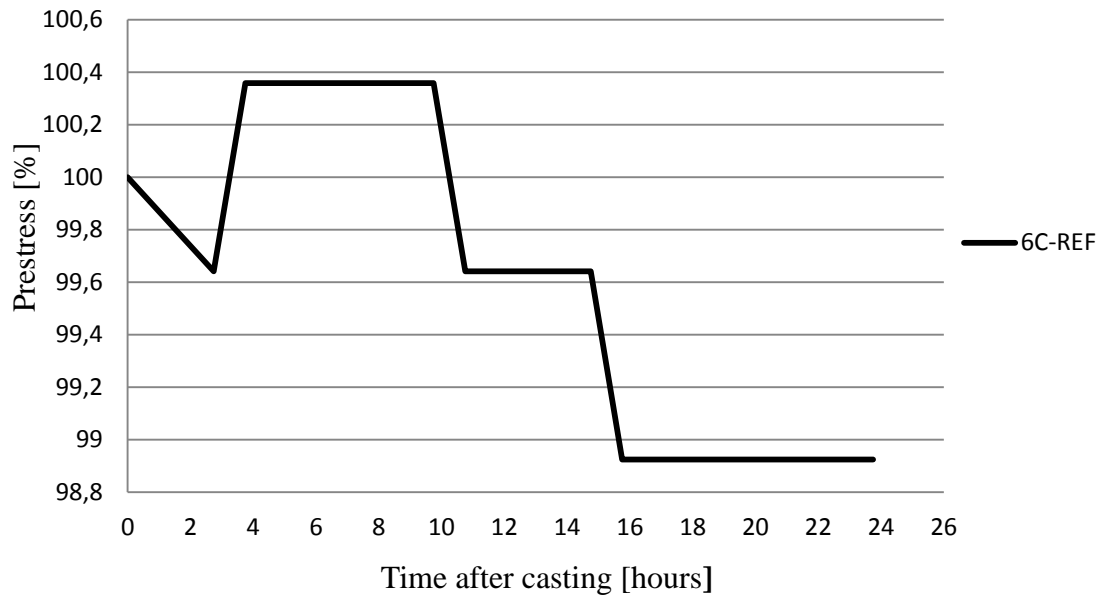


Figure 5.56 Illustrating of the variation of prestress in the steel strand within the concrete in the first sleeper on the active side of the bed during curing with reference values in Marijampolė factory.

FE-results of stress variation in the “naked” steel ends can be seen in Figure 5.57. The behavior is the same as in Vislanda factory, opposite of the temperature development, but the stress variation of the ends in Marijampolė is exactly the same.

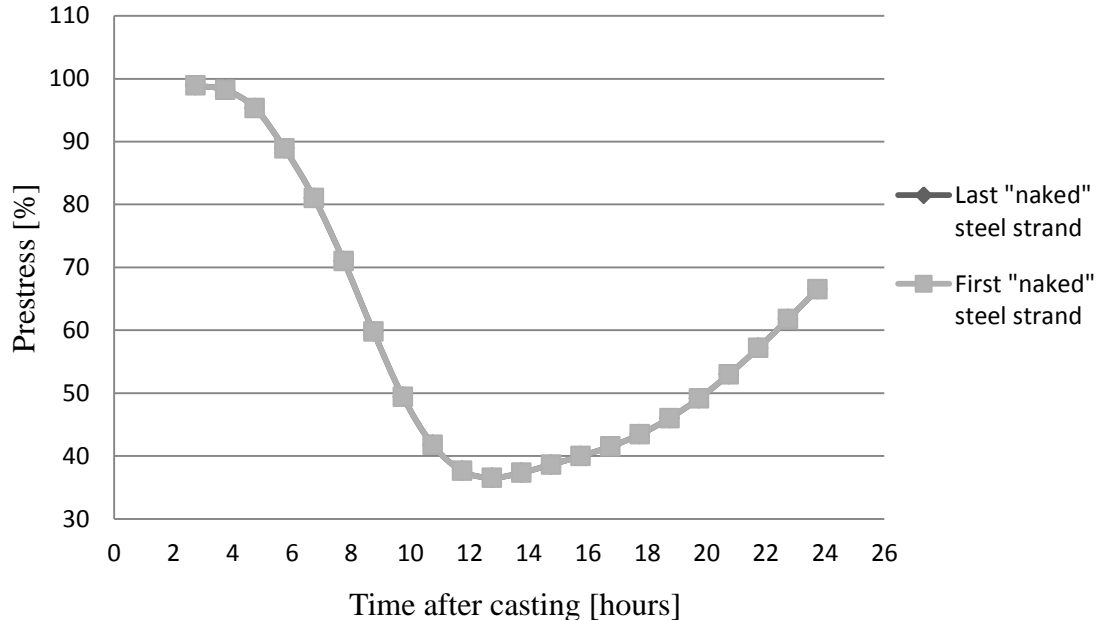


Figure 5.57 Variation of prestress of the “naked” steel strands in the ends according to reference values in Marijampolė factory.

Concrete stresses in the first and last sleepers, in both upper and lower elements, are illustrated in Figure 5.58. Same behaviour as in Vislanda factory was obtained, the lower elements became more compressed than the upper.

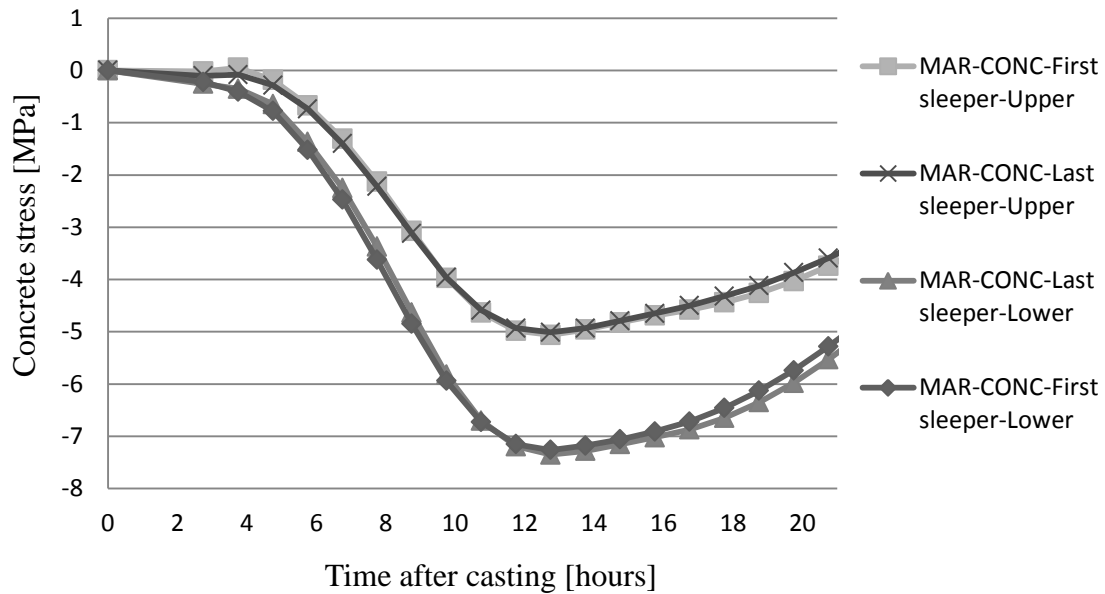


Figure 5.58 Concrete stresses in last and first sleeper of the bed in both upper and lower elements of the height according to reference values in Marijampolė factory.

FE-results of bond stresses during the curing period in first and last sleeper can be seen in Figure 5.59. Corresponding bond stresses along the entire bed is illustrated in Figure 5.60. The bond development behaviour in Marijampolė corresponds to the behaviour in Vislanda, mirrored bond stress between first and last sleeper. Bond stresses along the length is zero; bond stress occurs only in the ends due to transfer of prestress.

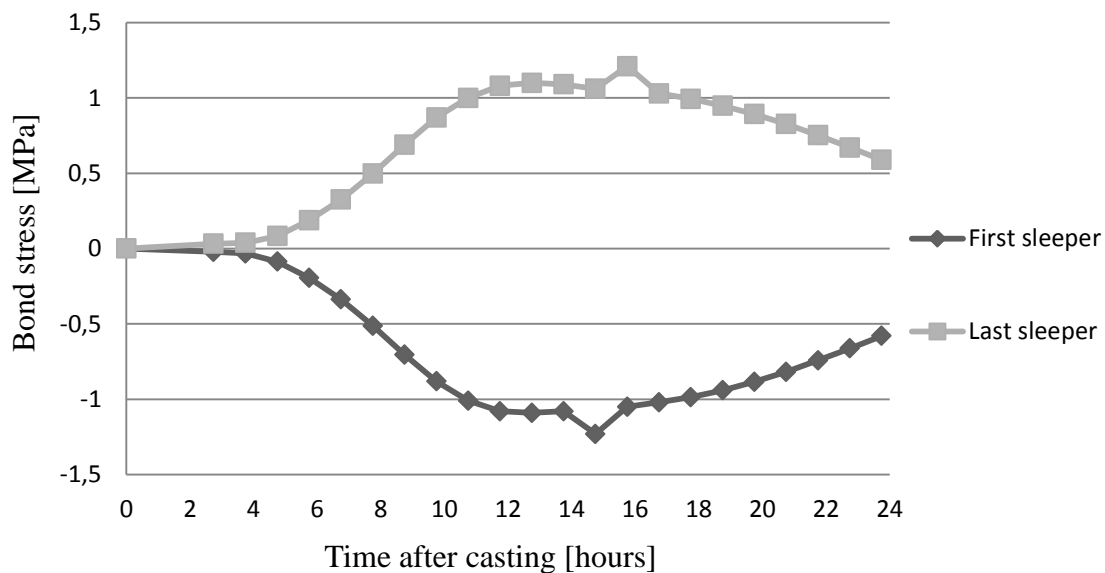


Figure 5.59 Bond stress depending on time after curing for the first and last sleepers with reference values in Marijampolė factory.

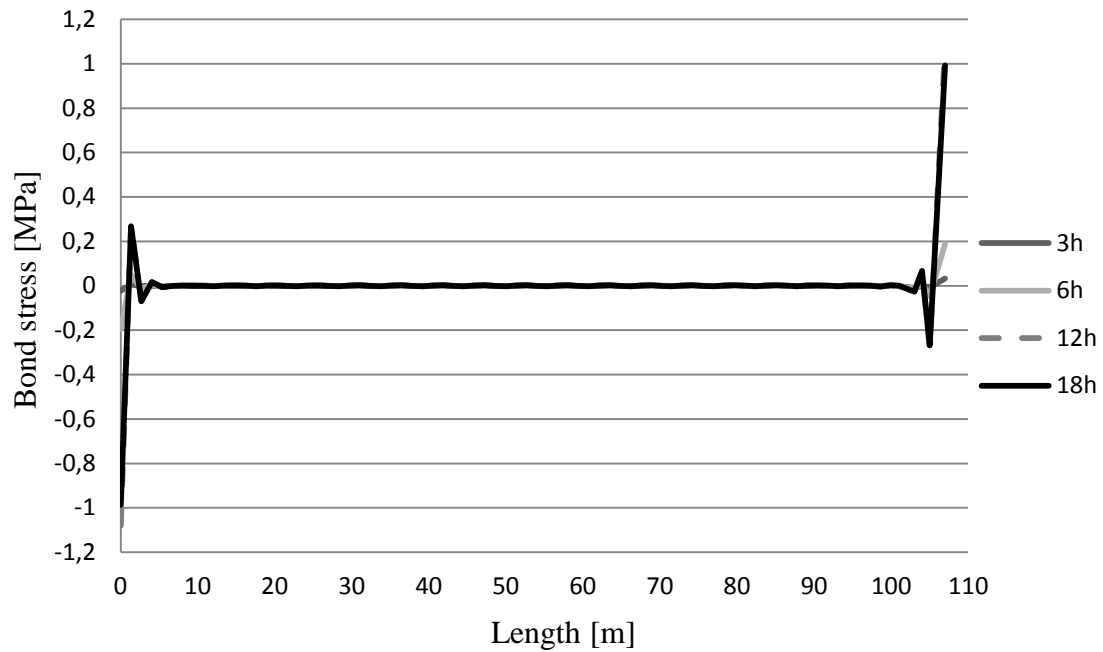


Figure 5.60 Variation of bond stress over the entire casting bed depending on different times according to reference values in Marijampolė factory.

5.6.3 Sollenau

FE-results of the prestress variation in the steel strand within the concrete along the bed in the Sollenau factory according to reference values, from casting to release of the prestress force can be seen in Figure 5.61. The general behaviour of the prestress variation of along the length is that the prestress increases in the active end and decreases in the passive end. The prestress “naked” steel ends decreases significantly to around 37 % of the initial steel stress after eighteen hours from casting.

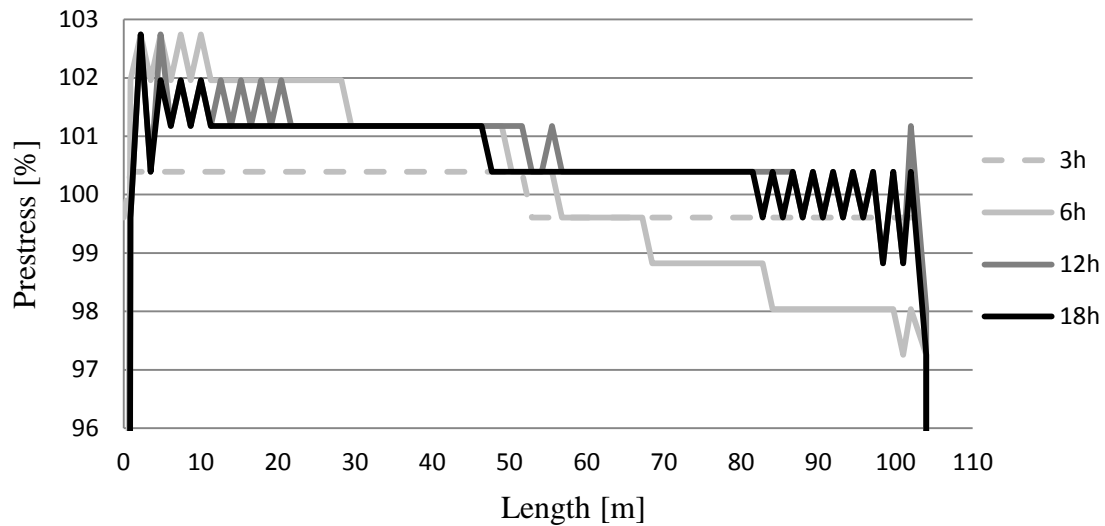


Figure 5.61 Results from FE-analysis of prestress variation in the steel strands within the concrete along the bed during different times, 3, 6, 12 and 18 hours after casting for Sollenau factory according to reference values.

Result of prestress variation and temperature development of the steel within the last sleeper compared to measured temperature and prestress loss can be seen in Figure 5.62 below. The prestress from FE-analysis decreases in the same amount as the measured prestressed loss during the first six hours after casting. Thereafter is the prestress in the last sleeper almost constant. The total loss of prestress during phase 2 was around 3 % in FE-analysis compared to 8 % in measurements.

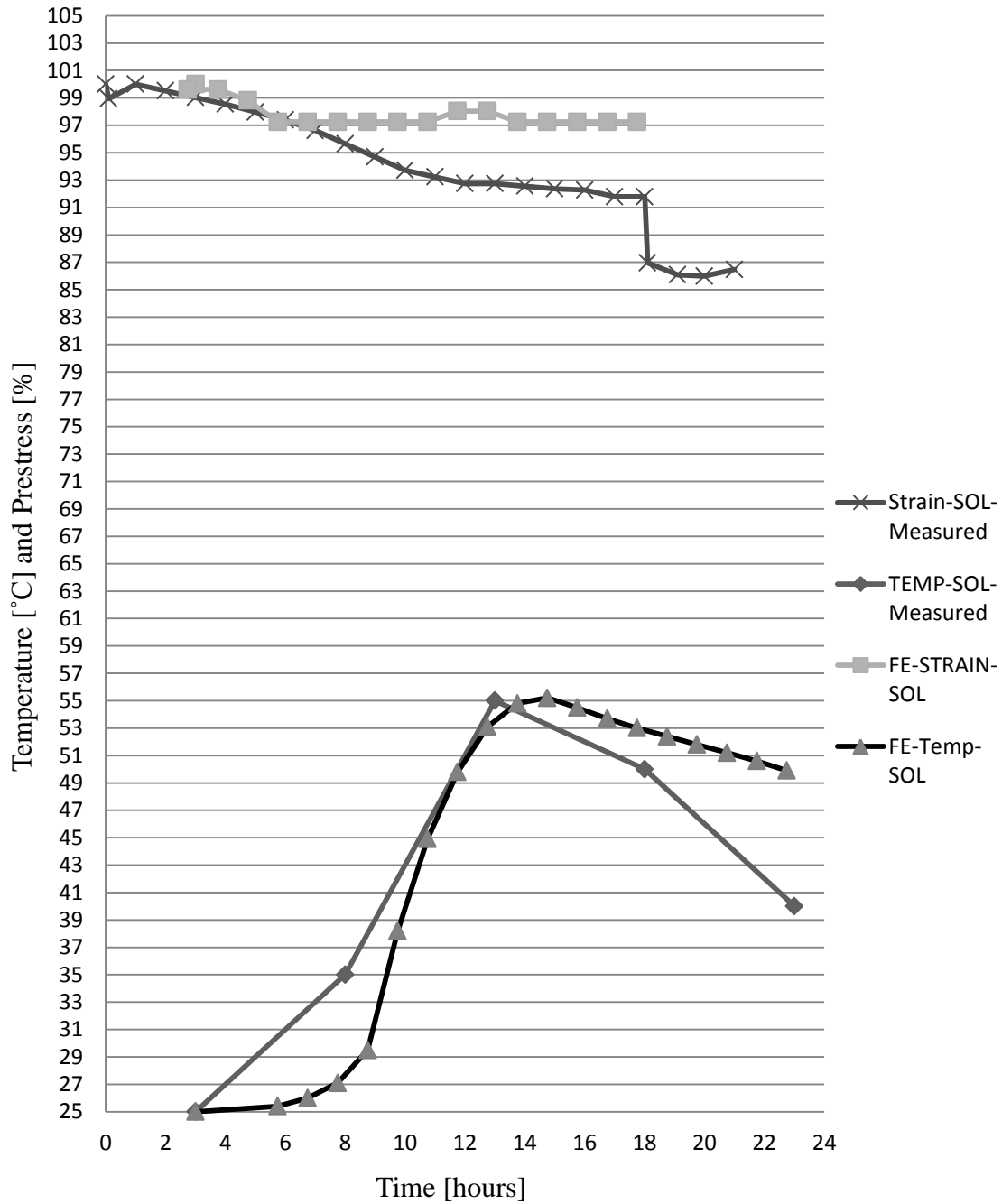


Figure 5.62 Results from the FE-analysis of prestress loss and temperature development compared to measures values in the steel strand within the concrete in the last bed for Marijampolė factory according to reference values.

Results of prestress and temperature development in the steel within the concrete in the first sleeper during phase 2 can be seen in Figure 5.63. The prestress variation increases until the bond starts and then decreases until maximum temperature occurs where it stays constant.

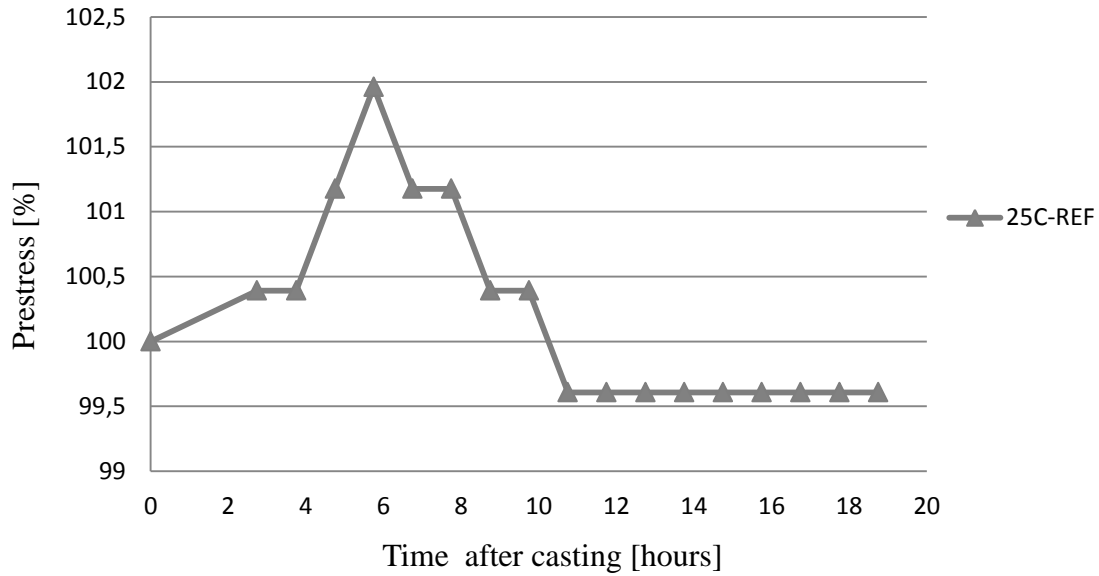


Figure 5.63 Illustrating of the variation of prestress in the steel strand within the concrete in the first sleeper on the active side of the bed during curing with reference values in Sollenau factory.

FE-results of the variation of prestress in the “naked” steel strands at the ends showed that the ends decreases until max temperature and thereafter increases back to 60 % of the initial prestress after 24 hours after casting, see Figure 5.64.

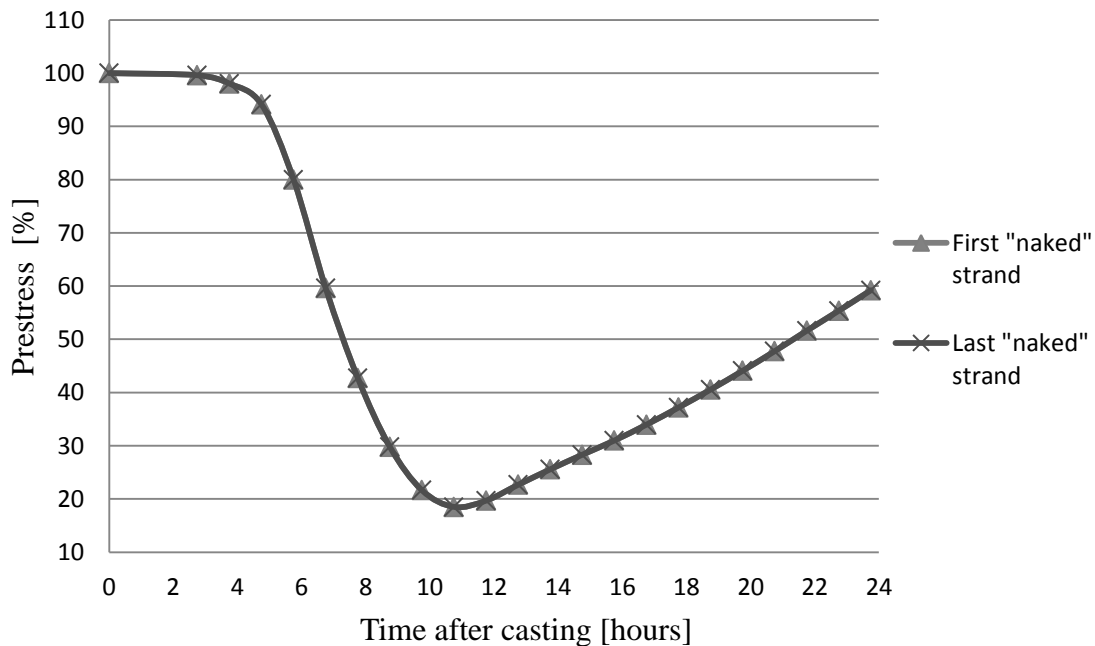


Figure 5.64 Variation of prestress of the “naked” steel strands in the ends according to reference values in Sollenau factory.

Concrete stresses in the first and last sleeper, in both upper and lower element, are illustrated in Figure 5.65. The behaviour is the same as in the other plants. Concrete stresses are highest in the lower part of the sleepers, due to restraint between the underneath mould and that the prestressed steel strand. Furthermore, the maturity de-

velopment of the concrete is also faster in the lower elements due to lower convection which causes higher concrete stresses.

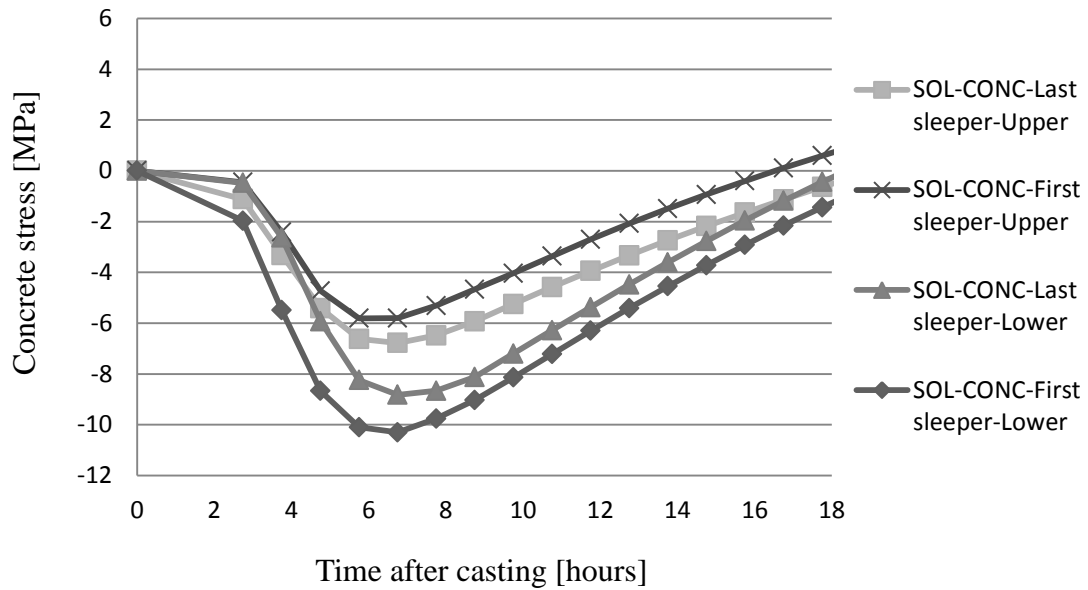


Figure 5.65 Concrete stresses in last and first sleepers of the bed in both upper and lower elements of the height according to reference values in Sollenau factory.

FE-results of bond stresses during the curing period in first and last sleeper can be seen in Figure 5.66. Corresponding bond stresses along the entire bed is illustrates in Figure 5.67. The bond stress variation during time was similar to the other plants and the bond stress behaviour along the bed is identical as in Marijampolė factory due to same production way with one long concrete bed.

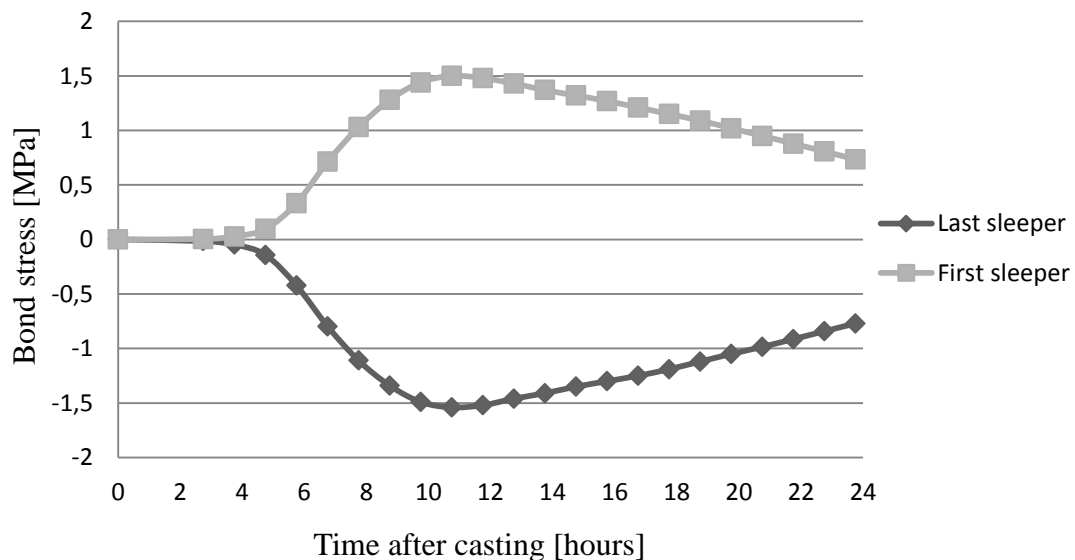


Figure 5.66 Bond stress depending on time after curing for the first and last sleepers with reference values in Sollenau factory.

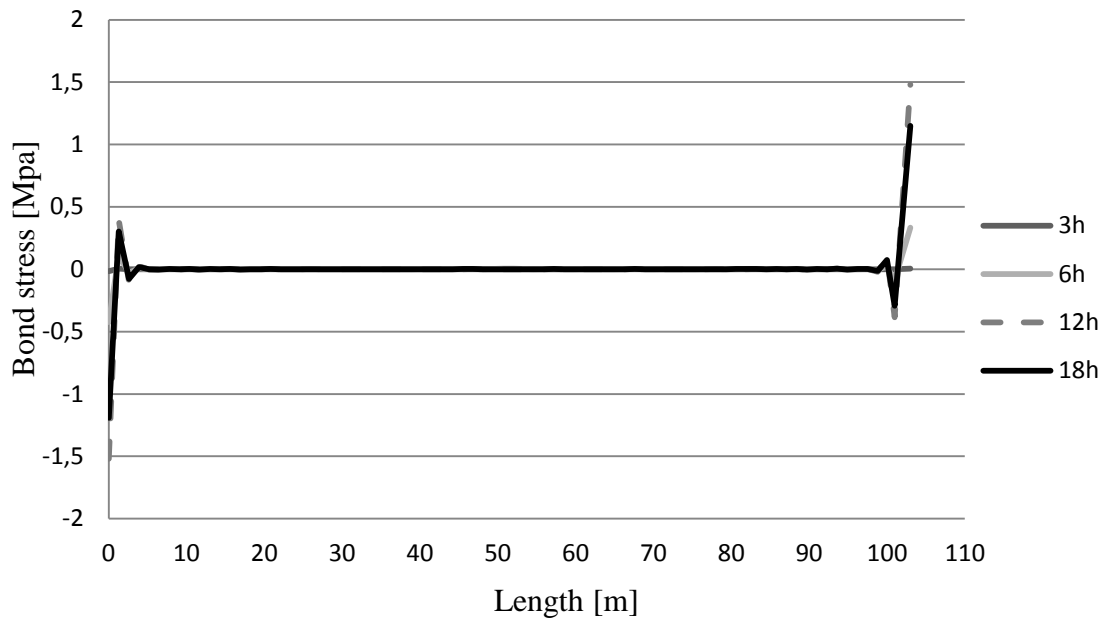


Figure 5.67 Variation of bond stress over the entire casting bed depending on different times according to reference values in Sollenau factory.

5.6.4 Comments to results

Generally comments are here given for analyses made for all the factories. All bond-stresses started at approximately four hours after casting, which was strange because they should start at different times according to the input values. The modulus of elasticity and bond behavior were verified with the equivalent time on small cube, maybe were these not applicable on the larger models.

Regarding the steel stress within the first and last sleepers, almost nothing happens before the bond starts, due to low temperature increase during the first hours after casting which was as expected.

Concerning the difference between the stresses in steel strands in the “naked” steel ends and the stresses in the steel within the concrete before any bond stresses occurs, the stress variation was almost the same with nearly no variation of the stresses from the initial steel stress. After the bond has started the stress in the “naked” steel ends decreases significantly and becomes also compressed sometimes. This could be a direct impact of a too large bond-stress at a too early age. Consequently, bond-development seems not to be entirely correct. However, even though the results are not quantitatively correct, they seem to be qualitatively consistent.

6 Parameter study

Different parameters were varied to study their influence on the prestress during the production of prestressed concrete sleepers in a qualitatively manner. The varied parameters were:

- The ambient air temperature
- Initial temperature of the steel strands
- Curing methods; without any sheeting or sheeting with polyethylene
- Bed arrangements of “The Long Line Method”
- Time of the concrete casting
- Expansion: different or equal.

The initial temperature of the concrete mixture was not included in the parameter study, since the equation of the adiabatic curves showed not so accurate effects on the resulting semi-adiabatic curves. If the initial concrete temperature would have been included in the parameter study, an adiabatic temperature curve had needed to be adopted, which would have created considerable uncertainty regarding the reliability of the results.

The results of the varied parameters can be seen for the Sollenau plant in the following subchapters. The other factories behaviour when changing the parameters can be seen in Table 6.1 in subchapter 6.7. All results in the parameter study were compared to reference values from Chapter 5.5.

6.1 The ambient air temperature

Higher ambient temperature resulted in increased prestress in the first sleeper and a lower gave a decreased prestress in relation to the reference curve, see Figure 6.1. Opposite behaviour occurred in the last sleeper at the passive side of the bed, see Figure 6.2. Stress variation in the “naked” steel strands for varying different external temperatures can be seen in Figure 6.3.

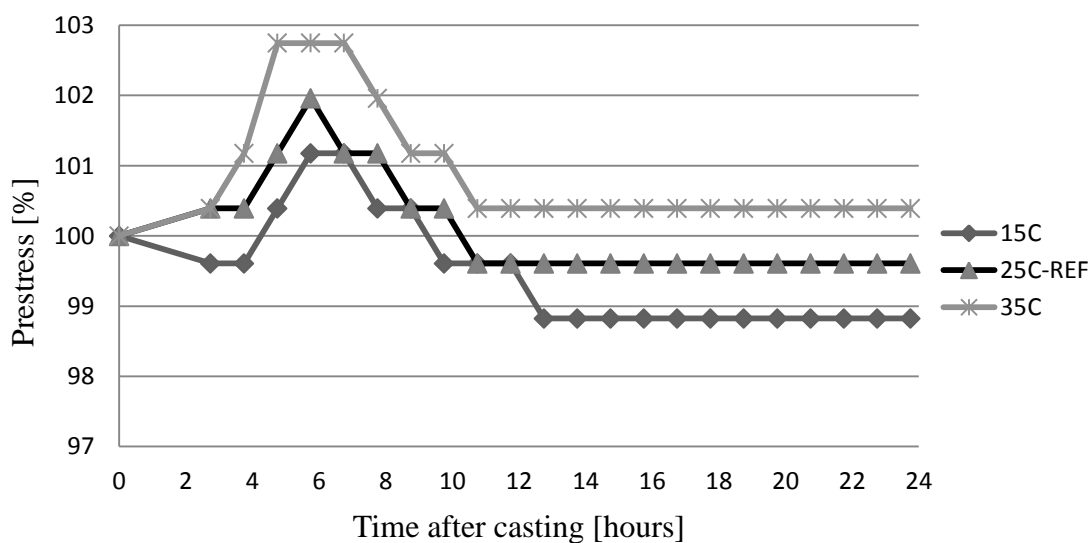


Figure 6.1 Stress variation of the first sleeper at the active side of the bed dependent of ambient temperature in the production hall.

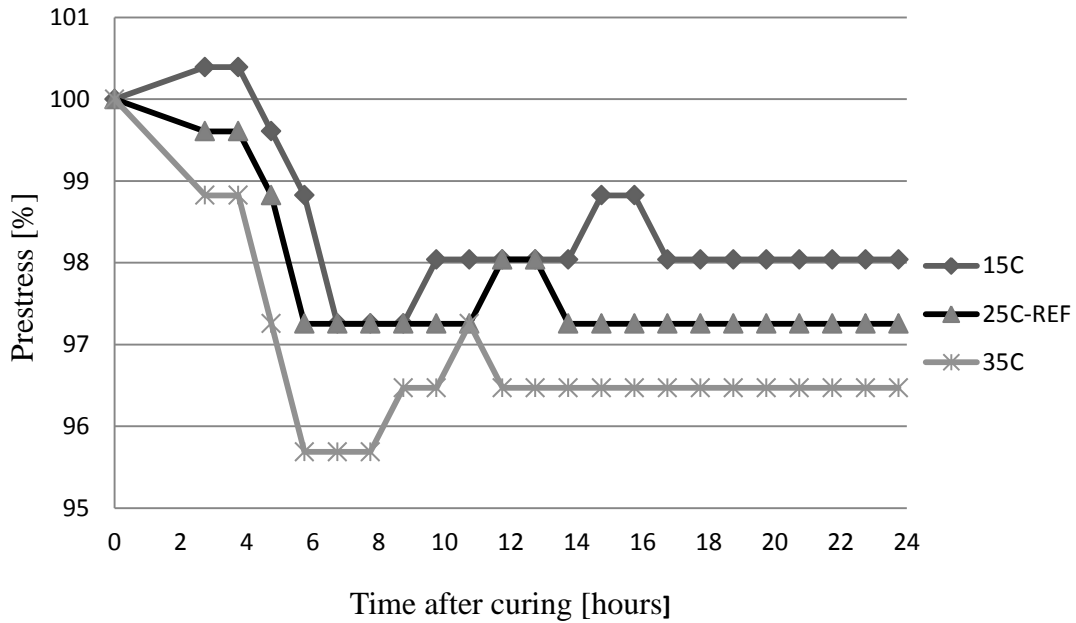


Figure 6.2 Stress variation of the last sleeper dependent of ambient temperature in the production hall.

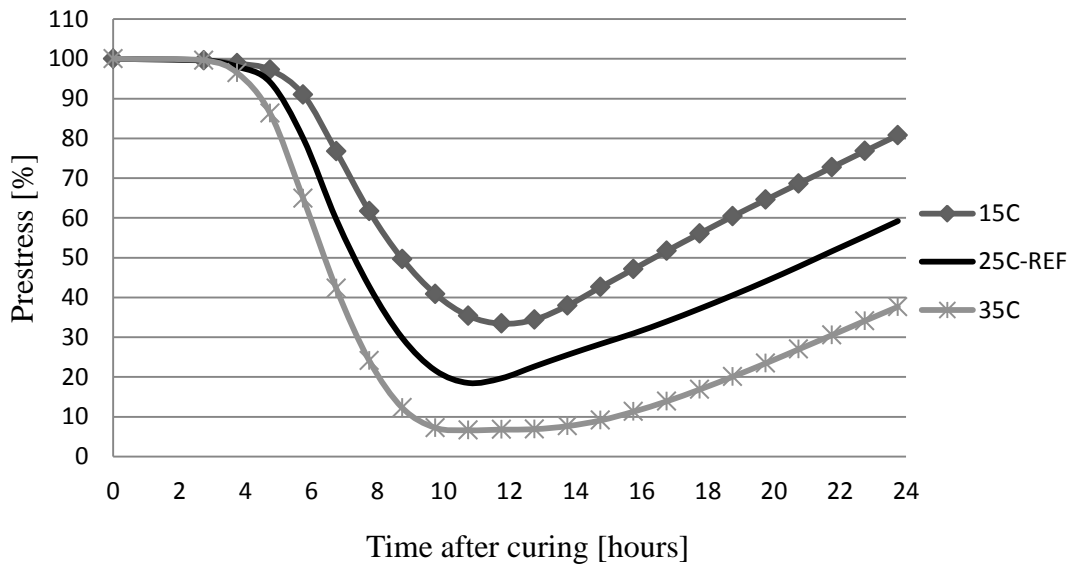


Figure 6.3 Stress variation of the “naked” steel strands dependent of ambient temperature in the production hall.

The influence of the external temperature on the prestress along the length can be seen in Figure 6.4. A decreased surrounding temperature resulted in more equal prestress in the steel strands within the concrete in different parts along the length.

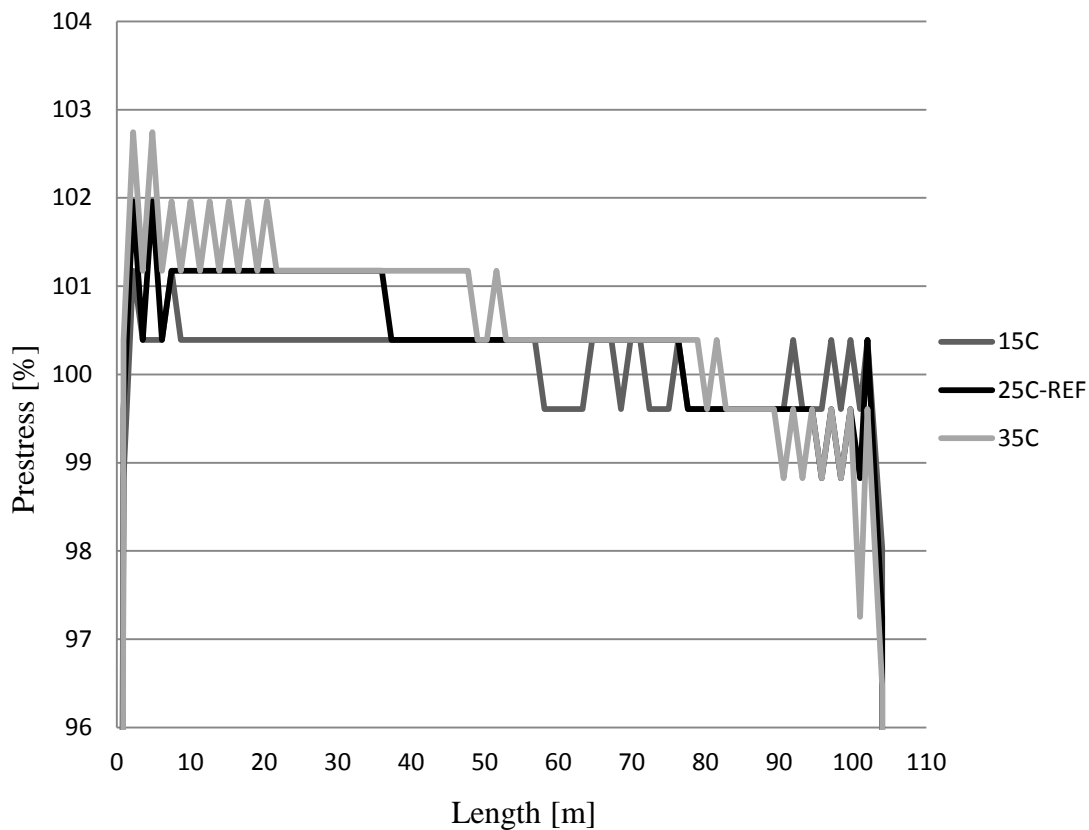


Figure 6.4 Varying external temperatures influence on the prestress variation along the length in Sollenau factory.

6.2 Initial temperature of the steel strands

Variations of the steel strands initial temperature were made. Results from FE-analysis showed that no variation of the prestress occurs in comparison to the reference curve. Consequently, preheating of steel strands does not influence the prestress variation.

6.3 Different curing methods

Different sheetings were compared in FE-analysis using different amount of convection, the reference used Polyethylene sheeting, see Figure 6.5 and Figure 6.6. Different convection values corresponded also to different amount of wind speed in the production hall. Constant convection along the bed was assumed in this study; though it was possible to vary the convection in different parts of the bed.

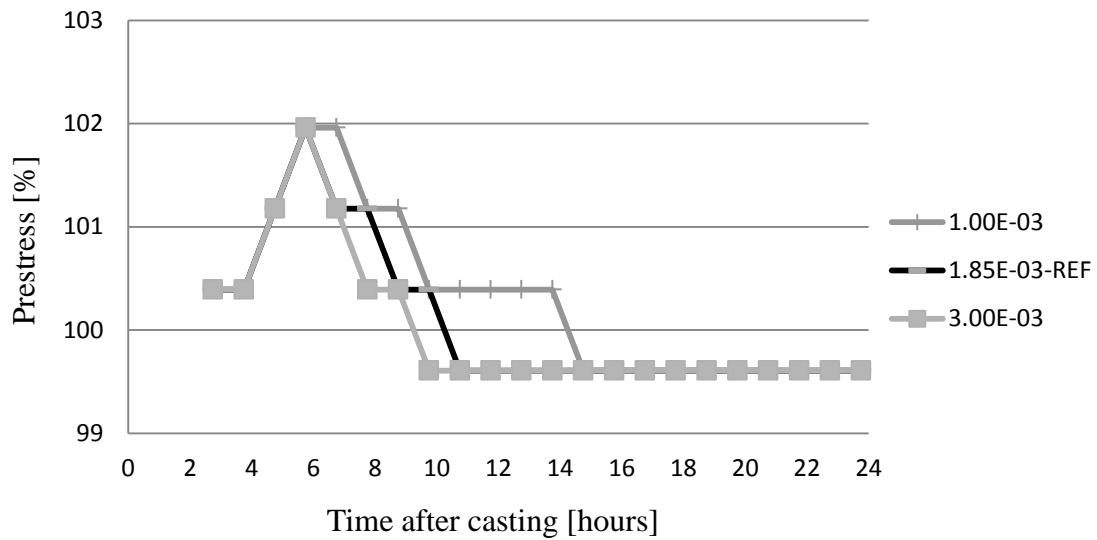


Figure 6.5 Stress variation of the first sleeper at the active side of the bed dependent of convection in the production hall.

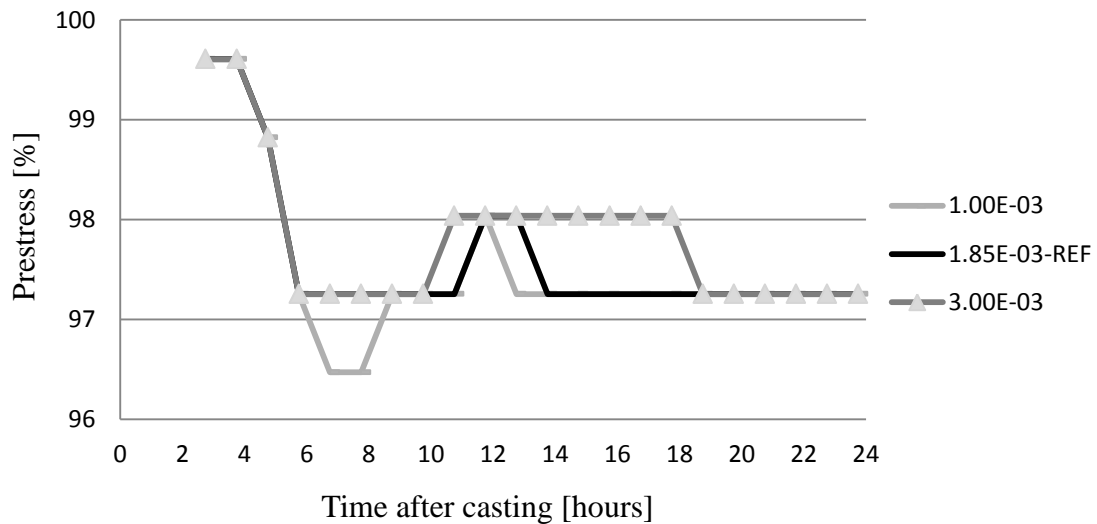


Figure 6.6 Stress variation of the last sleeper at the passive side of the bed dependent of convection in the production hall.

Figure 6.7 illustrate increased convection in the “naked” steel ends, which resulted in increased prestress in the contraction phase.

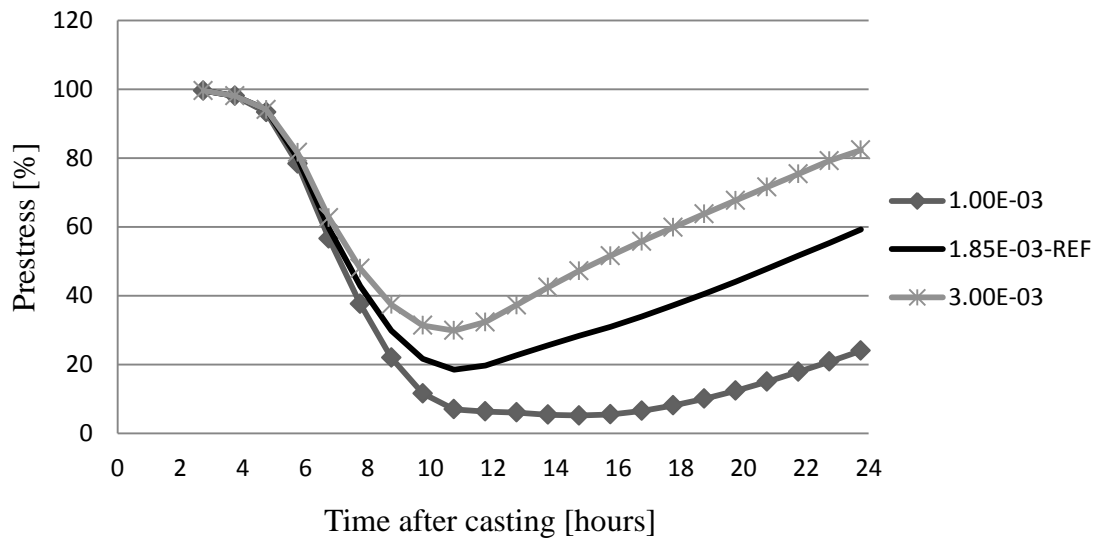


Figure 6.7 Stress variation of the “naked” steel strands depending on convection in the production hall.

6.4 Bed arrangements of “The Long Line Method”

Analysis of the different production conditions of “the Long Line Method”, casting in concrete package of four sleepers with “naked” steel parts in between (Vislanda factory) or casting with one set of moulds (Marijampolė and Sollenau), were made to verify which production method that gave most accurately results regarding prestress losses within the concrete sleepers. All thermal and mechanical properties in the Vislanda factory were applied on the casting bed in the plant in Sollenau. This corresponded to that the “naked” steel parts in the Vislanda factory were removed and replaced with the boundary conditions in Sollenau factory, with some simplification regarding the length which was different. Results of the FE-analyses can be seen in Figure 6.8, Figure 6.9 and Figure 6.10, which shows that the “Vislanda with Sollenau boundary conditions” had lower prestress than the reference bed arrangement in Vislanda.

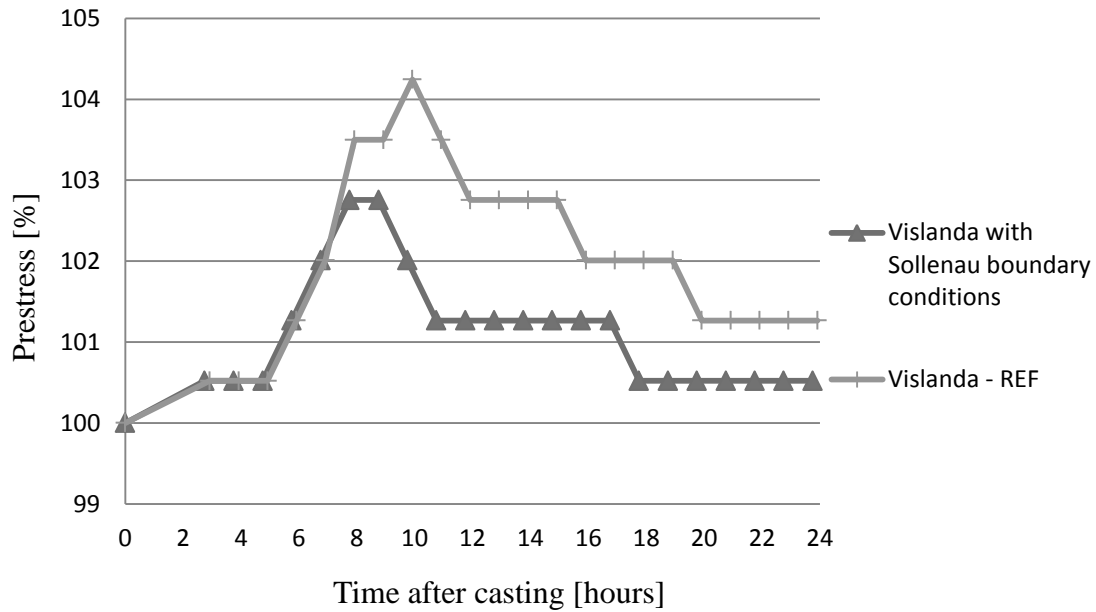


Figure 6.8 Comparison of variation in the steel strands within the first sleeper between Vislanda factory with boundary conditions of the casting bed according to Sollenau and ordinary conditions in Vislanda, Reference values were used.

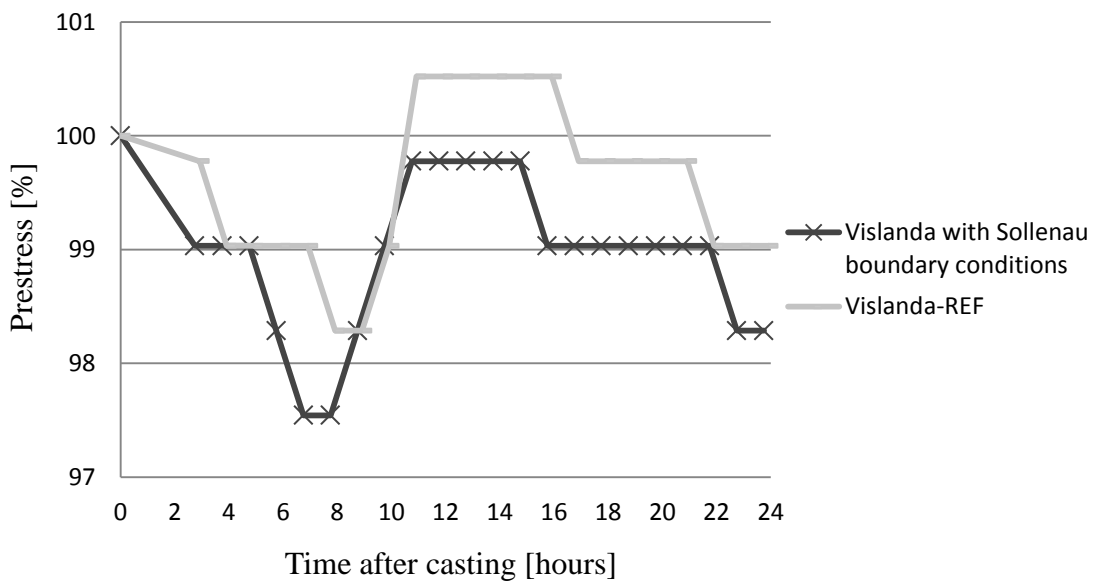


Figure 6.9 Comparison of variation in the steel strands within the last sleeper between Vislanda factory with boundary conditions of the casting bed according to Sollenau and ordinary conditions in Vislanda, Reference values were used.

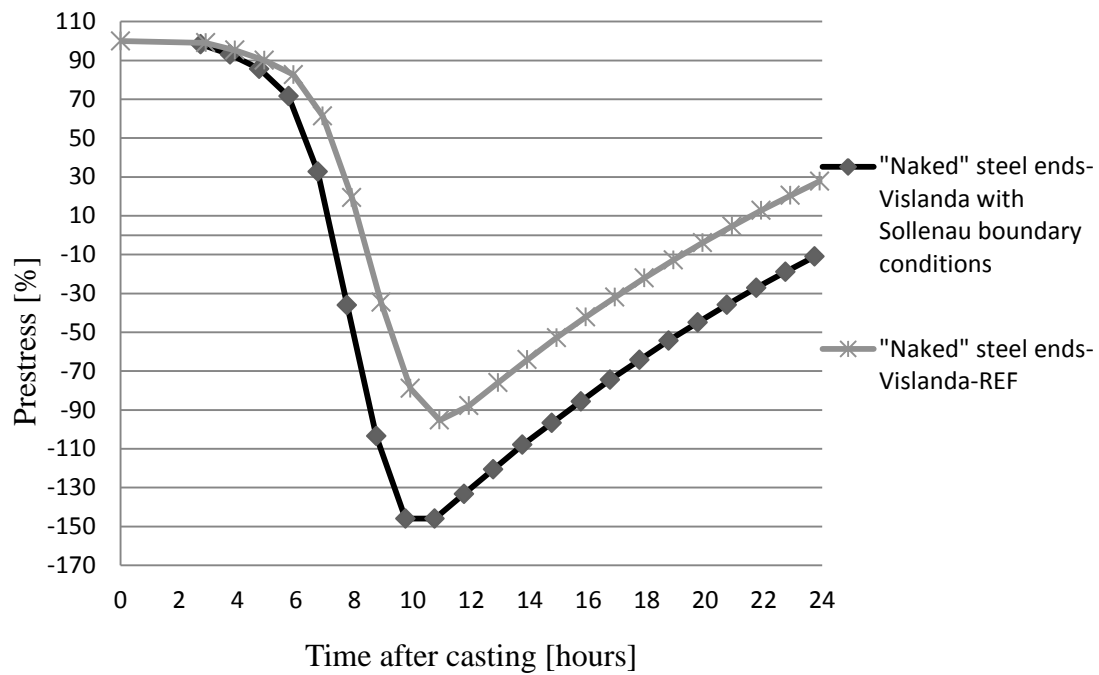


Figure 6.10 Comparison of variation in the “naked” steel ends between Vislanda factory with boundary conditions of the casting bed according to Sollenau and ordinary conditions in Vislanda, Reference values were used.

6.5 Different casting times

Analysis regarding how the time of casting influence on the prestress variation in the steel strand were further made. Results from the FE-analysis showed that long casting time affected the prestress force negatively in the last sleeper and positively in the first sleeper, especially during the first hours of the curing, see Figure 6.11 and Figure 6.12 for the first and last sleeper respectively. Zero casting time corresponded to casting the whole bed in one sequence which only is theoretically feasible, but has been chosen to be included in the analyses anyway.

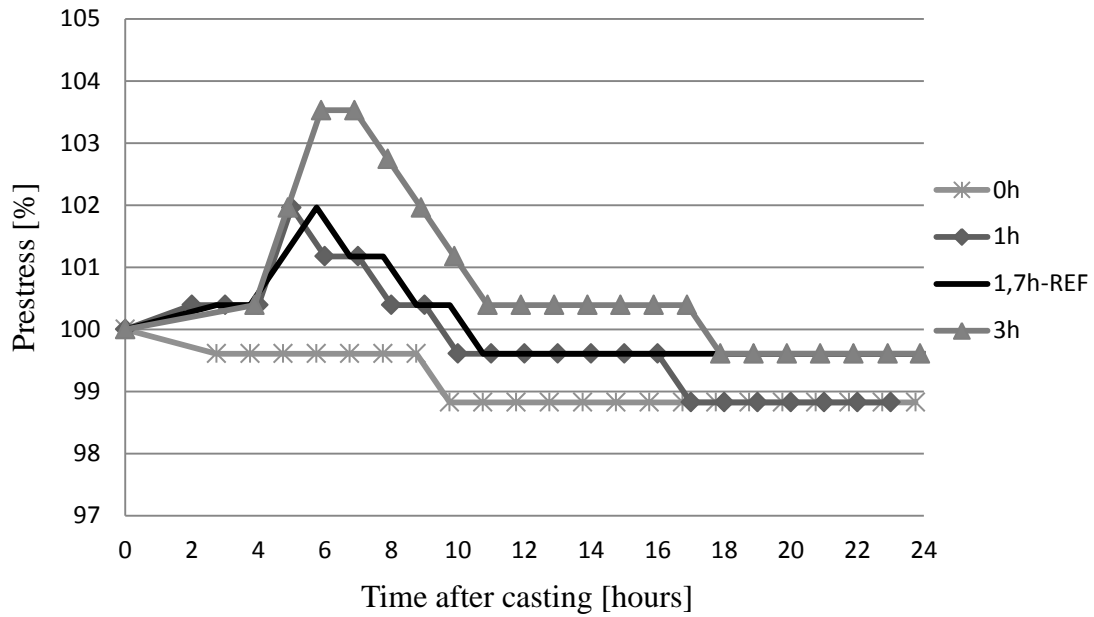


Figure 6.11 Stress variation of the first sleeper at the active side of the bed dependent of casting time in the production hall.

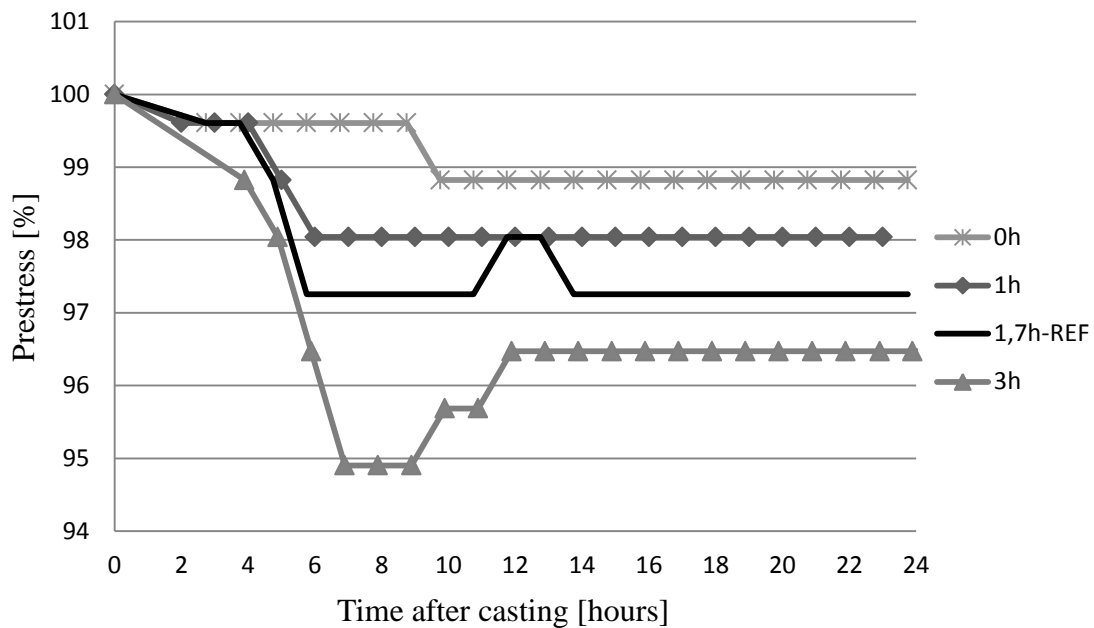


Figure 6.12 Stress variation of the last sleeper at the passive side of the bed dependent of casting time in the production hall.

In the “naked” steel strand was only a small variation was observed, see Figure 6.13.

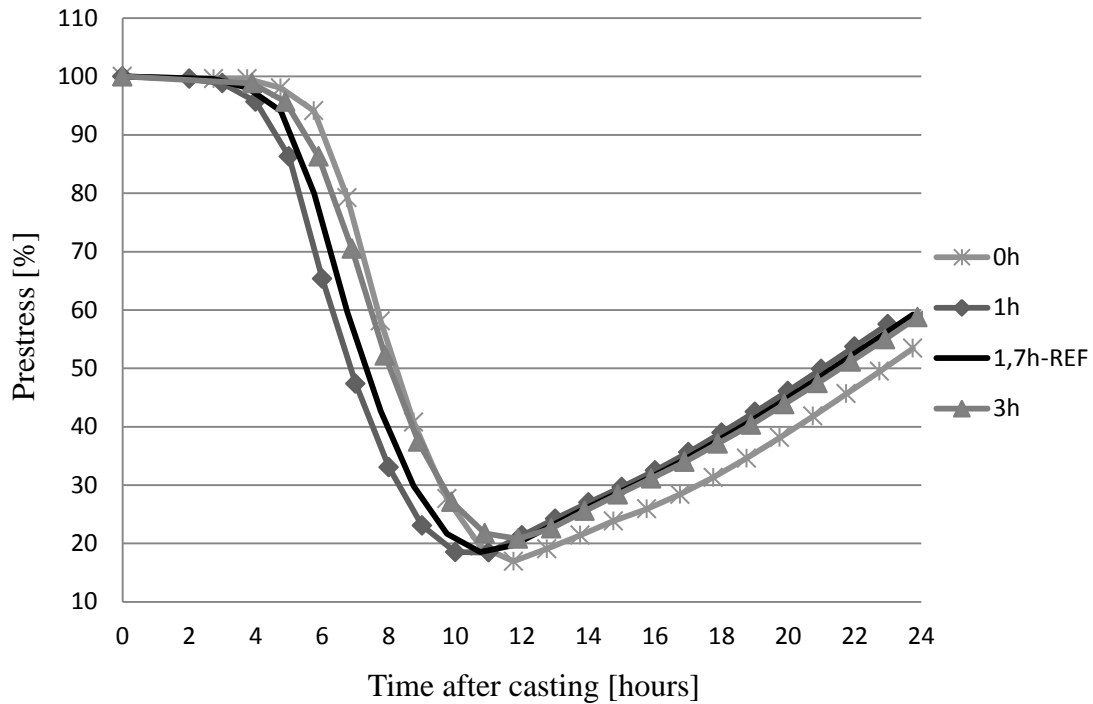


Figure 6.13 Stress variation of the “naked” steel strands depending on casting time in the production hall.

6.6 Expansion behaviour

Increasing the thermal expansion coefficient on concrete resulted in higher prestress in the first sleeper and lower prestress in the last bed, see Figure 6.14 and Figure 6.15. Analyses were also made with the same value of the expansion coefficients on steel and concrete; lower respectively higher than the reference curve. The analyses showed no influence of different thermal expansion coefficients of the steel strand.

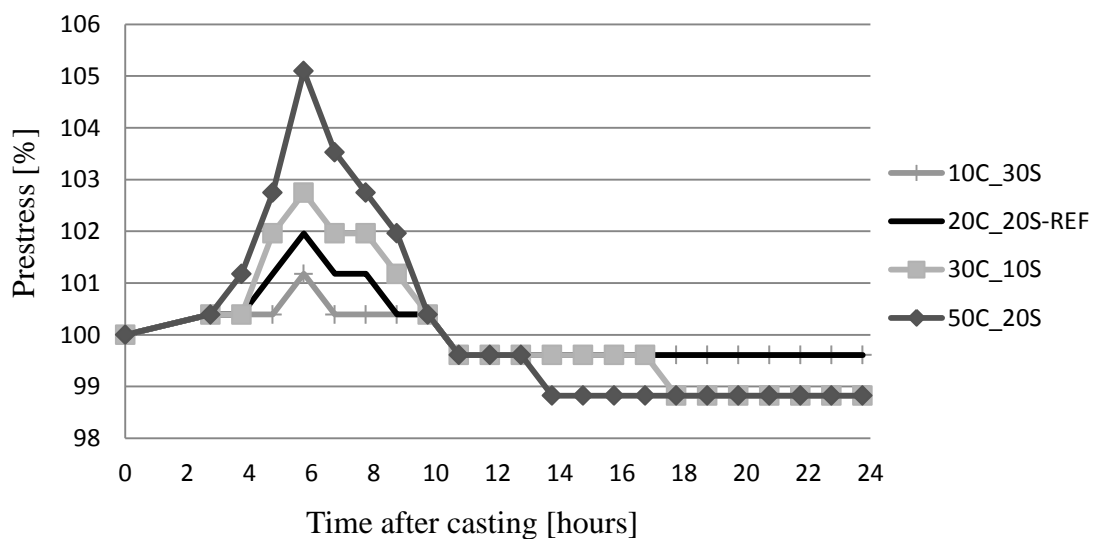


Figure 6.14 Stress variation of the first sleeper at the active side of expansion coefficients on steel and concrete.

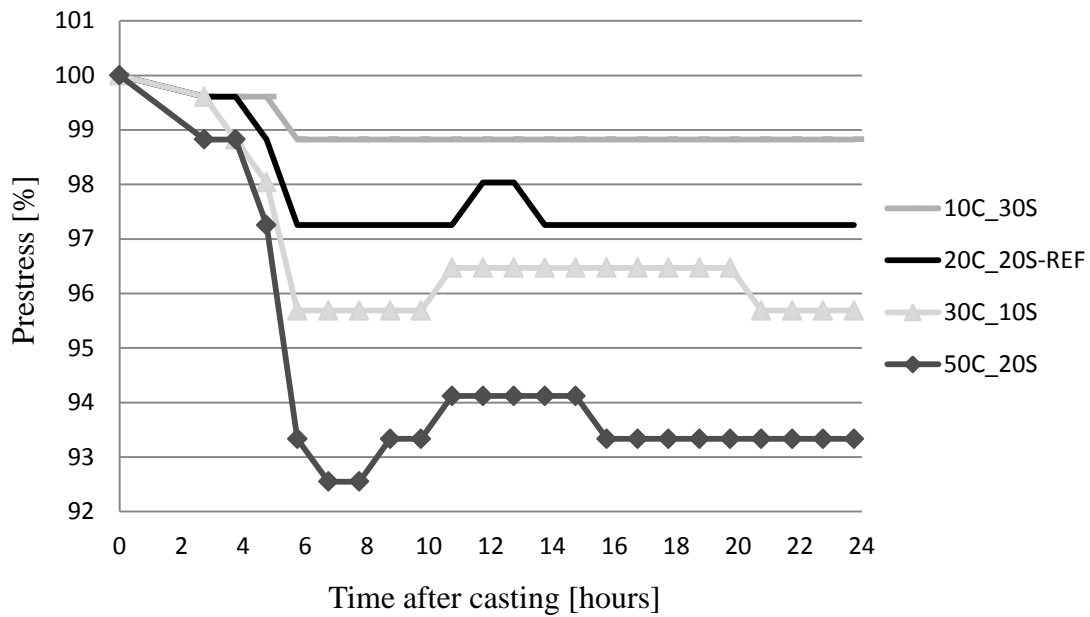


Figure 6.15 Stress variation of the last sleeper at the passive side of expansion coefficients on steel and concrete.

Higher expansion coefficient on concrete gave higher prestress losses in the “naked” steel strands, see Figure 6.16.

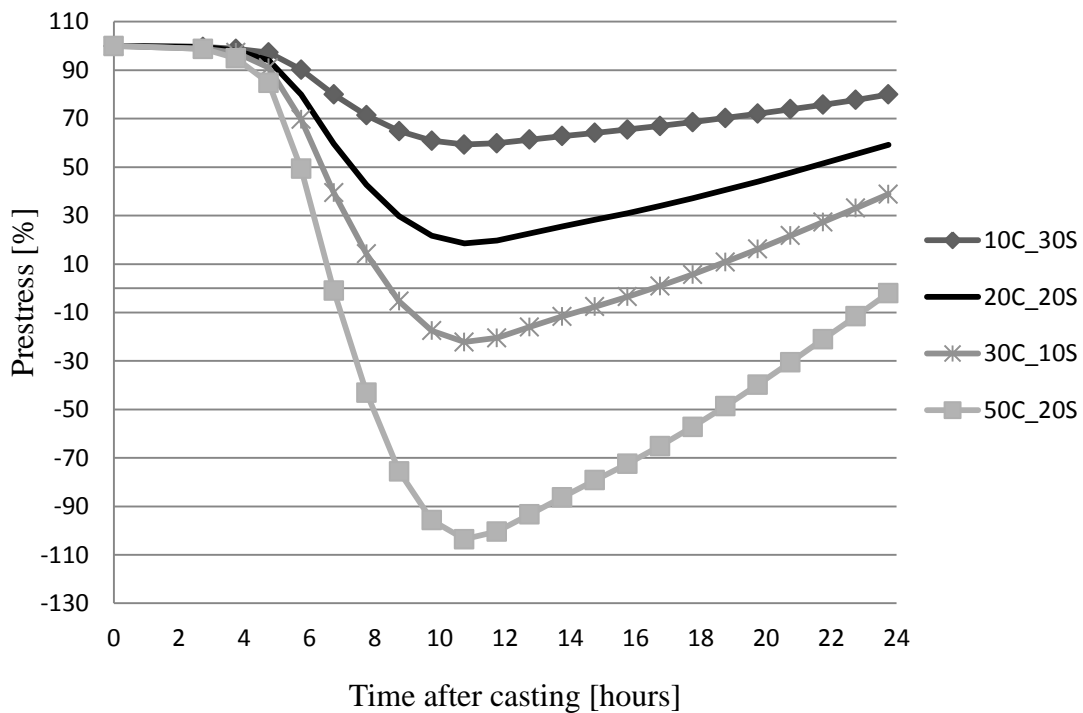


Figure 6.16 Stress variation of the “naked” steel strands dependent of expansion coefficients on steel and concrete.

6.7 Summary of results obtained in the parameter study

In Table 6.1 results from the parameter study are compiled. Positive or negative influences on the prestress loss in the steel strand within the concrete in first and last sleepers are given. The signs were in opposite way if the parameters should be decreased. Marijampolė factory was not included in the summary since very small variation occurred when the parameters were changed, due to almost negligible prestress losses in the FE-results.

Table 6.1 Summary of how different parameters influenced the prestress; + indicates larger prestress, - indicates smaller prestress (thus larger prestress loss).

Analyse time: 24 h Increase of:	Vislanda		Sollenau	
	First sleepers	Last sleepers	First sleepers	Last sleepers
Surrounding temperature	+	-	+	-
Convection coefficient	-	-	Unaffected	-
Concrete Expansion coefficient	+	Unaffected	+	-
Casting time	Unaffected	Unaffected	+	-

7 Achieved knowledge of principal phenomena influencing prestress losses during different phases of the sleeper production

Following subchapters describe the phenomenon of prestress losses in different phases of the concrete sleeper production. Figure 7.1 describe the different phases. As previously mentioned, this thesis focuses on phase 2 in Figure 7.1, the other phases were only studied in literature study. An illustration of the most important causes of prestress can be seen in Figure 7.2.

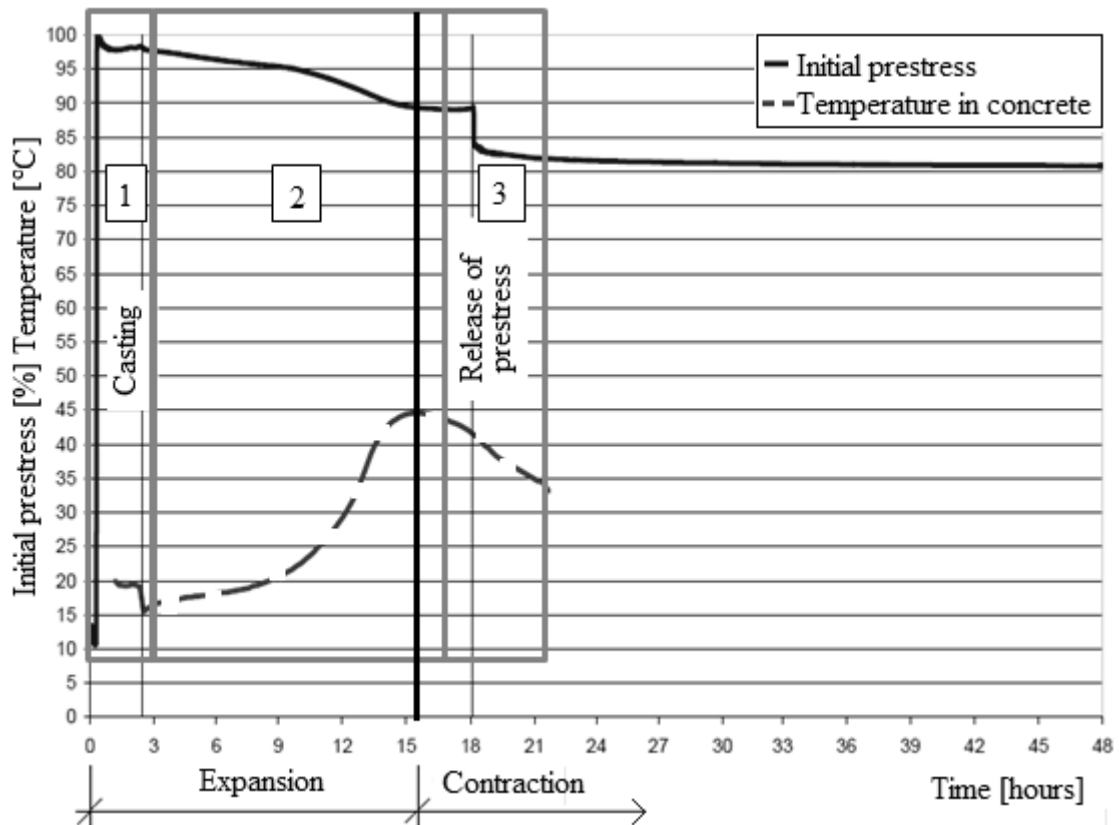


Figure 7.1 Different phases along the prestress loss during production, phase 1: before casting, phase 2: From casting to release of prestress and phase 3: release of prestress.

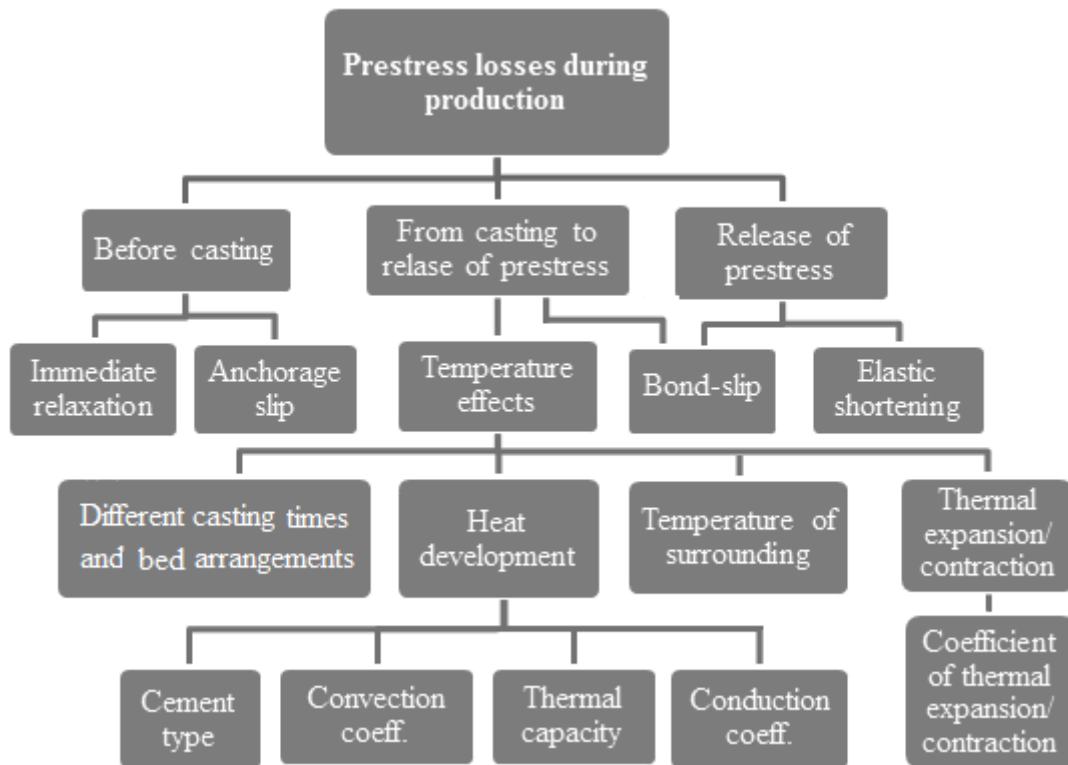


Figure 7.2 The most important causes of prestress losses during production.

7.1 Before casting

Phase 1 in Figure 7.1 includes the prestress losses before casting. They can be explained by:

- Immediate relaxation of steel strands
- Losses due to inner friction and leakage in hydraulic jack

Before the concrete is cast, prestress loss due to relaxation of the pre-tensioned strands occurs. This takes place during the period between the pre-tensioning of the strands and casting of concrete. This loss is very small due to very short time and use of low relaxation strands which only relax approximately 2,5 % after 1000 hours. Hand calculation of the relaxation according to Eurocode 2 showed a prestress loss of 0,38 %, 2,28 % and 0,49 % in Vislanda, Marijampolé and Sollenau respectively before casting, see Appendix A.3.

The pressure drop seen in measurements were most probably due to both internal friction and leakage between the two chambers of the hydraulic jack, see Andersen (2011).

7.2 From casting to release of prestress

The prestress losses that occurred from casting of concrete to release of the pre-tensioned steel strands, see phase 2 in Figure 7.1, can be described by:

- Temperature effects
 - Temperature of surroundings
 - Heat development

- Thermal expansion/contraction
- Different casting times and bed arrangements
- Bond-slip
- Relaxation of steel strands

Hand calculation of the relaxation showed a low prestress loss of 0,45 – 0,7 % for the factories in this phase, see Appendix A.3. Thus in this short time interval, relaxation losses were negligible.

When a temperature increase occurred in the concrete due to exothermal reaction in the hydration process, temperature was transferred from the concrete by conduction to the steel strands within the concrete. Because the conductivity of the steel is high, temperature development was almost identical in the two materials. When the temperature in the concrete increased, concrete and the steel strands expanded. However, when the concrete temperature decreased after the maximum value started the contraction phase, see Figure 7.1. If only temperature affected the prestress losses, the prestress decreased until the time for the maximum temperature occurred in the concrete. Opposite behaviour occurred in the contraction phase. Generally, temperature effects influenced the steel stress with a behaviour which looked like a mirrored temperature curve.

Bond stresses started approximately when the temperature increased significantly. Probably, bond strength did not increase more after the maximum temperature was reached. Before bond started, the prestress losses of the “naked” steel strands and the losses in the steel within the bed were equal. Losses depended mainly on temperature effects on the steel strand. However, due to casting in sequences, the temperature development along the bed was delayed, like a pulsing motion wave. This caused a delayed stiffness of the concrete which was in direct proportion to the maturity development. Consequently, stiffness was gained in the firstly casted concrete parts at the active side of the bed. The bed therefore expanded more to the passive side, because the concrete there had lower maturity. This behaviour generated increased steel stress within the concrete in the first part of the bed and decreased stress in the last part. The decreased prestress along the length were seen in results of analyses of all factories, but most clear in the Sollenau plant, see Figure 5.61 in Chapter 5.6.3. This behaviour verified why the sleepers in the first bed were better than the last, which were recognized in the factories.

When the bond started, concrete grabbed the steel strand and expanded it until maximum temperature was reached. Consequently, “naked” steel ends became compressed and the prestress in the steel within the bed increased. The stress development in the “naked” steel ends and the steel inside the concrete behaved therefore in opposite ways when the bond started in the FE-models. After maximum temperature was reached, the concrete wanted to contract. At this time only bond-slip occurred in the ends of the bed and in the mid part of the bed where concrete and steel were in full interaction. Consequently, the concrete could only contract in the ends, where bond stresses occurred, see Figure 5.67. Figure 7.3 illustrates the behaviour of steel and concrete in different parts at different times during the curing process according to the “The Long Line Method” used in Marijampolė and Sollenau factories.

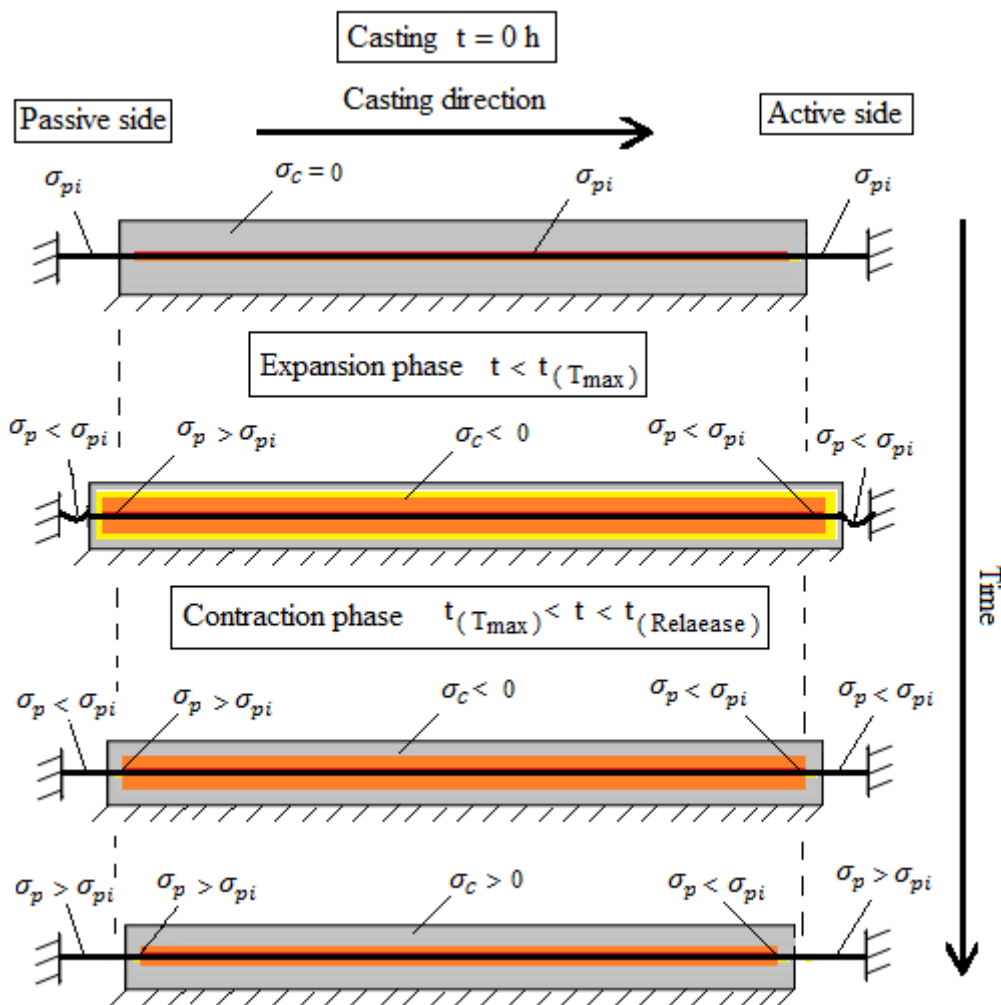


Figure 7.3 Behaviour during the production process illustrated in different phases along the length of the casting bed. Generally, prestress variation during time in the steel strand within the concrete was opposite in the first last beds. The steel stress, σ_p , varied from the initial steel stress, σ_{pi} , in different parts of the bed depended on both thermal- and mechanical properties over time. The figure illustrates the behaviour along the length in Marijampolė and Sollenau factories. In Vislanda factory, the behaviour was the same in the end parts, but due to “naked” steel strands in between every fourth sleeper, the stresses during expansion phase decreased, while they increased during the contraction phase.

The thermal coefficient of thermal expansion of young concrete was showed in the parameter study to have significant effect on the prestress variation. The explanation can be seen in Figure 7.4. The time when the concrete cured, the temperature development occurred, and concrete had its highest gradient of CTE. During the temperature increase, both the expansion phase and the bond development between the steel strands and concrete started. Since the concrete was cast in several sequences, along a long line, the casting time between the first and last sleeper differs with around 1-3 hours. If CTE instead was according to McCullough, higher expansion of concrete in the beginning occurred. Consequently, higher prestress losses in the last sleeper occurred due to a combination of increased bond, high expansion and delayed casting time along the casting bed. It should be noted though, that the input for the expansion

behaviour shown in Figure 7.4 actually is for cement paste; thus it should have been weighted with the aggregates according to equation 2.7.

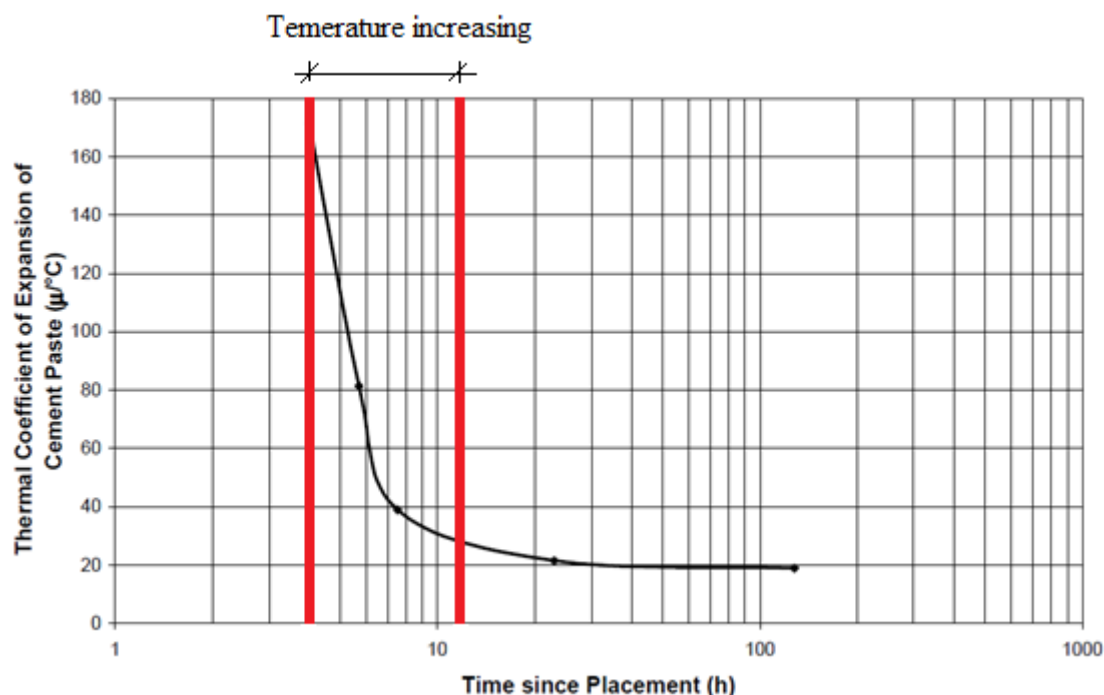


Figure 7.4 Development of thermal coefficient of expansion of Portland cement depended on time after curing. The major increase of temperature at the three different factories is marked in the figure, modified from McCullough (1998).

Hand calculations were made on the variation of the steel stress due to thermal effects. As input in the calculations, the semi-adiabatic temperature curves from measurements were used. The hand calculation did not take the bond between the steel and concrete into account. Consequently, prestress increased when the temperature development were maximum and started to cool down. This was not the case in the measurements, because bond occurred when maximum temperature took place. The results from hand calculations showed losses of prestress, from casting to maximum temperature, of around 3,3 – 6,7 % and 4,5 – 5,6 % for the factories with reference to EC2 and Engström (2011) respectively, see Table 7.1 and Appendix A.3.

Table 7.1 Summary of results from measurements and hand calculations calculated at the point when the maximum temperature occurs during curing.

[%]	Part of phase 2: From casting to maximum temperature							
	Relaxation	Shrinkage		Thermal effect		Total		
Factory	EC2	EC2	CEB-FIB	EC2	CEB-FIB	EC2	CEB/EC2	Test
Vislanda	0,5	0,3	0,02	3,6	5	5,0	4,4	6
Marijampolé	0,8	0,3	0,02	3,3	3,3	3,3	4,3	36
Sollenau	0,6	0,27	0,02	4,7	6,7	6,7	5,5	8

7.3 Release of prestress

At release of prestress, phase 3 in Figure 7.1, an instantaneous prestress loss occurred. This could be explained by a phenomenon called elastic shortening of the concrete, which was thoroughly described in Chapter 2.3.2.1. When the initial prestress force was released, instantaneous elastic shortening of the cast concrete took place which caused an immediate partial prestress loss. This occurred because the in-cast steel strands wanted to shrink back to its original length and therefore created a pressure force, which the concrete tried to resist. Due to almost fully bond between the two materials, forces were transferred from the steel strands to the concrete and equilibrium was achieved. The prestress loss during the release of the prestress force could also be related to bond-slip between the steel strands and the concrete, as full interaction was not reached. Hand calculations, in Appendix A.3, regarding the prestress losses at release of prestress force showed a prestress loss of 0,9 %, 2,6 % and 1 % in the Vislanda, Marijampolé and Sollenau respectively.

7.4 Comparison of prestress variation during the production between results from FE-analysis with reference values, hand calculation and measurement

Comparison of the prestress variation during casting in the steel strand within the concrete in the last sleeper for Vislanda, Marijampolé and Sollenau can be seen in Figure 7.5, Figure 7.6 and Figure 7.7 respectively.

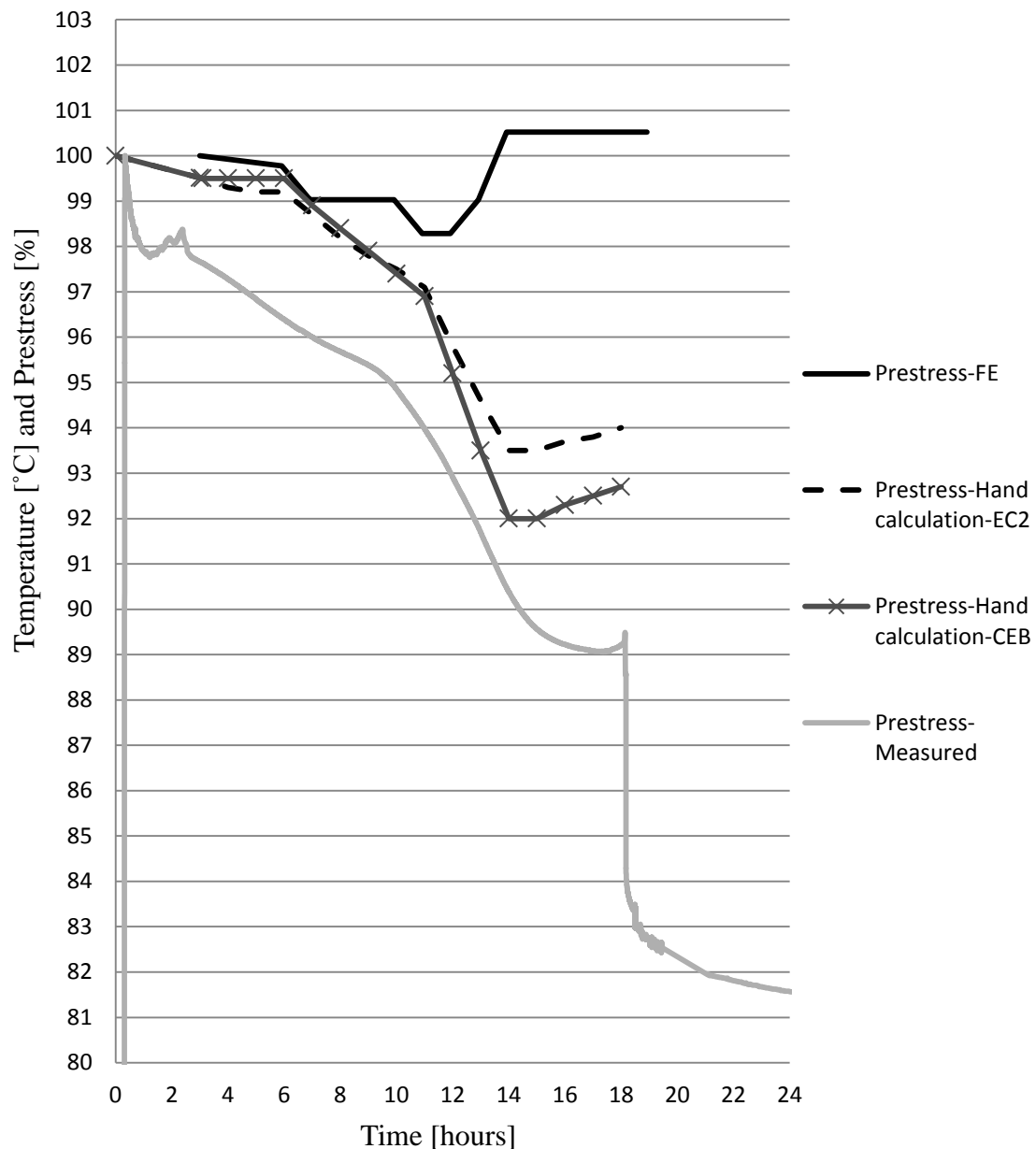


Figure 7.5 Comparison between prestress from FE-analysis, measurements and hand calculations according to both Eurocode 2 and CEB-FIB Model Code 1990 in the steel strand within the last sleeper in Vislanda factory.

The results of prestress variation from hand calculations in Figure 7.5 corresponded very well to the prestress loss in measurements. The main difference between hand calculations and measurements was the, approximately 2 %, decrease of the prestress which had occurred three hours after tensioning. This could be explained by the inner friction and leakage in the hydraulic jack. Even though the results differ quite a lot in values, for the first eight hours the same trend can be noticed in all of the results: measured, hand calculated and FE results. Thereafter, the measured prestress continued to decrease while the analysis results increased.

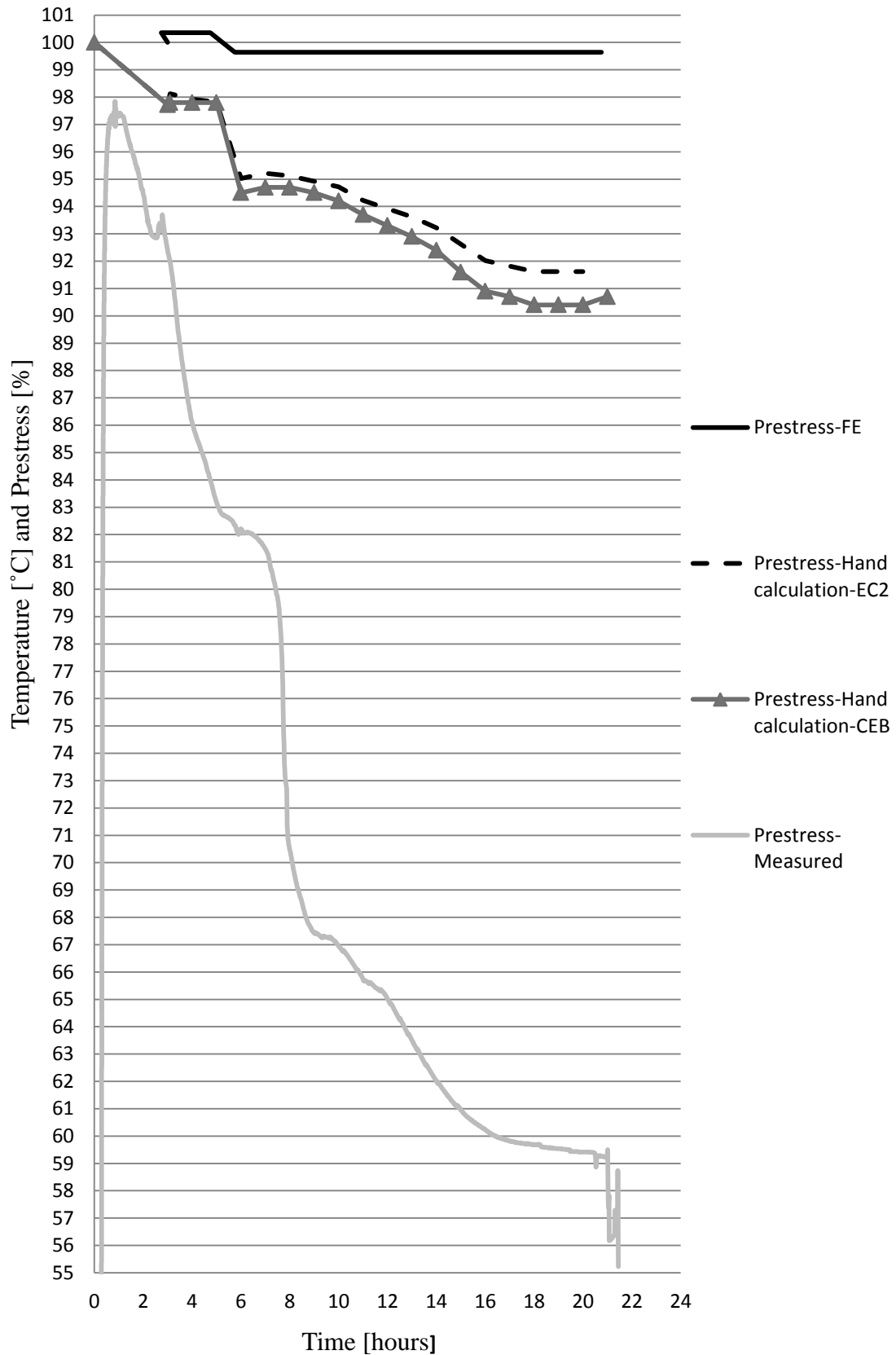


Figure 7.6 Comparison between prestress losses from FE-analysis, measurements and hand calculations according to both Eurocode 2 and CEB-FIB Model Code 1990 in the steel strand within the last sleeper in Mari-jampolé factory.

As Figure 7.6 illustrates, the prestress in the analyses did not agree very well with the measured. While the FE-analysis resulted in almost constant prestress in the last bed, the hand calculated results indicate a decrease but not as much as measured.

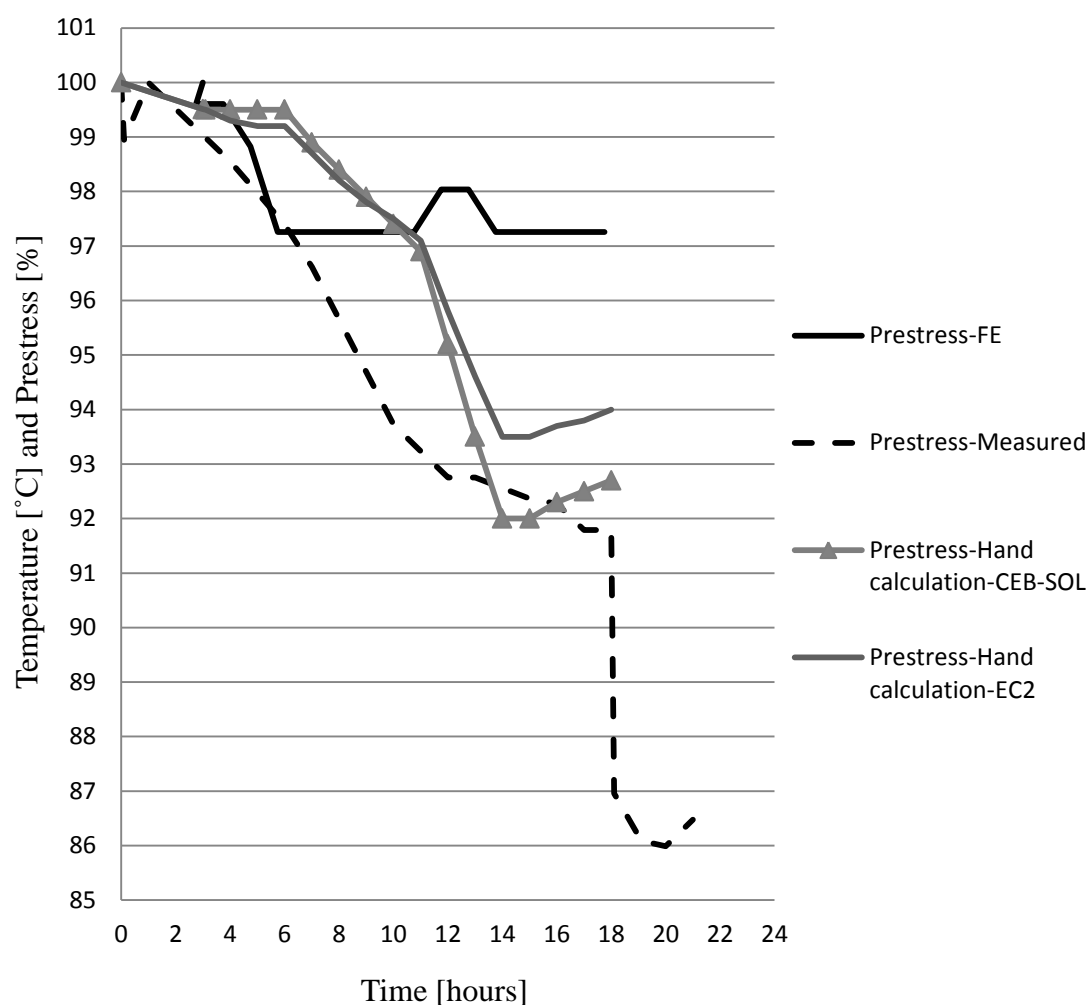


Figure 7.7 Comparison between prestress losses from FE-analysis, measurements and hand calculations according to both Eurocode 2 and CEB-FIB Model Code 1990 in the steel strand within the last sleeper in Sollenau factory.

The losses of prestress in the FE-results were larger in Sollenau factory compared to the other analyses. However, results from hand calculations corresponded better to measurements as Figure 7.7 shows.

8 Final remarks

8.1 Discussion

The aim of this master's thesis was to obtain better understanding about losses in prestress during production of sleepers and to explain which main parameters that influence the given prestress loss in three plants using the production process "The Long Line Method". Finite element models trying to characterize the boundary conditions during production at the plants were made using staggered flow-stress non-linear analysis. Results from the analyses indicates that the assumed bond-slip behaviour with maturity dependence between the young concrete and steel strands was too simplified to obtain the same prestress loss as in measurements. The general results from both hand calculations and FE-analyses showed less prestress losses compared to the measured results. Differences were largest in Marijampolė factory which had by far the coldest surrounding and largest prestress losses. Therefore, it was believed that cold surrounding environment had a significant influence on the losses. On the other hand, FE-analyses with reference values of thermal and mechanical properties showed that the cold external temperature did not affect the prestress losses in the Marijampolė. The sudden prestress losses observed in measurements could not be explained in the FE-analyses made in this master thesis. Instead, the opposite behaviour was shown in analyses of Marijampolė factory, with smallest losses during curing. This is due to slow development of the temperature and low maximum temperature which influenced the maturity development of the mechanical properties in the concrete. The reason for the contradicting results is though unknown.

In the analyses of the Sollenau factory, higher temperature and fastest temperature development occurred which resulted in larger prestress losses in the last sleepers in the casting bed. Consequently, the heat development in concrete, depending on the concrete composition, directly influenced the prestress loss. If not a considerable heat development occurred, mechanical properties in the concrete did not grow enough, which resulted in insufficient quality of the concrete strength. However, if too fast heat development occurred in combination with higher maximum temperature, the prestress varied more along the length, due to increase of both thermal and mechanical effects as expansion, bond-stresses etc. In reality, the temperature development can be regulated by adding admixtures in the concrete mixture.

The results from the FE-models cannot be completely reliable. One major reason is probably too large and too early bond stress development. However, the purpose with the FE-models was not to completely be able to reproduce the behaviour seen in measurements; instead the major purpose was to describe the principal behaviour. Probably the bond-slip with maturity dependence was too simplified and did not capture the actual behaviour during the curing process of young concrete. Maybe it is more accurate to model with slower increase of the bond-stress, assuming very small bond stress just before the maximum temperature occurs and then exponentially increase it up to maximum bond stress. In the maturity dependent bond-slip behaviour the bond stress was assumed to depend on the total slip; i.e. also slip that took place when the concrete had a low maturity will generate bond stresses when larger maturity is reached. Furthermore, the assumption of constant values on coefficient of thermal expansion, CTE, during curing was shown to have major influences on the results. If the value increased, the prestresses decreased significantly.

The influence of higher convection resulted in more even stresses in the steel strands along the bed, since the temperature development decreased. However, too much convection resulted in insufficient quality of the concrete. To have a rational production, “The Long Line Method” requires a fast curing period. Sheeting is therefore needed, but to obtain good quality of prestressed concrete sleepers, knowledge regarding convection coefficients of different sheetings is necessary.

8.2 Conclusions

Prestress losses of prestressed concrete sleepers using “The Long Line Method” were shown to be a complex problem with several influencing phenomena. These can be divided into thermal and mechanical parts in analysis, where the thermal is first analysed and then inserted as loads in each time-step in a structural analysis taking care of the mechanical properties.

The structural behaviour can be separated to three phases; before casting, from casting to release of prestress and at release of prestress. In the first phase; before casting, the prestress losses are due to inner friction and leakage in the hydraulic jack. A loss of prestress in this phase is easily calculated, and the initial prestress can then be updated with a force corresponding to the calculated prestress loss. Focus in this thesis was on phase 2; from casting to release of prestress. In this phase temperature effects such as expansion, contraction, and bond behaviour are important phenomena that influence the prestress changes along the bed.

The following parameters were shown to influence the principal behaviour of prestress variation within the casting bed at different times:

- The development of the concrete temperature, from hydration process, was found to be important. The maturity concept which includes the effect of temperature development in reference to the surrounding temperature is important because it relates to the stiffness and bond development.
- It is important to emphasize that slower temperature development makes the thermal effects, i.e. expansions and contractions, less pronounced, while other concrete properties such as strength and bond capacity become delayed. Hence, the relation between the thermal and mechanical properties is very important and is directly dependent of each other in a complex way.
- Lower ambient temperature resulted in a more even steel stress distribution along the bed while higher ambient temperature resulted in an uneven steel stress distribution.
- Initial temperature of the steel strands did not influence the results.
- To control the heat development in the bed, different sheeting can be used with desired properties.
- Two different bed arrangements were studied: long bed and small beds of four sleepers with “naked” steel in between. The factory in Vislanda which uses the bed arrangement with small beds had the largest steel stresses along the length. The effect was largest at the maximum temperature.
- Casting times, i.e. the time it takes to cast the whole bed, are preferable to keep as short as possible to get an even steel stress distribution.
- Expansion coefficients of concrete have a large influence of changes in the steel stress. Early temperature development results in higher expansion be-

cause the coefficient of expansion is very high during the first hours after casting.

A general conclusion from the parameter study was that there are many parameters influencing the prestress variation which if changed correctly, leads to a more even steel stress distribution along the bed in all plants.

8.3 Further studies

Further studies could include improvements regarding varying cross section of the sleepers and more accurate modelling of the steel strands where separate strands are modelled in correct positions can be made. Furthermore, the casting process was in this work also simplified assuming casting steps of five meters. A deeper investigation of the phases; before casting and at release of prestress can be performed. The finite element models created in this master's thesis can be improved by better control of bond-slip relation during early age and the implementation of a thermal expansion coefficient which depends on time. Friction between moulds and concrete can be introduced, which creates accumulated prestress losses along the length. There are also some thermal properties that can be varied according to the theory of material behaviours made in this report; specific heat capacity, conduction, convection and irradiation. It turned out during the literature study that it was difficult to find information regarding adiabatic temperature development of different concrete types, a suggestion for further studies is therefore to make adiabatic tests on different concrete mixtures in different surroundings to verify the temperature development and apply it to the created FE-models. A combination of different factors in the parameter study can be made to see how the combination influences the prestress.

The two-dimensional model can further be upgraded into a three-dimensional model where steel mould can be modelled. With three-dimensions it is also possible to model four separate equal beds bedside each other which can have influence on the heat transfer between the beds.

9 References

- ACI Committee (1999): *Heat Wheatear Concreting*. American Concrete Institute, Farmington Hills, Mich, 1999, pp. 305R-4 - 305R-5.
- Andersen, M., Bolmsvik, R. (2011): Measuring of prestress losses in Vislanda 2010. Abetong, växjö, Sweden, 2011, pp. 1-12.
- Andersen, M. (2011): Monitoring of the sleeper production in Marijampolé; prestress losses and temperature in concrete. Abetong, växjö, Sweden, 2011, pp. 3-12.
- ASM (2002): *Thermal properties of metals*. ASM International Material Properties Databad Committee, Ohio, USA, 2002, pp. 11, 337.
- Barr, P.J., Stanton, J.F., Eberhard, M.O. (2005): *Effects of temperature variation on precast prestressed concrete bridge girders*. American Society of Civil Engineers (ASCE), USA, 2005, pp. 6-8.
- Bennitz, A. (2008): *Mechanical Anchorage of Prestressed CFRP Tendons; Theory and Test*. Department of Civil, Mining and Environmental Engineering, Luleå University of Technology, Luleå, Sweden, 2008, 10 pp.
- Byfors, J. (1980): *Plain concrete at early ages*. Swedish cement and concrete research institute, Stockholm, Sweden, 1980, pp. 261, 268.
- Carino, N.J., Lew, H.S. (2001): *The maturity method; From theory to application*. Building and Fire Research Laboratory, National Institute of Standards and Technology, Gaithersburg, USA, 2001, pp. 3-8.
- CEB-FIB (1993): *CEB-FIB Model Code 1990*. Comité Euro-International du Béton, EPF Lausanne, Telford, London, Great Britain, 1993, 437 pp.
- CEN (2004): Eurocode 2: *Design of concrete structures – Part 1-1: General rules and rules for buildings*. European Committee for Standardization, Brussels, 2004, pp. 20-46, 76-82, 145-151, 173 -175, 202-204.
- Chen, Z., Liu, Z., Sun, G. (2011): *Thermal behaviour of steel cables in prestressed steel structures*. American Society of Civil Engineers, School of engineering, China, 2011, pp. 4-6.
- DIANA (2008): *Diana user's manual; Element library*, TNO DIANA BV, Delft, The Netherlands, 2008, pp. 29, 113, 117, 369-370, 503, 554.
- DIANA (2012): *Solutions for young hardening concrete*, TNO DIANA BV, Delft, The Netherlands, 2012, 2-3 pp.
- Domone, P., Illston, J.M. (2010): *Construction materials; Their Nature and Behaviour*. Spon Press, Milton Park, Abingdon, Oxon; New York, 2010, pp. 139-140.
- Engström, B. (2011): *Restraint cracking of reinforced concrete structures*. Department of Structural Engineering, Chalmers University of Technology, Göteborg, Sweden, 2011, pp. 23-24, 66-69, 84-89.
- Engström, B. (2011): *Design and analysis of prestressed concrete structures*. Department of Structural Engineering, Chalmers University of Technology, Göteborg, Sweden, 2011, pp. 11-12, 84-89.
- Esveld, C. (2001): *Modern Railway Track*. MRT-Productions, Zaltbommel, The Netherlands, 2001, pp. 212-226.

- Gahli, A., Favre, R. & Elbadry, M. (2002): *Concrete Structures; Stress and Deformation*. Spon Press, London; New York, 2002, pp. 350-358.
- Gere, J.M., Timoshenko, S.T. (1997): *Mechanics of Material*. PWS Pub Co, fourth Edition, Boston, USA, 1997.
- Gustavsson, R. (2002): *Structural Behaviour of Concrete Railway Sleepers*. Ph.D. Thesis. Department of Structural Engineering, Chalmers University of Technology, Publication no. 02-6, Göteborg, Sweden, 2002, pp. 4, 10-20,
- Hassoun, M.N. (2002): *Structural Concrete; Theory and Design*. Prentice-Hall, Inc. Upper Saddle River, New Jersey, 2002, pp. 1-5, 26.
- Ji, G. (2008): *Cracking risk of concrete structures in the hardening phase: Experiments; material modeling and finite element analysis*. Ph.D. Thesis. Department of Structural Engineering, The Norwegian University of Science and Technology, Trondheim, Norway, 2008, pp. 5-6, 14-16. 30-31, 41-42.
- Kim, J.K., Kim, K.H., Yang, J.K. (2000): *Thermal analysis of hydration heat in concrete structures with pipe-cooling system*. Department of Civil and Environmental Engineering, Chungwoon University, South Korea, 2000, 2 pp.
- Lienhard, J.H. IV., Lienhard, J.H. V. (2011): *A Heat Transfer Textbook*. Phlogiston Press. Department of Mechanical Engineering, Cambridge, Massachusetts, USA, 2011, 10 pp.
- Ljungkrantz, C., Möller, G. & Petersson, N. (1994): *Betonghandbok, material*. AB Svensk Byggtjänst, utgåva 2, Solna, Sverige, 1994, pp. 249-250, 459.
- Lundgren, M. (2005): *Development of strength and heat of hydration of young concrete at low temperatures*. Division of Building Materials, Lund Institute of Technology, Lund, Sweden, 2005, pp. 11-15.
- Mase, G.E., Mase, G.T. (2000): *Continuum mechanics for engineers*. CRC Press, Michigan, USA, 2000, p. 165.
- McCullough, B.F., Rasmussen, R.O. (1998): *Fast track paving; Concrete temperature control and traffic opening criteria for bonded concrete overlays*, Volume 1, Austin, USA, 1998, pp. 22, 37, 60-61, 65.
- Narang, V.A. (2005): *Heat transfer analysis in steel structures*. Worcester polytechnic institute, degree of Master of Science, Worcester, USA, 2005, pp 23-24.
- Nawy, E.G. (2000): *Presstressed concrete; a fundamental approach*. Prentice-Hall, Inc. Upper Saddle River, New Jersey, 2000, pp. 48-50.
- Nevander, L.E., Elmarsson, B. (2006): *Fukt handbok; praktik och teori*. AB Svensk byggtjänst, third edition, Sweden, Stockholm, 2006, pp. 305-236.
- Neville, A.M. (2003): *Properties of Concrete*. Prentice-Hall, London, England, 2003, pp. 10-26, 206, 425, 443-446, 449-452.
- Oluokun, F.A., Burdette, E.G., and Deatherage, J.H. (1991): *Young's modulus, Poisson's Ratio, and Compressive Strength Relationships at Early Ages*. ACI Materials Journal, V. 88, No. 1, 1991, pp. 3-9.
- Plos, M. (2000): *Finite element analyses of reinforced concrete structures*. Department of Structural Engineering, Chalmers University of Technology, Göteborg, Sweden, 2000, 8 pp.

- Russell, B.W., Burns, N.H. (1993): *Design guidelines for transfer, development and debonding of large diameter seven wire strands in pretensioned concrete girders*. State Department of Highway and Public Transportation, Texas, USA, 1993, pp 5-6, 11-21.
- Scmöllerl, H.R., Edl, M., Zehetner, J., Rinthoffer, G., Borensky, P. (2011): *Internal report; DMS measurements in emerging*. Sollenau, Austria, 2011, pp. 2-14.
- Tanabe, T., Kawasumi, M., Yamashita, Y. (1986): *Thermal stress analysis of massive concrete; seminar proceedings for finite element analysis of reinforced concrete structures*, Tokyo, Japan, 1985, ASCE, New York, N.Y.
- Vincenzo, N. (1999): *Strutture in acciaio precompresso. Prestressed steel structures*. Italy, 1999.
- Øverli, J.A., Høiseth, K., Bosnjak, D. (2002): *Heat and stress development during chemical hydration in concrete*. Taylor & Francis, Tokyo, Japan, 2002, pp. 115-121.

Appendix A Hand calculations

Hand calculations regarding thermal and structural analysis were made according to both Eurocode 2 and CEB-FIB MODEL CODE 1190. Measured temperatures during curing were used as input in the hand calculations due to lack of knowledge about the adiabatic temperature development. The thermal analysis, Appendix A.2, included the temperature development for each plant, and how the initial temperature could be weighted. In the structural analysis, Appendix A.3, was prestress losses due to shrinkage, relaxation and thermal effects during curing calculated. The immediate prestress loss occurred at de-tensioning were also calculated for the different factories. Calculations to verify the results from the FE-analysis were furthermore made, see Appendix A.4.

A.1 Input parameters

Name of the variables in the hand calculations

Vis = Vislanda

Mar = Marijampole

Sol = Sollenau

Time interval

$$t := 1..24 \quad (24\text{hr}=1\text{day})$$

Geometry

$$L_c := \begin{pmatrix} 110 \\ 108 \\ 104 \end{pmatrix} \cdot \text{m} \quad L_{\text{tot}} := \begin{pmatrix} 111.5 \\ 109 \\ 105 \end{pmatrix} \cdot \text{m} \quad \begin{array}{l} \text{Vislanda} \\ \text{Marijampole} \\ \text{Sololenau} \end{array} \quad L_{\text{step}} := 10\text{m}$$

$$H := 0.2\text{m}$$

Assume quadratic cross section

$$B := 0.2\text{m}$$

$$A_{\text{Long}} := 4 \cdot L_c \cdot H = \begin{pmatrix} 88 \\ 86.4 \\ 83.2 \end{pmatrix} \text{m}^2$$

$$A_{\text{Short}} := 2 \cdot B \cdot H = 0.08\text{m}^2$$

$$A_{\text{Tot}} := A_{\text{Long}} + A_{\text{Short}} = \begin{pmatrix} 88.08 \\ 86.48 \\ 83.28 \end{pmatrix} \text{m}^2$$

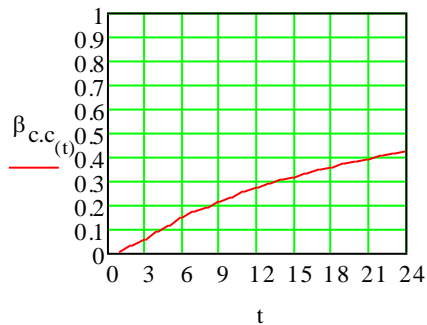
$$\text{RH} := 50\% \quad \text{Assumes: Indoor climate}$$

Material
Concrete
Strength

Class := "R"

$$s := \begin{cases} 0.2 & \text{if Class = "R"} \\ 0.25 & \text{if Class = "N"} \\ 0.38 & \text{if Class = "S"} \end{cases} = 0.2$$

$$\beta_{c,c(t)} := e^{\left[s \cdot \left(1 - \sqrt{\frac{28-24}{t}} \right) \right]}$$



$f_{c,m} := 48 \text{ MPa}$ From table 3.1

$f_{c,m(t)} := \beta_{c,c(t)} \cdot f_{c,m}$

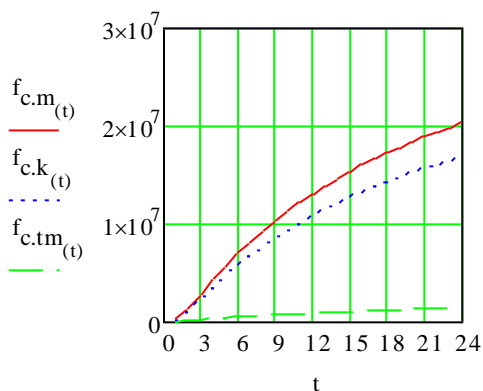
$f_{c,k} := 40 \text{ MPa}$ From table 3.1

$f_{c,k(t)} := \beta_{c,c(t)} \cdot f_{c,k}$ More precise values should be based on tests especially for $t < 3 \text{ days}$

$f_{c,tm} := 3.5 \text{ MPa}$ From table 3.1 $f_{c,mp} := 25 \text{ MPa}$

$\alpha := 1$ ($t < 28 \text{ days}$)

$f_{c,tm(t)} := \left[\beta_{c,c(t)} \right]^\alpha \cdot f_{c,tm}$



Elastic deformation

$$E_{c.m.Vis.} := 38 \text{ GPa} \quad E_{c.m.Mar.} := 38 \text{ GPa} \quad E_{c.m.Sol.} := 40 \text{ GPa} \quad \text{From table 3.1}$$

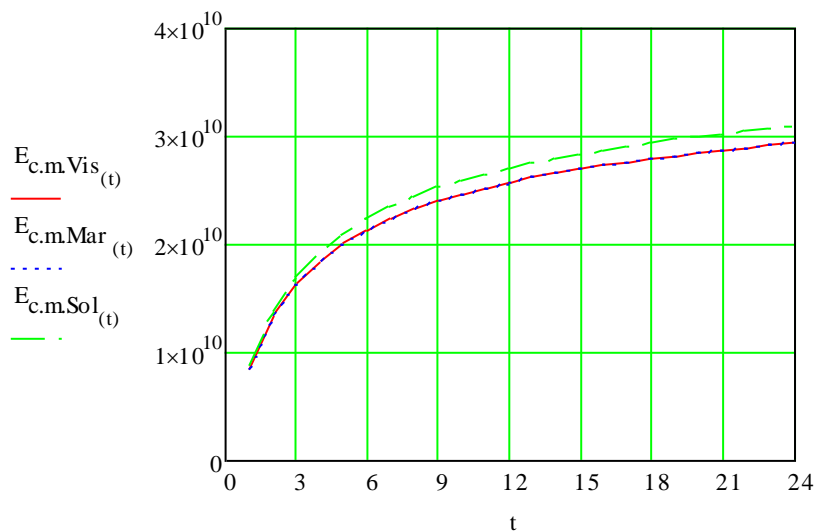
For limestone and sandstone aggregates reduce by 10% resp. 30%

For basalt aggregates increase by 20%

$$E_{c.m.Vis(t)} := \left[\frac{f_{c.m(t)}}{f_{c.m.}} \right]^{0.3} \cdot E_{c.m.Vis}$$

$$E_{c.m.Mar(t)} := \left[\frac{f_{c.m(t)}}{f_{c.m.}} \right]^{0.3} \cdot E_{c.m.Mar}$$

$$E_{c.m.Sol(t)} := \left[\frac{f_{c.m(t)}}{f_{c.m.}} \right]^{0.3} \cdot E_{c.m.Sol}$$



$$\nu := 0.2 \quad \text{Assumes: Uncracked concrete}$$

Prestressed steel

Strength

$$f_{p0.1k.Vis} := 1580 \text{ MPa} \quad f_{p0.1k.Mar} := 1860 \text{ MPa} \quad f_{p0.1k.Sol} := 1500 \text{ MPa}$$

$$f_{puk.Vis} := 1860 \text{ MPa} \quad f_{puk.Mar} := 1860 \text{ MPa} \quad f_{puk.Sol} := 1770 \text{ MPa}$$

$$\varepsilon_{uk} := 2.5\% \quad (\text{From Table 3.6 in "Design an analysis of prestressed concrete structures", Assumes: 3-wire strand, 7.5mm})$$

$$\gamma_S := 1.2$$

$$f_{pd.Vis} := \frac{f_{p0.1k.Vis}}{\gamma_S} = 1.317 \times 10^3 \cdot \text{MPa}$$

$$f_{pd.Mar} := \frac{f_{p0.1k.Mar}}{\gamma_S} = 1.55 \times 10^3 \cdot \text{MPa}$$

$$f_{pd.Sol} := \frac{f_{p0.1k.Sol}}{\gamma_S} = 1.25 \times 10^3 \cdot \text{MPa}$$

$$\varepsilon_{ud} := 0.9 \varepsilon_{uk}$$

$$E_p := 205 \cdot \text{GPa}$$

Sizes

Vislanda

$$d_{p.line.Vis} := 0.003 \text{ m}$$

$$n_{p.lines.in.1strand.Vis} := 3$$

$$n_{p.strand.Vis} := 14$$

$$n_{p.line.Total.Vis} := n_{p.strand.Vis} \cdot n_{p.lines.in.1strand.Vis} = 42$$

$$A_{p.line.Vis} := \frac{\pi (d_{p.line.Vis})^2}{4} = 7.069 \times 10^{-6} \text{ m}^2$$

$$A_{p.line.total.Vis} := A_{p.line.Vis} \cdot n_{p.line.Total.Vis} = 2.969 \times 10^{-4} \text{ m}^2$$

$$A_{O.line.Vis} := d_{p.line.Vis} \pi = 9.425 \times 10^{-3} \text{ m}$$

$$A_{O.strand.Vis} := n_{p.lines.in.1strand.Vis} \cdot d_{p.line.Vis} \pi = 0.028 \text{ m}$$

$$K_{red} := 0.6$$

$$A_{O.strand.Vis.red} := A_{O.strand.Vis} \cdot K_{red} = 0.017 \text{ m}$$

$$A_{O.line.Total.Vis} := n_{p.strand.Vis} \cdot A_{O.strand.Vis.red} = 0.238 \text{ m}$$

Marijampolé

$$d_{p.line.Mar} := 0.00315 \text{ m}$$

$$n_{p.lines.in.1strand.Mar} := 3$$

$$n_{p.strand.Mar} := 12$$

$$n_{p.line.Total.Mar} := n_{p.strand.Mar} \cdot n_{p.lines.in.1strand.Mar} = 36$$

$$A_{p.line.Mar} := \frac{\pi (d_{p.line.Mar})^2}{4} = 7.793 \times 10^{-6} \text{ m}^2$$

$$A_{p.line.total.Mar} := A_{p.line.Mar} \cdot n_{p.line.Total.Mar} = 2.806 \times 10^{-4} \text{ m}^2$$

$$A_{O.line.Mar} := d_{p.line.Mar} \cdot \pi = 9.425 \times 10^{-3} \text{ m}$$

$$A_{O.strand.Mar} := n_{p.lines.in.1strand.Mar} \cdot d_{p.line.Mar} \cdot \pi = 0.03 \text{ m}$$

$$K_{red} := 0.6$$

$$A_{O.strand.Mar.red} := A_{O.strand.Mar} \cdot K_{red} = 0.018 \text{ m}$$

$$A_{O.line.Total.Mar} := n_{p.strand.Mar} \cdot A_{O.strand.Mar.red} = 0.214 \text{ m}$$

Sollenau

$$d_{p.strand.Sol} := 0.006 \text{ m} = 6 \times 10^{-3} \text{ m}$$

$$n_{p.strand.Sol} := 14$$

$$A_{p.strand.Sol} := \frac{\pi (d_{p.strand.Sol})^2}{4} = 2.827 \times 10^{-5} \text{ m}^2$$

$$A_{p.line.total.Sol} := A_{p.strand.Sol} \cdot n_{p.strand.Sol} = 3.958 \times 10^{-4} \text{ m}^2$$

$$A_{O.Sol} := d_{p.strand.Sol} \cdot \pi = 0.019 \text{ m}$$

$$A_{O.Total.Sol} := n_{p.strand.Sol} \cdot A_{O.Sol} = 0.264 \text{ m}$$

A.2 Thermal analysis

$T_s := 20^\circ\text{C}$ Surface Temperature

$T_f := 45^\circ\text{C}$ Fluid Temperature

Temperatures

$T_{c,Vis} := 18.6^\circ\text{C}$

$T_{c,Mar} := 17^\circ\text{C}$ Concrete temperatures

$T_{c,Sol} := 25^\circ\text{C}$

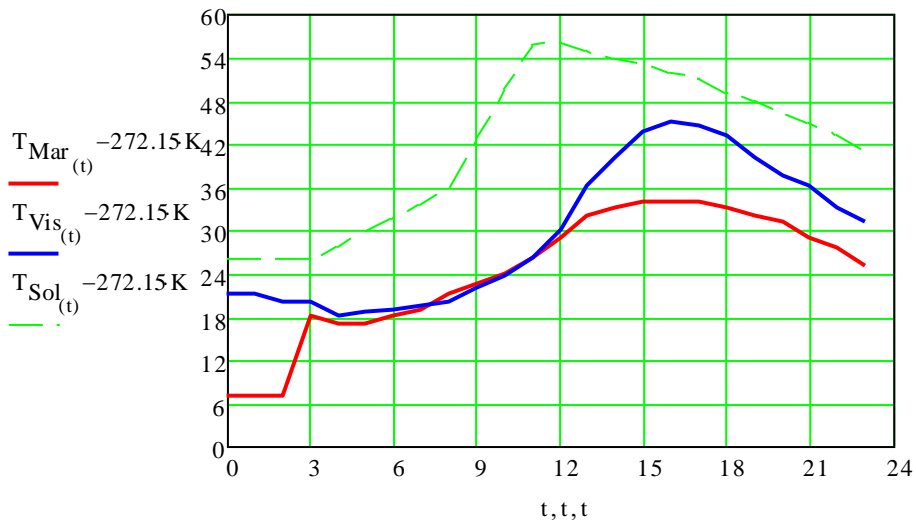
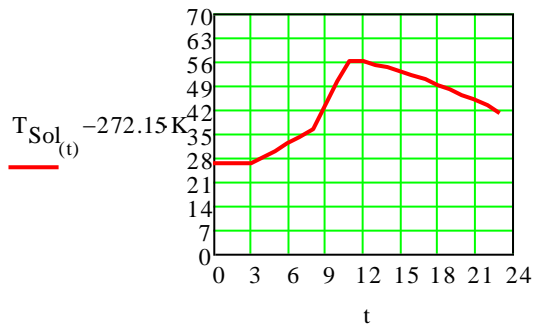
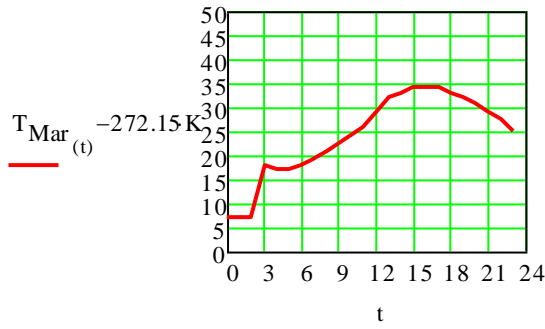
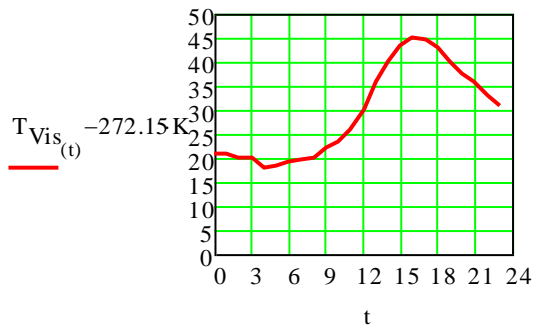
$T_{u,Vis} := 20^\circ\text{C}$

$T_{u,Mar} := 6^\circ\text{C}$

Surrounding temperatures

$T_{u,Sol} := 25^\circ\text{C}$

Time	$\begin{pmatrix} 20 \\ 20 \\ 19 \\ 19 \\ 17 \\ 17.5 \\ 18 \\ 18.5 \\ 19 \\ 21 \\ 22.5 \\ 25 \\ 29 \\ 35 \\ 39 \\ 42.5 \\ 44 \\ 43.5 \\ 42 \\ 39 \\ 36.5 \\ 35 \\ 32 \\ 30 \end{pmatrix}$	$T_{Vis} :=$	$^\circ\text{C}$	$\begin{pmatrix} 6 \\ 6 \\ 6 \\ 17 \\ 16 \\ 16 \\ 17 \\ 18 \\ 20 \\ 21.5 \\ 23 \\ 25 \\ 28 \\ 31 \\ 32 \\ 33 \\ 33 \\ 33 \\ 32 \\ 31 \\ 30 \\ 28 \\ 26.5 \\ 24 \end{pmatrix}$	$T_{Mar} :=$	$^\circ\text{C}$	$\begin{pmatrix} 25 \\ 25 \\ 25 \\ 25 \\ 27 \\ 29 \\ 31 \\ 33 \\ 35 \\ 42 \\ 49 \\ 55 \\ 55 \\ 54 \\ 53 \\ 52 \\ 51 \\ 50 \\ 48 \\ 47 \\ 45 \\ 44 \\ 42 \\ 40 \end{pmatrix}$	$T_{Sol} :=$	$^\circ\text{C}$	
$t_{End} := 2\text{h}$										
$t := 0..t_{End}$										



Starting temperature

$$\begin{array}{lll}
 c_{\text{Stone}} := 0.84 \frac{\text{J}}{\text{kg}\cdot\text{K}} & \rho_{\text{Stone}} := 2730 \frac{\text{kg}}{\text{m}^3} & T_{\text{Stone}} := 15^\circ\text{C} \\
 c_{\text{Sand}} := 0.84 \frac{\text{J}}{\text{kg}\cdot\text{K}} & \rho_{\text{Sand}} := 2650 \frac{\text{kg}}{\text{m}^3} & T_{\text{Sand}} := 15^\circ\text{C} \\
 c_{\text{Cement}} := 0.84 \frac{\text{J}}{\text{kg}\cdot\text{K}} & \rho_{\text{Cement}} := 3100 \frac{\text{kg}}{\text{m}^3} & T_{\text{Cement}} := 15^\circ\text{C} \\
 c_{\text{Concrete}} := 1.0 \frac{\text{J}}{\text{kg}\cdot\text{K}} & \rho_{\text{Concrete}} := 2350 \frac{\text{kg}}{\text{m}^3} & T_{\text{Concrete}} := 15^\circ\text{C}
 \end{array}$$

$$c := \begin{pmatrix} c_{\text{Stone}} \\ c_{\text{Sand}} \\ c_{\text{Cement}} \\ c_{\text{Concrete}} \end{pmatrix} \quad \rho := \begin{pmatrix} \rho_{\text{Stone}} \\ \rho_{\text{Sand}} \\ \rho_{\text{Cement}} \\ \rho_{\text{Concrete}} \end{pmatrix} \quad T := \begin{pmatrix} T_{\text{Stone}} \\ T_{\text{Sand}} \\ T_{\text{Cement}} \\ T_{\text{Concrete}} \end{pmatrix}$$

$$m_{\text{Stone}} := 1 \cdot \text{kg}$$

$$m_{\text{Sand}} := 1 \cdot \text{kg}$$

$$m_{\text{Cement}} := 1 \cdot \text{kg}$$

$$m_{\text{Concrete}} := 1 \cdot \text{kg}$$

$$G_{\text{Stone}} := m_{\text{Stone}} \cdot g = 9.807\text{N}$$

$$G_{\text{Sand}} := m_{\text{Sand}} \cdot g = 9.807\text{N}$$

$$G_{\text{Cement}} := m_{\text{Cement}} \cdot g = 9.807\text{N}$$

$$G_{\text{Concrete}} := m_{\text{Concrete}} \cdot g = 9.807\text{N}$$

$$G := \begin{pmatrix} G_{\text{Stone}} \\ G_{\text{Sand}} \\ G_{\text{Cement}} \\ G_{\text{Concrete}} \end{pmatrix}$$

Adding ice

$$c_{\text{ice}} := 1 \cdot \frac{\text{J}}{\text{kg}\cdot\text{K}} \quad c_{\text{w}} := 1 \cdot \frac{\text{J}}{\text{kg}\cdot\text{K}}$$

$$m_{\text{ice}} := 0.00 \text{ kg}$$

$$G_{\text{ice}} := m_{\text{ice}} \cdot g = 0$$

$$T_{\text{ice}} := 1^\circ\text{C}$$

$$L_{\text{ice}} := 335 \frac{\text{J}}{\text{kg}}$$

$$T_{\text{c.Vis.}} := \frac{\sum_{i=0}^3 (c_i \cdot G_i \cdot T_i) + c_{\text{ice}} \cdot G_{\text{ice}} \cdot T_{\text{ice}} - L_{\text{ice}} \cdot G_{\text{ice}}}{\sum_{i=0}^3 (c_i \cdot G_i) + c_w \cdot G_{\text{ice}}} = 15^\circ\text{C}$$

Adiabatic case

(Adiabatic temperature, no heat is released to the surrounding)

$$t_{\text{ad}} := 0..24 \quad (24\text{hr}=1\text{day})$$

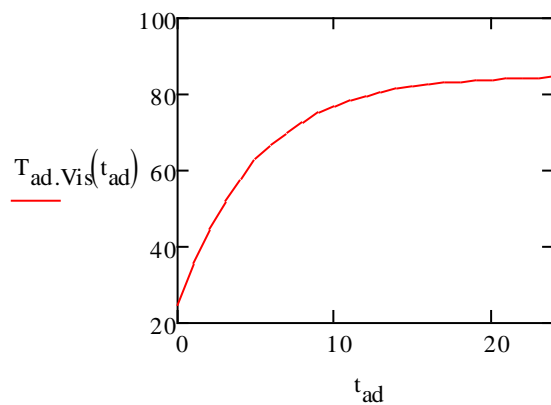
Vislanda

$$K_{\text{Vislanda}} := 60 \quad \text{Temperature increase}$$

$$T_{\text{initial}} := 25$$

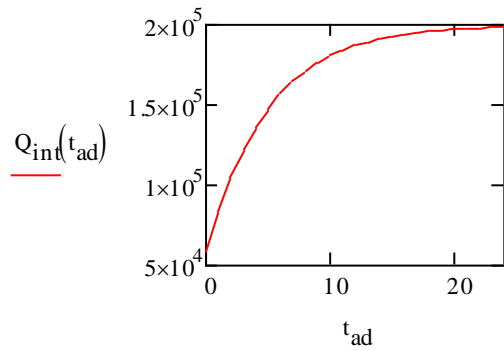
$$\alpha_{\text{ad.Vislanda}} := 0.2$$

$$T_{\text{ad.Vis}}(t_{\text{ad}}) := T_{\text{initial}} + K_{\text{Vis}} \cdot (1 - e^{-\alpha_{\text{ad.Vis}} \cdot t_{\text{ad}}})$$

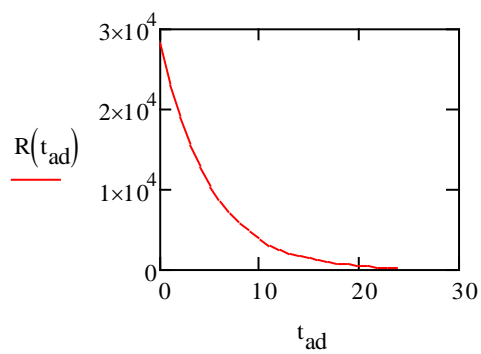


$$C_p := 1$$

$$Q_{\text{int}}(t_{\text{ad}}) := C_p \cdot \rho_{\text{Concrete}} \cdot T_{\text{ad.Vis}}(t_{\text{ad}})$$



$$R(t_{ad}) := K_{\text{Vislanda}} \cdot C_p \cdot \rho_{\text{Concrete}} \cdot \alpha_{ad, \text{Vislanda}} e^{-\alpha_{ad, \text{Vislanda}} t_{ad}}$$



Total heat of hydration

$$H_{C3s} := 500 \frac{\text{J}}{\text{g}}$$

$$H_{C2s} := 260 \frac{\text{J}}{\text{g}}$$

$$H_{C3A} := 850 \frac{\text{J}}{\text{g}} \quad [\text{J/g}]$$

$$H_{C4AF} := 420 \frac{\text{J}}{\text{g}}$$

$$H_C := 1165 \frac{\text{J}}{\text{g}}$$

$$H_{MgO} := 850 \frac{\text{J}}{\text{g}}$$

Compound composition for cement type I

$$p_{C3s} := 0.55$$

[-] ([%])

$$p_{C2s} := 0.19$$

$$P_{C3A} := 0.10$$

$$P_{C4AF} := 0.7$$

$$P_C := 0$$

$$P_{MgO} := 0.02 \quad (\text{Snabbh\u00e4rdande cement (SH) www.cementa.se})$$

$$H_u := P_{C3s} \cdot H_{C3s} + P_{C2s} \cdot H_{C2s} + P_{C3A} \cdot H_{C3A} + P_{C4AF} \cdot H_{C4AF} + P_C \cdot H_C + P_{MgO} \cdot H_{MgO}$$

$$H_{u.TypeI} := 460$$

Heat of hydration

$$T_{ref} := 20^\circ\text{C} \quad [\text{C}]$$

$$T_0 := 20$$

$$\Delta t := 1 \quad [\text{h}]$$

$$\Phi := 41750 \frac{\text{J}}{\text{mol}} \quad [\text{J/mol}]$$

Hydration parameters

$$\lambda_1 := 2.42$$

$$t_1 := 2.12$$

$$\kappa_1 := 0.85$$

$$R := 8.3144 \frac{\text{J}}{\text{mol}\cdot\text{K}}$$

$$T := \begin{pmatrix} T_0 \\ 19 \\ 19 \\ 20 \\ 17 \\ 17.5 \\ 18 \\ 18 \\ 18.5 \\ 19 \\ 21 \\ 22.5 \\ 25 \\ 29 \\ 35 \\ 39 \\ 42.5 \\ 44 \\ 43.5 \\ 42.5 \\ 41.5 \end{pmatrix} \text{ } ^\circ\text{C}$$

Assume temperature from Vis factory

$\beta_T :=$

292,15	293,15	0,984429	1,936051	0,031993	2,4965	
292,15	2,42	0,984429	2,400404	0,066591	2,4887	
293,15	2,12	1	2,872102	0,099038	2,2259	
290,15	0,85	0,95385	3,322032	0,125967	1,8383	
290,65	8,3144	0,961425	3,775534	0,149442	1,6037	
291,15	73,46036	0,969046	4,232631	0,169979	1,4078	
291,65	1	0,976714	4,693345	0,188076	1,2458	
292,15		0,984429	5,157698	0,204157	1,1116	
294,15		1,015761	5,636831	0,218882	1,0206	
295,65		1,039763	6,127285	0,232334	0,935	
298,15		1,080739	6,637068	0,244871	0,8731	
302,15		1,148882	7,178993	0,256851	0,8349	
308,15		1,25725	7,772036	0,268634	0,8204	
312,15		1,333747	8,401162	0,27987	0,783	
315,65		1,403565	9,063221	0,29052	0,7431	
317,15		1,434329	9,739791	0,30036	0,6884	
316,65		1,424018	10,4115	0,309249	0,624	
315,65		1,403565	11,07356	0,317276	0,5655	
314,65		1,383338	11,72607	0,324572	0,5155	
313,65		1,363335	11,89746	0,326397	0,4981	
312,65		1,343554	13,00291	0,337365	0,4349	
311,65		1,323994	13,62743	0,343015	0,4021	
310,65		1,304654	14,24284	0,348248	0,3731	
309,65		1,28553	14,84922	0,353113	0,3474	
308,65		1,266623	15,44668	0,357649	0,3244	
307,65		1,247931	16,03533	0,361892	0,3039	
306,65		1,229451	16,61526	0,36587	0,2853	

$(\Phi \ T_{ref} \ \lambda_1 \ t_1 \ \kappa_1 \ T \ R \ H_u \ C)$

$$\beta_{T(i)} := e^{\left[\frac{-\Phi}{R} \left(\frac{1}{T+273\cdot K} - \frac{1}{T_{ref}+273\cdot K} \right) \right]}$$

$$t_e := \sum_{i=1}^1 \beta_{T(i)}$$

$$\tau := 1 + \frac{t_e}{t_1}$$

$$\psi := e^{-\lambda_1 \cdot (\ln(\tau))^{-\kappa_1}}$$

$$Q_h := H_u \cdot C \cdot \psi \cdot \frac{\lambda_1 \cdot \kappa_1}{t_1} \cdot \frac{\ln(\tau)}{\tau} \cdot e^{\left[\frac{-\Phi}{R} \left(\frac{1}{T+273K} - \frac{1}{T_{ref}+273K} \right) \right]}$$

Heat Transfer

$$\rho_c := 2.3325 \quad [\text{g/m}^3]$$

Aggregate := "Limestone/Dolomite"

$$C_{p8} := \begin{cases} 0.91 & \text{if Aggregate} = \text{"Limestone/Dolomite"} = 0.91 \\ 0.77 & \text{if Aggregate} = \text{"Sandstone"} \\ 0.78 & \text{if Aggregate} = \text{"Granite/Gneiss"} \\ 0.77 & \text{if Aggregate} = \text{"Siliceous Gravel"} \\ 0.90 & \text{if Aggregate} = \text{"Basalt"} \end{cases} \quad [\text{J/(g} \cdot \text{C)}]$$

$$C_p := C_{p8} \cdot (1.25 - 0.25\psi)$$

$$k_{x8} := 0.612$$

$$k_x := k_{x8} \cdot (2 - \psi)$$

$$k_y := k_x$$

$$k_x \cdot \frac{d^2}{dx^2} T + k_y \cdot \frac{d^2}{dy^2} T + Q_h = \rho \cdot C_p \cdot \left(\frac{d}{dt} T \right)$$

$$RH := 0.5$$

$$C_m := \begin{cases} 1.18 & \text{if } 0 \leq RH < 0.2 \\ \frac{(1.80 - 1.18)}{(0.60 - 0.20)} \cdot RH + 0.90 & \text{if } 0.2 \leq RH < 0.6 \\ 1.8 & \text{if } 0.6 \leq RH < 0.75 \\ \frac{(1.80 - 1)}{(0.90 - 0.75)} \cdot RH + 400 & \text{if } 0.75 \leq RH < 0.90 \\ 1 & \text{if } 0.90 \leq RH < 100 \end{cases} = 1.675$$

$$\rho_C := 400 \frac{\text{kg}}{\text{m}^3}$$

$$\rho_{FA} := 0$$

$$\rho_{SF} := 0$$

$$\rho_{SL} := 0$$

$$\rho_{Fi} := 0$$

$$\rho_{Paste} := \rho_C + \rho_{FA} + \rho_{SF} + \rho_{SL} + \rho_{Fi} = 400 \frac{\text{kg}}{\text{m}^3}$$

$$V_{paste} := 0.5 \text{ m}^3$$

$$V_{agg} := 0.5 \text{ m}^3$$

$$V_{conc} := 1 \cdot \text{m}^3$$

$$\alpha_{agg} := \begin{cases} 6 & \text{if Aggregate} = \text{"Limestone/Dolomite"} = 6 \\ 11 & \text{if Aggregate} = \text{"Sandstone"} \\ 8 & \text{if Aggregate} = \text{"Granite/Gneiss"} \\ 10 & \text{if Aggregate} = \text{"Siliceous Gravel"} \\ 7 & \text{if Aggregate} = \text{"Basalt"} \end{cases}$$

$$\alpha_{paste} := 20$$

$$\alpha_{paste} := \begin{cases} 1.18 & \text{if } 0 \leq RH < 0.2 \\ \frac{(1.80 - 1.18)}{(0.60 - 0.20)} \cdot RH + 0.90 & \text{if } 0.2 \leq RH < 0.6 \\ 1.8 & \text{if } 0.6 \leq RH < 0.75 \\ \frac{(1.80 - 1)}{(0.90 - 0.75)} \cdot RH + 400 & \text{if } 0.75 \leq RH < 0.90 \\ 1 & \text{if } 0.90 \leq RH < 100 \end{cases} = 1.675$$

$$\alpha_{c.te} := C_m \left[\sum_{i=1}^1 \left(\alpha_{agg} \cdot 10^{-6} \cdot \frac{V_{agg}}{V_{conc}} \right) + \alpha_{paste} \cdot 10^{-6} \cdot \frac{V_{paste}}{V_{conc}} \right] = 6.428 \times 10^{-6}$$

A.3 Structural analysis

Thermal Contraction/Expansion strain

Coefficients for contraction/expansion

Assume same values for both contraction/expansion

$$\alpha_{c.tc} := 20 \cdot 10^{-6} \cdot \frac{1}{K} \quad \alpha_{c.te} := 20 \cdot 10^{-6} \cdot \frac{1}{K} \quad (\text{Table 4.3 in "Restraint cracking of reinforced concrete structures"})$$

Vislanda

$$T_{\text{Vis.max}(t)} := \max[T_{\text{Vis}(t)}]$$

$$\Delta T_{\text{max.Vis}(t)} := T_{\text{Vis.max}(t)} - T_{c.Vis}$$

$$T_{\text{Vis.max.const}} := \max(T_{\text{Vis.max}}) = 317.15K$$

(Valid for the Swedish construction cement, Dagenham Std P)

$$k_{0.Vis} := 0.64 + 0.003 \frac{T_{c.Vis} - 273.15K}{K} = 0.696$$

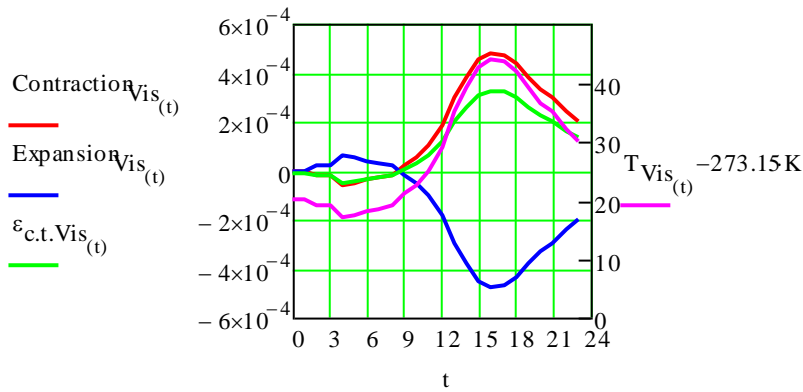
$$R := 1$$

$$\varepsilon_{c.t.Vis(t)} := R \cdot \left[\alpha_{c.tc} \cdot [T_{\text{Vis.max}(t)} - T_{u.Vis}] \cdots \right. \\ \left. + -\alpha_{c.te} \cdot (\Delta T_{\text{max.Vis}}) \cdot (1 - k_{0.Vis}) \right]$$

$$\varepsilon_{c.T.Vis(t)} := -\varepsilon_{c.t.Vis(t)}$$

$$\text{Contraction}_{\text{Vis}(t)} := \alpha_{c.tc} \cdot \left[\frac{T_{\text{Vis.max}(t)} - T_{u.Vis}}{K} \right]$$

$$\text{Expansion}_{\text{Vis}(t)} := -\alpha_{c.te} \cdot \left[\frac{T_{\text{Vis.max}(t)} - T_{u.Vis}}{K} \right]$$



Marijampolé

$$T_{\text{Mar.max}(t)} := \max(T_{\text{Mar}(t)})$$

$$\Delta T_{\text{max.Mar}(t)} := T_{\text{Mar.max}(t)} - T_{\text{c.Mar}}$$

$$T_{\text{Mar.max.const}} := \max(T_{\text{Mar}}) = 306.15 \text{ K}$$

(Valid for the Swedish construction cement, Degerhamn Std P)

$$k_{0,\text{Mar}} := 0.64 + 0.003 \frac{T_{\text{c.Mar}} - 273.15 \text{ K}}{\text{K}} = 0.691$$

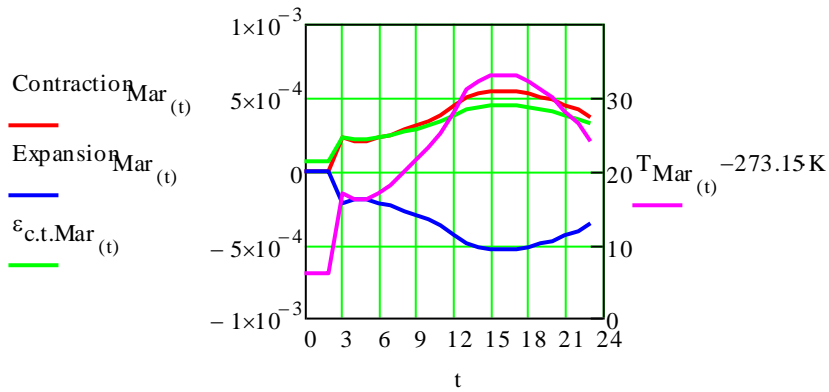
$$R := 1$$

$$\varepsilon_{\text{c.t.Mar}(t)} := R \cdot \left[\alpha_{\text{c.tc}} \cdot [T_{\text{Mar.max}(t)} - T_{\text{u.Mar}}] \cdots + -\alpha_{\text{c.te}} \cdot (\Delta T_{\text{max.Mar}(t)}) \cdot (1 - k_{0,\text{Mar}}) \right]$$

$$\varepsilon_{\text{c.T.Mar}(t)} := -\varepsilon_{\text{c.t.Mar}(t)}$$

$$\text{Contraction}_{\text{Mar}(t)} := \alpha_{\text{c.tc}} \cdot \left[\frac{T_{\text{Mar.max}(t)} - T_{\text{u.Mar}}}{\text{K}} \right]$$

$$\text{Expansion}_{\text{Mar}(t)} := -\alpha_{\text{c.te}} \cdot \left[\frac{T_{\text{Mar.max}(t)} - T_{\text{u.Mar}}}{\text{K}} \right]$$



Sollenau

$$T_{\text{Sol.max}(t)} := \max(T_{\text{Sol}t})$$

$$\Delta T_{\text{max.Sol}(t)} := T_{\text{Sol.max}(t)} - T_{\text{c.Sol}}$$

$$T_{\text{Sol.max.const}} := \max(T_{\text{Sol}}) = 328.15\text{K}$$

(Valid for the Swedish construction cement, Degerhamn Std P)

$$k_{0.\text{Sol}} := 0.64 + 0.003 \frac{T_{\text{c.Sol}} - 273.15\text{K}}{\text{K}} = 0.715$$

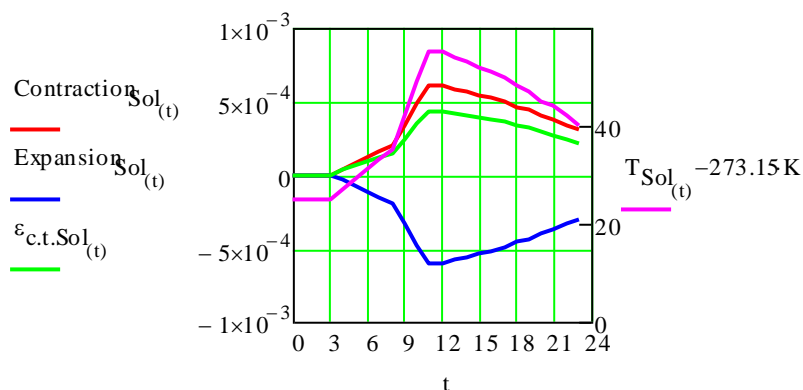
$$R := 1$$

$$\varepsilon_{\text{c.t.Sol}(t)} := R \cdot \left[\alpha_{\text{c.tc}} \left[T_{\text{Sol.max}(t)} - T_{\text{u.Sol}} \right] \dots \right. \\ \left. + -\alpha_{\text{c.te}} \left(\Delta T_{\text{max.Sol}(t)} \right) \cdot (1 - k_{0.\text{Sol}}) \right]$$

$$\varepsilon_{\text{c.T.Sol}(t)} := -\varepsilon_{\text{c.t.Sol}(t)}$$

$$\text{Contraction}_{\text{Sol}(t)} := \alpha_{\text{c.tc}} \left[\frac{T_{\text{Sol.max}(t)} - T_{\text{u.Sol}}}{\text{K}} \right]$$

$$\text{Expansion}_{\text{Sol}(t)} := -\alpha_{\text{c.te}} \left[\frac{T_{\text{Sol.max}(t)} - T_{\text{u.Sol}}}{\text{K}} \right]$$



Shrinkage

Vislanda

Drying shrinkage strain

$t_s := 0$ (Age of concrete at the beginning of drying shrinkage (or swelling).
Normally this is at the end of curing)

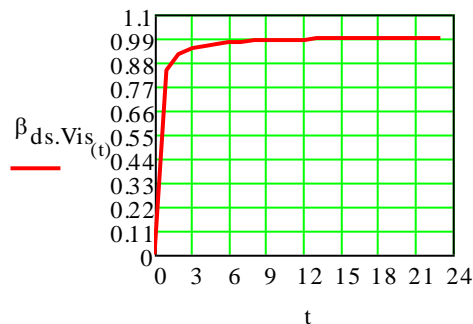
Should not be included when considering hydration process of young concrete!!!

$$A_c := H \cdot B = 0.04 \text{m}^2$$

$$u := 2 \cdot (B + H) = 0.8 \text{m}$$

$$h := 2 \cdot \frac{A_c}{u} = 0.1 \text{m}$$

$$\beta_{ds, Vis(t)} := \frac{(t - t_s)}{(t - t_s) + 0.04 \sqrt[3]{\frac{h}{m} \cdot 1000}}$$



$$k_{h, Vis} := \begin{cases} \frac{(0.85 - 1.0) \cdot h}{100 \cdot m} + 1.15 & \text{if } h < 200 \text{mm} \\ \frac{(0.75 - 0.85) \cdot h}{100 \cdot m} + 1.05 & \text{if } h \geq 200 \text{mm} \\ \frac{(0.7 - 0.75) \cdot h}{200 \cdot m} + 0.825 & \text{if } h \geq 300 \text{mm} \\ 0.7 & \text{if } h \geq 500 \text{mm} \end{cases} = 1.15$$

EN 1992-1-1: Annex B.2 Basic equations for determine the drying shrinkage

$$\alpha_{ds1} := \begin{cases} 3 & \text{if Class = "S"} \\ 4 & \text{if Class = "N"} \\ 6 & \text{if Class = "R"} \end{cases} = 6$$

$$\alpha_{ds2} := \begin{cases} 0.13 & \text{if Class = "S"} \\ 0.12 & \text{if Class = "N"} \\ 0.11 & \text{if Class = "R"} \end{cases} = 0.11$$

$$RH_0 := 100\%$$

$$\beta_{RH,Vis} := 1.55 \left[1 - \left(\frac{RH}{RH_0} \right)^3 \right] = 1.356$$

$$f_{c,m0} := 10 \text{ MPa}$$

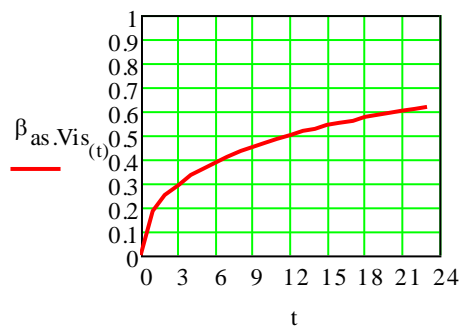
$$\varepsilon_{c,d,0,Vis} := 0.85 \left[(220 + 110 \alpha_{ds1}) \cdot \exp \left(-\alpha_{ds2} \cdot \frac{f_{c,m.}}{f_{c,m0}} \right) \right] \cdot 10^{-6} \cdot \beta_{RH,Vis} = 5.983 \times 10^{-4}$$

$$\varepsilon_{c,d,Vis(t)} := \beta_{ds,Vis(t)} \cdot k_{h,Vis} \cdot \varepsilon_{c,d,0,Vi}$$

Autogenous shrinkage strain

Negligible in precast element subjected to heat curing acc. to EN 1992-1-1:2004 Ch. 10.3.1.2(3)b)

$$\beta_{as,Vis(t)} := 1 - e^{-0.2 \cdot \sqrt{t}}$$



$$\varepsilon_{c,a,8,Vis} := 2.5 \left(\frac{f_{c,k.}}{\text{MPa}} - 10 \right) \cdot 10^{-6} = 7.5 \times 10^{-5}$$

$$\varepsilon_{c,a,Vis(t)} := \beta_{as,Vis(t)} \cdot \varepsilon_{c,a,8,Vi}$$

Total shrinkage strain

Not significant in precast element subjected to heat curing acc. to EN 1992-1-1:2004 Ch. 10.3.1.2(3)a)

Eurocode

$$\varepsilon_{c,s,Vis(t)} := \varepsilon_{c,d,Vis(t)} + \varepsilon_{c,a,Vis(t)} = \dots$$

CEB-FIP

$\beta := 8$ (Rapidly Hardening Concrete)

$$\varepsilon_{s,Vis(t)} := \left[160 + 10\beta \cdot \left[9 - \frac{f_{c,m(t)}}{f_{c,m0}} \right] \right] \cdot 10^{-6} = \dots$$

$$\beta_{RH,Vis} := \begin{cases} \left[1.55 \left[1 - \left(\frac{RH}{RH_0} \right)^3 \right] \right] & \text{if } 40\% \leq RH < 99\% \\ 0.5 & \text{if } RH \geq 99\% \end{cases} = -1.356$$

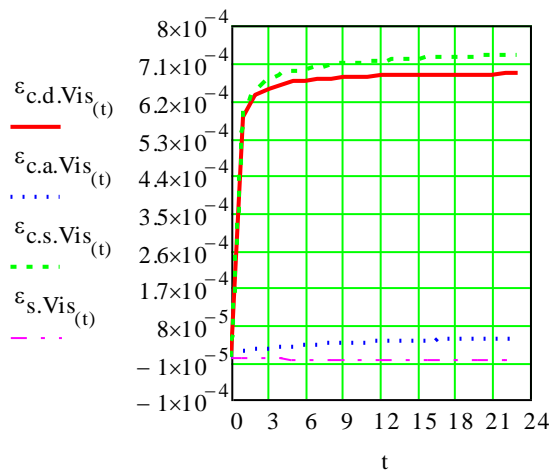
$$\varepsilon_{so,Vis(t)} := \varepsilon_{s,Vis(t)} \cdot \beta_{RH,Vis} = \dots$$

$h_0 := 0.001r$

$$\beta_{s,Vis(t)} := \left[\frac{(t - t_s)}{350 \left(\frac{h}{h_0} \right)^2 + (t - t_s)} \right]^{\frac{1}{2}} = \dots$$

$$\varepsilon_{s,Vis(t)} := (\varepsilon_{so,Vis})_{(t)} \cdot \beta_{s,Vis(t)} = \dots$$

Total



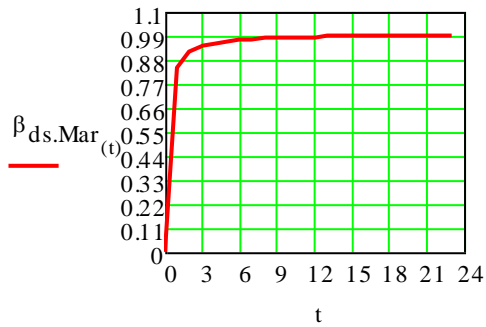
Marijampolė

Drying shrinkage strain

$t_s := 0$ (Age of concrete at the beginning of drying shrinkage or swelling). Normally this is at the end of curing)

Should not be included when considering hydration process of young concrete!!!

$$\beta_{ds.Mar}(t) := \frac{(t - t_s)}{(t - t_s) + 0.04 \sqrt[3]{\frac{h}{m} \cdot 1000}}$$



$$k_{h.Mar} := \begin{cases} \frac{(0.85 - 1.0)}{100} \cdot \frac{h}{m} + 1.15 & \text{if } h < 200 \text{ mm} \\ \frac{(0.75 - 0.85)}{100} \cdot \frac{h}{m} + 1.05 & \text{if } h \geq 200 \text{ mm} \\ \frac{(0.7 - 0.75)}{200} \cdot \frac{h}{m} + 0.825 & \text{if } h \geq 300 \text{ mm} \\ 0.7 & \text{if } h_0 \geq 500 \text{ mm} \end{cases} = 1.15$$

EN 1992-1-1: Annex B.2 Basic equations for determine the drying shrinkage

$$\alpha_{ds1} := \begin{cases} 3 & \text{if Class = "S"} \\ 4 & \text{if Class = "N"} \\ 6 & \text{if Class = "R"} \end{cases} = 6$$

$$\alpha_{ds2} := \begin{cases} 0.13 & \text{if Class = "S"} \\ 0.12 & \text{if Class = "N"} \\ 0.11 & \text{if Class = "R"} \end{cases} = 0.11$$

$$RH_0 := 100\%$$

$$\beta_{RH.Mar} := 1.55 \left[1 - \left(\frac{RH}{RH_0} \right)^3 \right] = 1.356$$

$$f_{c.m0} := 10 \text{ MPa}$$

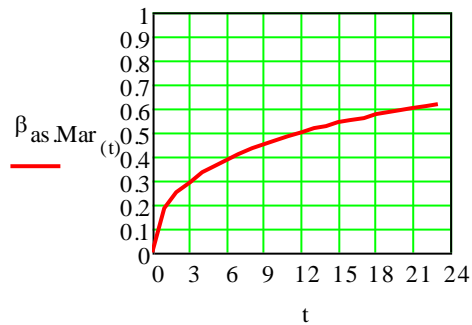
$$\varepsilon_{c.d.0.Mar} := 0.85 \left[\left(220 + 110 \alpha_{ds1} \right) \cdot \exp \left(-\alpha_{ds2} \cdot \frac{f_{c.m.}}{f_{c.m0}} \right) \right] \cdot 10^{-6} \cdot \beta_{RH.Mar}$$

$$\varepsilon_{c.d.Mar}(t) := \beta_{ds.Mar}(t) \cdot k_{h.Mar} \cdot \varepsilon_{c.d.0.Mar}$$

Autogenous shrinkage strain

Negligible in precast element subjected to heat curing acc. to EN 1992-1-1:2004 Ch. 10.3.1.2(3)b

$$\beta_{\text{as.Mar}}(t) := 1 - e^{-0.2 \cdot \sqrt{t}}$$



$$\varepsilon_{\text{c.a.8.Mar}} := 2.5 \left(\frac{f_{\text{c.k.}}}{\text{MPa}} - 10 \right) \cdot 10^{-6} = 7.5 \times 10^{-5}$$

$$\varepsilon_{\text{c.a.Mar}}(t) := \beta_{\text{as.Mar}}(t) \cdot \varepsilon_{\text{c.a.8.Mar}}$$

Total shrinkage strain

Not significant in precast element subjected to heat curing acc. to EN 1992-1-1:2004 Ch. 10.3.1.2(3)a

Eurocode

$$\varepsilon_{\text{c.s.Mar}}(t) := \varepsilon_{\text{c.d.Mar}}(t) + \varepsilon_{\text{c.a.Mar}}(t) = \dots$$

CEB-FIP

$$\beta := 8 \quad (\text{Rapidly Hardening Concrete})$$

$$\varepsilon_{\text{s.Mar}}(t) := \left[160 + 10\beta \cdot \left[9 - \frac{f_{\text{c.m}}(t)}{f_{\text{c.m0}}} \right] \right] \cdot 10^{-6} = \dots$$

$$\beta_{\text{RH.Mar}} := \begin{cases} \left[1.55 \left[1 - \left(\frac{\text{RH}}{\text{RH}_0} \right)^3 \right] \right] & \text{if } 40\% \leq \text{RH} < 99\% \\ 0.5 & \text{if } \text{RH} \geq 99\% \end{cases} = -1.356$$

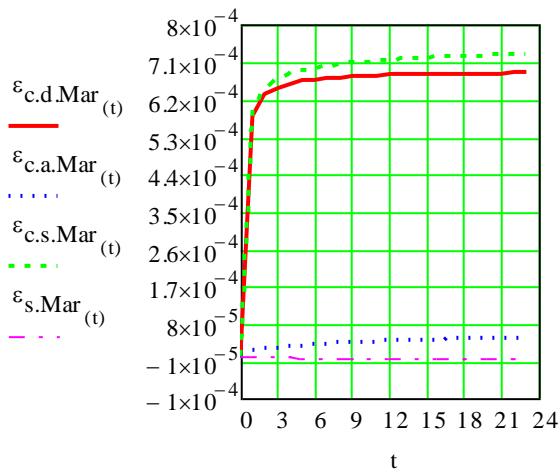
$$\varepsilon_{\text{so.Mar}}(t) := \varepsilon_{\text{s.Mar}}(t) \cdot \beta_{\text{RH.Mar}} = \dots$$

$$h_0 := 0.001 \text{ m}$$

$$\beta_{s.\text{Mar}}(t) := \left[\frac{(t - t_s)}{350 \left(\frac{h}{h_0} \right)^2 + (t - t_s)} \right]^{\frac{1}{2}} = \dots$$

$$\varepsilon_{s.\text{Mar}}(t) := (\varepsilon_{\text{so.Mar}})_{(t)} \cdot \beta_{s.\text{Mar}}(t) = \dots$$

Total



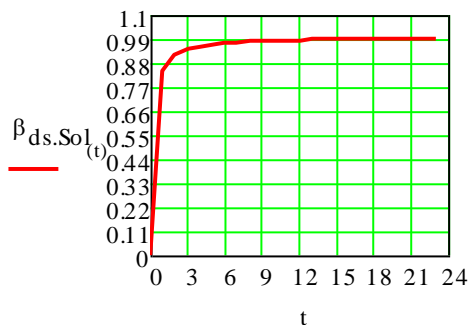
Sollenau

Drying shrinkage strain

$t_s := 0$ (Age of concrete at the beginning of drying shrinkage (or swelling).
Normally this is at the end of curing)

Should not be included when considering hydration process of young concrete!

$$\beta_{ds.\text{Sol}}(t) := \frac{(t - t_s)}{(t - t_s) + 0.04 \sqrt[3]{\frac{h}{\text{m}} \cdot 1000}}$$



$$k_{h.Sol} := \begin{cases} \frac{(0.85 - 1.0) \cdot h}{100} \cdot \frac{h}{m} + 1.15 & \text{if } h < 200\text{mm} \\ \frac{(0.75 - 0.85) \cdot h}{100} \cdot \frac{h}{m} + 1.05 & \text{if } h \geq 200\text{mm} \\ \frac{(0.7 - 0.75) \cdot h}{200} \cdot \frac{h}{m} + 0.825 & \text{if } h \geq 300\text{mm} \\ 0.7 & \text{if } h_0 \geq 500\text{mm} \end{cases}$$

EN 1992-1-1: Annex B.2 Basic equations for determine the drying shrinkage

$$\alpha_{ds1} := \begin{cases} 3 & \text{if Class = "S"} \\ 4 & \text{if Class = "N"} \\ 6 & \text{if Class = "R"} \end{cases} = 6$$

$$\alpha_{ds2} := \begin{cases} 0.13 & \text{if Class = "S"} \\ 0.12 & \text{if Class = "N"} \\ 0.11 & \text{if Class = "R"} \end{cases} = 0.11$$

$$RH_0 := 100\%$$

$$\beta_{RH.Sol} := 1.55 \left[1 - \left(\frac{RH}{RH_0} \right)^3 \right] = 1.356$$

$$f_{c.m0} := 10\text{MPa}$$

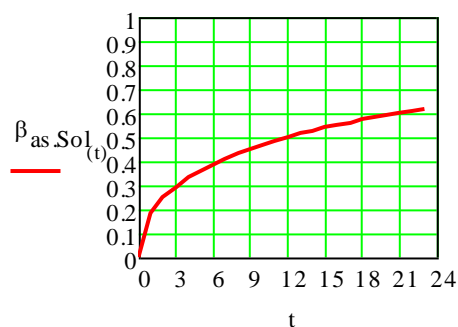
$$\varepsilon_{c.d.0.Sol} := 0.85 \left[(220 + 110 \alpha_{ds1}) \cdot \exp \left(-\alpha_{ds2} \cdot \frac{f_{c.m.}}{f_{c.m0}} \right) \right] \cdot 10^{-6} \cdot \beta_{RH.Sol} = 5.983 \times 10^{-4}$$

$$\varepsilon_{c.d.Sol(t)} := \beta_{ds.Sol(t)} \cdot k_{h.Sol} \cdot \varepsilon_{c.d.0.Sol}$$

Autogenous shrinkage strain

Negligible in precast element subjected to heat curing acc. to EN 1992-1-1:2004 Ch. 10.3.1.2(3)b

$$\beta_{as.Sol(t)} := 1 - e^{-0.2 \cdot \sqrt{t}}$$



$$\varepsilon_{c.a.8.Sol} := 2.5 \left(\frac{f_{c.k.}}{\text{MPa}} - 10 \right) \cdot 10^{-6} = 7.5 \times 10^{-5}$$

$$\varepsilon_{c.a.Sol(t)} := \beta_{as.Sol(t)} \cdot \varepsilon_{c.a.8.Sol}$$

Total shrinkage strain

Not significant in precast element subjected to heat curing acc. to EN 1992-1-1:2004 Ch. 10.3.1.2(3)a)

Eurocode

$$\varepsilon_{c.s.Sol(t)} := \varepsilon_{c.d.Sol(t)} + \varepsilon_{c.a.Sol(t)} = \dots$$

CEB-FIP

$\beta := 8$ (Rapidly Hardening Concrete)

$$\varepsilon_{s.Sol(t)} := \left[160 + 10\beta \cdot \left[9 - \frac{f_{c.m(t)}}{f_{c.m0}} \right] \right] \cdot 10^{-6} = \dots$$

$$\beta_{RH.Sol} := \begin{cases} \left[1.55 \left[1 - \left(\frac{RH}{RH_0} \right)^3 \right] \right] & \text{if } 40\% \leq RH < 99\% \\ 0.5 & \text{if } RH \geq 99\% \end{cases} = -1.356$$

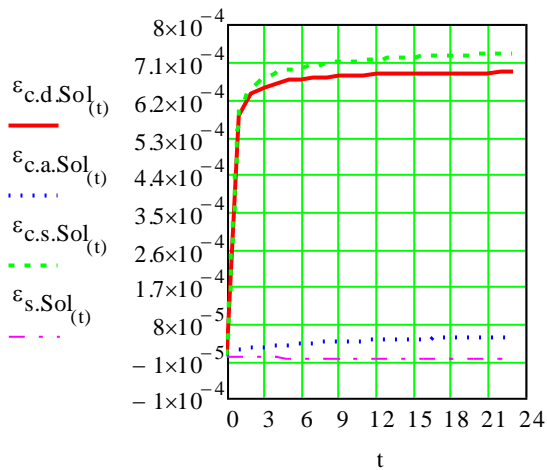
$$\varepsilon_{so.Sol(t)} := \varepsilon_{s.Sol(t)} \cdot \beta_{RH.Sol} = \dots$$

$h_0 := 0.001\text{m}$

$$\beta_{s.Sol(t)} := \left[\frac{(t - t_s)}{350 \left(\frac{h}{h_0} \right)^2 + (t - t_s)} \right]^{\frac{1}{2}} = \dots$$

$$\varepsilon_{s.Sol(t)} := (\varepsilon_{so.Sol(t)}) \cdot \beta_{s.Sol(t)} = \dots$$

Total



Prestressing force during tensioning

EN 1992-1-1:2004 Ch. 5.10.2

$$k_1 := 0.8$$

Assuming no overstressing

$$k_2 := 0.9$$

$$\sigma_{p,max,Vis} := \min(k_1 \cdot f_{puk,Vis}, k_2 \cdot f_{p0.1k,Vis}) = 1.422 \times 10^3 \cdot \text{MPa}$$

$$\sigma_{p,max,Mar} := \min(k_1 \cdot f_{puk,Mar}, k_2 \cdot f_{p0.1k,Mar}) = 1.488 \times 10^3 \cdot \text{MPa}$$

$$\sigma_{p,max,Sol} := \min(k_1 \cdot f_{puk,Sol}, k_2 \cdot f_{p0.1k,Sol}) = 1.35 \times 10^3 \cdot \text{MPa}$$

$$P_{max,Vis} := A_{p,line,total,Vis} \cdot \sigma_{p,max,Vis} = 422.164 \text{ kN}$$

$$P_{max,Mar} := A_{p,line,total,Mar} \cdot \sigma_{p,max,Mar} = 417.461 \text{ kN}$$

$$P_{max,Sol} := A_{p,line,total,Sol} \cdot \sigma_{p,max,Sol} = 534.385 \text{ kN}$$

Prestress force

EN 1992-1-1:2004 Ch. 5.10.2

$$k_7 := 0.75$$

$$k_8 := 0.85$$

$$\sigma_{p,m0,Vis} := \min(k_7 \cdot f_{puk,Vis}, k_8 \cdot f_{p0.1k,Vis}) = 1.343 \times 10^3 \cdot \text{MPa}$$

$$\sigma_{p,m0,Mar} := \min(k_7 \cdot f_{puk,Mar}, k_8 \cdot f_{p0.1k,Mar}) = 1.395 \times 10^3 \cdot \text{MPa}$$

$$\sigma_{p,m0,Sol} := \min(k_7 \cdot f_{puk,Sol}, k_8 \cdot f_{p0.1k,Sol}) = 1.275 \times 10^3 \cdot \text{MPa}$$

$$P_{m0.Vis} := A_{p.line.total.Vis} \sigma_{p.m0.Vis} = 398.711 \text{ kN}$$

$$P_{m0.Mar} := A_{p.line.total.Mar} \sigma_{p.m0.Mar} = 391.37 \text{ kN}$$

$$P_{m0.Sol} := A_{p.line.total.Sol} \sigma_{p.m0.Sol} = 504.697 \text{ kN}$$

Prestress losses

Vislanda

During the tensioning

Losses due to wedge draw-in of the anchorage device

Before the transfer of prestress to concrete

Losses due to shrinkage, relaxation of the prestressing steel and thermal effects

Relaxation

$$\Delta t := 1$$

$$\text{Class}_{rel} := "2"$$

$$\chi_{1000} := \begin{cases} 8\% & \text{if } \text{Class}_{rel} = "1" \\ 2.5\% & \text{if } \text{Class}_{rel} = "2" \\ 4\% & \text{if } \text{Class}_{rel} = "3" \end{cases} = 0.025$$

$$\varepsilon_{pi} := 0.006$$

$$\sigma_{p.i} := E_p \cdot \varepsilon_{pi} = 1.23 \times 10^3 \cdot \text{MPa} < \sigma_{p.max}$$

$$\sigma_{p.i.Vis} := \sigma_{p.m0.Vis} = 1.343 \times 10^3 \cdot \text{MPa}$$

$$\mu_{Vis} := \frac{\sigma_{p.i.Vis}}{f_{puk.Vis}} = 0.722$$

$$t_{eq.Vis} = \frac{1.14 \frac{T_{Vis.max} - 20^\circ\text{C}}{K}}{T_{Vis.max} - 20^\circ\text{C}} \cdot \sum_{i=1}^{20} \left[\left[T_{Vis(i)} - 20^\circ\text{C} \right] \cdot \Delta t \right] \quad (\text{EC2})$$

$t_{eq.Vis} :=$	317,15	293,15	1	0
		293,15		0
		292,15		-0,96717529
		292,15		-0,96717529
		290,15		-1
		290,65		-1
		291,15		-1
		291,65		-1
		292,15		-0,96717529
		294,15		0,967175286
		295,65		2,417938214
		298,15		4,835876428
		302,15		8,70457757
		308,15		14,50762928
		312,15		18,37633043
		315,65		21,76144392
		317,15		23,21220685
		316,65		22,72861921
		315,15		21,27785628
		312,15		18,37633043
		309,65		15,95839221
		308,15		14,50762928
		305,15		11,60610343
		303,15		9,671752855

Values lower than -1
has been changed to -1

$$(T_{Vis.max.const} T_{Vis} \Delta t)$$

$$\Delta\sigma_{p.r.Vis} := \begin{cases} \left[5.39 \times 1000 e^{6.7 \cdot \mu_{Vis}} \cdot \left(\frac{t_{eq.Vis} + \Delta t}{1000} \right)^{0.75 \cdot (1 - \mu_{Vis})} \cdot 10^{-3} \right] \cdot \sigma_{p.i.Vis} \text{ if Class}_{rel} = "1" \\ \left[0.66 \times 1000 e^{9.1 \cdot \mu_{Vis}} \cdot \left(\frac{t_{eq.Vis} + \Delta t}{1000} \right)^{0.75 \cdot (1 - \mu_{Vis})} \cdot 10^{-3} \right] \cdot \sigma_{p.i.Vis} \text{ if Class}_{rel} = "2" \\ \left[1.98 \times 1000 e^{8 \cdot \mu_{Vis}} \cdot \left(\frac{t_{eq.Vis} + \Delta t}{1000} \right)^{0.75 \cdot (1 - \mu_{Vis})} \cdot 10^{-3} \right] \cdot \sigma_{p.i.Vis} \text{ if Class}_{rel} = "3" \end{cases}$$

$$i := 21$$

$$\mu_{(0)} := \frac{\sigma_{p.i.Vis}}{f_{puk.Vis}} = 0.722$$

$$\mu_{Vis(t)} := \frac{\sigma_{p.i.Vis} + \sum_{i=1}^{21} \Delta\sigma_{p.r.Vis(i)}}{f_{puk.Vis}}$$

$$t_{e, \text{Vis}}(t) := 1000 \left[\frac{\sum_{i=1}^{i-1} \Delta\sigma_{\text{p.r.Vis}}(t)}{\left[\sigma_{\text{p.i.Vis}} + \sum_{i=1}^{i-1} \Delta\sigma_{\text{p.r.Vis}}(t) \right]} \cdot \frac{1}{\chi 1000 e^{6.7 \cdot \mu_{\text{Vis}}(t)}} \right]^{\frac{1}{\left[0.75 \left[1 - \mu_{\text{Vis}}(t) \right] \right]}} = \dots$$

$$\Delta\sigma_{\text{Vis.const1}}(t) := 5.39 \chi 1000 e^{6.7 \cdot \mu_{\text{Vis}}(t)} \left[\frac{t_{e, \text{Vis}}(t) + \Delta t}{1000} \right]^{0.75 \left[1 - \mu_{\text{Vis}}(t) \right]}$$

$$\Delta\sigma_{\text{Vis.const2}}(t) := \left[\sigma_{\text{p.i.Vis}} + \sum_{i=1}^{i-1} \Delta\sigma_{\text{p.r.Vis}}(t) \right] - \sum_{i=1}^{i-1} \Delta\sigma_{\text{p.r.Vis}}(t)$$

$$\Delta\sigma_{\text{Vis.const3}}(t) := 0.66 \chi 1000 e^{9.1 \cdot \mu_{\text{Vis}}(t)} \left[\frac{t_{e, \text{Vis}}(t) + \Delta t}{1000} \right]^{0.75 \left[1 - \mu_{\text{Vis}}(t) \right]}$$

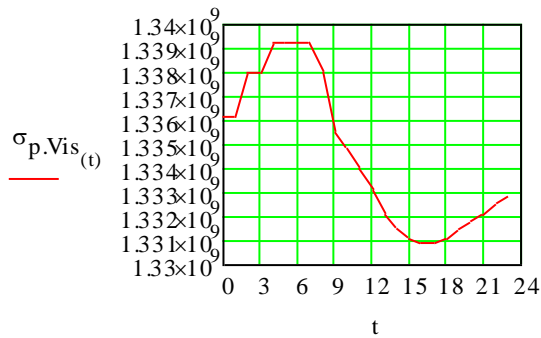
$$\Delta\sigma_{\text{Vis.const4}}(t) := \left[\sigma_{\text{p.i.Vis}} + \sum_{i=1}^{i-1} \Delta\sigma_{\text{p.r.Vis}}(t) \right] - \sum_{i=1}^{i-1} \Delta\sigma_{\text{p.r.Vis}}(t)$$

$$\Delta\sigma_{\text{Vis.const5}}(t) := 1.98 \chi 1000 e^{8 \cdot \mu_{\text{Vis}}(t)} \left[\frac{t_{e, \text{Vis}}(t) + \Delta t}{1000} \right]^{0.75 \left[1 - \mu_{\text{Vis}}(t) \right]}$$

$$\Delta\sigma_{\text{Vis.const6}}(t) := \left[\sigma_{\text{p.i.Vis}} + \sum_{i=1}^{i-1} \Delta\sigma_{\text{p.r.Vis}}(t) \right] - \sum_{i=1}^{i-1} \Delta\sigma_{\text{p.r.Vis}}(t)$$

$$\Delta\sigma_{\text{Vis}}(t) := \begin{cases} \left[\Delta\sigma_{\text{Vis.const1}}(t) \cdot \Delta\sigma_{\text{Vis.const2}}(t) \right] \cdot 10^{-3} & \text{if Class}_{\text{rel}} = "1" \\ \left[\left[\Delta\sigma_{\text{Vis.const3}}(t) \cdot \Delta\sigma_{\text{Vis.const4}}(t) \right] \right] \cdot 10^{-3} & \text{if Class}_{\text{rel}} = "2" \\ \left[\left[\Delta\sigma_{\text{Vis.const5}}(t) \cdot \Delta\sigma_{\text{Vis.const6}}(t) \right] \right] \cdot 10^{-3} & \text{if Class}_{\text{rel}} = "3" \end{cases}$$

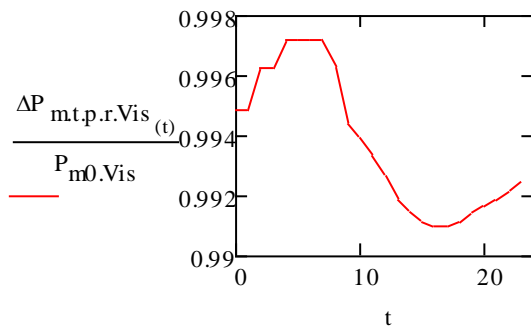
$$\sigma_{\text{p.Vis}}(t) := \sigma_{\text{p.i.Vis}} - \Delta\sigma_{\text{Vis}}(t)$$



Loss due to release of prestress force direct after de-tensioning

$$\Delta P_{p.r.Vis(t)} := A_{p.line.total.Vis} \cdot \Delta \sigma_{Vis(t)}$$

$$\Delta P_{m.t.p.r.Vis(t)} := P_{m0.Vis} - \Delta P_{p.r.Vis(t)}$$



Losses of prestress due to relaxation after 3 hours (before casting) and from casting to release of prestress force (18 hours)

$$x_{relaxationloss.3h.Vis} := 1 - \frac{\Delta P_{m.t.p.r.Vis_3}}{P_{m0.Vis}} = 3.753 \times 10^{-3}$$

$$x_{relaxationloss.18h.Vis} := \frac{\Delta P_{m.t.p.r.Vis_3} - \Delta P_{m.t.p.r.Vis_{18}}}{P_{m0.Vis}} = 4.382 \times 10^{-3}$$

Shrinkage

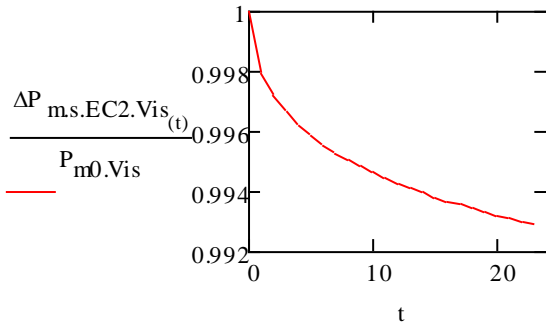
See "Structural analysis": "Shrinkage"

The autogenous part of the shrinkage is only considered in the calculations, according to EC2

According to EC2

$$\Delta P_{c.s.EC2.Vis(t)} := A_{p.line.total.Vis} \cdot E_p \cdot \epsilon_{c.a.Vis(t)}$$

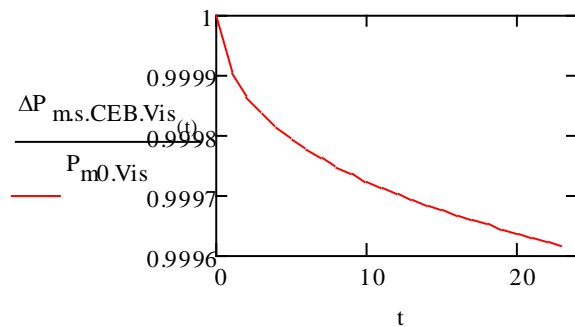
$$\Delta P_{m.s.EC2.Vis(t)} := P_{m0.Vis} - \Delta P_{c.s.EC2.Vis(t)}$$



CEB-FIB (used in DIANA)

$$\Delta P_{c.s.CEB.Vis(t)} := A_{p.line.total.Vis} E_p \cdot (-\varepsilon_{s.Vis}(t))$$

$$\Delta P_{m.s.CEB.Vis(t)} := P_{m0.Vis} - \Delta P_{c.s.CEB.Vis(t)}$$



Losses of prestress due to shrinkage during 18 hours from casting

$$x_{shrinkageloss.EC2.Vis} := \frac{\Delta P_{m.s.EC2.Vis_3} - \Delta P_{m.s.EC2.Vis_{21}}}{P_{m0.Vis}} = 3.518 \times 10^{-3}$$

$$x_{shrinkageloss.CEB.Vis} := \frac{\Delta P_{m.s.CEB.Vis_3} - \Delta P_{m.s.CEB.Vis_{21}}}{P_{m0.Vis}} = 2.054 \times 10^{-4}$$

Thermal EN 1992-1-1:2004 Ch. 10.5.2 Losses of prestress

According to Eurocode

$$\varepsilon_{c.t.EC2.Vis(t)} := \alpha_{c.te} \cdot [(T_{Vis}(t) - T_{c.Vis})]$$

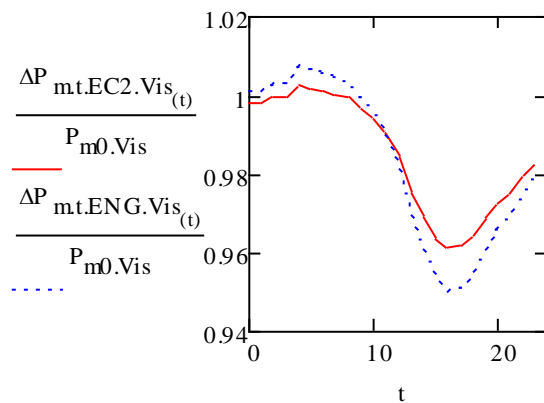
$$\Delta P_{\theta, EC2, Vis(t)} := 0.5 A_{p, line, total, Vis} E_p \cdot \varepsilon_{c, t, EC2, Vis(t)}$$

$$\Delta P_{m, t, EC2, Vis(t)} := P_{m0, Vis} - (\Delta P_{\theta, EC2, Vis(t)})$$

According to Engström

$$\Delta P_{\theta, ENG, Vis(t)} := A_{p, line, total, Vis} E_p \cdot \varepsilon_{c, t, Vis(t)}$$

$$\Delta P_{m, t, ENG, Vis(t)} := P_{m0, Vis} - \Delta P_{\theta, ENG, Vis(t)}$$



Loss due to thermal effects after 19 hours

$$\chi_{thermalloss, ENG, Vis} := \frac{\Delta P_{m, t, ENG, Vis_3} - \Delta P_{m, t, ENG, Vis_2}}{P_{m0, Vis}} = 0.034$$

$$\chi_{thermalloss, EC2, Vis} := \frac{\Delta P_{m, t, EC2, Vis_3} - \Delta P_{m, t, EC2, Vis_2}}{P_{m0, Vis}} = 0.024$$

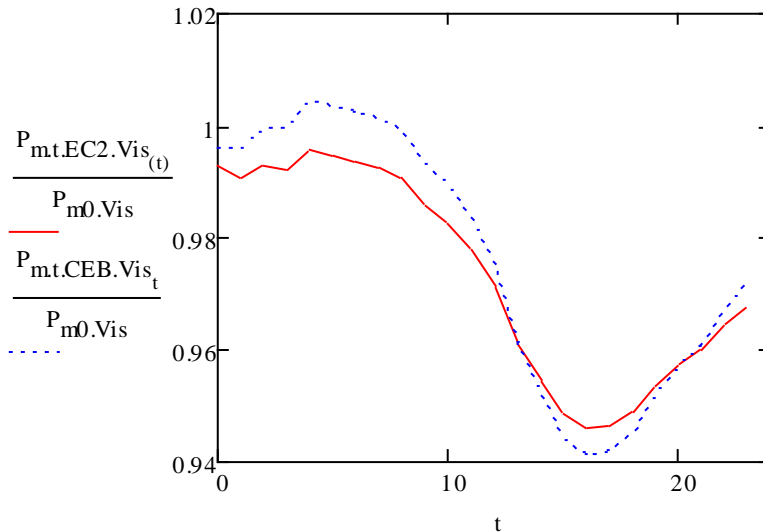
Total prestress loss

According to CEB-FIB and Engström

$$P_{m, t, CEB, Vis(t)} := P_{m0, Vis} - \Delta P_{p, r, Vis(t)} \dots \\ + (-\Delta P_{c, s, CEB, Vis(t)}) - \Delta P_{\theta, ENG, Vis(t)}$$

According to Eurocode

$$P_{m, t, EC2, Vis(t)} := P_{m0, Vis} - \Delta P_{p, r, Vis(t)} \dots \\ + -\Delta P_{c, s, EC2, Vis(t)} - \Delta P_{\theta, EC2, Vis(t)}$$



Total loss after 19 hours except release of prestress

$$\chi_{\text{totloss.CEB.Vis}} := \chi_{\text{thermalloss.ENG.Vis}} + \chi_{\text{shrinkageloss.CEB.Vis}} + \chi_{\text{relaxationloss.18h.Vis}} = 0.039$$

$$\chi_{\text{totloss.EC2.Vis}} := \chi_{\text{thermalloss.EC2.Vis}} + \chi_{\text{shrinkageloss.EC2.Vis}} + \chi_{\text{relaxationloss.18h.Vis}} = 0.032$$

At the transfer of prestress to concrete

Losses due to elastic deformation and relaxation due to elastic deformation of the concrete

Elastic deformation

$$\varepsilon_{p.el} := 0.001$$

Relaxation, due to elastic shortening of the concrete EN 1992-1-1:2004 Annex D

$$\sigma_{p.i.el} := E_p \cdot \varepsilon_{p.el} = 205 \text{ MPa} \quad i := 23 \quad t_{rel} := 18..19$$

$$\mu_{rel.Vis(18)} := \frac{\sigma_{p.i.Vis} + \sum_{i=1}^{21} \Delta\sigma_{p.r.Vis(18)}}{f_{puk.Vis}}$$

$$\mu_{rel.Vis(19)} := \frac{\sum_{i=1}^{21} \Delta\sigma_{p.r.Vis(19)}}{f_{puk.Vis}}$$

$$t_{e,rel.Vis}(t_{rel}) := 1000 \left[\frac{\sum_{i=1}^{i-1} \Delta\sigma_{p,r.Vis}(t_{rel})}{\left[\sigma_{p,i} + \sum_{i=1}^{i-1} \Delta\sigma_{p,r.Vis}(t_{rel}) \right] \chi 1000 e} \right] \cdot \frac{1}{\left[\frac{1}{0.75 \cdot \left[1 - \mu_{rel.Vis}(t_{rel}) \right]} \right]} = \dots$$

$$\Delta\sigma_{pr.el.rel.c1.Vis}(t_{rel}) := 5.39 \chi 1000 e \cdot \left[\frac{t_{e,rel.Vis}(t_{rel}) + \Delta t}{1000} \right]^{6.7 \cdot \mu_{rel.Vis}(t_{rel})} \cdot \left[1 - \mu_{rel.Vis}(t_{rel}) \right]^{0.75}$$

$$\Delta\sigma_{pr.el.rel.c2.Vis}(t_{rel}) := \left[\sigma_{p,i.Vis} + \sum_{i=1}^{i-1} \Delta\sigma_{p,r.Vis}(t_{rel}) \right] - \sum_{i=1}^{i-1} \Delta\sigma_{p,r.Vis}(t_{rel})$$

$$\Delta\sigma_{pr.el.rel.c3.Vis}(t_{rel}) := 0.66 \chi 1000 e \cdot \left[\frac{t_{e,rel.Vis}(t_{rel}) + \Delta t}{1000} \right]^{9.1 \cdot \mu_{rel.Vis}(t_{rel})} \cdot \left[1 - \mu_{rel.Vis}(t_{rel}) \right]^{0.75}$$

$$\Delta\sigma_{pr.el.rel.c4.Vis}(t_{rel}) := \left[\sigma_{p,i.Vis} + \sum_{i=1}^{i-1} \Delta\sigma_{p,r.Vis}(t_{rel}) \right] - \sum_{i=1}^{i-1} \Delta\sigma_{p,r.Vis}(t_{rel})$$

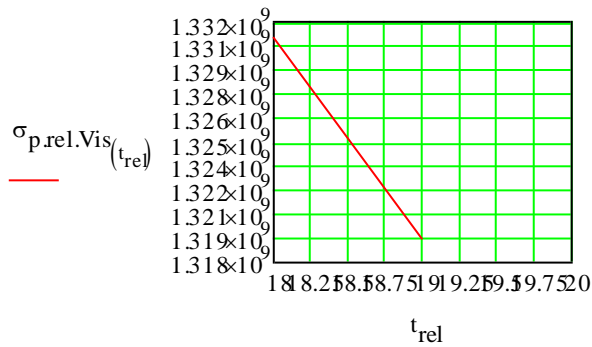
$$\Delta\sigma_{pr.el.rel.c5.Vis}(t_{rel}) := 1.98 \chi 1000 e \cdot \left[\frac{t_{e,rel.Vis}(t_{rel}) + \Delta t}{1000} \right]^{8 \cdot \mu_{rel.Vis}(t_{rel})} \cdot \left[1 - \mu_{rel.Vis}(t_{rel}) \right]^{0.75}$$

$$\Delta\sigma_{pr.el.rel.c6.Vis}(t_{rel}) := \left[\sigma_{p,i.Vis} + \sum_{i=1}^{i-1} \Delta\sigma_{p,r.Vis}(t_{rel}) \right] - \sum_{i=1}^{i-1} \Delta\sigma_{p,r.Vis}(t_{rel})$$

$$\Delta\sigma_{pr.el.rel.Vis}(t_{rel}) := \begin{cases} \left[\Delta\sigma_{pr.el.rel.c1.Vis}(t_{rel}) \cdot \Delta\sigma_{pr.el.rel.c2.Vis}(t_{rel}) \right] \cdot 10^{-3} & \text{if Class}_{rel} = "1" \\ \left[\Delta\sigma_{pr.el.rel.c3.Vis}(t_{rel}) \cdot \Delta\sigma_{pr.el.rel.c4.Vis}(t_{rel}) \right] \cdot 10^{-3} & \text{if Class}_{rel} = "2" \\ \left[\Delta\sigma_{pr.el.rel.c5.Vis}(t_{rel}) \cdot \Delta\sigma_{pr.el.rel.c6.Vis}(t_{rel}) \right] \cdot 10^{-3} & \text{if Class}_{rel} = "3" \end{cases}$$

$$\sigma_{p,rel.Vis_{18}} := \sigma_{p.Vis_{18}}$$

$$\sigma_{p,rel.Vis_{19}} := \sigma_{p.Vis_{18}} - \Delta\sigma_{pr.el.rel.Vis_{18}}$$



Loss due to release of prestress force direct after de-tensioning

$$\chi_{\text{releaseloss.EC2.Vis}} := 1 - \frac{\sigma_{\text{p.rel.Vis}}_{19}}{\sigma_{\text{p.Vis}}_{18}} = 8.926 \times 10^{-3}$$

Total loss during curing inclusive loss due to release

$$\chi_{\text{TOT.EC2.Vis}} = \chi_{\text{relaxationloss.3h.Vis}} + \chi_{\text{totloss.EC2.Vis}} + \chi_{\text{releaseloss.EC2.Vis}} = 0.045$$

$$\chi_{\text{TOT.CEB.Vis}} = \chi_{\text{relaxationloss.3h.Vis}} + \chi_{\text{totloss.CEB.Vis}} + \chi_{\text{releaseloss.EC2.Vis}} = 0.051$$

Marijampolé

During the tensioning

Losses due to wedge draw-in of the anchorage device

Before the transfer of prestress to concrete

Losses due to shrinkage, relaxation of the prestressing steel and thermal effects

Relaxation

$$\text{Class}_{\text{rel}} := "2"$$

$$\chi_{1000} := \begin{cases} 8\% & \text{if } \text{Class}_{\text{rel}} = "1" \\ 2.5\% & \text{if } \text{Class}_{\text{rel}} = "2" \\ 4\% & \text{if } \text{Class}_{\text{rel}} = "3" \end{cases}$$

$$\varepsilon_{\text{pi}} := 0.006$$

$$\sigma_{p.i} := E_p \cdot \varepsilon_{pi} = 1.23 \times 10^3 \cdot \text{MPa} < \sigma_{p.ma}$$

$$\sigma_{p.i.Mar} := \sigma_{p.m0.Mar} = 1.395 \times 10^3 \cdot \text{MPa}$$

$$\mu_{Mar} := \frac{\sigma_{p.i.Mar}}{f_{puk.Mar}} = 0.75$$

$$t_{eq.Mar} = \frac{\frac{T_{Mar.max} - 20^\circ\text{C}}{\text{K}} \cdot 1.14}{T_{Mar.max} - 20^\circ\text{C}} \cdot \sum_{i=1}^{20} \left[\left[T_{Mar(i)} - 20^\circ\text{C} \right] \cdot \Delta t \right] \quad (\text{EC2})$$

$t_{eq.Mar} :=$

306,15	279,15	1	0
	279,15		0
	279,15		0
	290,15		14,01070236
	289,15		12,73700214
	289,15		12,73700214
	290,15		14,01070236
	291,15		15,28440257
	293,15		17,831803
	294,65		19,74235332
	296,15		21,65290365
	298,15		24,20030407
	301,15		28,02140472
	304,15		31,84250536
	305,15		33,11620558
	306,15		34,38990579
	306,15		34,38990579
	306,15		34,38990579
	305,15		33,11620558
	304,15		31,84250536
	303,15		30,56880515
	301,15		28,02140472
	299,65		26,1108544
	297,15		22,92660386

$$\left(T_{Mar.max} \cdot \text{const} \cdot T_{Mar} \cdot \Delta t \right)$$

$$\Delta\sigma_{p.r.Mar} := \begin{cases} \left[5.39 \chi_{1000} e^{6.7 \cdot \mu_{Mar}} \cdot \left(\frac{t_{eq.Mar} + \Delta t}{1000} \right)^{0.75 \cdot (1 - \mu_{Mar})} \cdot 10^{-3} \right] \cdot \sigma_{p.i.Mar} & \text{if Class}_{rel} = "1" \\ \left[0.66 \chi_{1000} e^{9.1 \cdot \mu_{Mar}} \cdot \left(\frac{t_{eq.Mar} + \Delta t}{1000} \right)^{0.75 \cdot (1 - \mu_{Mar})} \cdot 10^{-3} \right] \cdot \sigma_{p.i.Mar} & \text{if Class}_{rel} = "2" \\ \left[1.98 \chi_{1000} e^{8 \cdot \mu_{Mar}} \cdot \left(\frac{t_{eq.Mar} + \Delta t}{1000} \right)^{0.75 \cdot (1 - \mu_{Mar})} \cdot 10^{-3} \right] \cdot \sigma_{p.i.Mar} & \text{if Class}_{rel} = "3" \end{cases}$$

i := 23

$$\mu_{Mar(t)} := \frac{\sigma_{p.i.Mar} + \sum_{i=1}^{23} \Delta\sigma_{p.r.Mar(t)}}{f_{puk.Mar}}$$

$$t_{e.Mar(t)} := 1000 \left[\frac{\sum_{i=1}^{i-1} \Delta\sigma_{p.r.Mar(t)}}{\left[\sigma_{p.i} + \sum_{i=1}^{i-1} \Delta\sigma_{p.r.Mar(t)} \right] \chi_{1000} e^{6.7 \cdot \mu_{Mar(t)}}} \cdot \frac{1}{\left[0.75 \cdot \left[1 - \mu_{Mar(t)} \right] \right]} \right] = \dots$$

$$\Delta\sigma_{Mar.const1(t)} := 5.39 \chi_{1000} e^{6.7 \cdot \mu_{Mar(t)}} \cdot \left[\frac{t_{e.Mar(t)} + \Delta t}{1000} \right]^{0.75 \cdot [1 - \mu_{Mar(t)}]}$$

$$\Delta\sigma_{Mar.const2(t)} := \left[\sigma_{p.i.Mar} + \sum_{i=1}^{i-1} \Delta\sigma_{p.r.Mar(t)} \right] - \sum_{i=1}^{i-1} \Delta\sigma_{p.r.Mar(t)}$$

$$\Delta\sigma_{Mar.const3(t)} := 0.66 \chi_{1000} e^{9.1 \cdot \mu_{Mar(t)}} \cdot \left[\frac{t_{e.Mar(t)} + \Delta t}{1000} \right]^{0.75 \cdot [1 - \mu_{Mar(t)}]}$$

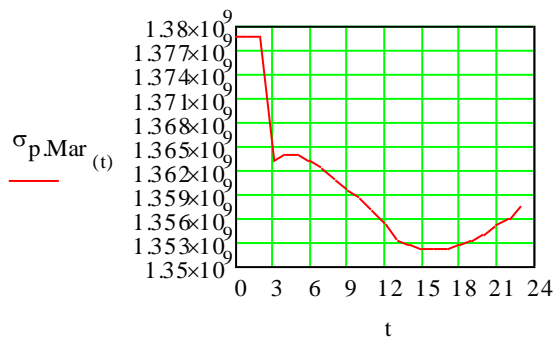
$$\Delta\sigma_{Mar.const4(t)} := \left[\sigma_{p.i.Mar} + \sum_{i=1}^{i-1} \Delta\sigma_{p.r.Mar(t)} \right] - \sum_{i=1}^{i-1} \Delta\sigma_{p.r.Mar(t)}$$

$$\Delta\sigma_{\text{Marconst5}(t)} := 1.98 \times 1000^e \cdot 8 \cdot \mu_{\text{Mar}(t)} \cdot \left[\frac{t_{e,\text{Mar}(t)} + \Delta t}{1000} \right]^{0.75} \cdot [1 - \mu_{\text{Mar}(t)}]$$

$$\Delta\sigma_{\text{Mar.const6}(t)} := \left[\sigma_{\text{p.i.Mar}} + \sum_{i=1}^{i-1} \Delta\sigma_{\text{p.r.Mar}(t)} \right] - \sum_{i=1}^{i-1} \Delta\sigma_{\text{p.r.Mar}(t)}$$

$$\Delta\sigma_{\text{Mar}(t)} := \begin{cases} \left[\Delta\sigma_{\text{Mar.const1}(t)} \cdot \Delta\sigma_{\text{Marconst2}(t)} \right] \cdot 10^{-3} & \text{if Class}_{\text{rel}} = "1" \\ \left[\left[\Delta\sigma_{\text{Mar.const3}(t)} \cdot \Delta\sigma_{\text{Mar.const4}(t)} \right] \right] \cdot 10^{-3} & \text{if Class}_{\text{rel}} = "2" \\ \left[\left[\Delta\sigma_{\text{Marconst5}(t)} \cdot \Delta\sigma_{\text{Mar.const6}(t)} \right] \right] \cdot 10^{-3} & \text{if Class}_{\text{rel}} = "3" \end{cases}$$

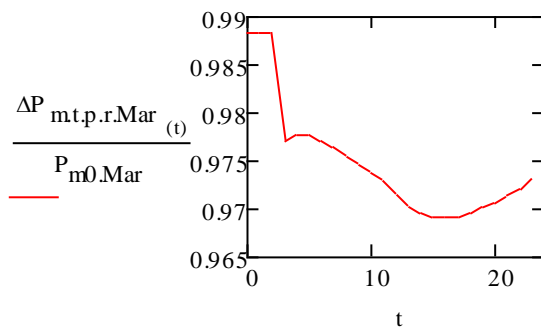
$$\sigma_{\text{p.Mar}(t)} := \sigma_{\text{p.i.Mar}} - \Delta\sigma_{\text{Mar}(t)}$$



Loss due to release of prestress force direct after de-tensioning

$$\Delta P_{\text{p.r.Mar}(t)} := A_{\text{p.line.total.Mar}} \cdot \Delta\sigma_{\text{Mar}(t)}$$

$$\Delta P_{\text{m.t.p.r.Mar}(t)} := P_{\text{m0.Mar}} - \Delta P_{\text{p.r.Mar}(t)}$$



Losses of prestress due to relaxation after 3 hours (before casting) and losses from casting to release of prestress force (18 hours)

$$\chi_{\text{relaxationloss.3h.Mar}} := 1 - \frac{\Delta P_{\text{m.t.p.r.Mar}_5}}{P_{\text{m0.Mar}}} = 0.023$$

$$\chi_{\text{relaxationloss.18h.Mar}} := \frac{\Delta P_{\text{m.t.p.r.Mar}_5} - \Delta P_{\text{m.t.p.r.Mar}_{21}}}{P_{\text{m0.Mar}}} = 5.734 \times 10^{-3}$$

Shrinkage

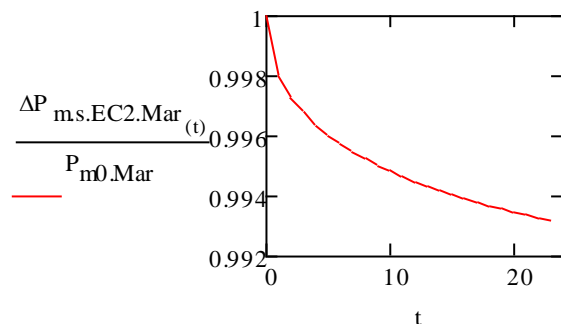
See "Structural analysis": "Shrinkage"

The autogenous part of the shrinkage is only considered in the calculations

According to EC2

$$\Delta P_{\text{c.s.EC2.Mar}(t)} := A_{\text{p.line.total.Mar}} E_p \cdot \varepsilon_{\text{c.a.Mar}(t)}$$

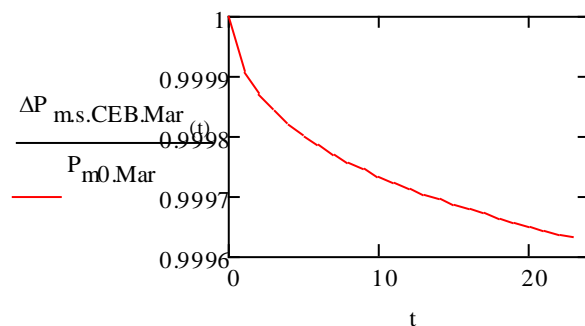
$$\Delta P_{\text{m.s.EC2.Mar}(t)} := P_{\text{m0.Mar}} - \Delta P_{\text{c.s.EC2.Mar}(t)}$$



CEB-FIB (used in DIANA)

$$\Delta P_{\text{c.s.CEB.Mar}(t)} := A_{\text{p.line.total.Mar}} E_p \cdot (-\varepsilon_{\text{s.Mar}}(t))$$

$$\Delta P_{\text{m.s.CEB.Mar}(t)} := P_{\text{m0.Mar}} - \Delta P_{\text{c.s.CEB.Mar}(t)}$$



$$x_{\text{thermalloss.EC2.Mar}} := \frac{\Delta P_{m.t.EC2.Mar_3} - \Delta P_{m.t.EC2.Mar_2_1}}{P_{m0.Mar}} = 0.016$$

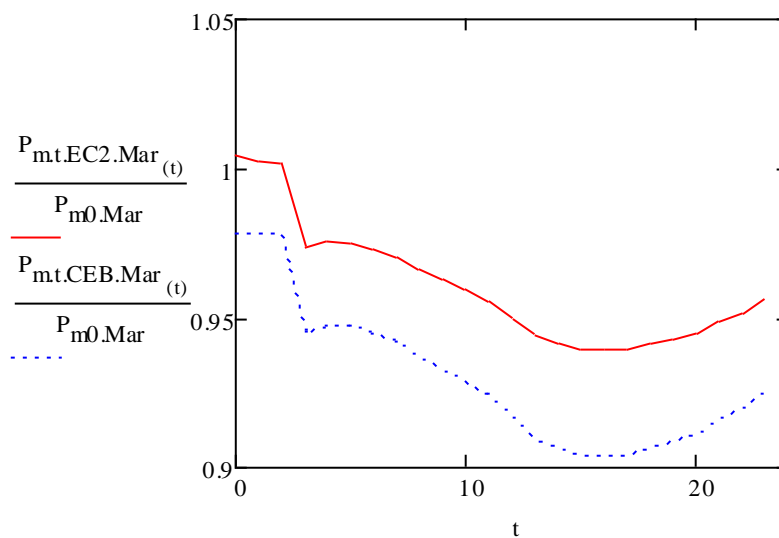
Total prestress loss

According to CEB-FIB and Engström

$$P_{m.t.CEB.Mar(t)} := P_{m0.Mar} - \Delta P_{p.r.Mar(t)} \dots \\ + -\Delta P_{c.s.CEB.Mar(t)} - \Delta P_{\theta.ENG.Mar(t)}$$

According to Eurocode

$$P_{m.t.EC2.Mar(t)} := P_{m0.Mar} - \Delta P_{p.r.Mar(t)} \dots \\ + -\Delta P_{c.s.EC2.Mar(t)} - \Delta P_{\theta.EC2.Mar(t)}$$



Total loss after 20 hours except release of prestress

$$x_{\text{totloss.CEB.Mar}} := x_{\text{thermalloss.ENG.Mar}} + x_{\text{shrinkageloss.CEB.Mar}} \dots = 0.028 \\ + x_{\text{relaxationloss.18h.Mar}}$$

$$x_{\text{totloss.EC2.Mar}} := x_{\text{thermalloss.EC2.Mar}} + x_{\text{shrinkageloss.EC2.Mar}} \dots = 0.025 \\ + x_{\text{relaxationloss.18h.Mar}}$$

At the transfer of prestress to concrete

Losses due to elastic deformation and relaxation due to elastic deformation of the concrete

Elastic deformation

$$\varepsilon_{p.el} := 0.00$$

Relaxation, due to elastic shortening of the concrete

EN 1992-1-1:2004 Annex D

$$\sigma_{p.i.el} := E_p \cdot \varepsilon_{p.el} = 205 \text{ MPa} \quad i := 23 \quad t_{rel} := 18.19$$

$$\mu_{rel.Mar(18)} := \frac{\sigma_{p.i.Mar} + \sum_{i=1}^{21} \Delta\sigma_{p.r.Mar(18)}}{f_{puk.Mar}}$$

$$\mu_{rel.Mar(19)} := \frac{\sum_{i=1}^{21} \Delta\sigma_{p.r.Mar(19)}}{f_{puk.Mar}}$$

$$t_{e.rel.Mar}(t_{rel}) := 1000 \left[\frac{\sum_{i=1}^{i-1} \Delta\sigma_{p.r.Mar}(t_{rel})}{\left[\sigma_{p.i} + \sum_{i=1}^{i-1} \Delta\sigma_{p.r.Mar}(t_{rel}) \right] \chi 1000^e} \cdot \frac{1}{6.7 \cdot \mu_{rel.Mar}(t_{rel})} \right] \frac{1}{\left[0.75 \cdot \left[1 - \mu_{rel.Mar}(t_{rel}) \right] \right]} = \dots$$

$$\Delta\sigma_{pr.el.rel.c1.Mar}(t_{rel}) := 5.39 \chi 1000^e \cdot \frac{6.7 \cdot \mu_{rel.Mar}(t_{rel}) \left[\frac{t_{e.rel.Mar}(t_{rel}) + \Delta t}{1000} \right]}{0.75 \cdot \left[1 - \mu_{rel.Mar}(t_{rel}) \right]}$$

$$\Delta\sigma_{pr.el.rel.c2.Mar}(t_{rel}) := \left[\sigma_{p.i.Mar} + \sum_{i=1}^{i-1} \Delta\sigma_{p.r.Mar}(t_{rel}) \right] - \sum_{i=1}^{i-1} \Delta\sigma_{p.r.Mar}(t_{rel})$$

$$\Delta\sigma_{pr.el.rel.c3.Mar}(t_{rel}) := 0.66 \chi 1000^e \cdot \frac{9.1 \cdot \mu_{rel.Mar}(t_{rel}) \left[\frac{t_{e.rel.Mar}(t_{rel}) + \Delta t}{1000} \right]}{0.75 \cdot \left[1 - \mu_{rel.Mar}(t_{rel}) \right]}$$

$$t_{\text{eq.Sollenau}} := \frac{\frac{T_{\text{Sollenau.max}} - 20^{\circ}\text{C}}{\text{K}} \cdot 1.14}{T_{\text{Sollenau.max}} - 20^{\circ}\text{C}} \cdot \sum_{i=1}^{20} \left[\left[T_{\text{Sollenau}(i)} - 20^{\circ}\text{C} \right] \cdot \Delta t \right]$$

$t_{\text{eq.Sollenau}} :=$

328.15	298.15	1	0
	298.15		0
	298.15		0
	298.15		0
	300.15		3.396677239
	302.15		6.793354478
	304.15		10.19003172
	306.15		13.58670896
	308.15		16.98338619
	315.15		28.87175653
	322.15		40.76012687
	328.15		50.95015858
	328.15		50.95015858
	327.15		49.25181996
	326.15		47.55348134
	325.15		45.85514272
	324.15		44.15680411
	323.15		42.45846549
	321.15		39.06178825
	320.15		37.36344963
	318.15		33.96677239
	317.15		32.26843377
	315.15		28.87175653
	313.15		25.47507929

$$\left(T_{\text{Sollenau.max.const}} \quad T_{\text{Sollenau}} \quad \Delta t \right)$$

$$\Delta\sigma_{\text{pr.el.rel.c4.Mar}(t_{\text{rel}})} := \left[\sigma_{\text{p.i.Mar}} + \sum_{i=1}^{i-1} \Delta\sigma_{\text{p.r.Mar}(t_{\text{rel}})} \right] - \sum_{i=1}^{i-1} \Delta\sigma_{\text{p.r.Mar}(t_{\text{rel}})}$$

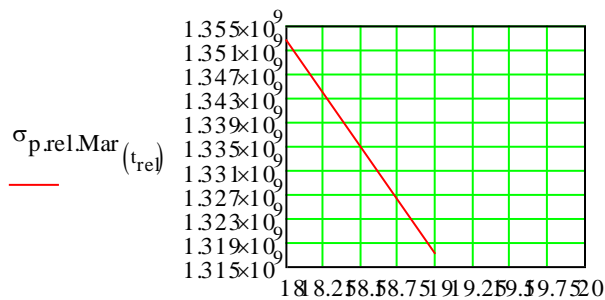
$$\Delta\sigma_{\text{pr.el.rel.c5.Mar}(t_{\text{rel}})} := 1.98 \times 1000 e^{8 \cdot \mu_{\text{rel.Mar}}(t_{\text{rel}})} \left[\frac{t_{\text{e.rel.Mar}}(t_{\text{rel}}) + \Delta t}{1000} \right]^{0.75 \cdot [1 - \mu_{\text{rel.Mar}}(t_{\text{rel}})]}$$

$$\Delta\sigma_{\text{pr.el.rel.c6.Mar}(t_{\text{rel}})} := \left[\sigma_{\text{p.i.Mar}} + \sum_{i=1}^{i-1} \Delta\sigma_{\text{p.r.Mar}(t_{\text{rel}})} \right] - \sum_{i=1}^{i-1} \Delta\sigma_{\text{p.r.Mar}(t_{\text{rel}})}$$

$$\Delta\sigma_{\text{pr.el.rel.Mar}(t_{\text{rel}})} := \begin{cases} \left[\Delta\sigma_{\text{pr.el.rel.c1.Mar}(t_{\text{rel}})} \cdot \Delta\sigma_{\text{pr.el.rel.c2.Mar}(t_{\text{rel}})} \right] \cdot 10^{-3} & \text{if Class}_{\text{rel}} = "1" \\ \left[\left[\Delta\sigma_{\text{pr.el.rel.c3.Mar}(t_{\text{rel}})} \cdot \Delta\sigma_{\text{pr.el.rel.c4.Mar}(t_{\text{rel}})} \right] \right] \cdot 10^{-3} & \text{if Class}_{\text{rel}} = "2" \\ \left[\left[\Delta\sigma_{\text{pr.el.rel.c5.Mar}(t_{\text{rel}})} \cdot \Delta\sigma_{\text{pr.el.rel.c6.Mar}(t_{\text{rel}})} \right] \right] \cdot 10^{-3} & \text{if Class}_{\text{rel}} = "3" \end{cases}$$

$$\sigma_{\text{p.rel.Mar}_{18}} := \sigma_{\text{p.Mar}_{18}}$$

$$\sigma_{\text{p.rel.Mar}_{19}} := \sigma_{\text{p.Mar}_{18}} - \Delta\sigma_{\text{pr.el.rel.Mar}_{18}}$$



$$x_{\text{releaselos.EC2.Mar}} := 1 - \frac{\sigma_{\text{p.rel.Mar}_{19}}}{\sigma_{\text{p.Mar}_{18}}} = 0.026$$

Total loss during curing inclusive loss due to release

$$x_{\text{TOT.EC2.Mar}} = x_{\text{relaxationloss.3h.Mar}} \dots = 0.074$$

$$+ x_{\text{totloss.EC2.Mar}} + x_{\text{releaselos.EC2.Mar}}$$

$$x_{\text{TOT.CEB.Mar}} = x_{\text{relaxationloss.3h.Mar}} \dots = 0.077$$

$$+ x_{\text{totloss.CEB.Mar}} + x_{\text{releaselos.EC2.Mar}}$$

Sollenau

During the tensioning

Losses due to wedge draw-in of the anchorage device

Losses due to shrinkage, relaxation of the prestressing steel and thermal effects

Relaxation

$$\Delta t := 1$$

$$\text{Class}_{\text{rel}} := "2"$$

$$\chi_{1000} := \begin{cases} 8\% & \text{if } \text{Class}_{\text{rel}} = "1" \\ 2.5\% & \text{if } \text{Class}_{\text{rel}} = "2" \\ 4\% & \text{if } \text{Class}_{\text{rel}} = "3" \end{cases} = 0.025$$

$$\varepsilon_{\text{pi}} := 0.006$$

$$< \sigma_{\text{p,max}}$$

$$\sigma_{\text{p,i}} := E_{\text{p}} \cdot \varepsilon_{\text{pi}} = 1.23 \times 10^3 \cdot \text{MPa}$$

$$\sigma_{\text{p,i.Sollenau}} := \sigma_{\text{p,m0.Sollenau}} = 1.275 \times 10^3 \cdot \text{MPa}$$

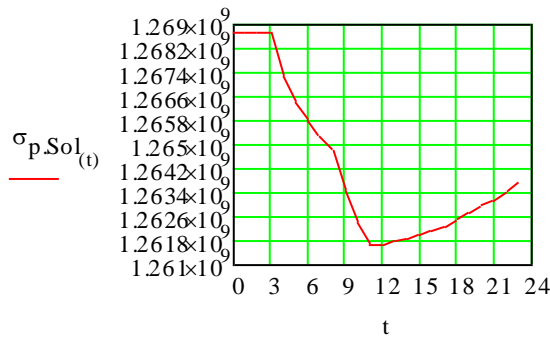
$$\mu_{\text{Sollenau}} := \frac{\sigma_{\text{p,i.Sollenau}}}{f_{\text{puk.Sollenau}}} = 0.72$$

$$t_{\text{eq.Sollenau}} := \frac{1.14}{T_{\text{Sollenau,max}} - 20^{\circ}\text{C}} \cdot \frac{T_{\text{Sollenau,max}} - 20^{\circ}\text{C}}{\text{K}} \cdot \sum_{i=1}^{20} \left[\left[T_{\text{Sollenau}(i)} - 20^{\circ}\text{C} \right] \cdot \Delta t \right]$$

$$t_{\text{e.Sol}(t)} := 1000 \left[\frac{\sum_{i=1}^{i-1} \Delta \sigma_{\text{p,r.Sol}(t)}}{\left[\sigma_{\text{p,i}} + \sum_{i=1}^{i-1} \Delta \sigma_{\text{p,r.Sol}(t)} \right] \chi_{1000} e^{6.7 \cdot \mu_{\text{Sol}(t)}}} \right]^{\frac{1}{0.75 \cdot [1 - \mu_{\text{Sol}(t)})}} = \dots$$

$$\Delta \sigma_{\text{Sol, const1}(t)} := 5.39 \chi_{1000} e^{6.7 \cdot \mu_{\text{Sol}(t)}} \cdot \left[\frac{t_{\text{e.Sol}(t)} + \Delta t}{1000} \right]^{0.75 \cdot [1 - \mu_{\text{Sol}(t)})}$$

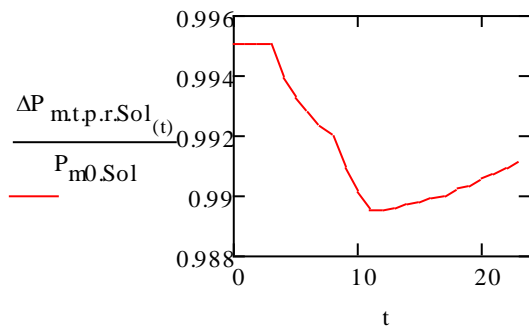
$$\Delta \sigma_{\text{Sol, const2}(t)} := \left[\sigma_{\text{p,i.Sol}} + \sum_{i=1}^{i-1} \Delta \sigma_{\text{p,r.Sol}(t)} \right] - \sum_{i=1}^{i-1} \Delta \sigma_{\text{p,r.Sol}(t)}$$



Loss due to release of prestress force direct after de-tensioning

$$\Delta P_{p.r.Sol(t)} := A_{p.line.total.Sol} \Delta \sigma_{Sol(t)}$$

$$\Delta P_{m.t.p.r.Sol(t)} := P_{m0.Sol} - \Delta P_{p.r.Sol(t)}$$



Losses of prestress due to relaxation after 3 hours (before casting) and loss of prestress from casting to release of prestress (20 hours).

$$x_{relaxationloss.3h.Sol} := 1 - \frac{\Delta P_{m.t.p.r.Sol_3}}{P_{m0.Sol}} = 4.904 \times 10^{-3}$$

$$x_{relaxationloss.20h.Sol} := \frac{\Delta P_{m.t.p.r.Sol_3} - \Delta P_{m.t.p.r.Sol_{23}}}{P_{m0.Sol}} = 3.866 \times 10^{-3}$$

Shrinkage

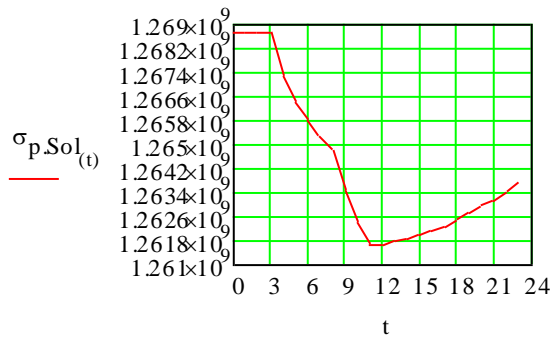
See "Structural analysis": "Shrinkage"

The autogenous part of the shrinkage is only considered in the calculations

According to EC2

$$\Delta P_{c.s.EC2.Sol(t)} := A_{p.line.total.Sol} E_p \cdot \epsilon_{c.a.Sol(t)}$$

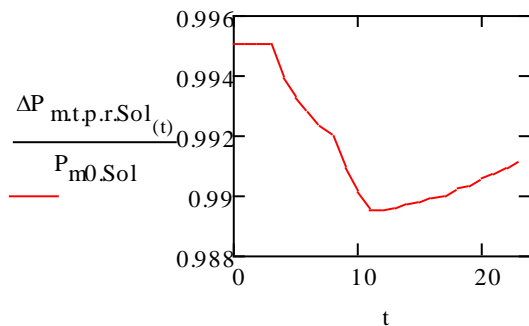
$$\Delta P_{m.s.EC2.Sol(t)} := P_{m0.Sol} - \Delta P_{c.s.EC2.Sol(t)}$$



Loss due to release of prestress force direct after de-tensioning

$$\Delta P_{p.r.Sol(t)} := A_{p.line.total.Sol} \Delta \sigma_{Sol(t)}$$

$$\Delta P_{m.t.p.r.Sol(t)} := P_{m0.Sol} - \Delta P_{p.r.Sol(t)}$$



Losses of prestress due to relaxation after 3 hours (before casting) and loss of prestress from casting to release of prestress (20 hours)

$$x_{relaxationloss.3h.Sol} := 1 - \frac{\Delta P_{m.t.p.r.Sol_3}}{P_{m0.Sol}} = 4.904 \times 10^{-3}$$

$$x_{relaxationloss.20h.Sol} := \frac{\Delta P_{m.t.p.r.Sol_3} - \Delta P_{m.t.p.r.Sol_{23}}}{P_{m0.Sol}} = 3.866 \times 10^{-3}$$

Shrinkage

See "Structural analysis": "Shrinkage"

The autogenous part of the shrinkage is only considered in the calculations

According to EC2

$$\Delta P_{c.s.EC2.Sol(t)} := A_{p.line.total.Sol} E_p \cdot \epsilon_{c.a.Sol(t)}$$

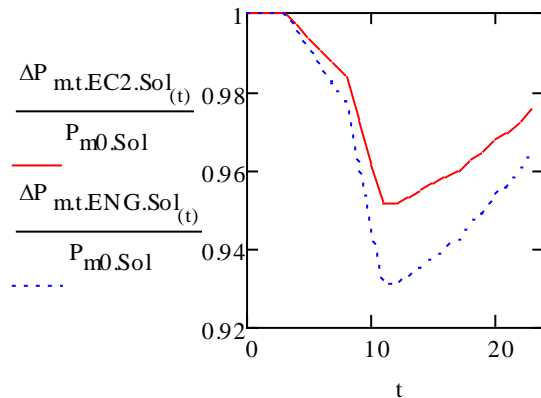
$$\Delta P_{m.s.EC2.Sol(t)} := P_{m0.Sol} - \Delta P_{c.s.EC2.Sol(t)}$$

$$\Delta P_{m.t.EC2.Sol(t)} := P_{m0.Sol} - \Delta P_{\theta.EC2.Sol(t)}$$

According to Engström

$$\Delta P_{\theta.ENG.Sol(t)} := A_{p.line.total.Sol} E_p \cdot \varepsilon_{c.t.Sol(t)}$$

$$\Delta P_{m.t.ENG.Sol(t)} := P_{m0.Sol} - \Delta P_{\theta.ENG.Sol(t)}$$



Loss due to only thermal effects after 20 hours from casting

$$\chi_{thermalloss.ENG.Sol} = \frac{\Delta P_{m.t.ENG.Sol_3} - \Delta P_{m.t.ENG.Sol_{23}}}{P_{m0.Sol}} = 0.034$$

$$\chi_{thermalloss.EC2.Sol} = \frac{\Delta P_{m.t.EC2.Sol_3} - \Delta P_{m.t.EC2.Sol_{23}}}{P_{m0.Sol}} = 0.024$$

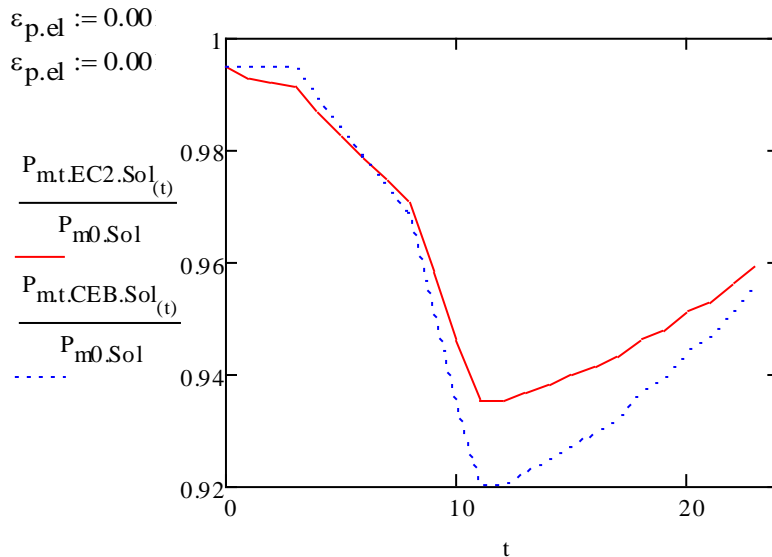
Total prestress loss

According to CEB-FIB and Engström

$$P_{m.t.CEB.Sol(t)} := P_{m0.Sol} - \Delta P_{p.r.Sol(t)} - \Delta P_{c.s.CEB.Sol(t)} \cdot \cdot \\ + -\Delta P_{\theta.ENG.Sol(t)}$$

According to Eurocode

$$P_{m.t.EC2.Sol(t)} := P_{m0.Sol} - \Delta P_{p.r.Sol(t)} - \Delta P_{c.s.EC2.Sol(t)} \cdot \cdot \\ + -\Delta P_{\theta.EC2.Sol(t)}$$



Total loss after 20 hours from tensioning except release of prestress

$$x_{totloss,CEB,Sol} := x_{thermalloss,ENG,Sol} + x_{shrinkageloss,CEB,Sol} + x_{relaxationloss,20h,Sol} = 0.039$$

$$x_{totloss,EC2,Sol} := x_{thermalloss,EC2,Sol} + x_{shrinkageloss,EC2,Sol} + x_{relaxationloss,20h,Sol} = 0.032$$

At the transfer of prestress to concrete

Losses due to elastic deformation and relaxation due to elastic deformation of the concrete

Elastic deformation

$$\varepsilon_{p,el} := 0.001$$

Relaxation, due to elastic shortening of the concrete EN 1992-1-1:2004 Annex D

$$\sigma_{p,i,el,Sol} := E_p \cdot \varepsilon_{p,el} = 205 \text{ MPa} \quad i := 21 \quad t_{rel} := 18..19$$

$$\mu_{rel,Sol(18)} := \frac{\sigma_{p,i,Sol} + \sum_{i=1}^{21} \Delta\sigma_{p,r,Sol(18)}}{f_{puk,Sol}}$$

$$\mu_{rel,Sol(19)} := \frac{\sum_{i=1}^{21} \Delta\sigma_{p,r,Sol(19)}}{f_{puk,Sol}}$$

$$t_{e,rel.Sol}(t_{rel}) := 1000 \left[\frac{\sum_{i=1}^{i-1} \Delta\sigma_{p,r.Sol}(t_{rel})}{\left[\sigma_{p,i} + \sum_{i=1}^{i-1} \Delta\sigma_{p,r.Sol}(t_{rel}) \right] \chi 1000 e} \right] \cdot \frac{1}{\left[\frac{1}{0.75 \cdot \left[1 - \mu_{rel.Sol}(t_{rel}) \right]} \right]} = \dots$$

$$\Delta\sigma_{pr.el.rel.c1.Sol}(t_{rel}) := 5.39 \chi 1000 e^{6.7 \cdot \mu_{rel.Sol}(t_{rel})} \cdot \left[\frac{t_{e,rel.Sol}(t_{rel}) + \Delta t}{1000} \right]^{0.75 \cdot \left[1 - \mu_{rel.Sol}(t_{rel}) \right]}$$

$$\Delta\sigma_{pr.el.rel.c2.Sol}(t_{rel}) := \left[\sigma_{p,i.Sol} + \sum_{i=1}^{i-1} \Delta\sigma_{p,r.Sol}(t_{rel}) \right] - \sum_{i=1}^{i-1} \Delta\sigma_{p,r.Sol}(t_{rel})$$

$$\Delta\sigma_{pr.el.rel.c3.Sol}(t_{rel}) := 0.66 \chi 1000 e^{9.1 \cdot \mu_{rel.Sol}(t_{rel})} \cdot \left[\frac{t_{e,rel.Sol}(t_{rel}) + \Delta t}{1000} \right]^{0.75 \cdot \left[1 - \mu_{rel.Sol}(t_{rel}) \right]}$$

$$\Delta\sigma_{pr.el.rel.c4.Sol}(t_{rel}) := \left[\sigma_{p,i.Sol} + \sum_{i=1}^{i-1} \Delta\sigma_{p,r.Sol}(t_{rel}) \right] - \sum_{i=1}^{i-1} \Delta\sigma_{p,r.Sol}(t_{rel})$$

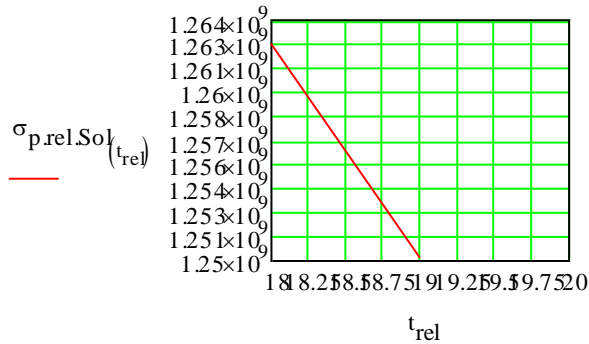
$$\Delta\sigma_{pr.el.rel.c5.Sol}(t_{rel}) := 1.98 \chi 1000 e^{8 \cdot \mu_{rel.Sol}(t_{rel})} \cdot \left[\frac{t_{e,rel.Sol}(t_{rel}) + \Delta t}{1000} \right]^{0.75 \cdot \left[1 - \mu_{rel.Sol}(t_{rel}) \right]}$$

$$\Delta\sigma_{pr.el.rel.c6.Sol}(t_{rel}) := \left[\sigma_{p,i.Sol} + \sum_{i=1}^{i-1} \Delta\sigma_{p,r.Sol}(t_{rel}) \right] - \sum_{i=1}^{i-1} \Delta\sigma_{p,r.Sol}(t_{rel})$$

$$\Delta\sigma_{pr.el.rel.Sol}(t_{rel}) := \begin{cases} \left[\Delta\sigma_{pr.el.rel.c1.Sol}(t_{rel}) \cdot \Delta\sigma_{pr.el.rel.c2.Sol}(t_{rel}) \right] \cdot 10^{-3} & \text{if Class}_{rel} = "1" \\ \left[\left[\Delta\sigma_{pr.el.rel.c3.Sol}(t_{rel}) \cdot \Delta\sigma_{pr.el.rel.c4.Sol}(t_{rel}) \right] \right] \cdot 10^{-3} & \text{if Class}_{rel} = "2" \\ \left[\left[\Delta\sigma_{pr.el.rel.c5.Sol}(t_{rel}) \cdot \Delta\sigma_{pr.el.rel.c6.Sol}(t_{rel}) \right] \right] \cdot 10^{-3} & \text{if Class}_{rel} = "3" \end{cases}$$

$$\sigma_{p.rel.Sol_{18}} := \sigma_{p.Sol_{18}}$$

$$\sigma_{p.rel.Sol_{19}} := \sigma_{p.Sol_{18}} - \Delta\sigma_{pr.el.rel.Sol_{18}}$$



Loss due to release of prestress force direct after de-tensioning

$$x_{\text{releaseloss.EC2.Sol}} := 1 - \frac{\sigma_{p.rel.Sol_{19}}}{\sigma_{p.Sol_{18}}} = 9.849 \times 10^{-3}$$

Total loss during curing inclusive loss due to release

$$x_{\text{TOT.EC2.Sol}} = x_{\text{relaxationloss.3h.Sol}} + x_{\text{totloss.EC2.Sol}} + x_{\text{releaseloss.EC2.Sol}} = 0.047$$

$$x_{\text{TOT.CEB.Sol}} = x_{\text{relaxationloss.3h.Sol}} + x_{\text{totloss.CEB.Sol}} + x_{\text{releaseloss.EC2.Sol}} = 0.053$$

Summary of Prestress Loss

During the different phases to release of prestress

Prestress Loss	Vislanda		Marijampole		Sollenau	
	EC2	CEB-FIP	EC2	CEB-FIP	EC2	CEB-FIP
Before casting	0,38%	-	2,28%	-	0,49%	-
Cast-Release	3,23%	3,86%	2,53%	2,83%	3,19%	3,86%
At release	0,89%	-	2,63%	-	0,98%	-
Total	4,50%	5,13%	7,44%	7,74%	4,66%	5,33%

RE - Calculation, using prestress loss at max temperature, due to the assumption of full bond at that point.

Vislanda

Max temperature after 15 hours

$$x_{\text{relaxationloss.12h.Vis}} = \frac{\Delta P_{\text{m.t.p.r.Vis}_3} - \Delta P_{\text{m.t.p.r.Vis}_{15}}}{P_{\text{m0.Vis}}} = 5.14 \times 10^{-3}$$

$$x_{\text{shrinkageloss.EC2.Vis.12h}} = \frac{\Delta P_{\text{m.s.EC2.Vis}_3} - \Delta P_{\text{m.s.EC2.Vis}_{15}}}{P_{\text{m0.Vis}}} = 2.82 \times 10^{-3}$$

$$x_{\text{shrinkageloss.CEB.Vis.12h}} = \frac{\Delta P_{\text{m.s.CEB.Vis}_3} - \Delta P_{\text{m.s.CEB.Vis}_{15}}}{P_{\text{m0.Vis}}} = 1.603 \times 10^{-4}$$

$$x_{\text{thermalloss.ENG.Vis.12h}} = \frac{\Delta P_{\text{m.t.ENG.Vis}_3} - \Delta P_{\text{m.t.ENG.Vis}_{15}}}{P_{\text{m0.Vis}}} = 0.05$$

$$x_{\text{thermalloss.EC2.Vis.12h}} = \frac{\Delta P_{\text{m.t.EC2.Vis}_3} - \Delta P_{\text{m.t.EC2.Vis}_{15}}}{P_{\text{m0.Vis}}} = 0.036$$

$$x_{\text{totloss.CEB.Vis.12h}} = x_{\text{thermalloss.ENG.Vis.12h}} + x_{\text{shrinkageloss.CEB.Vis.12h}} + x_{\text{relaxationloss.12h.Vis}} = 0.055$$

$$x_{\text{totloss.EC2.Vis.12h}} = x_{\text{thermalloss.EC2.Vis.12h}} + x_{\text{shrinkageloss.EC2.Vis.12h}} + x_{\text{relaxationloss.12h.Vis}} = 0.044$$

Marijampole

Max temperature after 17 hours

$$x_{\text{relaxationloss.14h.Mar}} := \frac{\Delta P_{\text{m.t.p.r.Mar}_3} - (\Delta P_{\text{m.t.p.r.Mar}})_{17}}{P_{\text{m0.Mar}}} = 7.898 \times 10^{-3}$$

$$x_{\text{shrinkageloss.EC2.Mar.14h}} := \frac{\Delta P_{\text{m.s.EC2.Mar}_3} - \Delta P_{\text{m.s.EC2.Mar}}_{17}}{P_{\text{m0.Mar}}} = 2.963 \times 10^{-3}$$

$$x_{\text{shrinkageloss.CEB.Mar.14h}} := \frac{\Delta P_{\text{m.s.CEB.Mar}_3} - \Delta P_{\text{m.s.CEB.Mar}}_{17}}{P_{\text{m0.Mar}}} = 1.699 \times 10^{-4}$$

$$x_{\text{thermalloss.ENG.Mar.14h}} := \frac{(\Delta P_{\text{m.t.ENG.Mar}})_3 - \Delta P_{\text{m.t.ENG.Mar}}_{17}}{P_{\text{m0.Mar}}} = 0.032$$

$$x_{\text{thermalloss.EC2.Mar.14h}} := \frac{\Delta P_{\text{m.t.ENG.Mar}_3} - \Delta P_{\text{m.t.ENG.Mar}}_{17}}{P_{\text{m0.Mar}}} = 0.032$$

$$x_{\text{totloss.CEB.Mar.14h}} := x_{\text{thermalloss.ENG.Mar.14h}} + x_{\text{shrinkageloss.CEB.Mar.14h}} \dots = 0.041$$
$$+ x_{\text{relaxationloss.14h.Mar}}$$

$$x_{\text{totloss.EC2.Mar.14h}} := x_{\text{thermalloss.EC2.Mar.14h}} + x_{\text{shrinkageloss.EC2.Mar.14h}} \dots = 0.043$$
$$+ x_{\text{relaxationloss.14h.Mar}}$$

Sollenau

Max temperature after 13 hours

$$x_{\text{relaxationloss.10h.Sol}} := \frac{(\Delta P_{\text{m.t.p.r.Sol}})_3 - \Delta P_{\text{m.t.p.r.Sol}}_{13}}{P_{\text{m0.Sol}}} = 5.473 \times 10^{-3}$$

$$x_{\text{shrinkageloss.EC2.Sol.10h}} := \frac{\Delta P_{\text{m.s.EC2.Sol}_3} - \Delta P_{\text{m.s.EC2.Sol}}_{13}}{P_{\text{m0.Sol}}} = 2.665 \times 10^{-3}$$

$$x_{\text{shrinkage loss.CEB.Sol.10hr}} = \frac{\Delta P_{\text{m.s.CEB.Sol}_3} - \Delta P_{\text{m.s.CEB.Sol}_3}}{P_{\text{m0.Sol}}} = 1.501 \times 10^{-4}$$

$$x_{\text{thermal loss.ENG.Sol.10hr}} = \frac{\Delta P_{\text{m.t.ENG.Sol}_3} - \Delta P_{\text{m.t.ENG.Sol}_3}}{P_{\text{m0.Sol}}} = 0.067$$

$$x_{\text{thermal loss.EC2.Sol.10hr}} = \frac{\Delta P_{\text{m.t.EC2.Sol}_3} - \Delta P_{\text{m.t.EC2.Sol}_3}}{P_{\text{m0.Sol}}} = 0.047$$

$$x_{\text{tot loss.CEB.Sol.10hr}} = x_{\text{thermal loss.ENG.Sol.10hr}} + x_{\text{shrinkage loss.CEB.Sol.10hr}} + x_{\text{relaxation loss.10h.Sol}} = 0.072$$

$$x_{\text{tot loss.EC2.Sol.10hr}} = x_{\text{thermal loss.EC2.Sol.10hr}} + x_{\text{shrinkage loss.EC2.Sol.10hr}} + x_{\text{relaxation loss.10h.Sol}} = 0.055$$

SUMMARY

Only take the prestress losses the time until the maximum temperature occurs in the Concrete.

Prestress losses at maximum temperature for the different plants. Hand calculations take not into account for bond, and therefore should these values be more accurate. But the equations takes not into account for the surrounding temperatures on a good way and the semi-adiabatic curves from test are used as indata.

Prestress Loss	Vislanda		Marijampole		Sollenau	
	EC2	CEB-FIP	EC2	CEB-FIP	EC2	CEB-FIP
Before casting	0,38%	-	2,28%	-	0,49%	-
Cast-Release	4,38%	5,52%	4,34%	4,06%	5,48%	7,23%
At release	0,89%	-	2,63%	-	0,98%	-
Total	5,65%	6,79%	9,25%	8,97%	6,95%	8,71%

Only Phase2

Pre. Loss	From casting to max. temperature							
	Relaxation		Shrinkage		Thermal effect		Total	
	EC2	CEB	EC2	CEB	EC2	CEB	EC2	CEB
Vislanda	0,51%	0,28%	0,02%	0,02%	3,59%	4,99%	4,38%	5,52%
Marijampole	0,79%	0,30%	0,02%	0,02%	3,25%	3,25%	4,34%	4,06%
Sollenau	0,55%	0,27%	0,02%	0,02%	4,66%	6,67%	5,48%	7,23%

A.4 FE-verification

Thermal expansion due to constant temperature

1D and 2D Concrete

$$\Delta T := 45 \text{ K}$$

$$\varepsilon_{c,t,FE} := \alpha_{c,te} \cdot \Delta T = 9 \times 10^{-4}$$

$$\varepsilon_{c,t,FE} + \varepsilon_{c,T,FE} = \text{C}$$

$$\varepsilon_{c,T,FE} := -\varepsilon_{c,t,FE} = -9 \times 10^{-4}$$

$$\sigma_{c,t,FE} := \varepsilon_{c,T,FE} E_{c,m,Vis} = -34.2 \text{ MPa}$$

$$A_{c,FE} := B \cdot H = 0.04 \text{ m}^2$$

$$N_{c,FE} := \sigma_{c,t,FE} A_{c,FE} = -1.368 \times 10^3 \text{ kN}$$

Steel

$$\alpha_{s,te} := 12 \cdot 10^{-6} \cdot \frac{1}{\text{K}}$$

$$\varepsilon_{s,t,FE} := \alpha_{s,te} \cdot \Delta T = 5.4 \times 10^{-4}$$

$$\varepsilon_{s,t,FE} + \varepsilon_{s,T,FE} = \text{C}$$

$$\varepsilon_{s,T,FE} := -\varepsilon_{s,t,FE} = -5.4 \times 10^{-4}$$

$$\sigma_{s,t,FE} := \varepsilon_{s,T,FE} E_p = -110.7 \text{ MPa}$$

$$N_{s,FE} := \sigma_{s,t,FE} A_{p,line,total,Vis} = -32.865 \text{ kN}$$

Appendix B Input data files for DIANA

Appendix B includes input data files, DAT-, FGC- and DCF-files, of all the finite element analyses made in this thesis. Some parts of the input data files were reduced, due to for example large amount of coordinates, elements etc. The rows that were taken out were replaced with: "..."

B.1 Verification of thermal properties

B.1.1 Hydration process of the young concrete and heat transfer

DAT-file, materi, was used in all FGC-files in the Appendix B.1.2

:materi

ADIAB 0. 25.0

1.800E+04 2.606E+01

3.600E+04 3.231E+01

5.400E+04 3.992E+01

7.200E+04 4.387E+01

9.000E+04 4.608E+01

1.080E+05 4.740E+01

1.206E+05 4.799E+01

1.512E+05 4.873E+01

1.800E+05 4.898E+01

The nonlinear staggered heat transient analysis running file, DCF-file, below was used in all the FE-analysis in this Chapter.

- **DCF-file**

*FILOS

INITIA

*HEATTR

MODEL MATRIX CAPACI LUMPED

BEGIN INITIA

NONLIN HYDRAT DGRINI 0.01

TEMPER

END INITIA

BEGIN EXECUT

ALPHA 0.67

NONLIN ITERAT MAXITE 100

SIZES 3600(240)

END EXECUT

BEGIN OUTPUT

FILE "Thermal"

REACTI TOTAL INTPNT

TEMPER

END OUTPUT

```

BEGIN OUTPUT
  TABULA
  FILE "Thermal"
  REACTI TOTAL INTPNT
  TEMPER
END OUTPUT
*NONLIN
BEGIN EXECUT
  TIME STEPS EXPLIC SIZES 3600(240)
  BEGIN ITERAT
  BEGIN CONVER
  DISPLA OFF
  ENERGY
  FORCE OFF
  END CONVER
  END ITERAT
END EXECUT
BEGIN OUTPUT
  FILE "Structural"
  TEXT "New Block"
  DISPLA TOTAL TRANSL GLOBAL
  MATURI TOTAL
  STRAIN TEMPER GREEN LOCAL
  STRAIN TOTAL GREEN LOCAL
  STRESS TOTAL CAUCHY LOCAL
END OUTPUT
BEGIN OUTPUT
  TABULA
  FILE "Structural"
  TEXT "New Block"
  DISPLA TOTAL TRANSL GLOBAL
  MATURI TOTAL
  STRAIN TEMPER GREEN LOCAL
  STRAIN TOTAL GREEN LOCAL
  STRESS TOTAL CAUCHY LOCAL
END OUTPUT
*END

```

B.1.1.1 Hydration of the young concrete with adiabatic conditions

- **FGC-file**

```

PROPERTY FE-PROG DIANA HTSTAG_2D
yes
UTILITY SETUP UNITS LENGTH METER
UTILITY SETUP UNITS MASS KILOGRAM
UTILITY SETUP UNITS FORCE NEWTON

```

```

UTILITY SETUP UNITS TIME SECOND
UTILITY SETUP UNITS TEMPERATURE CELSIUS
!!                               block 1
CONSTRUCT SPACE WORK-BOX 10. 0.2 0.
EYE FRAME WORK-BOX
!!                               end block 1
!!                               block 2
GEOMETRY POINT 0.0
GEOMETRY POINT 10.0
GEOMETRY POINT 10.0 0.2
GEOMETRY POINT 0.0 0.2
GEOMETRY SURFACE 4POINTS P1 P2 P3 P4
VIEW GEOMETRY ALL VIOLET
LABEL GEOMETRY POINTS
LABEL GEOMETRY LINES ALL VIOLET
!!picgen utility setup plotter format postscript colour
!!picgen drawing save plotfile geom.ps
!!picgen yes
!!picgen
!!                               end block 2
!!                               block 3
MESHING TYPES ALL QU4 Q8MEM
MESHING DIVISION L1 99
MESHING DIVISION L2 2
MESHING DIVISION L3 99
MESHING DIVISION L4 2
MESHING TYPES L1 BE2 B2HT
MESHING TYPES L2 BE2 B2HT
MESHING TYPES L3 BE2 B2HT
MESHING TYPES L4 BE2 B2HT
MESHING GENERATE
VIEW OPTIONS SHRINK
VIEW MESH
LABEL MESH NODES
LABEL MESH ELEMENTS

```

```

!!picgen drawing save plotfile mesh.ps
!!picgen yes
!!picgen
!!
                                end block 3
!!Thermal Properties
property material ma1 flow isotrop 0.002 2640
property material ma1 external external "materi.dat"
property material ma2 flow boundary convecti 0.001E-200
property material ma3 flow boundary convecti 0.001E-200
property material ma1 therconc isotrop 80E-6
!!Mechanical Properties
property material ma1 elastic isotrop 38000 0.2
PROPERTY PHYSICAL PH1 GEOMETRY PLANSTRS THORTHOT 0.2 0.04
0.04 0.04 0.04
!!
                                block 4
PROPERTY ATTACH S1 MA1
PROPERTY ATTACH S1 PH1
PROPERTY ATTACH L1 MA3
PROPERTY ATTACH L2 MA3
PROPERTY ATTACH L3 MA2
PROPERTY ATTACH L4 MA3
!!
                                end block 4
!!
                                block 5
PROPERTY INITIAL INITEMP ALL 25
LABEL MESH OFF
LABEL MESH INITIAL ALL BLUE
!!picgen drawing save plotfile initem.ps
!!picgen yes
!!picgen
!!
                                end block 5
!!
                                block 6
PROPERTY BOUNDARY MPC RBEAM CO6 L2 P2 X
PROPERTY BOUNDARY MPC RBEAM CO7 L4 P1 X
PROPERTY BOUNDARY CONSTRAINT CO8 P1 X
PROPERTY BOUNDARY CONSTRAINT CO9 P1 Y

```

```

PROPERTY BOUNDARY CONSTRAINT CO10 P2 X
PROPERTY BOUNDARY CONSTRAINT CO11 P2 Y
LABEL MESH OFF
LABEL MESH CONSTRNT
!!picgen drawing save plotfile bcons.ps
!!picgen yes
!!picgen
!!                                     end block 6

```

- **DAT-file**

```

FEMGEN MODEL      : 20X2ADIABATIC
ANALYSIS TYPE     : Heatflow-Stress Staggered 2D
MODEL DESCRIPTION : From archive file
'UNITS'
LENGTH M
TIME SEC
TEMPER CELSIU
FORCE N
'COORDINATES' DI=2

```

1	0.000000E+00	0.000000E+00
2	1.010101E-01	0.000000E+00
3	2.020202E-01	0.000000E+00
...		
98	9.797979E+00	0.000000E+00
99	9.898990E+00	0.000000E+00
100	1.000000E+01	0.000000E+00
101	1.000000E+01	1.000000E-01
102	1.000000E+01	2.000000E-01
103	9.898990E+00	2.000000E-01
...		
199	2.020206E-01	2.000000E-01
200	1.010103E-01	2.000000E-01
201	0.000000E+00	2.000000E-01
202	0.000000E+00	1.000000E-01
203	1.010102E-01	1.000000E-01

: Rows are shortened

204 2.020205E-01 1.000000E-01
...
298 9.696970E+00 1.000000E-01
299 9.797979E+00 1.000000E-01
300 9.898990E+00 1.000000E-01

'ELEMENTS'

CONNECTIVITY

1 B2HT 1 2
2 B2HT 2 3
3 B2HT 3 4

...

200 B2HT 200 201
201 B2HT 201 202
202 B2HT 202 1
203 Q8MEM 1 2 203 202
204 Q8MEM 2 3 204 203
205 Q8MEM 3 4 205 204

...

398 Q8MEM 298 299 104 105
399 Q8MEM 299 300 103 104
400 Q8MEM 300 101 102 103

MATERIALS

/ 203-400 / 1
/ 102-200 / 2
/ 1-101 201 202 / 3

GEOMETRY

/ 203-400 / 1

'MATERIALS'

1 CONDUCT 2.000000E-03
CAPACI 2.640000E+03
YOUNG 3.800000E+04
POISON 2.000000E-01
THERMX 8.000000E-05
ADIAB 0. 25.0
1.800E+04 2.606E+01

```

3.600E+04 3.231E+01
5.400E+04 3.992E+01
7.200E+04 4.387E+01
9.000E+04 4.608E+01
1.080E+05 4.740E+01
1.206E+05 4.799E+01
1.512E+05 4.873E+01
1.800E+05 4.898E+01
2 CONVEC 9.999666E-42
3 CONVEC 9.999666E-42
'GEOMETRY'
1 THICK 2.000000E-01
MEMP 4.000000E-02 4.000000E-02 4.000000E-02
4.000000E-02
'SUPPORTS'
/ 1 100 / TR 1
/ 1 100 / TR 2
'TYINGS'
FIX TR 1
101 100 TR 1 1.0
102 100 TR 1 1.0
FIX TR 1
201 1 TR 1 1.0
202 1 TR 1 1.0
'INIVAR'
TEMPER 1
/ 1-300 / 0.250000E+02
'DIRECTIONS'
1 1.000000E+00 0.000000E+00 0.000000E+00
2 0.000000E+00 1.000000E+00 0.000000E+00
3 0.000000E+00 0.000000E+00 1.000000E+00
'END'

```

B.1.1.2 Hydration of the young concrete with semi-adiabatic conditions with heat flux from all surfaces

- **FGC-file**

```
PROPERTY FE-PROG DIANA HTSTAG_2D
yes
UTILITY SETUP UNITS LENGTH METER
UTILITY SETUP UNITS MASS KILOGRAM
UTILITY SETUP UNITS TIME SECOND
UTILITY SETUP UNITS TEMPERATURE CELSIUS
!!                               block 1
CONSTRUCT SPACE WORK-BOX 10. 0.2 0.
EYE FRAME WORK-BOX
!!                               end block 1
!!                               block 2
GEOMETRY POINT 0.0
GEOMETRY POINT 10.0
GEOMETRY POINT 10.0 0.2
GEOMETRY POINT 0.0 0.2
GEOMETRY SURFACE 4POINTS P1 P2 P3 P4
VIEW GEOMETRY ALL VIOLET
LABEL GEOMETRY POINTS
LABEL GEOMETRY LINES ALL VIOLET
!!picgen utility setup plotter format postscript colour
!!picgen drawing save plotfile geom.ps
!!picgen yes
!!picgen
!!                               end block 2
!!                               block 3
MESHING TYPES ALL QU4 Q8MEM
MESHING DIVISION L1 99
MESHING DIVISION L2 2
MESHING DIVISION L3 99
MESHING DIVISION L4 2
MESHING TYPES L1 BE2 B2HT
MESHING TYPES L2 BE2 B2HT
MESHING TYPES L3 BE2 B2HT
MESHING TYPES L4 BE2 B2HT
MESHING GENERATE
VIEW OPTIONS SHRINK
VIEW MESH
LABEL MESH NODES
LABEL MESH ELEMENTS
!!picgen drawing save plotfile mesh.ps
!!picgen yes
!!picgen
!!                               end block 3
!!Thermal Properties
property material ma1 flow isotrop 0.0024 2640
```

```

property material ma1 external external "materi.dat"
property material ma2 flow boundary convecti 0.002
property material ma3 flow boundary convecti 0.002
property material ma1 therconc isotrop 80E-6
!!Mechanical Properties
property material ma1 elastic isotrop 38000 0.2
PROPERTY PHYSICAL PH1 GEOMETRY PLANSTRS THORTHOT 0.2 0.04
0.04 0.04 0.04
!!                                block 4
PROPERTY ATTACH S1 MA1
PROPERTY ATTACH S1 PH1
PROPERTY ATTACH L1 MA3
PROPERTY ATTACH L2 MA3
PROPERTY ATTACH L3 MA2
PROPERTY ATTACH L4 MA3
!!                                end block 4
!!                                block 5
PROPERTY LOADS EXTTEMP L1 25
CONSTRUCT TCURVE LIST 0.0 1.0 864000 1.0
PROPERTY ATTACH LOADCASE 1 TC1
PROPERTY LOADS EXTTEMP L2 25
CONSTRUCT TCURVE LIST 0.0 1.0 864000 1.0
PROPERTY ATTACH LOADCASE 1 TC1
PROPERTY LOADS EXTTEMP L3 25
CONSTRUCT TCURVE LIST 0.0 1.0 864000 1.0
PROPERTY ATTACH LOADCASE 1 TC1
PROPERTY LOADS EXTTEMP L4 25
CONSTRUCT TCURVE LIST 0.0 1.0 864000 1.0
PROPERTY ATTACH LOADCASE 1 TC1
PROPERTY INITIAL INITEMP ALL 25
LABEL MESH OFF
LABEL MESH INITIAL ALL BLUE
!!picgen drawing save plotfile initem.ps
!!picgen yes
!!picgen
!!                                end block 5
!!                                block 6
PROPERTY BOUNDARY MPC RBEAM CO6 L2 P2 X
PROPERTY BOUNDARY MPC RBEAM CO7 L4 P1 X
PROPERTY BOUNDARY CONSTRAINT CO8 P1 X
PROPERTY BOUNDARY CONSTRAINT CO9 P1 Y
PROPERTY BOUNDARY CONSTRAINT CO10 P2 X
PROPERTY BOUNDARY CONSTRAINT CO11 P2 Y
LABEL MESH OFF
LABEL MESH CONSTRNT
!!picgen drawing save plotfile bcons.ps
!!picgen yes
!!picgen
!!                                end block 6

```

- **DAT-file**

FEMGEN MODEL : 20X2SEMI-ADIABATICAL

ANALYSIS TYPE : Heatflow-Stress Staggered 2D

MODEL DESCRIPTION : From archive file

'UNITS'

MASS KG

LENGTH M

TIME SEC

TEMPER CELSIU

'COORDINATES' DI=2

: Same as Appendix B.1.2.1 above

MATERIALS

/ 203-400 / 1

/ 102-200 / 2

/ 1-101 201 202 / 3

GEOMETRY

/ 203-400 / 1

'MATERIALS'

1 CONDUCT 2.400000E-03

CAPACI 2.640000E+03

YOUNG 3.800000E+04

POISON 2.000000E-01

THERMX 8.000000E-05

ADIAB 0. 25.0

1.800E+04 2.606E+01

3.600E+04 3.231E+01

5.400E+04 3.992E+01

7.200E+04 4.387E+01

9.000E+04 4.608E+01

1.080E+05 4.740E+01

1.206E+05 4.799E+01

1.512E+05 4.873E+01

1.800E+05 4.898E+01

2 CONVEC 2.000000E-03

3 CONVEC 2.000000E-03

```
'GEOMETRY'
  1 THICK  2.000000E-01
    MEMP  4.000000E-02  4.000000E-02  4.000000E-02
      4.000000E-02
```

```
'SUPPORTS'
```

```
/ 1 100 / TR  1
/ 1 100 / TR  2
```

```
'TYINGS'
```

```
FIX TR 1
```

```
  101  100 TR 1 1.0
  102  100 TR 1 1.0
```

```
FIX TR 1
```

```
  201   1 TR 1 1.0
  202   1 TR 1 1.0
```

```
'BOUNDA'
```

```
CASE 1
```

```
ELEMEN
```

```
  1 EXTEMP  0.250000E+02
```

```
...
```

: Rows are shortened

```
202 EXTEMP  0.250000E+02
```

```
'TIMEBO'
```

```
BOUNDA 1
```

```
TIMES 0.000000E+00  0.864000E+06 /
```

```
FACTOR 0.100000E+01  0.100000E+01 /
```

```
'INIVAR'
```

```
TEMPER 1
```

```
/ 1-300 /  0.250000E+02
```

```
'DIRECTIONS'
```

```
  1  1.000000E+00  0.000000E+00  0.000000E+00
  2  0.000000E+00  1.000000E+00  0.000000E+00
  3  0.000000E+00  0.000000E+00  1.000000E+00
```

```
'END'
```

B.1.1.3 Hydration of the young concrete with semi-adiabatic conditions with heat flux from only top surface

: Same FGC- and DAT-file as Appendix B.1.2.3 above except:

- **FGC-file**

property material ma3 flow boundary convecti 0.001e-200

- **DAT-file**

FEMGEN MODEL : 20X2SEMI-ADIABATIC TOP
3 CONVEC 9.999666E-42

B.1.2 Casting of young concrete in sequences

- **FGC-file**

```
PROPERTY FE-PROG DIANA HTSTAG_2D
yes
UTILITY SETUP UNITS LENGTH METER
UTILITY SETUP UNITS MASS KILOGRAM
UTILITY SETUP UNITS TIME SECOND
UTILITY SETUP UNITS TEMPERATURE CELSIUS
!!                               block 1
CONSTRUCT SPACE WORK-BOX 10. 0.2 0.
EYE FRAME WORK-BOX
!!                               end block 1
!!                               block 2
CONSTRUCT SET OPEN G1
GEOMETRY POINT 0.0
GEOMETRY POINT 5.0
GEOMETRY POINT 5.0 0.2
GEOMETRY POINT 0.0 0.2
GEOMETRY SURFACE 4POINTS P1 P2 P3 P4
CONSTRUCT SET CLOSE

CONSTRUCT SET OPEN G2
GEOMETRY POINT 10.0
GEOMETRY POINT 10.0 0.2
GEOMETRY SURFACE 4POINTS P2 P5 P6 P3
CONSTRUCT SET CLOSE

VIEW GEOMETRY ALL VIOLET
LABEL GEOMETRY POINTS
LABEL GEOMETRY LINES ALL VIOLET
!!picgen utility setup plotter format postscript colour
!!picgen drawing save plotfile geom.ps
!!picgen yes
!!picgen
```

```

!!                               end block 2
!!                               block 3
!!GROUP1
MESHING DIVISION L1 99
MESHING DIVISION L2 2
MESHING DIVISION L3 99
MESHING DIVISION L4 2
MESHING TYPES S1 QU4 Q8MEM

!!GROUP2
MESHING DIVISION L5 99
MESHING DIVISION L6 2
MESHING DIVISION L7 99
MESHING TYPES S2 QU4 Q8MEM

!!GROUP1
MESHING TYPES L1 BE2 B2HT
MESHING TYPES L3 BE2 B2HT
MESHING TYPES L4 BE2 B2HT
MESHING TYPES L2 BE2 B2HT

!!GROUP2
MESHING TYPES L5 BE2 B2HT
MESHING TYPES L6 BE2 B2HT
MESHING TYPES L7 BE2 B2HT

MESHING GENERATE
VIEW OPTIONS SHRINK
VIEW MESH
LABEL MESH NODES
LABEL MESH ELEMENTS
!!picgen drawing save plotfile mesh.ps
!!picgen yes
!!picgen
!!                               end block 3
!!                               block 4
!!Thermal Properties
property material ma1 flow isotrop 0.0024 2640
property material ma1 external external "materi.dat"
property material ma2 flow boundary convecti 0.002
property material ma3 flow boundary convecti 0.001e-200
property material ma1 therconc isotrop 80E-6
!!Mechanical Properties
property material ma1 elastic isotrop 38000 0.2
PROPERTY PHYSICAL PH1 GEOMETRY PLANSTRS THORTHOT 0.2 0.04
0.04 0.04 0.04
!!
PROPERTY ATTACH S1 MA1
Property attach S1 PH1
PROPERTY ATTACH S2 MA1

```

```

Property attach S2 PH1
PROPERTY ATTACH L4 MA3
PROPERTY ATTACH L1 MA3
PROPERTY ATTACH L5 MA3
PROPERTY ATTACH L6 MA3
PROPERTY ATTACH L3 MA2
PROPERTY ATTACH L7 MA2
!!                               end block 4
!!                               block 5
PROPERTY INITIAL INITEMP ALL 25.0
LABEL MESH OFF
LABEL MESH INITIAL ALL BLUE
!!picgen drawing save plotfile init em.ps
!!picgen yes
!!picgen
!!                               end block 5
!!                               block 6
PROPERTY BOUNDARY MPC RBEAM CO6 L6 P5 X
PROPERTY BOUNDARY MPC RBEAM CO7 L4 P1 X
PROPERTY BOUNDARY CONSTRAINT CO8 P1 X
PROPERTY BOUNDARY CONSTRAINT CO9 P1 Y
PROPERTY BOUNDARY CONSTRAINT CO10 P5 X
PROPERTY BOUNDARY CONSTRAINT CO11 P5 Y
PROPERTY BOUNDARY CONSTRAINT CO12 P2 Y
LABEL MESH OFF
LABEL MESH CONSTRNT
!!picgen drawing save plotfile bcons.ps
!!picgen yes
!!picgen
!!                               end block 6

```

- **DAT-file**

```

FEMGEN MODEL      : HHYDR2STEP
ANALYSIS TYPE    : Heatflow-Stress Staggered 2D
MODEL DESCRIPTION : From archive file
'UNITS'
MASS   KG
LENGTH M
TIME   SEC
TEMPER CELSIU
'COORDINATES' DI=2
  1   0.000000E+00  0.000000E+00
  2   5.050505E-02  0.000000E+00
  3   1.010101E-01  0.000000E+00

```

: Rows are shortened

```
...
98  4.898990E+00  0.000000E+00
99  4.949495E+00  0.000000E+00
100 5.000000E+00  0.000000E+00
101 5.000000E+00  2.000000E-01
102 4.949495E+00  2.000000E-01
103 4.898990E+00  2.000000E-01
...
198 1.010103E-01  2.000000E-01
199 5.050516E-02  2.000000E-01
200 0.000000E+00  2.000000E-01
201 0.000000E+00  1.000000E-01
202 5.050505E+00  0.000000E+00
203 5.101010E+00  0.000000E+00
204 5.151515E+00  0.000000E+00
...
298 9.898990E+00  0.000000E+00
299 9.949495E+00  0.000000E+00
300 1.000000E+01  0.000000E+00
301 1.000000E+01  1.000000E-01
302 1.000000E+01  2.000000E-01
303 9.949495E+00  2.000000E-01
...
398 5.151515E+00  2.000000E-01
399 5.101010E+00  2.000000E-01
400 5.050505E+00  2.000000E-01
401 5.050512E-02  1.000000E-01
402 1.010102E-01  1.000000E-01
403 1.515150E-01  1.000000E-01
...
595 9.848485E+00  1.000000E-01
596 9.898990E+00  1.000000E-01
597 9.949495E+00  1.000000E-01
```

'ELEMENTS'

CONNECTIVITY

1 B2HT 1 2
 2 B2HT 2 3
 ...
 399 B2HT 399 400
 400 B2HT 400 101
 401 Q8MEM 1 2 401 201
 402 Q8MEM 2 3 402 401
 ...
 498 Q8MEM 98 99 498 497
 499 Q8MEM 99 100 499 498
 500 Q8MEM 201 401 199 200
 501 Q8MEM 401 402 198 199
 597 Q8MEM 497 498 102 103
 598 Q8MEM 498 499 101 102
 ...
 599 Q8MEM 100 202 500 499
 600 Q8MEM 202 203 501 500
 ...
 696 Q8MEM 298 299 597 596
 697 Q8MEM 299 300 301 597
 698 Q8MEM 499 500 400 101
 699 Q8MEM 500 501 399 400
 ...
 795 Q8MEM 596 597 303 304
 796 Q8MEM 597 301 302 303

MATERIALS

/ 401-796 / 1
 / 100-198 302-400 / 2
 / 1-99 199-301 / 3

GEOMETRY

/ 401-796 / 1

'MATERIALS'

1 CONDUCT 2.400000E-03
 CAPACIT 2.640000E+03
 YOUNG 3.800000E+04

```

POISON  2.000000E-01
THERMX  8.000000E-05
ADIAB 0. 25.0
    1.800E+04 2.606E+01
    3.600E+04 3.231E+01
    5.400E+04 3.992E+01
    7.200E+04 4.387E+01
    9.000E+04 4.608E+01
    1.080E+05 4.740E+01
    1.206E+05 4.799E+01
    1.512E+05 4.873E+01
    1.800E+05 4.898E+01
2 CONVEC  2.000000E-03
3 CONVEC  9.999666E-42
'GEOMETRY'
1 THICK  2.000000E-01
  MEMP  4.000000E-02  4.000000E-02  4.000000E-02
    4.000000E-02
'GROUPS'
ELEMEN
  1 G1 / 1-200 401-598 /
NODES
  2 G1_N / 1-201 401-499 /
ELEMEN
  3 G2 / 201-400 599-796 /
NODES
  4 G2_N / 100 101 202-400 499-597 /
'SUPPORTS'
/ 1 300 / TR  1
/ 1 100 300 / TR  2
'TYINGS'
FIX TR 1
  301  300 TR 1 1.0
  302  300 TR 1 1.0
FIX TR 1

```

```

200 1 TR 1 1.0
201 1 TR 1 1.0
'INIVAR'
TEMPER 1
/1-597/ 0.250000E+02
'DIRECTIONS'
1 1.000000E+00 0.000000E+00 0.000000E+00
2 0.000000E+00 1.000000E+00 0.000000E+00
3 0.000000E+00 0.000000E+00 1.000000E+00
'END'

```

- **DAT-file: Bounda1**

```

'BOUNDA'
CASE 1
ELEMEN
1 EXTEMP 25
...
202 EXTEMP 25

'TIMEBO'
BOUNDA 1
TIMES 0.00000E+000 8.64000E+005 /
FACTOR 1.00000E+000 1.00000E+000 /

```

- **DAT-file: Bounda2**

```

'BOUNDA'
CASE 1
ELEMEN
1 EXTEMP 25
...
402 EXTEMP 25

'TIMEBO'
BOUNDA 1
TIMES 0.00000E+000 8.64000E+005 /

```

FACTOR 1.00000E+000 1.00000E+000 /

- **DCF-file**

```
*FILOS
INITIA
*INPUT
BEGIN READ
  APPEND
  FILE "Bounda1.dat"
  BEGIN TABLE
    BOUNDA
    TIMEBO
  END TABLE
END READ
*PHASE
BEGIN ACTIVE
  ELEMEN G1 /
  REINFO
END ACTIVE
*HEATTR
MODEL MATRIX CAPACI LUMPED
BEGIN INITIA
  NONLIN HYDRAT
  TEMPER
END INITIA
BEGIN EXECUT
  ALPHA 0.67
  BEGIN NONLIN
    HYDRAT ITERAT
    ITERAT MAXITE 100
  END NONLIN
  SIZES 1800(2)
END EXECUT
BEGIN OUTPUT
  FILE "Thermal-PHASE1"
  REACTI TOTAL INTPNT
  TEMPER
END OUTPUT
BEGIN OUTPUT
  TABULA
  FILE "Thermal-PHASE1"
  REACTI TOTAL INTPNT
  TEMPER
END OUTPUT
*NONLIN
EXECUT START INITIA STRESS
BEGIN EXECUT
  TIME STEPS EXPLIC SIZES 1800(2)
  BEGIN ITERAT
```

```

BEGIN CONVER
  DISPLA OFF
  ENERGY
  FORCE OFF
END CONVER
END ITERAT
END EXECUT
BEGIN OUTPUT
  FILE "Structural-PHASE1"
  TEXT "New Block"
  DISPLA TOTAL TRANSL GLOBAL
  MATURI TOTAL
  STRAIN TEMPER GREEN LOCAL
  STRAIN TOTAL GREEN LOCAL
  STRESS TOTAL CAUCHY LOCAL
END OUTPUT
BEGIN OUTPUT
  TABULA
  FILE "Structural-PHASE1"
  TEXT "New Block"
  DISPLA TOTAL TRANSL GLOBAL
  MATURI TOTAL
  STRAIN TEMPER GREEN LOCAL
  STRAIN TOTAL GREEN LOCAL
  STRESS TOTAL CAUCHY LOCAL
END OUTPUT
*INPUT
BEGIN DELETE
  BEGIN TABLE
    BOUNDA
    TIMEBO
  END TABLE
END DELETE
BEGIN READ
  APPEND
  FILE "Bounda2.dat"
  BEGIN TABLE
    BOUNDA
    TIMEBO
  END TABLE
END READ
*PHASE
BEGIN ACTIVE
  ELEMEN G1 G2 /
  REINFO
END ACTIVE
*HEATTR
MODEL MATRIX CAPACI LUMPED
BEGIN INITIA
  NONLIN HYDRAT

```

```

TEMPER
TIME0 3600
END INITIA
BEGIN EXECUT
  ALPHA 0.67
  BEGIN NONLIN
    HYDRAT ITERAT
    ITERAT MAXITE 100
  END NONLIN
  SIZES 3600(24)
END EXECUT
BEGIN OUTPUT
  FILE "Thermal-PHASE2"
  REACTI TOTAL INTPNT
  TEMPER
END OUTPUT
BEGIN OUTPUT
  TABULA
  FILE "Thermal-PHASE2"
  REACTI TOTAL INTPNT
  TEMPER
END OUTPUT
*NONLIN
BEGIN EXECUT
  BEGIN START
    INITIA STRESS PHASE
    STEPS EXPLIC
    TIME 3600
  END START
  BEGIN ITERAT
    BEGIN CONVER
      DISPLA OFF
      ENERGY
      FORCE OFF
    END CONVER
  END ITERAT
END EXECUT
BEGIN EXECUT
  TIME STEPS EXPLIC SIZES 3600(24)
  BEGIN ITERAT
    BEGIN CONVER
      DISPLA OFF
      ENERGY
      FORCE OFF
    END CONVER
  END ITERAT
END EXECUT
BEGIN OUTPUT
  FILE "Structural-PHASE2"
  TEXT "New Block"

```

```

DISPLA TOTAL TRANSL GLOBAL
MATURI TOTAL
STRAIN TEMPER GREEN LOCAL
STRAIN TOTAL GREEN LOCAL
STRESS TOTAL CAUCHY LOCAL
END OUTPUT
BEGIN OUTPUT
TABULA
FILE "Structural-PHASE2"
TEXT "New Block"
DISPLA TOTAL TRANSL GLOBAL
MATURI TOTAL
STRAIN TEMPER GREEN LOCAL
STRAIN TOTAL GREEN LOCAL
STRESS TOTAL CAUCHY LOCAL
END OUTPUT
*END

```

B.2 Verification of mechanical properties

B.2.1 Thermal expansion due to constant temperature

The Linear staggered analysis FGC-file below was used in this Appendix B.2.1.

- **FGC-file**

```

*FILOS
INITIA
*LINSTA
BEGIN OUTPUT
FILE "Structural"
DISPLA TOTAL TRANSL GLOBAL
FORCE RESIDU TRANSL GLOBAL
FORCE REACTI TRANSL GLOBAL
STRAIN TOTAL GREEN GLOBAL
STRAIN TOTAL GREEN PRINCI
STRAIN TOTAL GREEN GLOBAL INTPNT
STRESS TOTAL CAUCHY GLOBAL
STRESS TOTAL CAUCHY PRINCI
END OUTPUT
BEGIN OUTPUT
TABULA
FILE "Structural"
DISPLA TOTAL TRANSL GLOBAL
FORCE RESIDU TRANSL GLOBAL
FORCE REACTI TRANSL GLOBAL
STRAIN TOTAL GREEN GLOBAL
STRAIN TOTAL GREEN PRINCI
STRESS TOTAL CAUCHY GLOBAL
STRESS TOTAL CAUCHY PRINCI
END OUTPUT
*END

```

B.2.1.1 Homogenous concrete specimen, 1D

- FGC-file

```
PROPERTY FE-PROG DIANA HTSTAG_2D
yes
UTILITY SETUP UNITS LENGTH METER
UTILITY SETUP UNITS MASS KILOGRAM
UTILITY SETUP UNITS TIME SECOND
UTILITY SETUP UNITS TEMPERATURE CELSIUS
!!                               block 1
CONSTRUCT SPACE WORK-BOX 10. 0.2 0.
EYE FRAME WORK-BOX
!!                               end block 1
!!                               block 2
GEOMETRY POINT 0.0
GEOMETRY POINT 10.0
GEOMETRY LINE STRAIGHT P1 P2
VIEW GEOMETRY ALL VIOLET
LABEL GEOMETRY POINTS
LABEL GEOMETRY LINES ALL VIOLET
!!picgen utility setup plotter format postscript colour
!!picgen drawing save plotfile geom.ps
!!picgen yes
!!picgen
!!                               end block 2
!!                               block 3
MESHING DIVISION L1 20
MESHING TYPES L1 L2TRU
MESHING GENERATE
VIEW OPTIONS SHRINK
VIEW MESH
LABEL MESH NODES
LABEL MESH ELEMENTS
!!picgen drawing save plotfile mesh.ps
!!picgen yes
!!picgen
!!                               end block 3
!!                               block 4
property material ma1 elastic isotrop 38E9 0.2
PROPERTY MATERIAL MA1 THERCONC ISOTROP 80E-6 0
PROPERTY PHYSICAL PH1 GEOMETRY BEAM CLASSI PREDEFIN RECTAN
0.2 0.2
PROPERTY ATTACH L1 MA1
PROPERTY ATTACH L1 PH1
!!                               end block 4
!!                               block 5
PROPERTY LOADS TEMPERAT LO1 1 L1 45 0 0
LABEL MESH OFF
LABEL MESH INITIAL ALL BLUE
```

```

!!picgen drawing save plotfile init em.ps
!!picgen yes
!!picgen
!!                               end block 5
!!                               block 6
PROPERTY BOUNDARY CONSTRAINT CO1 P1 X
PROPERTY BOUNDARY CONSTRAINT CO2 P1 Y
PROPERTY BOUNDARY CONSTRAINT CO3 P2 X
PROPERTY BOUNDARY CONSTRAINT CO4 P2 Y
LABEL MESH OFF
LABEL MESH CONSTRNT
!!picgen drawing save plotfile bcons.ps
!!picgen yes
!!picgen
!!                               end block 6

```

- **DAT-file**

```

FEMGEN MODEL   : CONSTANTTEMP1D
ANALYSIS TYPE  : Heatflow-Stress Staggered 2D
MODEL DESCRIPTION : From archive file

```

'UNITS'

MASS KG

LENGTH M

TIME SEC

TEMPER CELSIU

'COORDINATES' DI=2

```

 1  0.000000E+00  0.000000E+00
 2  5.000000E-01  0.000000E+00
 3  1.000000E+00  0.000000E+00

```

...

: Rows are shortened

```

19  9.000000E+00  0.000000E+00
20  9.500000E+00  0.000000E+00
21  1.000000E+01  0.000000E+00

```

'ELEMENTS'

CONNECTIVITY

1 L2TRU 1 2

2 L2TRU 2 3

3 L2TRU 3 4

...

```

18 L2TRU 18 19
19 L2TRU 19 20
20 L2TRU 20 21
MATERIALS
/ 1-20 / 1
GEOMETRY
/ 1-20 / 1
'MATERIALS'
  1 YOUNG  3.800000E+10
    POISON  2.000000E-01
    THERMX  8.000000E-05
'GEOMETRY'
  1 RECTAN  2.000000E-01  2.000000E-01
'SUPPORTS'
/ 1 21 /  TR  1
/ 1 21 /  TR  2
'LOADS'
CASE 1
ELEMEN
  1 TEMPER  0.450000E+02  0.450000E+02
  ...
  20 TEMPER  0.450000E+02  0.450000E+02
'DIRECTIONS'
  1 1.000000E+00  0.000000E+00  0.000000E+00
  2 0.000000E+00  1.000000E+00  0.000000E+00
  3 0.000000E+00  0.000000E+00  1.000000E+00
'END'

```

B.2.1.2 Homogenous concrete specimen, 2D

- **FGC-file**

```

PROPERTY FE-PROG DIANA HTSTAG_2D
yes
UTILITY SETUP UNITS LENGTH METER
UTILITY SETUP UNITS MASS KILOGRAM
UTILITY SETUP UNITS TIME SECOND
UTILITY SETUP UNITS TEMPERATURE CELSIUS
!!                               block 1

```

```

CONSTRUCT SPACE WORK-BOX 10. 0.2 0.
EYE FRAME WORK-BOX
!!                               end block 1
!!                               block 2
GEOMETRY POINT 0.0
GEOMETRY POINT 10.0
GEOMETRY POINT 10.0 0.2
GEOMETRY POINT 0.0 0.2
GEOMETRY SURFACE 4POINTS P1 P2 P3 P4
VIEW GEOMETRY ALL VIOLET
LABEL GEOMETRY POINTS
LABEL GEOMETRY LINES ALL VIOLET
!!picgen utility setup plotter format postscript colour
!!picgen drawing save plotfile geom.ps
!!picgen yes
!!picgen
!!                               end block 2
!!                               block 3
MESHING DIVISION L1 20
MESHING DIVISION L2 2
MESHING DIVISION L3 20
MESHING DIVISION L4 2
MESHING TYPES ALL QU8 CQ16M
MESHING GENERATE
VIEW OPTIONS SHRINK
VIEW MESH
LABEL MESH NODES
LABEL MESH ELEMENTS
!!picgen drawing save plotfile mesh.ps
!!picgen yes
!!picgen
!!                               end block 3
!!                               block 4
PROPERTY MATERIAL MA1 FLOW ISOTROP 0.0024 0
property material ma1 elastic isotrop 38E9 0.2
PROPERTY MATERIAL MA1 THERCONC ISOTROP 80E-6 0
PROPERTY PHYSICAL PH1 GEOMETRY PLANSTRS THREGULR 0.2
PROPERTY ATTACH S1 MA1
Property attach S1 PH1
!!                               end block 4
!!                               block 5
PROPERTY LOADS TEMPERAT LO1 1 ALL 45 0 0
LABEL MESH OFF
LABEL MESH INITIAL ALL BLUE
!!picgen drawing save plotfile init em.ps
!!picgen yes
!!picgen
!!                               end block 5
!!                               block 6
PROPERTY BOUNDARY MPC RBEAM CO6 L2 P2 X

```

```

PROPERTY BOUNDARY MPC RBEAM CO7 L4 P1 X
PROPERTY BOUNDARY CONSTRAINT CO8 P1 X
PROPERTY BOUNDARY CONSTRAINT CO9 P1 Y
PROPERTY BOUNDARY CONSTRAINT CO10 P2 X
PROPERTY BOUNDARY CONSTRAINT CO11 P2 Y
LABEL MESH OFF
LABEL MESH CONSTRNT
!!picgen drawing save plotfile bcons.ps
!!picgen yes
!!picgen
!!                                     end block 6

```

- **DAT-file**

```

FEMGEN MODEL      : CONSTANTTEMP2D
ANALYSIS TYPE     : Heatflow-Stress Staggered 2D
MODEL DESCRIPTION : From archive file
'UNITS'
MASS   KG
LENGTH M
TIME   SEC
TEMPER CELSIU
'COORDINATES' DI=2
  1  0.000000E+00  0.000000E+00
  2  1.000000E+00  0.000000E+00
  ...
 10  9.000000E+00  0.000000E+00
 11  1.000000E+01  0.000000E+00
 12  0.000000E+00  2.000000E-01
 13  1.000000E+00  2.000000E-01
  ...
 21  9.000000E+00  2.000000E-01
 22  1.000000E+01  2.000000E-01
 23  5.000000E-01  0.000000E+00
 24  1.500000E+00  0.000000E+00
  ...
 31  8.500000E+00  0.000000E+00
 32  9.500000E+00  0.000000E+00
 33  0.000000E+00  1.000000E-01

```

34	1.000000E+00	1.000000E-01
...		
42	9.000000E+00	1.000000E-01
43	1.000000E+01	1.000000E-01
44	5.000000E-01	2.000000E-01
45	1.500000E+00	2.000000E-01
...		
52	8.500000E+00	2.000000E-01
53	9.500000E+00	2.000000E-01

'ELEMENTS'

CONNECTIVITY

1 CQ16M	1 23 2 34 13 44 12 33
2 CQ16M	2 24 3 35 14 45 13 34
3 CQ16M	3 25 4 36 15 46 14 35
4 CQ16M	4 26 5 37 16 47 15 36
5 CQ16M	5 27 6 38 17 48 16 37
6 CQ16M	6 28 7 39 18 49 17 38
7 CQ16M	7 29 8 40 19 50 18 39
8 CQ16M	8 30 9 41 20 51 19 40
9 CQ16M	9 31 10 42 21 52 20 41
10 CQ16M	10 32 11 43 22 53 21 42

MATERIALS

/ 1-10 / 1

GEOMETRY

/ 1-10 / 1

'MATERIALS'

1 CONDUCT	2.400000E-03
YOUNG	3.800000E+10
POISON	2.000000E-01
THERMX	8.000000E-05

'GEOMETRY'

1 THICK	2.000000E-01
---------	--------------

'SUPPORTS'

/ 1 11 / TR	1
/ 1 11 / TR	2

```

'TYINGS'
FIX TR 1
  22  11 TR 1 1.0
  43  11 TR 1 1.0
FIX TR 1
  12   1 TR 1 1.0
  33   1 TR 1 1.0
'LOADS'
CASE 1
ELEMEN
  1 TEMPER  0.450000E+02  0.450000E+02  0.450000E+02  0.450000E+02
    0.450000E+02  0.450000E+02  0.450000E+02  0.450000E+02
...
 10 TEMPER  0.450000E+02  0.450000E+02  0.450000E+02  0.450000E+02
    0.450000E+02  0.450000E+02  0.450000E+02  0.450000E+02
'DIRECTIONS'
  1  1.000000E+00  0.000000E+00  0.000000E+00
  2  0.000000E+00  1.000000E+00  0.000000E+00
  3  0.000000E+00  0.000000E+00  1.000000E+00
'END'

```

B.2.1.3 Steel strands

B.2.1.3.1 Without initial stress

- **FGC-file**

```

PROPERTY FE-PROG DIANA HTSTAG_2D
yes
UTILITY SETUP UNITS LENGTH METER
UTILITY SETUP UNITS MASS KILOGRAM
UTILITY SETUP UNITS TIME SECOND
UTILITY SETUP UNITS TEMPERATURE CELSIUS
!!                               block 1
CONSTRUCT SPACE WORK-BOX 10. 0.2 0.
EYE FRAME WORK-BOX
!!                               end block 1
!!                               block 2
GEOMETRY POINT 0.0
GEOMETRY POINT 10.0
GEOMETRY LINE STRAIGHT P1 P2
VIEW GEOMETRY ALL VIOLET
LABEL GEOMETRY POINTS

```

```

LABEL GEOMETRY LINES ALL VIOLET
!!picgen utility setup plotter format postscript colour
!!picgen drawing save plotfile geom.ps
!!picgen yes
!!picgen
!!                               end block 2
!!                               block 3
MESHING DIVISION L1 20
MESHING TYPES L1 L2TRU
MESHING GENERATE
VIEW OPTIONS SHRINK
VIEW MESH
LABEL MESH NODES
LABEL MESH ELEMENTS
!!picgen drawing save plotfile mesh.ps
!!picgen yes
!!picgen
!!                               end block 3
!!                               block 4
property material ma1 elastic isotrop 205E9 0.3
PROPERTY MATERIAL MA1 THERCONC ISOTROP 12E-6 0
PROPERTY PHYSICAL PH1 GEOMETRY TRUSCABL 8.764E-5
PROPERTY ATTACH L1 MA1
PROPERTY ATTACH L1 PH1
!!                               end block 4
!!                               block 5
PROPERTY LOADS TEMPERAT LO1 1 L1 45 0 0
!!PROPERTY INITIAL INITEMP ALL 0.0
LABEL MESH OFF
LABEL MESH INITIAL ALL BLUE
!!picgen drawing save plotfile init em.ps
!!picgen yes
!!picgen
!!                               end block 5
!!                               block 6
PROPERTY BOUNDARY CONSTRAINT CO1 P1 X
PROPERTY BOUNDARY CONSTRAINT CO2 P1 Y
PROPERTY BOUNDARY CONSTRAINT CO3 P2 X
PROPERTY BOUNDARY CONSTRAINT CO4 P2 Y
LABEL MESH OFF
LABEL MESH CONSTRNT
!!picgen drawing save plotfile bcons.ps
!!picgen yes
!!picgen
!!                               end block 6

```

- **DAT-file**

```

FEMGEN MODEL      : ONLYSTEEL
ANALYSIS TYPE    : Heatflow-Stress Staggered 2D

```

MODEL DESCRIPTION : From archive file

'UNITS'

MASS KG

LENGTH M

TIME SEC

TEMPER CELSIU

'COORDINATES' DI=2

1 0.000000E+00 0.000000E+00

2 5.000000E-01 0.000000E+00

...

20 9.500000E+00 0.000000E+00

21 1.000000E+01 0.000000E+00

: Rows are shortened

'ELEMENTS'

CONNECTIVITY

1 L2TRU 1 2

2 L2TRU 2 3

...

19 L2TRU 19 20

20 L2TRU 20 21

MATERIALS

/ 1-20 / 1

GEOMETRY

/ 1-20 / 1

'MATERIALS'

1 YOUNG 2.050000E+11

POISON 3.000000E-01

THERMX 1.200000E-05

'GEOMETRY'

1 CROSSE 8.764000E-05

'SUPPORTS'

/ 1 21 / TR 1

/ 1 21 / TR 2

'LOADS'

CASE 1

ELEMEN

```

1 TEMPER 0.450000E+02 0.450000E+02
...
20 TEMPER 0.450000E+02 0.450000E+02
'DIRECTIONS'
1 1.000000E+00 0.000000E+00 0.000000E+00
2 0.000000E+00 1.000000E+00 0.000000E+00
3 0.000000E+00 0.000000E+00 1.000000E+00
'END'

```

B.2.1.3.2 With initial stress

: Same DAT-file as Appendix B.2.1.3.1 above, except from

- **DAT-file**

```

'LOADS'
CASE 1
ELEMEN
1 TEMPER 0.450000E+02 0.450000E+02
...
20 TEMPER 0.450000E+02 0.450000E+02
/ 1-20 / PRESTR 1400E6

```

: Rows are shortened

B.2.2 Full interaction between concrete and induced steel strand

B.2.2.1 Constant temperature load

- **FGC-file**

```

PROPERTY FE-PROG DIANA HTSTAG_2D
yes
UTILITY SETUP UNITS LENGTH METER
UTILITY SETUP UNITS FORCE NEWTON
UTILITY SETUP UNITS TIME SECOND
UTILITY SETUP UNITS TEMPERATURE KELVIN
!!                               block 1
CONSTRUCT SPACE WORK-BOX 11. 0.2 0.
EYE FRAME WORK-BOX
!!                               end block 1
!!                               block 2
!!CONCRETE
GEOMETRY POINT 0.0
GEOMETRY POINT 10.0
GEOMETRY POINT 10.0 0.1
GEOMETRY POINT 0.0 0.1

```

GEOMETRY POINT 10.0 0.2
 GEOMETRY POINT 0.0 0.2

 GEOMETRY SURFACE 4POINTS P1 P2 P3 P4
 GEOMETRY SURFACE 4POINTS P4 P3 P5 P6

 !!STEEL ENDS
 GEOMETRY POINT -0.5 0.1
 GEOMETRY POINT 10.5 0.1

 GEOMETRY LINE P7 P4
 GEOMETRY LINE P3 P8

 !!STEEL BETWEEN
 GEOMETRY LINE P4 P3

 !!STEEL
 GEOMETRY POINT 0.0 0.1
 GEOMETRY POINT 10.0 0.1

 !!INTERFACE BOND-SLIP
 GEOMETRY SURFACE 4POINTS P3 P4 P8 P9

 !!INTERFACE HEAT
 GEOMETRY SURFACE 4POINTS P3 P4 P8 P9

 VIEW GEOMETRY ALL VIOLET
 LABEL GEOMETRY POINTS
 LABEL GEOMETRY LINES ALL VIOLET
 !!picgen utility setup plotter format postscript colour
 !!picgen drawing save plotfile geom.ps
 !!picgen yes
 !!picgen
 !! end block 2
 !! block 3
 !!CONCRETE
 MESHING TYPES ALL QU4 Q8MEM
 MESHING DIVISION L1 80
 MESHING DIVISION L2 1
 MESHING DIVISION L3 80
 MESHING DIVISION L4 1
 MESHING DIVISION L5 1
 MESHING DIVISION L6 80
 MESHING DIVISION L7 1

 !!STEEL ENDS
 MESHING DIVISION L8 1
 MESHING DIVISION L9 1

```

!!STEEL
MESHING DIVISION L10 80

!!INTERFACE
MESHING DIVISION L11 1
MESHING DIVISION L12 80
MESHING DIVISION L13 1

!!SURROUNDING CONCRETE
MESHING TYPES L1 BE2 B2HT
MESHING TYPES L2 BE2 B2HT
MESHING TYPES L4 BE2 B2HT
MESHING TYPES L5 BE2 B2HT
MESHING TYPES L6 BE2 B2HT
MESHING TYPES L7 BE2 B2HT

!!STEEL ENDS
MESHING TYPES L8 BE2 L2TRU
MESHING TYPES L9 BE2 L2TRU

!!STEEL BETWEEN
MESHING TYPES L10 BE2 L2TRU

!!INTERFACE BOND-SLIP
MESHING TYPES S3 IL22 L8IF

!!INTERFACE HEAT
MESHING TYPES S4 IL22 IL4HT

MESHING GENERATE
VIEW OPTIONS SHRINK
VIEW MESH
LABEL MESH NODES
LABEL MESH ELEMENTS
!!picgen drawing save plotfile mesh.ps
!!picgen yes
!!picgen
!!                                     end block 3
!!CONCRETE
PROPERTY PHYSICAL PH1 GEOMETRY PLANSTRS THREGULR 0.2
PROPERTY MATERIAL MA1 FLOW ISOTROP 0.0024 2640
PROPERTY MATERIAL MA1 ELASTIC ISOTROP 38E9 0.2
PROPERTY MATERIAL MA1 THERCONC ISOTROP 80E-6
!!PROPERTY MATERIAL MA1 LIBRARY CONCRETE MC1990 REINFORC
C50 NONLIN TIME RS AGING SHRINKAG 0.15 1E-05
!!2500 3.9E+10 3.9E+15 20 80 80 20 0 0

PROPERTY MATERIAL MA2 FLOW BOUNDARY CONVECTI 0.002
PROPERTY MATERIAL MA3 FLOW BOUNDARY CONVECTI 0.001e-200

```

!!INTERFACE BOND-SLIP
PROPERTY PHYSICAL PH2 GEOMETRY INTERFAC LINE BONDSL 0.057
PROPERTY MATERIAL MA4 ELASTIC INTERFAC 785E6 785E6
PROPERTY MATERIAL MA4 STATNONL INTERFAC BONDSLIP DOERR
4.6E3 0.00018

!!INTERFACE HEAT
PROPERTY MATERIAL MA6 FLOW INTERFAC 45

!!STEEL
PROPERTY MATERIAL MA5 FLOW ISOTROP 0.05 3611
PROPERTY MATERIAL MA5 ELASTIC ISOTROP 2.05E+11 0.3
PROPERTY MATERIAL MA5 THERCONC ISOTROP 12E-6
PROPERTY PHYSICAL PH3 GEOMETRY TRUSCABL 2.629E-4
!! block 4

!!CONCRETE
PROPERTY ATTACH S1 MA1
PROPERTY ATTACH S1 PH1
PROPERTY ATTACH S2 MA1
PROPERTY ATTACH S2 PH1
PROPERTY ATTACH L1 MA3
PROPERTY ATTACH L2 MA3
PROPERTY ATTACH L5 MA3
PROPERTY ATTACH L4 MA3
PROPERTY ATTACH L7 MA3
PROPERTY ATTACH L6 MA2

!!INTERFACE BOND-SLIP
PROPERTY ATTACH S3 MA4
PROPERTY ATTACH S3 PH2

!!INTERFACE HEAT
PROPERTY ATTACH S4 MA6

!!STEEL
PROPERTY ATTACH L8 MA5
PROPERTY ATTACH L9 MA5
PROPERTY ATTACH L10 MA5
PROPERTY ATTACH L8 PH3
PROPERTY ATTACH L9 PH3
PROPERTY ATTACH L10 PH3

!! end block 4

!! block 5

PROPERTY LOADS TEMPERAT LO1 1 ALL 45 0 0

LABEL MESH OFF

LABEL MESH INITIAL ALL BLUE

!!picgen drawing save plotfile initem.ps

!!picgen yes

!!picgen

!! end block 5

!! block 6

PROPERTY BOUNDARY CONSTRAINT CO1 L1 Y

```

PROPERTY BOUNDARY CONSTRAINT CO2 P7 X
PROPERTY BOUNDARY CONSTRAINT CO3 P8 X
PROPERTY BOUNDARY CONSTRAINT CO4 P7 Y
PROPERTY BOUNDARY CONSTRAINT CO5 P8 Y
LABEL MESH OFF
LABEL MESH CONSTRNT
!!picgen drawing save plotfile bcons.ps
!!picgen yes
!!picgen
!!                               end block 6

```

- **DAT-file**

```

FEMGEN MODEL      : FULLINTCONSTTEMP
ANALYSIS TYPE    : Heatflow-Stress Staggered 2D
MODEL DESCRIPTION : From archive file
'UNITS'
LENGTH M
TIME SEC
TEMPER KELVIN
FORCE N

```

```
'COORDINATES' DI=2
```

```

 1  0.000000E+00  0.000000E+00
 2  1.250000E-01  0.000000E+00
 3  2.500000E-01  0.000000E+00
...
79  9.750000E+00  0.000000E+00
80  9.875000E+00  0.000000E+00
81  1.000000E+01  0.000000E+00
82  1.000000E+01  1.000000E-01
83  0.000000E+00  1.000000E-01
84  1.000000E+01  2.000000E-01
85  9.875000E+00  2.000000E-01
86  9.750000E+00  2.000000E-01
...
162 2.500000E-01  2.000000E-01
163 1.250000E-01  2.000000E-01
164 0.000000E+00  2.000000E-01
165 -5.000000E-01  1.000000E-01

```

: Rows are shortened

166	1.050000E+01	1.000000E-01
167	1.250000E-01	1.000000E-01
...		
243	9.625000E+00	1.000000E-01
244	9.750000E+00	1.000000E-01
245	9.875000E+00	1.000000E-01
246	1.250000E-01	1.000000E-01
247	2.500000E-01	1.000000E-01
248	3.750000E-01	1.000000E-01
...		
323	9.750000E+00	1.000000E-01
324	9.875000E+00	1.000000E-01
325	0.000000E+00	1.000000E-01
326	1.312494E-01	1.000000E-01
327	2.624998E-01	1.000000E-01
328	3.937502E-01	1.000000E-01
...		
402	1.010625E+01	1.000000E-01
403	1.023750E+01	1.000000E-01
404	1.036875E+01	1.000000E-01

'ELEMENTS'

CONNECTIVITY

1 B2HT 1 2

...

2 B2HT 2 3

245 L2TRU 244 245

246 L2TRU 245 82

247 Q8MEM 1 2 246 83

248 Q8MEM 2 3 247 246

249 Q8MEM 3 4 248 247

...

326 Q8MEM 80 81 82 324

327 Q8MEM 83 246 163 164

328 Q8MEM 246 247 162 163

329 Q8MEM 247 248 161 162

...
 405 Q8MEM 323 324 85 86
 406 Q8MEM 324 82 84 85
 407 L8IF 82 324 325 326
 408 L8IF 324 323 326 327
 409 L8IF 323 322 327 328
 ...
 485 L8IF 247 246 403 404
 486 L8IF 246 83 404 166
 487 IL4HT 82 324 325 326
 488 IL4HT 324 323 326 327
 489 IL4HT 323 322 327 328
 ...
 564 IL4HT 248 247 402 403
 565 IL4HT 247 246 403 404
 566 IL4HT 246 83 404 166

MATERIALS

/ 247-406 / 1
 / 84-163 / 2
 / 1-83 164 / 3
 / 407-486 / 4
 / 487-566 / 5
 / 165-246 / 6

GEOMETRY

/ 247-406 / 1
 / 407-486 / 2
 / 165-246 / 3

'MATERIALS'

1 CONDUCT 2.400000E-03
 CAPACIT 2.640000E+03
 YOUNG 38.000000E+03
 POISON 2.000000E-01
 THERMX 8.000000E-05
 2 CONVEC 2.000000E-03
 3 CONVEC 9.999666E-42

```

4 DSTIF  7.850000E+08  7.850000E+08
  BONDSL 1
  SLPVAL  4.600000E+20  1.800000E-20
5 DFLUX  4.500000E+01
6 CONDUCT  5.000000E-02
  CAPACI  3.611000E+03
  YOUNG  205.0000E+03
  POISON  3.000000E-01
  THERMX  1.200000E-05
'GEOMETRY'
  1 THICK  2.000000E-01
  2 THICK  1.290000E-02
  CONFIG BONDSL
  3 CROSSE  8.764000E-05
'SUPPORTS'
/ 165 166 / TR  1
:/ 286 42 123 / TR  1
/ 1-81 165 166 / TR  2
/ 82-83 167-245 / TR  2
'LOADS'
CASE 1
ELEMEN
  165 TEMPER  0.450000E+02
  247 TEMPER  0.450000E+02  0.450000E+02  0.450000E+02  0.450000E+02
  ...
  406 TEMPER  0.450000E+02  0.450000E+02  0.450000E+02  0.450000E+02
  166 TEMPER  0.450000E+02
'DIRECTIONS'
  1  1.000000E+00  0.000000E+00  0.000000E+00
  2  0.000000E+00  1.000000E+00  0.000000E+00
  3  0.000000E+00  0.000000E+00  1.000000E+00
'END'

```

B.2.2.2 Heat development with semi-adiabatic conditions and heat flux from top surface

- **DCF-file**

```

*FILOS
INITIA
*HEATTR
MODEL MATRIX CAPACI LUMPED
BEGIN INITIA
  NONLIN HYDRAT
  TEMPER
END INITIA
BEGIN EXECUT
  ALPHA 0.67
  BEGIN NONLIN
  HYDRAT ITERAT
  ITERAT MAXITE 100
  END NONLIN
  SIZES 3600(24)
END EXECUT
BEGIN OUTPUT
  FILE "Thermal"
  REACTI TOTAL INTPNT
  TEMPER
END OUTPUT
BEGIN OUTPUT
  TABULA
  FILE "Thermal"
  REACTI TOTAL INTPNT
  TEMPER
END OUTPUT
*NONLIN
EXECUT START INITIA STRESS
BEGIN EXECUT
  TIME STEPS EXPLIC SIZES 3600(24)
  BEGIN ITERAT
  BEGIN CONVER
  DISPLA OFF
  ENERGY
  FORCE OFF
  END CONVER
  END ITERAT
END EXECUT
BEGIN OUTPUT
  FILE "Structural"
  TEXT "New Block"
  DISPLA TOTAL TRANSL GLOBAL
  MATURI TOTAL
  STRAIN TEMPER GREEN LOCAL
  STRAIN TOTAL GREEN LOCAL
  STRESS TOTAL CAUCHY LOCAL
  STRESS TOTAL TRACTI
END OUTPUT

```

```

BEGIN OUTPUT
  TABULA
  FILE "Structural"
  TEXT "New Block"
  DISPLA TOTAL TRANSL GLOBAL
  MATURI TOTAL
  STRAIN TEMPER GREEN LOCAL
  STRAIN TOTAL GREEN LOCAL
  STRESS TOTAL CAUCHY LOCAL
  STRESS TOTAL TRACTI
END OUTPUT
*END

```

- **DAT-file**

```

FEMGEN  MODEL  :  EXTENDED
ANALYSIS TYPE  :  Heatflow-Stress Staggered 2D
MODEL DESCRIPTION  :  From archive file
'UNITS'
LENGTH  M
TIME  SEC
TEMPER  CELSIU
FORCE  N
'COORDINATES'  DI=2
:GROUP  1
  1  0  0
  2  0.1  0
  ...
  100  9.9  0
  101  10  0
  102  0  0.1
  103  0.1  0.1
  104  0.2  0.1
  ...
  201  9.9  0.1
  202  10  0.1
  203  0  0.2
  204  0.1  0.2
  ...

```

: Rows are shortened

```

302  9.9  0.2
303  10   0.2
:Steel Ends
304  -0.5 0.1
305  10.5 0.1
:Steel
306  0    0.1
307  0.1  0.1
...
405  9.9  0.1
406  10   0.1

```

'ELEMENTS'

CONNECTIVITY

```

:Group 1+2
  1  B2HT  1  2
  2  B2HT  2  3
...
100 B2HT 100 101
101 B2HT 101 202
102 B2HT 202 303
103 B2HT 303 302
104 B2HT 302 301
...
202 B2HT 204 203
203 B2HT 203 102
204 B2HT 102  1
:Group 1
400 Q8MEM  1  2 103 102
401 Q8MEM  2  3 104 103
...
598 Q8MEM 200 201 302 301
599 Q8MEM 201 202 303 302

```

1000 L2TRU 304 306
 1001 L2TRU 306 307
 1002 L2TRU 307 308
 ...
 1100 L2TRU 405 406
 1101 L2TRU 406 305

 2000 L8IF 306 307 102 103
 2001 L8IF 307 308 103 104
 ...
 2098 L8IF 404 405 200 201
 2099 L8IF 405 406 201 202

 3000 IL4HT 306 307 102 103
 3001 IL4HT 307 308 103 104
 ...
 3098 IL4HT 404 405 200 201
 3099 IL4HT 405 406 201 202

MATERIALS

/ 400-599 / 1
 / 101-204 / 2
 :/ 4000-4009 / 2
 / 1-100 / 3
 / 2000-2099 / 4
 / 1000-1101 / 5
 / 3000-3099 / 6

GEOMETRY

/ 400-599 / 1
 / 2000-2099 / 2
 / 1000-1101 / 3

'MATERIALS'

1 NAME CONCRETE
 CONDUCT 2.4E-3
 CAPACIT 2.64E+03

YOUNG 3.80E+04
 POISON 2.00E-01
 THERMX 8.00E-05
 ADIAB 0.25.0
 1.800E+04 2.606E+01
 3.600E+04 3.231E+01
 5.400E+04 3.992E+01
 7.200E+04 4.387E+01
 9.000E+04 4.608E+01
 1.080E+05 4.740E+01
 1.206E+05 4.799E+01
 1.512E+05 4.873E+01
 1.800E+05 4.898E+01
 2 NAME AIR
 CONVEC 2E-03
 3 NAME FORM
 CONVEC 3.60E-06
 4 NAME INTERFACE
 DSTIF 785E5 785E5
 5 NAME PRESTRESSEDSTEEL
 CONDUCT 0.05
 CAPACI 3611
 YOUNG 2.05E+05
 POISON 3.00E-01
 THERMX 2.00E-05
 6 NAME HEATINTERFACE
 DFLUX 2
 'GEOMET'
 1 NAME CONCRETE
 THICK 2.00E-01
 2 NAME INTERFACE
 THICK 0.129
 CONFIG BONDSL
 3 NAME STEEL
 CROSSE 0.00008764

```

'LOADS'
CASE 1
ELEMEN
/1000-1101/PRESTR 1.40E+03
'BOUNDA'
CASE 1
ELEMEN
  1000 EXTEMP 25
  1 EXTEMP 25
  ...
  204 EXTEMP 25
  1101 EXTEMP 25
'TIMEBO'
BOUNDA 1
TIMES 0.000000E+00 0.864000E+06 /
FACTOR 0.100000E+01 0.100000E+01 /
'SUPPORTS'
/ 304 305 / TR 1
/ 304 305 1-101 / TR 2
:/ 304-406 1-101 / TR 2
'INIVAR'
TEMPER 1
/ 1-303 / 25
/ 304-406 / 25
'DIRECTIONS'
  1 1.00E+00 0.00E+00 0.00E+00
  2 0.00E+00 1.00E+00 0.00E+00
  3 0.00E+00 0.00E+00 1.00E+00
'END'

```

B.2.3 Shrinkage of young concrete

- **DAT-file**

```

FEMGEN MODEL : CONSTANTTEMP2D
ANALYSIS TYPE : Heatflow-Stress Staggered 2D

```

MODEL DESCRIPTION : From archive file

'UNITS'

MASS KG

LENGTH M

TIME SEC

TEMPER CELSIU

'COORDINATES' DI=2

1 0.000000E+00 0.000000E+00

2 1.000000E+00 0.000000E+00

...

: Rows are shortened

10 9.000000E+00 0.000000E+00

11 1.000000E+01 0.000000E+00

12 0.000000E+00 2.000000E-01

13 1.000000E+00 2.000000E-01

...

21 9.000000E+00 2.000000E-01

22 1.000000E+01 2.000000E-01

23 0.000000E+00 1.000000E-01

24 1.000000E+00 1.000000E-01

...

32 9.000000E+00 1.000000E-01

33 1.000000E+01 1.000000E-01

'ELEMENTS'

CONNECTIVITY

1 Q8MEM 1 2 24 23

2 Q8MEM 2 3 25 24

...

19 Q8MEM 31 32 21 20

20 Q8MEM 32 33 22 21

21 B2HT 1 2

22 B2HT 2 3

...

43 B2HT 12 23

44 B2HT 23 1

MATERIALS

/ 1-20 / 1
 / 21-44 / 2
 GEOMETRY
 / 1-20 / 1
 'INIVAR'
 TEMPER 1
 / 1-20 / 0
 'MATERIALS'
 1 CONDUCT 1.000000E-02
 CAPACI 2640
 YOUNG 3.800000E+10
 POISON 2.000000E-01
 THERMX 1.000000E-20
 SHRINN MC1990
 FCM28 73
 H 100
 CEMTYP RS
 RH 50
 CURAGE 0
 2 CONVEC 1E-40
 'GEOMETRY'
 1 THICK 2.000000E-01
 'SUPPORTS'
 / 1 11 / TR 1
 / 1 11 / TR 2
 'BOUNDA'
 CASE 1
 ELEMEN
 21 EXTEMP 0.450000E+02
 ...
 44 EXTEMP 0.450000E+02
 'TIMEBO'
 BOUNDA 1
 TIMES 0.000000E+00 0.864000E+06 /
 FACTOR 0.100000E+01 0.100000E+01 /

```

'TYINGS'
FIX TR 1
  22  11 TR 1 1.0
  33  11 TR 1 1.0
FIX TR 1
  12   1 TR 1 1.0
  23   1 TR 1 1.0
'DIRECTIONS'
  1  1.000000E+00  0.000000E+00  0.000000E+00
  2  0.000000E+00  1.000000E+00  0.000000E+00
  3  0.000000E+00  0.000000E+00  1.000000E+00
'END'

```

- **DCF-file**

```

*FILOS
INITIA
*HEATTR
BEGIN INITIA
  NONLIN HYDRAT DGRINI 0.01
  TEMPER
END INITIA
EXECUT SIZES 3600(24)
BEGIN OUTPUT
  FILE "ThermalCube-24h"
  TEMPER
END OUTPUT
BEGIN OUTPUT
  TABULA
  FILE "ThermalCube-24h"
  TEMPER
END OUTPUT
*NONLIN
EXECUT TIME STEPS EXPLIC SIZES 3600(24)
BEGIN OUTPUT
  FILE "StructuralCube-24h"
  DISPLA TOTAL TRANSL GLOBAL
  FORCE RESIDU TRANSL GLOBAL
  FORCE REACTI TRANSL GLOBAL
  STRAIN TOTAL GREEN GLOBAL
  STRAIN TOTAL GREEN PRINCI
  STRESS TOTAL CAUCHY GLOBAL
  STRESS TOTAL CAUCHY PRINCI
END OUTPUT
BEGIN OUTPUT

```

```

TABULA
FILE "StructuralCube-24h"
DISPLA TOTAL TRANSL GLOBAL
FORCE RESIDU TRANSL GLOBAL
FORCE REACTI TRANSL GLOBAL
STRAIN TOTAL GREEN GLOBAL
STRAIN TOTAL GREEN PRINCI
STRESS TOTAL CAUCHY GLOBAL
STRESS TOTAL CAUCHY PRINCI
END OUTPUT
*END

```

B.2.4 Development of Young's modulus of elasticity

- **DAT-file**

```

FEMGEN MODEL      : 20X2
ANALYSIS TYPE    : Heatflow-Stress Staggered 2D
MODEL DESCRIPTION : From archive file
'DIRECTIONS'
  1 1.00000E+000 0.00000E+000 0.00000E+000
  2 0.00000E+000 1.00000E+000 0.00000E+000
  3 0.00000E+000 0.00000E+000 1.00000E+000
'COORDINATES'
  1 0 0 0
  2 0.05 0 0
  3 0.05 0.05 0
  4 0 0.05 0
'MATERI'
  1 NAME CONCRETE
    POWER 0.1 0 0 0
    CONDUCT 2E-3
    CAPACI 2.64000E+003
    YOUNG 38E3
    POISON 2.00000E-001
    EQUAGE ARRTYP
    TEMREF 25
    ARRHEN 6000
    ADIAB 0.25.0

```

1.800E+04 2.606E+01
3.600E+04 3.231E+01
5.400E+04 3.992E+01
7.200E+04 4.387E+01
9.000E+04 4.608E+01
1.080E+05 4.740E+01
1.206E+05 4.799E+01
1.512E+05 4.873E+01
1.800E+05 4.898E+01
2419200 49

: SEC AND CELSIUS

: CEB-FIP MC 1990 CASE

:9.4.3

YOUHAR MC1990
YOUN28 38E3
CEMTYP RS

2 NAME AIR

CONVEC 9.999666E-42

'GEOMET'

1 NAME CONCRETE

THICK 0.05

'ELEMENTS'

CONNECT

1 Q8MEM 1 2 3 4

2 B2HT 1 2

3 B2HT 2 3

4 B2HT 3 4

5 B2HT 4 1

MATERI

/ 1 / 1

/ 2-5 / 2

GEOMET

/ 1 / 1

'BOUNDA'
CASE 1
ELEMEN
2 EXTEMP 25
...
5 EXTEMP 25
'TIMEBO'
BOUND A 1
TIMES 0.00000E+000 2419200 /
FACTOR 1.00000E+000 1.00000E+000 /
'LOADS'
CASE 2
NODAL
3 FORCE 2 -100
4 FORCE 2 -100
'TIMELO'
LOAD 2
TIMES 0.00000E+000 2419200 /
FACTOR 0.00000E+000 0.00000E+000 /
'SUPPOR'
/ 2-3 / TR 1
/ 1-2 / TR 2
'INIVAR'
TEMPER 1
/ 1-4 / 25
'UNITS'
LENGTH M
TIME SEC
TEMPER CELSIUS
FORCE N
'END'

- **DCF-file: For 1/10/24h**

*FILOS
INITIA

```

*HEATTR
BEGIN INITIA
  NONLIN HYDRAT DGRINI 0.01
  TEMPER
  EQUAGE
END INITIA
EXECUT SIZES 3600(1/10/24)
BEGIN OUTPUT
  FILE "ThermalCube-1h/10h/24h"
  REACTI TOTAL INTPNT
  TEMPER
  EQUAGE
END OUTPUT
BEGIN OUTPUT
  TABULA
  FILE "ThermalCube-1h/10h/24h "
  REACTI
  TEMPER
  EQUAGE
END OUTPUT

*NONLIN
EXECUT TIME STEPS EXPLIC SIZES 3600(1/10/24)
BEGIN EXECUT
  LOAD STEPS EXPLIC SIZES 0.1(10)
  BEGIN ITERAT
    BEGIN CONVER
      ENERGY CONTIN TOLCON=0.001
      FORCE CONTIN TOLCON=0.01
      DISPLA CONTIN TOLCON=0.01
    END CONVER
  END ITERAT
END EXECUT
BEGIN OUTPUT
  FILE "StructuralCube-1h/10h/24h "
  DISPLA TOTAL TRANSL GLOBAL
  FORCE EXTERN TRANSL GLOBAL
END OUTPUT
BEGIN OUTPUT
  TABULA
  FILE "StructuralCube-1h/10h/24h "
  LAYOUT COMBIN
  DISPLA TOTAL TRANSL GLOBAL
  FORCE EXTERN TRANSL GLOBAL
END OUTPUT
*END

```

B.2.5 Bond-slip behaviour between concrete and induced steel strand

B.2.5.1 Bond-slip with prescribed curve

- **DCF-file**

```
*FILOS
INITIA
*NONLIN
TYPE PHYSIC
BEGIN EXECUT
LOAD STEPS EXPLIC SIZES 0.1(10)
BEGIN ITERAT
METHOD SECANT BFGS
MAXITE=25
BEGIN CONVER
ENERGY CONTIN TOLCON=0.001
FORCE CONTIN TOLCON=0.01
DISPLA CONTIN TOLCON=0.01
END CONVER
END ITERAT
END EXECUT
BEGIN OUTPUT
FILE "Structural"
DISPLA TOTAL TRANSL GLOBAL
STRESS TOTAL TRACTI LOCAL
END OUTPUT
BEGIN OUTPUT
TABULA
FILE "Structural"
DISPLA TOTAL TRANSL GLOBAL
STRESS TOTAL TRACTI LOCAL
END OUTPUT
*END
```

- **DAT-file**

```
FEMGEN MODEL : 20X2
ANALYSIS TYPE : Heatflow-Stress Staggered 2D
MODEL DESCRIPTION : From archive file
'DIRECTIONS'
1 1.00000E+000 0.00000E+000 0.00000E+000
2 0.00000E+000 1.00000E+000 0.00000E+000
3 0.00000E+000 0.00000E+000 1.00000E+000
'COORDINATES'
1 0 0 0
2 0.05 0 0
```

3 0.05 0.025 0
4 0.05 0.05 0
5 0 0.05 0
6 0 0.025 0
1001 0 0.025 0
1002 0.05 0.025 0

'MATERI'

1 NAME CONCRETE
YOUNG 38E9
POISON 2.0000E-001
2 NAME INTERFACE
DSTIF 0 0
BONDSL 3
SLPVAL 0 0

9.969583537 0.0000001
2.703615875 0.0000007
741.7989731 0.0000194
1045.229162 0.0000282
1092.908555 0.0000302
1193.815385 0.0000314
1454.122901 0.0000339
1995.268515 0.0000415
2443.477335 0.0000472
2667.595826 0.0000534
3209.05123 0.000057
3864.255639 0.000063
4493.409584 0.00007
5462.486899 0.0000798
6240.058089 0.0000866
7418.947261 0.0000972
8358.735404 0.0001054
9797.002724 0.0001174
10877.32257 0.0001274
12264.89709 0.0001525
13145.82526 0.000178

14212.62703 0.0002273
14957.81115 0.0002632
16077.84035 0.0003132
16853.44016 0.00035
17874.90003 0.0004052
18565.73021 0.0004481
19436.51982 0.000512
20027.37254 0.0005588
20869.15461 0.0006249
21433.81605 0.0006736
22175.90228 0.0007437
22714.09082 0.0007951
23348.03242 0.0008691
23794.97391 0.0009232
24392.30405 0.0009983
24810.80125 0.0010539
25388.13589 0.0011321
26263.99479 0.0012709
26576.60037 0.0013301
27038.46808 0.0014128
27300.38087 0.0014734
27604.53766 0.0015603
27860.81791 0.0016231
28201.58616 0.0017104
28694.43281 0.0018642
28857.77627 0.0019296
29108.42399 0.0020215

3 NAME STEEL

YOUNG 2.05000E+011

POISON 3.00000E-001

'GEOMET'

1 NAME CONCRETE

THICK 0.05

2 NAME INTERFACE

```

THICK 0.129
CONFIG BONDSL
3 NAME STEEL
CROSSE 8.76400E-004
'ELEMENTS'
CONNECT
1 Q8MEM 1 2 3 6
2 Q8MEM 6 3 4 5
100 L8IF 1001 1002 6 3
200 L2TRU 1001 1002
MATERI
/ 1-2 / 1
/ 100 / 2
/ 200 / 3
GEOMET
/ 1-2 / 1
/ 100 / 2
/ 200 / 3
'LOADS'
CASE 1
DEFORM
/ 1001 1002 / TR 1 0.0020215
'SUPPOR'
/ 1-6 1001 1002 / TR 1
/ 1-6 1001 1002 / TR 2
'UNITS'
LENGTH M
TIME SEC
FORCE N
'END'

```

B.2.5.2 Bond-slip with cubic-function

- **DCF-file**

*FILOS

```

INITIA
*NONLIN
TYPE PHYSIC
BEGIN EXECUT
LOAD STEPS EXPLIC SIZES 0.025(40)
BEGIN ITERAT
METHOD SECANT BFGS
MAXITE=25
BEGIN CONVER
ENERGY CONTIN TOLCON=0.001
FORCE CONTIN TOLCON=0.01
DISPLA CONTIN TOLCON=0.01
END CONVER
END ITERAT
END EXECUT
BEGIN OUTPUT
FILE "Structural"
DISPLA TOTAL TRANSL GLOBAL
STRESS TOTAL TRACTI LOCAL
END OUTPUT
BEGIN OUTPUT
TABULA
FILE "Structural"
DISPLA TOTAL TRANSL GLOBAL
STRESS TOTAL TRACTI LOCAL
END OUTPUT
*END

```

- **DAT-file**

```

FEMGEN MODEL      : 20X2
ANALYSIS TYPE     : Heatflow-Stress Staggered 2D
MODEL DESCRIPTION : From archive file
'DIRECTIONS'
  1 1.00000E+000 0.00000E+000 0.00000E+000
  2 0.00000E+000 1.00000E+000 0.00000E+000
  3 0.00000E+000 0.00000E+000 1.00000E+000
'COORDINATES'
  1 0 0 0
  2 0.05 0 0
  3 0.05 0.025 0
  4 0.05 0.05 0
  5 0 0.05 0
  6 0 0.025 0

```

1001 0 0.025 0
 1002 0.05 0.025 0
 'MATERI'
 1 NAME CONCRETE
 CONDUCT 2E-3
 CAPACI 2.64000E+003
 YOUNG 38E3
 POISON 2.00000E-001
 : THERMX 8.00000E-005
 EQUAGE ARRTYP
 TEMREF 25
 ARRHEN 6000
 ADIAB 0. 25.0
 1.800E+04 2.606E+01
 3.600E+04 3.231E+01
 5.400E+04 3.992E+01
 7.200E+04 4.387E+01
 9.000E+04 4.608E+01
 1.080E+05 4.740E+01
 1.206E+05 4.799E+01
 1.512E+05 4.873E+01
 1.800E+05 4.898E+01
 2 NAME INTERFACE
 DSTIF 0 0
 BONDSL 1
 SLPVAL 5.5E6 0.0025
 3 NAME STEEL
 CAPACI 2.00000E+003
 YOUNG 2.05000E+05
 POISON 3.00000E-001
 'GEOMET'
 1 NAME CONCRETE
 THICK 0.05
 2 NAME INTERFACE
 THICK 0.129

CONFIG BONDSL
3 NAME STEEL
CROSSE 8.76400E-004
'ELEMENTS'
CONNECT
1 Q8MEM 1 2 3 6
2 Q8MEM 6 3 4 5
100 L8IF 1001 1002 6 3
200 L2TRU 1001 1002
MATERI
/ 1-2 / 1
/ 100 / 2
/ 200 / 3
GEOMET
/ 1-2 / 1
/ 100 / 2
/ 200 / 3
'INIVAR'
TEMPER 1
/ 1-6 / 25
/ 1001-1002 / 25
'LOADS'
CASE 1
DEFORM
/ 1001 1002 / TR 1 0.01
'SUPPOR'
/ 1-6 1001 1002 / TR 1
/ 1-6 1001 1002 / TR 2
'UNITS'
LENGTH M
TIME SEC
TEMPER CELSIUS
FORCE N
'END'

B.2.5.3 Bond-slip with cubic-function and maturity dependence

- DCF-file: for 1/7/12/18/24h.

```
*FILOS
INITIA
*INPUT
READ FILE "/beda/users/home/simonc/CubeBondSlipMaturity.dat"
*FORTRAN
TAKE "usrifc.f"
*HEATTR
BEGIN INITIA
  BEGIN NONLIN
  EQUAGE
  HYDRAT DGRINI=0.01
  END NONLIN
  TEMPER
END INITIA
BEGIN EXECUT
  ALPHA 0.67
  BEGIN NONLIN
  HYDRAT ITERAT
  ITERAT MAXITE 100
  END NONLIN
  SIZES 3600(1/7/12/18/24)
END EXECUT
BEGIN OUTPUT
  FILE "Thermal-1h1h/7h/12h/18h/24h"
  EQUAGE
  TEMPER
END OUTPUT
BEGIN OUTPUT
  TABULA
  FILE "Thermal-1h/7h/12h/18h/24h"
  EQUAGE
  TEMPER
END OUTPUT
*NONLIN
EXECUT TIME STEPS EXPLIC SIZES 3600(1/7/12/18/24)
BEGIN EXECUT
  LOAD STEPS EXPLIC SIZES 0.0125(80)
  BEGIN ITERAT
  BEGIN CONVER
  ENERGY CONTIN TOLCON=0.001
  FORCE CONTIN TOLCON=0.01
  DISPLA CONTIN TOLCON=0.01
  END CONVER
  END ITERAT
END EXECUT
BEGIN OUTPUT
```

```

FILE "Structural-1h/7h/12h/18h/24h"
DISPLA TOTAL TRANSL GLOBAL
STRESS TOTAL TRACTI LOCAL
END OUTPUT
BEGIN OUTPUT
TABULA
FILE "Structural-1h/7h/12h/18h/24h"
DISPLA TOTAL TRANSL GLOBAL
STRESS TOTAL TRACTI LOCAL
END OUTPUT
*END

```

- **DAT-file**

```

FEMGEN MODEL      : 20X2
ANALYSIS TYPE    : Heatflow-Stress Staggered 2D
MODEL DESCRIPTION : From archive file
'DIRECTIONS'
  1 1.0000E+000 0.00000E+000 0.00000E+000
  2 0.00000E+000 1.00000E+000 0.00000E+000
  3 0.00000E+000 0.00000E+000 1.00000E+000
'COORDINATES'
  1 0 0 0
  2 0.05 0 0
  3 0.05 0.025 0
  4 0.05 0.05 0
  5 0 0.05 0
  6 0 0.025 0
1001 0 0.025 0
1002 0.05 0.025 0
'MATERI'
  1 NAME  CONCRETE
    CONDUCT 2E-3
    CAPACI 2.64000E+003
    YOUNG  38E3
    POISON 2.00000E-001
:  THERMX 8.00000E-005
    EQUAGE ARRTYP
    TEMREF 25

```

```

ARRHEN 6000
ADIAB 0. 25.0
    1.800E+04 2.606E+01
    3.600E+04 3.231E+01
    5.400E+04 3.992E+01
    7.200E+04 4.387E+01
    9.000E+04 4.608E+01
    1.080E+05 4.740E+01
    1.206E+05 4.799E+01
    1.512E+05 4.873E+01
    1.800E+05 4.898E+01
2 NAME INTERFACE
    DSTIF 10E10 10E10

    CAPACI 2.00000E+003
    CONDUCT 2E-3
    DFLUX 0.00001E-20
    USRIFC BAGE
    USRVAL 2E-3 5.5E6 201345.66 30347.29
    USRSTA 0
3 NAME STEEL
    CAPACI 2.00000E+003
    YOUNG 2.05000E+05
    POISON 3.00000E-001
4 NAME BOUNDARY
    CONVEC 9.999666E-42
'GEOMET'
1 NAME CONCRETE
    THICK 0.05
2 NAME INTERFACE
    THICK 0.129
    CONFIG BONDSL
3 NAME STEEL
    CROSSE 8.764000E-005
'ELEMENTS'

```

CONNECT

1 Q8MEM 1 2 3 6

2 Q8MEM 6 3 4 5

3 B2HT 1 2

4 B2HT 2 4

5 B2HT 4 5

6 B2HT 5 1

100 L8IF 1001 1002 6 3

200 L2TRU 1001 1002

MATERI

/ 1-2 / 1

/ 100 / 2

/ 200 / 3

/ 3-6 / 4

GEOMET

/ 1-2 / 1

/ 100 / 2

/ 200 / 3

'BOUNDA'

CASE 1

ELEMEN

3 EXTEMP 0.250000E+02

...

6 EXTEMP 0.250000E+02

'TIMEBO'

BOUNDA 1

TIMES 0.000000E+00 0.864000E+06 /

FACTOR 0.100000E+01 0.100000E+01 /

'INIVAR'

TEMPER 1

/ 1-6 / 25

/ 1001-1002 / 25

'LOADS'

CASE 2

DEFORM

```

/ 1001 1002 / TR 1 0.01
'TIMELO'
LOAD 2
TIMES 0.00000E+000 2419200 /
FACTOR 0.00000E+000 0.00000E+000 /
'SUPPOR'
/ 1-6 1001 1002 / TR 1
/ 1-6 1001 1002 / TR 2
'UNITS'
LENGTH M
TIME SEC
TEMPER CELSIUS
FORCE N
'END'

```

- **Subroutine code**

A Subroutine code was made to take into account for bond-slip with maturity dependence. Cubic-function was used to characteristic the bond-slip development until the maximum bond ($1,9 \cdot \text{tensile strength}$) occurs, then was the bond constant. The tensile strength during equivalent time was assumed to vary in three different phases:

- Phase 1: From casting until the bond starts to develop, which was assumed occurs at 7 hours after casting in Vislanda and Marijampolé factories, and at 4 h Sollenau factory. The tensile strength, f_t , was assumed to be very small, almost constant zero.
- Phase 2: From bond starts until the maximum tensile strength had reached. The increase of the tensile strength was assumed vary linearly between when the bond started, $t_{eq.start}$, and maximum tensile strength, $t_{eq.max}$.
- Phase 3: After the maximum tensile strength had occurred. The tensile strength was assumed to be constant, see Figure B.2.

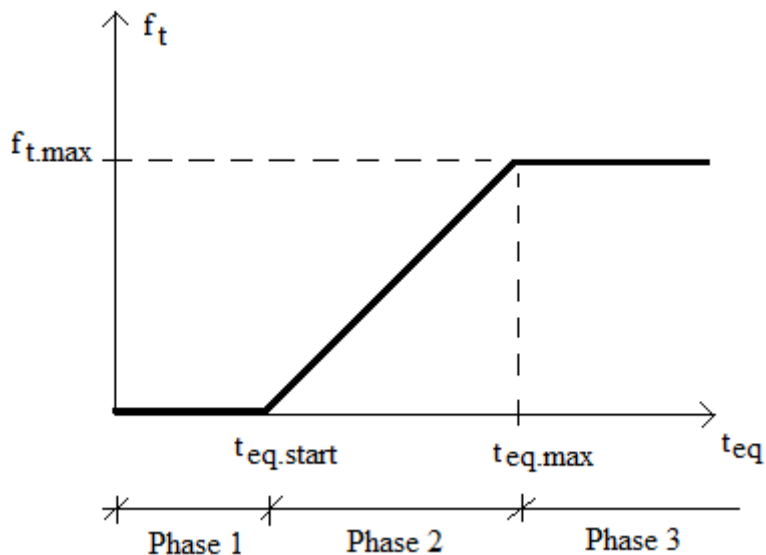


Figure B.2 Tensile strength depending on equivalent time in different phases.

*** Subroutine that varies bond depending on element age

```

SUBROUTINE USRIFC( U0, DU, NT, AGE0, DTIME, TEMP0, DTEMP,
$   ELEMEN, INTPT, COORD, SE, ITER, USRMOD, USRVAL, NUV,
$   USRSTA, NUS, USRIND, NUI, TRA, STIFF )

INTEGER  NUI, NT, NUV, USRIND(NUI),ELEMEN, INTPT, ITER, NUS,
$   TE
CHARACTER*6 USRMOD
DOUBLE PRECISION  U0(NT), DU(NT), AGE0, DTIME, TEMP0, DTEMP,
$   COORD(3), TRA(NT), STIFF(NT,NT), SE(NT,NT),
$   USRVAL(NUV), USRSTA(NUS), DSTIF(2), SL, TT, TTMAX

IF (USRMOD .NE. 'BAGE') THEN
  PRINT *, 'No model chosen in the inputfile'
  CALL PRGERR ('USRIFC', 1)
ENDIF
IF (NT .NE. 2 ) THEN
  PRINT *, 'Model can only be used in line interface element'
  CALL PRGERR ('USRIFC', 2)
ENDIF

CALL GTC( './MATERI/DSTIF', DSTIF, 2 )
STIFF(1,1)= DSTIF(1)
STIFF(2,1)= 0.0
STIFF(1,2)= 0.0

TRA(1) = TRA(1)+STIFF(1,1)*DU(1)+ STIFF(1,2)*DU(2)

SL = ABS(U0(2)+DU(2))
IF (U0(2)+DU(2) .EQ. 0 )THEN

```

```

TE = 1
ELSE
TE = SL/(U0(2)+DU(2))
ENDIF

```

: Calculating the equivalent time according to

```

$      USRSTA(1) = USRSTA(1) +
      EXP(6000*(1/298.15-1/(TEMP0+DTEMP+273.15)))*DTIME

```

: Check if interval is; on the plateau (phase 3, after linearly increase of tensile strength), before the linearly increase (phase 1) or at the linearly decrease of the tensile strength (phase 2).

```

IF (USRSTA(1) .GE. USRVAL(3)) THEN
  TTMAX = USRVAL(2)
ELSEIF (USRSTA(1) .LE. USRVAL(4)) THEN
  TTMAX = 0.1E5
ELSE
  TTMAX = (USRVAL(2)*USRSTA(1)/(USRVAL(3)-USRVAL(4))) -
976091.6
ENDIF

```

: Linearly increase of the tensile strength from almost zero until the maximum value (plateau).

```

IF (SL .LE. USRVAL(1)) THEN
  TT = TTMAX*(5*(SL/USRVAL(1))-4.5*(SL/USRVAL(1))**2+
$      1.4*(SL/USRVAL(1))**3)
  TRA(2) = TE*TT
  STIFF(2,2)= TT/SL

ELSE
  STIFF(2,2)= 0.0
  TRA(2) = 1.9*TE*TTMAX
ENDIF
CALL PRIVAL(USRSTA(1), 'USRSTA(1)')
CALL PRIVAL(TTMAX, 'TTMAX')
CALL PRIVAL(TEMP0, 'TEMP0')
CALL PRIVAL(DTEMP, 'DTEMP')
CALL PRIVAL(AGE0, 'AGE0')
CALL PRIVAL(DTIME, 'DTIME')

END

```

B.2.6 Verification of the relationship between all parameters

Same nonlinear transient heat staggered analysis, DCF-file, as Appendix B.3.1.2

- **DAT-file**

FEMGEN MODEL : 10metersallparameters
 ANALYSIS TYPE : Heatflow-Stress Staggered 2D
 MODEL DESCRIPTION : From archive file

'UNITS'

LENGTH M

TIME SEC

TEMPER CELSIU

FORCE N

'COORDINATES' DI=2

:GROUP 1

1 0 0

2 0.1 0

...

100 9.9 0

101 10 0

102 0 0.1

103 0.1 0.1

104 0.2 0.1

...

201 9.9 0.1

202 10 0.1

203 0 0.2

204 0.1 0.2

...

302 9.9 0.2

303 10 0.2

:Steel Ends

304 -0.5 0.1

305 10.5 0.1

:Steel

306 0 0.1

307 0.1 0.1

...

405 9.9 0.1

: Rows are shortened

406 10 0.1

'ELEMENTS'

CONNECTIVITY

:Group 1+2

1 B2HT 1 2

2 B2HT 2 3

...

100 B2HT 100 101

101 B2HT 101 202

102 B2HT 202 303

103 B2HT 303 302

104 B2HT 302 301

...

202 B2HT 204 203

203 B2HT 203 102

204 B2HT 102 1

:Group 1

400 Q8MEM 1 2 103 102

401 Q8MEM 2 3 104 103

...

598 Q8MEM 200 201 302 301

599 Q8MEM 201 202 303 302

1000 L2TRU 304 306

1001 L2TRU 306 307

1002 L2TRU 307 308

...

1100 L2TRU 405 406

1101 L2TRU 406 305

2000 L8IF 306 307 102 103

2001 L8IF 307 308 103 104

...

2098 L8IF 404 405 200 201

2099 L8IF 405 406 201 202

3000 IL4HT 306 307 102 103

3001 IL4HT 307 308 103 104

...

3098 IL4HT 404 405 200 201

3099 IL4HT 405 406 201 202

MATERIALS

/ 400-599 / 1

/ 101-204 / 2

:/ 4000-4009 / 2

/ 1-100 / 3

/ 2000-2099 / 4

/ 1000-1101 / 5

/ 3000-3099 / 6

GEOMETRY

/ 400-599 / 1

/ 2000-2099 / 2

/ 1000-1101 / 3

'MATERIALS'

1 NAME CONCRETE

POWER 0.1 0 0 0

CONDUCT 2.4E-3

CAPACIT 2.64E+03

YOUNG 3.80E+04

POISON 2.00E-01

THERMX 20.00E-06

EQUAGE ARRTYP

TEMREF 25

ARRHEN 6000

ADIAB 0. 25.0

1.800E+04 2.606E+01

3.600E+04 3.231E+01

5.400E+04 3.992E+01

7.200E+04 4.387E+01
 9.000E+04 4.608E+01
 1.080E+05 4.740E+01
 1.206E+05 4.799E+01
 1.512E+05 4.873E+01
 1.800E+05 4.898E+01
 YOUHAR MC1990
 YOUN28 3.80E+04
 CEMTYP RS
 2 NAME AIR
 CONVEC 2E-03
 3 NAME FORM
 CONVEC 3.60E-06
 4 NAME INTERFACE
 DSTIF 785E5 785E5
 CAPACI 2.00000E+003
 CONDOC 2E-3
 DFLUX 0.00001E-20
 USRIFC BAGE
 USRVAL 2E-3 5.5E6 191413
 USRSTA 0
 5 NAME PRESTRESSEDSTEEL
 CONDOC 0.05
 CAPACI 3611
 YOUNG 2.05E+05
 POISON 3.00E-01
 THERMX 20.00E-06
 6 NAME HEATINTERFACE
 DFLUX 2
 'GEOMET'
 1 NAME CONCRETE
 THICK 2.00E-01
 2 NAME INTERFACE
 THICK 0.129
 CONFIG BONDSL

```

3 NAME STEEL
  CROSSE 0.00008764
'LOADS'
CASE 1
ELEMEN
/1000-1101/PRESTR 1.40E+03
'BOUNDA'
CASE 1
ELEMEN
  1000 EXTEMP 25
  1 EXTEMP 25
  ...
  204 EXTEMP 25
  1101 EXTEMP 25
'TIMEBO'
BOUNDA 1
TIMES 0.000000E+00 0.864000E+06 /
FACTOR 0.100000E+01 0.100000E+01 /
'SUPPORTS'
/ 304 305 / TR 1
/ 304 305 1-101 / TR 2
:/ 304-406 1-101 / TR 2
'INIVAR'
TEMPER 1
/ 1-303 / 25
/ 304-406 / 25
'DIRECTIONS'
  1 1.00E+00 0.00E+00 0.00E+00
  2 0.00E+00 1.00E+00 0.00E+00
  3 0.00E+00 0.00E+00 1.00E+00
'END'

```

B.3 FE-Model

The complete FE-codes for the different factories can be seen in subchapters below.

B.3.1 Vislanda

- **DAT-file**

FEMGEN MODEL : EXTENDED
ANALYSIS TYPE : Heatflow-Stress Staggered 2D
MODEL DESCRIPTION : From archive file
'UNITS'
LENGTH M
TIME SEC
TEMPER CELSIU
FORCE N
'COORDINATES' DI=2
:GROUP 1
1 0 0
2 1.25 0
3 2.5 0
4 3.75 0
5 5 0
6 0 0.1
7 1.25 0.1
8 2.5 0.1
9 3.75 0.1
10 5 0.1
11 0 0.2
12 1.25 0.2
13 2.5 0.2
14 3.75 0.2
15 5 0.2
...
:GROUP 22
286 106.75 0
287 108 0
288 109.25 0
289 110.5 0
290 106.75 0.1
291 108 0.1
292 109.25 0.1

293 110.5 0.1
294 106.75 0.2
295 108 0.2
296 109.25 0.2
297 110.5 0.2

:Steel Ends

331 -0.5 0.1
332 111 0.1

:Steel

333 0 0.1
334 1.25 0.1
...
430 109.25 0.1
431 110.5 0.1

'ELEMENTS'

CONNECTIVITY

:Group 1

1 B2HT 1 2
2 B2HT 2 3
...
99 B2HT 119 114
100 B2HT 114 109

101 B2HT 136 137

:Group 22

568 Q8MEM 275 286 290 280
569 Q8MEM 286 287 291 290
...
574 Q8MEM 291 292 296 295
575 Q8MEM 292 293 297 296

1000 L2TRU 331 333

1000 L2TRU 333 334
 ...
 1098 L2TRU 430 431
 1099 L2TRU 431 332

 2000 L8IF 333 334 6 7
 2001 L8IF 334 335 7 8
 ...
 2086 L8IF 429 430 291 292
 2087 L8IF 430 431 292 293

 3000 IL4HT 333 334 6 7
 3001 IL4HT 334 335 7 8
 ...
 3086 IL4HT 429 430 291 292
 3087 IL4HT 430 431 292 293

 4001 B2HT 333 334
 4002 B2HT 334 335

 4097 B2HT 429 430
 4098 B2HT 430 431

MATERIALS

/ 400-575 / 1
 / 9-20 29-40 49-60 69-80 89-100 109-120 129-140 149-160 169-180
 189-200 209-220 / 2
 / 1-8 21-28 41-48 61-68 81-88 101-108 121-128 141-148 161-168
 181-188 201-208 / 3
 / 2000-2087 / 4
 / 1000-1099 / 5
 / 3000-3087 / 6
 / 4001-4098 / 7

GEOMETRY

/ 400-575 / 1
 / 2000-2087 / 2

/ 1000-1099 / 3

'MATERIALS'

1 NAME CONCRETE
POWER 0.1 0 0 0
CONDUCT 2.40E-03
CAPACI 2.64E+03
YOUNG 3.80E+04
POISON 2.00E-01
THERMX 2.00E-05
EQUAGE ARRTYP
TEMREF 20
ARRHEN 6000
ADIAB 0 18.60
3600 18.7
7200 18.8
10800 18.9
14400 19
18000 19.2
21600 19.5
25200 20.5
28800 21.5
32400 22.5
36000 24
39600 28.0
43200 36.0
46800 46.0
50400 47.0
54000 47.1
57600 47.2
61200 47.3
64800 47.4
68400 47.5
72000 47.6
75600 47.7
79200 47.8

82800 47.9
 86400 48.0
 YOUHAR MC1990
 YOUN28 3.80E+04
 CEMTYP RS
 2 NAME AIR
 CONVEC 1.853E-03
 3 NAME FORM
 CONVEC 3.60E-06
 4 NAME INTERFACE
 DSTIF 7.85E5 7.85E-3
 CAPACI 2.00E+03
 CONDOC 2.00E-03
 DFLUX 1.00E-25
 USRIFC BAGE
 USRVAL 2.00E-03 5.20E+06 120000 25500
 USRSTA 0
 5 NAME PRESTRESSEDSTEEL
 CONDOC 0.05
 CONVEC 3.600000E-6
 CAPACI 3611
 YOUNG 2.05E+05
 POISON 2.00E-01
 THERMX 2.00E-05
 6 NAME HEATINTERFACE
 DFLUX 1
 7 CONVEC 3.60E-6
 'GEOMET'
 1 NAME CONCRETE
 THICK 2.00E-01
 2 NAME INTERFACE
 THICK 0.129
 CONFIG BONDSL
 3 NAME STEEL
 CROSSE 8.76400E-005

'LOADS'

CASE 1

ELEMEN

/1000-1099/PRESTR 1343

'GROUPS'

ELEMEN

1 CONC1 / 1-20 400-407 /
2 CONC1+2 / 1-20 400-415 /
3 CONC3 / 21-40 416-423 /
4 CONC3+4 / 21-40 416-431 /
5 CONC5 / 41-60 432-439 /
6 CONC5+6 / 41-60 432-447 /
7 CONC7 / 61-80 448-455 /
8 CONC7+8 / 61-80 448-463 /
9 CONC9 / 81-100 464-471 /
10 CONC9+10 / 81-100 464-479 /
11 CONC11 / 101-120 480-487 /
12 CONC11+12 / 101-120 480-495 /
13 CONC13 / 121-140 496-503 /
14 CONC13+14 / 121-140 496-511 /
15 CONC15 / 141-160 512-519 /
16 CONC15+16 / 141-160 512-527 /
17 CONC17 / 161-180 528-535 /
18 CONC17+18 / 161-180 528-543 /
19 CONC19 / 181-200 544-551 /
20 CONC19+20 / 181-200 544-559 /
21 CONC21 / 201-220 560-567 /
22 CONC21+22 / 201-220 560-575 /
30 STEELIF / 1000-1099 2000-2087 4001-4098 3000-3087 /

'SUPPORTS'

/ 331 332 / TR 1

/ 331-431 / TR 2

/ 1-8 21-28 41-48 61-68 81-88 101-108 121-128 141-148 161-168
181-188 201-208 / TR 2

'INIVAR'

```

TEMPER 1
/ 1-297 / 18.6
/ 331-431 / 20
'TEMPER'
NODES
    0 8.64E7
/ 331 332 /
    20 20
'DIRECTIONS'
    1 1.000000E+00 0.000000E+00 0.000000E+00
    2 0.000000E+00 1.000000E+00 0.000000E+00
    3 0.000000E+00 0.000000E+00 1.000000E+00
'END'

```

B.3.2 Marijampolé

- **DAT-file**

```

FEMGEN MODEL : EXTENDED
ANALYSIS TYPE : Heatflow-Stress Staggered 2D
MODEL DESCRIPTION : From archive file
'UNITS'
LENGTH M
TIME SEC
TEMPER KELVIN
FORCE N
'COORDINATES' DI=2
:GROUP 1
: 108
    1 0 0
    2 1.35 0
    ...
    14 4.05 0.2
    15 5.4 0.2

:GROUP 20
    232 103.95 0

```

```

233 105.3 0
...
242 106.65 0.2
243 108 0.2

:Steel
303 0 0.1
304 1.35 0.1
...
382 106.65 0.1
383 108 0.1
:Steel Ends
301 -0.5 0.1
302 108.5 0.1

'ELEMENTS'
CONNECTIVITY
1 B2HT 1 2
2 B2HT 2 3
...
162 B2HT 12 11
163 B2HT 11 6
164 B2HT 6 1
:Group 1
400 Q8MEM 1 2 7 6
401 Q8MEM 2 3 8 7
...
406 Q8MEM 8 9 14 13
407 Q8MEM 9 10 15 14
...
:Group 20
552 Q8MEM 223 232 236 227
553 Q8MEM 232 233 237 236
...
558 Q8MEM 237 238 242 241

```

559	Q8MEM	238	239	243	242
1000	L2TRU	301	303		
1001	L2TRU	303	304		
...					
1080	L2TRU	382	383		
1081	L2TRU	383	302		
2000	L8IF	303	304	6	7
2001	L8IF	304	305	7	8
...					
2078	L8IF	381	382	237	238
2079	L8IF	382	383	238	239
3000	IL4HT	303	304	6	7
3001	IL4HT	304	305	7	8
...					
3078	IL4HT	381	382	237	238
3079	IL4HT	382	383	238	239
4001	B2HT	303	304		
4002	B2HT	304	305		
...					
4079	B2HT	381	382		
4080	B2HT	382	383		

MATERIALS

/	400-559	/	1
/	81-164	/	2
/	1-80	/	3
/	2000-2079	/	4
/	1000-1081	/	5
/	3000-3079	/	6
/	4001-4080	/	7

GEOMETRY

/	400-559	/	1
---	---------	---	---

/ 2000-2079 / 2

/ 1000-1081 / 3

'MATERIALS'

1 NAME CONCRETE

POWER 0.1 0 0 0

CONDUCT 2.40E-03

CAPACIT 2.64E+03

YOUNG 3.80E+04

POISSON 2.00E-01

THERMX 2.00E-05

EQUATION ARRTYP

TEMPREF 6

ARRHEN 6000

ADIAB 0 17

3600 17.2

7200 18.7

10800 19.4

14400 19.9

18000 21.0

21600 25.0

25200 28.0

28800 34.0

32400 39.0

36000 43.0

39600 44.0

43200 47.0

46800 50.0

50400 51.0

54000 51.5

57600 52.3

61200 52.7

64800 53.0

68400 53.2

72000 53.4

75600 53.5

79200 53.6
 82800 53.7
 86400 53.8
 YOUHAR MC1990
 YOUN28 3.80E+04
 CEMTYP RS
 2 NAME AIR
 CONVEC 1.853E-03
 3 NAME FORM
 CONVEC 3.60E-06
 4 NAME INTERFACE
 DSTIF 7.85E5 7.85E-3
 CAPACI 2.00E+03
 CONDOC 2.00E-03
 DFLUX 1.00E-25
 USRIFC BAGE
 USRVAL 2.00E-03 4.80E+06 191000 58000
 USRSTA 0
 5 NAME PRESTRESSEDSTEEL
 CONDOC 0.05
 CONVEC 3.600000E-6
 CAPACI 3611
 YOUNG 2.05E+05
 POISON 2.00E-01
 THERMX 2.00E-05
 6 NAME HEATINTERFACE
 DFLUX 1
 7 CONVEC 3.60E-6
 'GEOMET'
 1 NAME CONCRETE
 THICK 2.00E-01
 2 NAME INTERFACE
 THICK 0.214
 CONFIG BONDSL
 3 NAME STEEL

CROSSE 2.806E-04

'LOADS'

CASE 1

ELEMEN

/1000-1081/PRESTR 1395

'GROUPS'

ELEMEN

1 CONC1 / 1-4,159-164,400-407 /

ELEMEN

2 CONC1+2 / 1-8,155-164,400-415 /

ELEMEN

3 CONC3 / 1-12,151-164,416-423 /

ELEMEN

4 CONC3+4 / 1-16,147-164,416-431 /

ELEMEN

5 CONC5 / 1-20,143-164,432-439 /

ELEMEN

6 CONC5+6 / 1-24,139-164,432-447 /

ELEMEN

7 CONC7 / 1-28,135-164,448-455 /

ELEMEN

8 CONC7+8 / 1-32,131-164,448-463 /

ELEMEN

9 CONC9 / 1-36,127-164,464-471 /

ELEMEN

10 CONC9+10 / 1-40,123-164,464-479 /

ELEMEN

11 CONC11 / 1-44,119-164,480-487 /

ELEMEN

12 CONC11+12 / 1-48,115-164,480-495 /

ELEMEN

13 CONC13 / 1-52,111-164,496-503 /

ELEMEN

14 CONC13+14 / 1-56,107-164,496-511 /

ELEMEN

```

15 CONC15 / 1-60,103-164,512-519 /
ELEMEN
16 CONC15+16 / 1-64,99-164,512-527 /
ELEMEN
17 CONC17 / 1-68,95-164,528-535 /
ELEMEN
18 CONC17+18 / 1-72,91-164,528-543 /
ELEMEN
19 CONC19 / 1-76,87-164,544-551 /
ELEMEN
20 CONC19+20 / 1-164,544-559 /
ELEMEN
30 STEELIF / 1000-1081,2000-2079,4001-4080,3000-3079 /
'SUPPORTS'
/ 301,302 / TR 1
/ 301-383 / TR 2
/ 1-5,16-19,28-31,40-43,52-55,64-67,76-79,88-91,100-103,112-115,124-127,136-
139,148-151,160-163,172-175,184-187,196-199,208-211,220-223,232-235 / TR
2
'INIVAR'
TEMPER 1
/ 1-243 / 17
/ 301-383 / 6
'TEMPER'
NODES
0 8.64E7
/ 301 302 /
6 6
'DIRECTIONS'
1 1.00E+00 0.00E+00 0.00E+00
2 0.00E+00 1.00E+00 0.00E+00
3 0.00E+00 0.00E+00 1.00E+00
'END'

```

B.3.3 Sollenau

- **DAT-file**

FEMGEN MODEL : EXTENDED
ANALYSIS TYPE : Heatflow-Stress Staggered 2D
MODEL DESCRIPTION : From archive file
'UNITS'
LENGTH M
TIME SEC
TEMPER KELVIN
FORCE N
'COORDINATES' DI=2
:GROUP 1
: 104
1 0 0
2 1.3 0
...
14 3.9 0.2
15 5.2 0.2
...
242 102.7 0.2
243 104 0.2

:Steel
303 0 0.1
304 1.3 0.1
...
381 101.4 0.1
382 102.7 0.1
383 104 0.1
:Steel Ends
301 -0.5 0.1
302 104.5 0.1

'ELEMENTS'
CONNECTIVITY
:Group 1

1 B2HT 1 2
 2 B2HT 2 3
 ...
 162 B2HT 12 11
 163 B2HT 11 6
 164 B2HT 6 1
 :Group 1
 400 Q8MEM 1 2 7 6
 401 Q8MEM 2 3 8 7
 ...
 406 Q8MEM 8 9 14 13
 407 Q8MEM 9 10 15 14

 :Group 20
 552 Q8MEM 223 232 236 227
 553 Q8MEM 232 233 237 236
 ...
 558 Q8MEM 237 238 242 241
 559 Q8MEM 238 239 243 242

 1000 L2TRU 301 303
 1001 L2TRU 303 304
 ...
 1080 L2TRU 382 383
 1081 L2TRU 383 302

 2000 L8IF 303 304 6 7
 2001 L8IF 304 305 7 8
 ...
 2078 L8IF 381 382 237 238
 2079 L8IF 382 383 238 239

 3000 IL4HT 303 304 6 7
 3001 IL4HT 304 305 7 8
 ...

3078 IL4HT 381 382 237 238
3079 IL4HT 382 383 238 239

4001 B2HT 303 304
4002 B2HT 304 305

...

4079 B2HT 381 382
4080 B2HT 382 383

MATERIALS

/ 400-559 / 1
/ 81-164 / 2
/ 1-80 / 3
/ 2000-2079 / 4
/ 1000-1081 / 5
/ 3000-3079 / 6
/ 4001-4080 / 7

GEOMETRY

/ 400-559 / 1
/ 2000-2079 / 2
/ 1000-1081 / 3

'MATERIALS'

1 NAME CONCRETE
POWER 0.1 0 0 0
CONDUCT 2.40E-03
CAPACI 2.64E+03
YOUNG 4.00E+04
POISON 2.00E-01
THERMX 2.00E-05
EQUAGE ARRTYP
TEMREF 25
ARRHEN 6000
ADIAB 0 25.00
3600 35.88
7200 44.78

10800	52.07
14400	58.04
18000	62.1
21600	62.4
25200	62.6
28800	62.89
32400	65.08
36000	66.88
39600	68.35
43200	69.56
46800	70.54
50400	71.35
54000	72.01
57600	72.55
61200	73.00
64800	73.36
68400	73.66
72000	73.90
75600	74.10
79200	74.26
82800	74.40
86400	74.51

YOUHAR MC1990
 YOUN28 4.00E+04
 CEMTYP RS
 2 NAME AIR
 CONVEC 1.853E-03
 3 NAME FORM
 CONVEC 3.60E-06
 4 NAME INTERFACE
 DSTIF 7.85E5 7.85E-3
 CAPACI 2.00E+03
 CONDOC 2.00E-03
 DFLUX 1.00E-25
 USRIFC BAGE

```

USRVAL 2.00E-03 6.30E+06 82000 14800
USRSTA 0
5 NAME PRESTRESSEDSTEEL
CONDUCT 0.05
CONVEC 3.600000E-6
CAPACI 3611
YOUNG 2.05E+05
POISON 2.00E-01
THERMX 2.00E-05
6 NAME HEATINTERFACE
DFLUX 1
7 CONVEC 3.60E-6
'GEOMET'
1 NAME CONCRETE
THICK 2.00E-01
2 NAME INTERFACE
THICK 0.264
CONFIG BONDSL
3 NAME STEEL
CROSSE 3.958E-04
'LOADS'
CASE 1
ELEMEN
/1000-1081/PRESTR 1275
'GROUPS'
ELEMEN
1 CONC1 / 1-4,159-164,400-407 /
ELEMEN
2 CONC1+2 / 1-8,155-164,400-415 /
ELEMEN
3 CONC3 / 1-12,151-164,416-423 /
ELEMEN
4 CONC3+4 / 1-16,147-164,416-431 /
ELEMEN
5 CONC5 / 1-20,143-164,432-439 /

```

ELEMEN

6 CONC5+6 / 1-24,139-164,432-447 /

ELEMEN

7 CONC7 / 1-28,135-164,448-455 /

ELEMEN

8 CONC7+8 / 1-32,131-164,448-463 /

ELEMEN

9 CONC9 / 1-36,127-164,464-471 /

ELEMEN

10 CONC9+10 / 1-40,123-164,464-479 /

ELEMEN

11 CONC11 / 1-44,119-164,480-487 /

ELEMEN

12 CONC11+12 / 1-48,115-164,480-495 /

ELEMEN

13 CONC13 / 1-52,111-164,496-503 /

ELEMEN

14 CONC13+14 / 1-56,107-164,496-511 /

ELEMEN

15 CONC15 / 1-60,103-164,512-519 /

ELEMEN

16 CONC15+16 / 1-64,99-164,512-527 /

ELEMEN

17 CONC17 / 1-68,95-164,528-535 /

ELEMEN

18 CONC17+18 / 1-72,91-164,528-543 /

ELEMEN

19 CONC19 / 1-76,87-164,544-551 /

ELEMEN

20 CONC19+20 / 1-164,544-559 /

ELEMEN

30 STEELIF / 1000-1081,2000-2079,4001-4080,3000-3079 /

'SUPPORTS'

/ 301,302 / TR 1

/ 301-383 / TR 2

```

/ 1-5,16-19,28-31,40-43,52-55,64-67,76-79,88-91,100-103,112-115,124-127,136-
139,148-151,160-163,172-175,184-187,196-199,208-211,220-223,232-235 / TR
2
'INIVAR'
TEMPER 1
/ 1-243 / 25
/ 301-383 / 25
'TEMPER'
NODES
0 8.64E7
/ 301 302 /
25 25
'DIRECTIONS'
1 1.00E+00 0.00E+00 0.00E+00
2 0.00E+00 1.00E+00 0.00E+00
3 0.00E+00 0.00E+00 1.00E+00
'END'

```